POLISH ACADEMY OF SCIENCES
INSTITUTE OF FUNDAMENTAL TECHNOLOGICAL RESEARCH

BIBLIOTEKA MECHANIKI STOSOWANEJ

Seria B. Podręczniki i opracowania inżynierskie

WYDAWNICTWO NAUKOWE PWN
POLISH SCIENTIFIC PUBLISHERS PWN

POLISH ACADEMY OF SCIENCES
INSTITUTE OF FUNDAMENTAL TECHNOLOGICAL RESEARCH

ANTONI SAWCZUK and JOANNA SOKÓŁ-SUPEL

LIMIT ANALYSIS OF PLATES

WARSZAWA 1993

This book is supported by
TEMPUS — JOINT EUROPEAN PROJECTS No. 0438-91/92

Cover design
MARIA DUSZEK

MAREK KWIECIŃSKI — Translation Editor
Faculty of Civil Engineering
Warsaw University of Technology

ISBN 83-01-11181-X

PRINTED IN POLAND

Ark. wyd. 15,25. Ark. druk. 15,75. Papier offsetowy kl. III. 80 g. 70×100 cm. Oddano do składania w sierpniu 1992 r. Druk ukończono w marcu 1993 r.

Skład: **GP-BIT** Warszawa, ul. Marymoncka 34

Druk i oprawa: Warszawa, ul. Potażowa 8

TABLE OF CONTENTS

PREFACE

Limit analysis is concerned with the development of effective methods for computing the ultimate load of many types of structures. It is especially for thin plates that limit analysis supplies relatively simple and reliable results of intense interest to practicing engineers and to the students of plasticity alike.

The prime objective of this book is to present basic features of the limit analysis of plates. Emphasis is placed both on mathematical aspects of the plastic plate equations and on the solutions for a broad class of plates obeying various yield conditions. Methods of the limit analysis for plates are explained and approximate theories such as the yield-line method, are discussed on the background of the general theory.

It is hoped that this book will prove useful to both the research workers and graduate students in the field of applied plasticity as well as to the civil and structural engineers.

The first draft of this book was prepared during my stay at the Mexico National University (UNAM) in Mexico City. A certain part of the material covers the lectures delivered by Professor Antoni Sawczuk at the International Centre for Mechanical Sciences (CISM) in Udine, Italy. The results obtained by his research group at the Institute of Fundamental Technological Research of the Polish Academy of Sciences are also included.

Untimely death of Professor Sawczuk interfered with the prompt preparation of the book. The present updated text was finally prepared and the encouragement of Professor Wojciech Szczepiński is appreciated.

I would like to gratefully acknowledge the help of Professor Marek Kwieciński of the Warsaw University of Technology, who read the whole draft and made useful corrections. Thanks are also due to him for the editing of the English translation.

I am also greatly indebted to Professor Marek Janas of the Polish Academy of Sciences for his assistance in commenting on and improving the final version of the book.

Last but by no means least, I would like to thank Dr. Jerzy A. Supel, my husband, for his patience and encouragement.

Joanna Sokół-Supel

Warsaw, November 1991

CHAPTER 1

INTRODUCTION

1.1. Preliminaries

The theory of plasticity has a broad range of applications in many branches of technology. Its methods permit to describe metal-forming processes, allow to estimate safety of structures against collapse, make possible to evaluate flow of bulk materials and stability of slopes. Stress analysis and design of structural elements in chemical engineering, aeronautics, power engineering, machine and ship building, civil engineering, nuclear technology is nowadays made taking into account methods and solutions furnished by the theory of plasticity and by its specialized branches such as limit analysis, thermoplasticity, shakedown analysis or study of post-yield behaviour, [15], [17], [27], [43], [55], [58], [59], [79].

Mathematical models of plastic response are useful in studies of vehicle collisions and response of containments to transient loadings, in designing machines for earthwork and mining, as well as in studying landslides and avalanches.

Implementation of methods of plastic analysis in engineering appears to have been unsufficient, considering properties the real materials possess to sustain plastic deformation. The main reason for this is the wealth of accumulated and diffused knowledge about elastic response as well as linearity of equations governing infinitesimal elastic deformations. Methods of elastic analysis and design, various sets of useful formulae, tables and diagrams are available in the technical literature and constitute a substantial aid to designer's work. There is, however, a natural trend to produce appropriate collections of design aids within the plastic approach and place them as useful tools in the hands of engineer.

To make any theory a powerful and reliable tool of engineering at least three conditions must be satisfied. In the first place the theory must be sound, that is well set analytically and properly verified experimentally. Clearly stated assumptions and a solid mathematical structure make the necessary part of such a theory. Several theories of plastic behaviour satisfy this requirement.

Secondly, a theory should be provided with appropriate methods for solving boundary or initial value problems for systems of govering differential equations. Moreover, a sufficient number of solutions to practically important problems should be known so that structural engineer could assess the relevance of the theory. The third requirement is that the results a theory furnishes must be properly presented in the form of collections of tables, formulae and algorithms or programs so as to permit a straightforward application of the information to the problem at hand. In this specific domain a large amount of work has yet to be done to bring the plasticity theories to everyday applications in structural analysis.

It is also important to have methods of plastic analysis and design incorporated in the codes of practice for design of civil and mechanical engineering structures. Further, if the methods are admitted, as it is now mostly the case, it is necessary to have available appropriate recommendations or routines.

In this book we intend to combine theoretical aspects of plasticity with practical implementations, possibly in the form of design aids. The considerations will be restricted to the limit analysis of plates. Before passing to specific problems it appears, however, worthwhile to discern the place kept by the limit analysis theory in the mosaic of plastic methods of structural analysis.

1.2. Plastic analysis

The most developed branch of plastic analysis of structures is the theory of limit analysis. Fairly advanced are the studies regarding the shakedown analysis as well as the post-yield behaviour, including changes in the structural shape in the process of plastic flow. There also exists an extensive literature on dynamics of plastic structures and on optimal plastic design. In general the rigid-perfectly plastic or the elastic-perfectly plastic models of material response are employed, [18], [29], [36], [38], [49], [61], [64], [65], [75].

The theory of limit analysis studies the behaviour of ideally plastic structures. The main purpose is to determine the value of the load multiplier at which a given structure collapses, i.e. transforms into a mechanism. To solve a problem of analysis and to establish the intensity of the load a structure or a machine element can support it is necessary to solve a system of differential equations of equilibrium and flow, supplemented by algebraic relations representing a yield condition. The obtained system is usually nonlinear.

Most of the real structures are subjected to multi-parameter loadings. In many instances we know only the range of the loading program in the loading

space. Such ranges are, for example, prescribed by the codes of practice. The loads act independently, varying in magnitude, direction and sense. They are repetitive and usually vary within prescribed limits, neither the sequence of loading nor its frequency being specified. This results in repeated and fluctuating deformations which may either stabilize or evolve, resulting in shakedown or in unserviceability, respectively. The shakedown analysis studies behaviour of elastic-ideally plastic structures under variablerepeated loading. It answers the question whether an elastic-plastic structure will respond elastically after passing a certain stage of plastic deformation and developing a field of residual stresses. In shakedown analysis we are mostly interested in finding the boundaries of the loading range where the response is elastic but differs from the response of a structure without residual stresses, [36].

In many situations the deformations of a structure under sustained load become significant and thus the shape of a structure changes so that it influences the state of stress. The original and the current configurations of a structure have to be distinguished. The problem of post-yield behaviour can be properly set in terms of geometrically nonlinear theories. Geometric changes are of importance in design as they can either be useful or dangerous. For certain loading combinations the post-yield behaviour results in "strengthening" of a structure, in some other instability occurs resulting in a catastrophic collapse.

Besides the limit analysis, the shakedown theory and the post-yield behaviour, the plastic analysis includes dynamics of plastic structures. An ideal elastic-plastic structure, if loaded impulsively can carry loads exceeding the static collapse load. The induced accelerations result in plastic motion which ceases when the kinetic energy introduced is dissipated in the process of plastic flow.

A specific domain of the theory of plastic structures is that of optimum design, [3], [65]. Most of the optimum design problems in plasticity constitute counterparts of the analysis. Such structural shapes or cross-sectional sizes are sought for which lead to the minimum material consumption to support prescribed ultimate load.

1.3. Scope

In the present book we shall confine our attention solely to the limit analysis of plates. Several yield criteria will be employed in order to give a feeling to what extent the form of a yield condition influences methods of solution and characteristic features of a solution itself. Emphasis is put both on mathematical aspects of the plastic plate equations and on the solutions

for a broad class of plates obeying various yield criteria. Methods of limit analysis of plates are explained and approximate theories like the yield-line method are discussed on the background of a general theory. A collection of tables and design aids are given.

To make the presentation self contained the basic equations of perfect plasticity are briefly shown in Chapter 2. The plate equations are analyzed in Chapter 3. Chapter 4 concerns with circular plates under rotationally symmetric loading when ordinary differential equations govern the plastic behaviour. Analytical and numerical solutions are given. Bounding techniques that furnish estimates to the collapse load intensity are explained in Chapter 5, whereas in the next chapter orthotropic and nonhomogeneous plates are briefly considered. Chapter 8 is devoted to bending of plates of arbitrary shape. Special attention is given to plates obeying a square yield criterion in the plane of principal moments. A number of new complete solutions is presented allowing to assess the accuracy of results furnished by the yield line theory, which is presented in Chapter 7 and accompanied by a set of tables.

CHAPTER 2

PRINCIPLES OF LIMIT ANALYSIS

2.1. Basic assumptions

2.1.1. Mathematical model of plastic behaviour. Mechanical behaviour of rate insensitive elastic-plastic, non-hardening solids is idealized in the stress-strain diagram shown in Fig. 2.1a. Unconstrained plastic flow begins in uniaxial tension at the yield stress σ_0^+ and in uniaxial compression at σ_0^-.

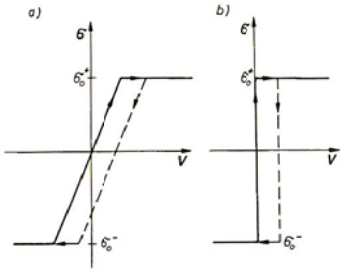

Fig. 2.1. (a) Elastic-perfectly plastic, (b) rigid-perfectly plastic models of materials

In problems regarding unconstrained plastic motion the elastic strains can usually be disregarded when compared with the prevailing plastic strains. The rigid-plastic model of material response is hence obtained, Fig. 2.1b. The constitutive equation of rigid-perfectly plastic solids involves the stress tensor $\boldsymbol{\sigma}$ and the strain rate tensor $\mathbf{V}$

$$\boldsymbol{\sigma} = \boldsymbol{\sigma}(\mathbf{V}). \tag{2.1}$$

Its general form is subjected to the condition that the stress components be homogeneous functions of order zero with respect to time, i.e. with respect to the strain rates as well. The homogeneity requirement: $\boldsymbol{\sigma}(\alpha\,\mathbf{V}) = \alpha^0\,\boldsymbol{\sigma}(\mathbf{V})$, α being a constant, results in the system of equations

$$\frac{\partial \sigma_{ij}}{\partial V_{rs}} V_{rs} = 0 \tag{2.2}$$

which expresses analytically the essential property of the rate insensitive plastic flow, namely that the state of stress at yield does not depend on how fast this state has been reached. From now on a repeated index denotes a sum according to the summation convention.

In view of the homogeneity requirement not all stress components are independent since they are expressible in terms of the ratios of strain rate components. Since $\sigma_{ij} = \sigma_{ji}$, six stress components σ_{ij} are expressible in terms of five ratios of strain rate components. On eliminating the parameters the yield criterion is obtained

$$F(\sigma_{ij}) = 0 \quad \text{or} \quad f(\sigma_{ij}) - c = 0, \tag{2.3}$$

where c is a material constant.

The yield criterion can be represented as a surface in the six-dimensional stress space. The yield locus (2.3) is the boundary of the elastic domain where $F(\sigma_{ij}) < 0$. The states $F(\sigma_{ij}) > 0$ are not admissible for a perfectly plastic solid. The surface (2.3) is convex.

2.1.2. Yield criteria. The yield criterion (2.3) for specific materials is specified on the grounds of experimental data. For metals two criteria are generally accepted, namely the Huber-Mises and the Tresca criteria. In both the influence of hydrostatic stress component on the onset of yielding is neglected.

The Huber-Mises yield criterion states that a material becomes plastic when the elastic distortion energy per unit volume reaches a critical value

$$F = 3\sigma_{ij}\sigma_{ij} - \sigma_{ii}\sigma_{jj} - 2\sigma_0^2 = 0. \tag{2.4}$$

In the state of plane stress the condition (2.4) represents an ellipsoid

$$\sigma_x^2 - \sigma_x\sigma_y + \sigma_y^2 + 3\tau_{xy}^2 = \sigma_0^2. \tag{2.5}$$

The Tresca yield criterion states that a material becomes plastic when the maximum shearing stress reaches a limiting value

$$\sup(|\sigma_1 - \sigma_2|, |\sigma_2 - \sigma_3|, |\sigma_3 - \sigma_1|) = \sigma_0. \tag{2.6}$$

In the case of plane stress, $\sigma_3 = 0$, the condition (2.6) takes the form of the following three equations

$$\begin{aligned} F_1 &= -(\sigma_x - \sigma_0)(\sigma_y - \sigma_0) + \sigma_{xy}^2 = 0, \\ F_2 &= -(\sigma_x + \sigma_0)(\sigma_y + \sigma_0) + \sigma_{xy}^2 = 0, \\ F_3 &= (\sigma_x - \sigma_y)^2 + 4\sigma_{xy}^2 - \sigma_0^2 = 0. \end{aligned} \tag{2.7}$$

The elastic region is therefore bounded by two cones $F_1 = 0$, $F_2 = 0$ and by an elliptic cylinder $F_3 = 0$.

The equations describing plastic behaviour of structures can be simplified by using certain approximate yield criteria such as the maximum reduced stress criterion

$$\sup|\sigma_i - (\sigma_1 + \sigma_2 + \sigma_3)/3| = \frac{2}{3}\sigma_0, \qquad i = 1, 2, 3. \tag{2.8}$$

In the space of principal stresses it represents a regular hexagonal prism circumscribing the Tresca criterion and having common symmetry planes. In plane stress the criterion becomes

$$\sup(|\sigma_1 - \frac{1}{2}\sigma_2|, |\sigma_2 - \frac{1}{2}\sigma_1|, \frac{1}{2}|\sigma_1 + \sigma_2|) = \sigma_0. \tag{2.9}$$

In plate analysis a yield criterion of maximum normal stress is also employed. For the case of plane stress it reduces to the first two of Eqs.(2.7) and represents two intersecting cones.

Comparison of Huber-Mises, Tresca, maximum reduced stress and maximum normal stress criteria for plane stress in the plane of principal stresses is shown in Fig. 2.2.

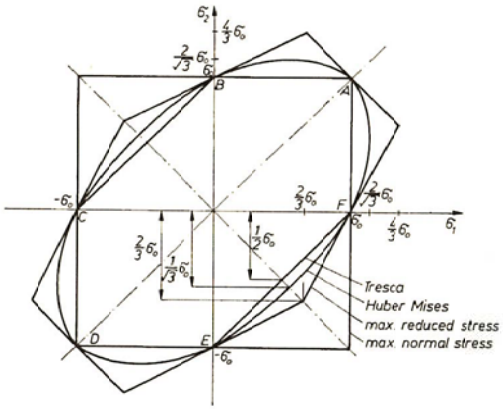

Fig. 2.2. Comparison of Huber-Mises, Tresca, maximum reduced stress and maximum normal stress yield criteria

2.1.3. Power of dissipation. The power of dissipation in plastic flow at a generic particle whose stress state is described by σ and the strain rate state by $\mathbf{V}$ is

$$d = \sigma \cdot \mathbf{V}. \tag{2.10}$$

This power is assumed to be fully dissipated in the form of heat during plastic flow and is regarded positive.

The constitutive equation of plastic solid relates the stress tensor σ only to the tensor of the plastic strain rates $\mathbf{V}$, (2.1), and it is homogeneous of order zero; thus

a) the power of dissipation is a single valued function of the strain rate

$$d = d(\mathbf{V}), \tag{2.11}$$

b) the dissipation rate function $d(\mathbf{V})$ is homogeneous of the order one with respect to the strain rates

$$d(\alpha \mathbf{V}) = \alpha d(\mathbf{V}), \qquad \alpha > 0$$

or

$$\frac{\partial d}{\partial \mathbf{V}} \cdot \mathbf{V} = d. \tag{2.12}$$

The latter property expresses the inviscid nature of plastic flow.

2.1.4. Constitutive equation of limit analysis. The yield criterion predicts at what state of stress the plastic motion can take place. In order to answer the question what is the mechanism of motion at a particle stressed so that the yield criterion is satisfied it is necessary to know a flow rule, i.e. the constitutive relation governing plastic motion. Various theories of plasticity exist depending upon the form of the constitutive relation.

In limit analysis the associated flow rule is accepted in which the yield function (2.3) is taken as the plastic potential:

$$V_{ij} = \nu \frac{\partial F}{\partial \sigma_{ij}} = \nu \frac{\partial f}{\partial \sigma_{ij}}, \qquad \nu \geqslant 0. \tag{2.13}$$

This means that the strain rate vector $\mathbf{V}$ is directed along the outer normal to the surface $F = 0$, Fig. 2.3. Since the yield surface (2.3) is convex,

$$\frac{\partial f}{\partial \sigma_{ij}} \sigma_{ij} \geqslant 0, \tag{2.14}$$

and the power of dissipation (2.10) is nonnegative thus the scalar multiplier ν is nonnegative.

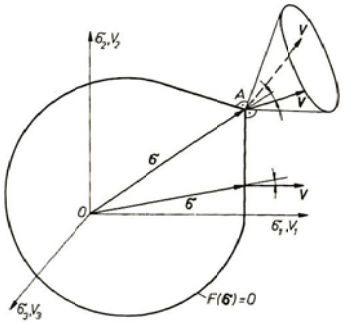

Fig. 2.3. Associated flow rule

Taking $f(\sigma_{ij})$ as a homogeneous function of order $n>0$ in stress it is found that

$$\nu = \frac{d}{nf} = \frac{d}{nc}. \tag{2.15}$$

When the yield surface has ridges and corners, as at A in Fig. 2.3, the gradient there is not uniquely defined. The plastic potential flow law at the singular points where k surfaces $F_k=0$ meet is then generalized to take the form

$$V_{ij} = \nu_k \frac{\partial F_k}{\partial \sigma_{ij}} \tag{2.16}$$

and all ν_k are nonnegative. The strain rate vector remains within the fan defined by the normals to the surfaces meeting at singular points. Such a situation takes place for the Tresca yield condition (2.7) on the ridges of the corresponding yield surface.

2.1.5. Description of limit analysis problem. In the theory of limit analysis an incipient motion of perfectly plastic structures and continua is studied. Its objective is to solve boundary value problems for equations governing plastic motion under a system of loads increasing quasistatically, starting from zero. The term quasistatic means that the loading process is so slow that all dynamic effects can be disregarded.

The classical presentation of the limit analysis theory concerns a system of loads increasing in proportion to a single parameter μ and is described as follows:

$$\mathbf{T}(\mathbf{x},t) = \mu(t)\, \mathbf{P}(\mathbf{x}), \tag{2.17}$$

POLISH ACADEMY OF SCIENCES
INSTITUTE OF FUNDAMENTAL TECHNOLOGICAL RESEARCH

BIBLIOTEKA
MECHANIKI
STOSOWANEJ

Seria B. Podręczniki i opracowania inżynierskie

WYDAWNICTWO NAUKOWE PWN
POLISH SCIENTIFIC PUBLISHERS PWN

POLISH ACADEMY OF SCIENCES
INSTITUTE OF FUNDAMENTAL TECHNOLOGICAL RESEARCH

ANTONI SAWCZUK and JOANNA SOKÓŁ-SUPEL

LIMIT ANALYSIS OF PLATES

WARSZAWA 1993

POLISH ACADEMY OF SCIENCES
INSTITUTE OF FUNDAMENTAL TECHNOLOGICAL RESEARCH

BIBLIOTEKA MECHANIKI STOSOWANEJ

Seria B. Podręczniki i opracowania inżynierskie

WYDAWNICTWO NAUKOWE PWN
POLISH SCIENTIFIC PUBLISHERS PWN

POLISH ACADEMY OF SCIENCES
INSTITUTE OF FUNDAMENTAL TECHNOLOGICAL RESEARCH

ANTONI SAWCZUK and JOANNA SOKÓŁ-SUPEL

LIMIT ANALYSIS OF PLATES

WARSZAWA 1993

This book is supported by
TEMPUS — JOINT EUROPEAN PROJECTS No. 0438-91/92

Cover design
MARIA DUSZEK

MAREK KWIECIŃSKI — Translation Editor
Faculty of Civil Engineering
Warsaw University of Technology

ISBN 83-01-11181-X

PRINTED IN POLAND

Ark. wyd. 15,25. Ark. druk. 15,75. Papier offsetowy kl. III. 80 g. 70×100 cm. Oddano do składania w sierpniu 1992 r. Druk ukończono w marcu 1993 r.

Skład: **GP-BIT** Warszawa, ul. Marymoncka 34

Druk i oprawa: Warszawa, ul. Potażowa 8

TABLE OF CONTENTS

PREFACE

Limit analysis is concerned with the development of effective methods for computing the ultimate load of many types of structures. It is especially for thin plates that limit analysis supplies relatively simple and reliable results of intense interest to practicing engineers and to the students of plasticity alike.

The prime objective of this book is to present basic features of the limit analysis of plates. Emphasis is placed both on mathematical aspects of the plastic plate equations and on the solutions for a broad class of plates obeying various yield conditions. Methods of the limit analysis for plates are explained and approximate theories such as the yield-line method, are discussed on the background of the general theory.

It is hoped that this book will prove useful to both the research workers and graduate students in the field of applied plasticity as well as to the civil and structural engineers.

The first draft of this book was prepared during my stay at the Mexico National University (UNAM) in Mexico City. A certain part of the material covers the lectures delivered by Professor Antoni Sawczuk at the International Centre for Mechanical Sciences (CISM) in Udine, Italy. The results obtained by his research group at the Institute of Fundamental Technological Research of the Polish Academy of Sciences are also included.

Untimely death of Professor Sawczuk interfered with the prompt preparation of the book. The present updated text was finally prepared and the encouragement of Professor Wojciech Szczepiński is appreciated.

I would like to gratefully acknowledge the help of Professor Marek Kwieciński of the Warsaw University of Technology, who read the whole draft and made useful corrections. Thanks are also due to him for the editing of the English translation.

I am also greatly indebted to Professor Marek Janas of the Polish Academy of Sciences for his assistance in commenting on and improving the final version of the book.

Last but by no means least, I would like to thank Dr. Jerzy A. Supel, my husband, for his patience and encouragement.

Joanna Sokół-Supel

Warsaw, November 1991

Secondly, a theory should be provided with appropriate methods for solving boundary or initial value problems for systems of govering differential equations. Moreover, a sufficient number of solutions to practically important problems should be known so that structural engineer could assess the relevance of the theory. The third requirement is that the results a theory furnishes must be properly presented in the form of collections of tables, formulae and algorithms or programs so as to permit a straightforward application of the information to the problem at hand. In this specific domain a large amount of work has yet to be done to bring the plasticity theories to everyday applications in structural analysis.

It is also important to have methods of plastic analysis and design incorporated in the codes of practice for design of civil and mechanical engineering structures. Further, if the methods are admitted, as it is now mostly the case, it is necessary to have available appropriate recommendations or routines.

In this book we intend to combine theoretical aspects of plasticity with practical implementations, possibly in the form of design aids. The considerations will be restricted to the limit analysis of plates. Before passing to specific problems it appears, however, worthwhile to discern the place kept by the limit analysis theory in the mosaic of plastic methods of structural analysis.

1.2. Plastic analysis

The most developed branch of plastic analysis of structures is the theory of limit analysis. Fairly advanced are the studies regarding the shakedown analysis as well as the post-yield behaviour, including changes in the structural shape in the process of plastic flow. There also exists an extensive literature on dynamics of plastic structures and on optimal plastic design. In general the rigid-perfectly plastic or the elastic-perfectly plastic models of material response are employed, [18], [29], [36], [38], [49], [61], [64], [65], [75].

The theory of limit analysis studies the behaviour of ideally plastic structures. The main purpose is to determine the value of the load multiplier at which a given structure collapses, i.e. transforms into a mechanism. To solve a problem of analysis and to establish the intensity of the load a structure or a machine element can support it is necessary to solve a system of differential equations of equilibrium and flow, supplemented by algebraic relations representing a yield condition. The obtained system is usually nonlinear.

Most of the real structures are subjected to multi-parameter loadings. In many instances we know only the range of the loading program in the loading space. Such ranges are, for example, prescribed by the codes of practice. The loads act independently, varying in magnitude, direction and sense. They are repetitive and usually vary within prescribed limits, neither the sequence of loading nor its frequency being specified. This results in repeated and fluctuating deformations which may either stabilize or evolve, resulting in shakedown or in unserviceability, respectively. The shakedown analysis studies behaviour of elastic-ideally plastic structures under variablerepeated loading. It answers the question whether an elastic-plastic structure will respond elastically after passing a certain stage of plastic deformation and developing a field of residual stresses. In shakedown analysis we are mostly interested in finding the boundaries of the loading range where the response is elastic but differs from the response of a structure without residual stresses, [36].

In many situations the deformations of a structure under sustained load become significant and thus the shape of a structure changes so that it influences the state of stress. The original and the current configurations of a structure have to be distinguished. The problem of post-yield behaviour can be properly set in terms of geometrically nonlinear theories. Geometric changes are of importance in design as they can either be useful or dangerous. For certain loading combinations the post-yield behaviour results in "strengthening" of a structure, in some other instability occurs resulting in a catastrophic collapse.

Besides the limit analysis, the shakedown theory and the post-yield behaviour, the plastic analysis includes dynamics of plastic structures. An ideal elastic-plastic structure, if loaded impulsively can carry loads exceeding the static collapse load. The induced accelerations result in plastic motion which ceases when the kinetic energy introduced is dissipated in the process of plastic flow.

A specific domain of the theory of plastic structures is that of optimum design, [3], [65]. Most of the optimum design problems in plasticity constitute counterparts of the analysis. Such structural shapes or cross-sectional sizes are sought for which lead to the minimum material consumption to support prescribed ultimate load.

1.3. Scope

In the present book we shall confine our attention solely to the limit analysis of plates. Several yield criteria will be employed in order to give a feeling to what extent the form of a yield condition influences methods of solution and characteristic features of a solution itself. Emphasis is put both on mathematical aspects of the plastic plate equations and on the solutions

for a broad class of plates obeying various yield criteria. Methods of limit analysis of plates are explained and approximate theories like the yield-line method are discussed on the background of a general theory. A collection of tables and design aids are given.

To make the presentation self contained the basic equations of perfect plasticity are briefly shown in Chapter 2. The plate equations are analyzed in Chapter 3. Chapter 4 concerns with circular plates under rotationally symmetric loading when ordinary differential equations govern the plastic behaviour. Analytical and numerical solutions are given. Bounding techniques that furnish estimates to the collapse load intensity are explained in Chapter 5, whereas in the next chapter orthotropic and nonhomogeneous plates are briefly considered. Chapter 8 is devoted to bending of plates of arbitrary shape. Special attention is given to plates obeying a square yield criterion in the plane of principal moments. A number of new complete solutions is presented allowing to assess the accuracy of results furnished by the yield line theory, which is presented in Chapter 7 and accompanied by a set of tables.

CHAPTER 2

PRINCIPLES OF LIMIT ANALYSIS

2.1. Basic assumptions

2.1.1. Mathematical model of plastic behaviour. Mechanical behaviour of rate insensitive elastic-plastic, non-hardening solids is idealized in the stress-strain diagram shown in Fig. 2.1a. Unconstrained plastic flow begins in uniaxial tension at the yield stress σ_0^+ and in uniaxial compression at σ_0^-.

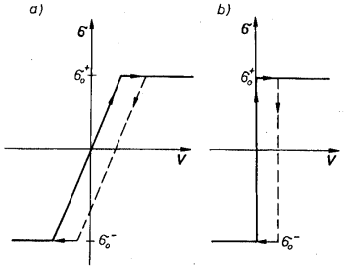

Fig. 2.1. (a) Elastic-perfectly plastic, (b) rigid-perfectly plastic models of materials

In problems regarding unconstrained plastic motion the elastic strains can usually be disregarded when compared with the prevailing plastic strains. The rigid-plastic model of material response is hence obtained, Fig. 2.1b. The constitutive equation of rigid-perfectly plastic solids involves the stress tensor $\boldsymbol{\sigma}$ and the strain rate tensor $\mathbf{V}$

$$\boldsymbol{\sigma} = \boldsymbol{\sigma}(\mathbf{V}). \tag{2.1}$$

Its general form is subjected to the condition that the stress components be homogeneous functions of order zero with respect to time, i.e. with respect to the strain rates as well. The homogeneity requirement: $\boldsymbol{\sigma}(\alpha\,\mathbf{V}) = \alpha^0\boldsymbol{\sigma}(\mathbf{V})$, α being a constant, results in the system of equations

$$\frac{\partial \sigma_{ij}}{\partial V_{rs}} V_{rs} = 0 \tag{2.2}$$

which expresses analytically the essential property of the rate insensitive plastic flow, namely that the state of stress at yield does not depend on how fast this state has been reached. From now on a repeated index denotes a sum according to the summation convention.

In view of the homogeneity requirement not all stress components are independent since they are expressible in terms of the ratios of strain rate components. Since $\sigma_{ij} = \sigma_{ji}$, six stress components σ_{ij} are expressible in terms of five ratios of strain rate components. On eliminating the parameters the yield criterion is obtained

$$F(\sigma_{ij}) = 0 \qquad \text{or} \qquad f(\sigma_{ij}) - c = 0, \tag{2.3}$$

where c is a material constant.

The yield criterion can be represented as a surface in the six-dimensional stress space. The yield locus (2.3) is the boundary of the elastic domain where $F(\sigma_{ij}) < 0$. The states $F(\sigma_{ij}) > 0$ are not admissible for a perfectly plastic solid. The surface (2.3) is convex.

2.1.2. Yield criteria. The yield criterion (2.3) for specific materials is specified on the grounds of experimental data. For metals two criteria are generally accepted, namely the Huber-Mises and the Tresca criteria. In both the influence of hydrostatic stress component on the onset of yielding is neglected.

The Huber-Mises yield criterion states that a material becomes plastic when the elastic distortion energy per unit volume reaches a critical value

$$F = 3\sigma_{ij}\sigma_{ij} - \sigma_{ii}\sigma_{jj} - 2\sigma_0^2 = 0. \tag{2.4}$$

In the state of plane stress the condition (2.4) represents an ellipsoid

$$\sigma_x^2 - \sigma_x\sigma_y + \sigma_y^2 + 3\tau_{xy}^2 = \sigma_0^2. \tag{2.5}$$

The Tresca yield criterion states that a material becomes plastic when the maximum shearing stress reaches a limiting value

$$\sup(|\sigma_1 - \sigma_2|, |\sigma_2 - \sigma_3|, |\sigma_3 - \sigma_1|) = \sigma_0. \tag{2.6}$$

In the case of plane stress, $\sigma_3 = 0$, the condition (2.6) takes the form of the following three equations

$$\begin{aligned} F_1 &= -(\sigma_x - \sigma_0)(\sigma_y - \sigma_0) + \sigma_{xy}^2 = 0, \\ F_2 &= -(\sigma_x + \sigma_0)(\sigma_y + \sigma_0) + \sigma_{xy}^2 = 0, \\ F_3 &= (\sigma_x - \sigma_y)^2 + 4\sigma_{xy}^2 - \sigma_0^2 = 0. \end{aligned} \tag{2.7}$$

The elastic region is therefore bounded by two cones $F_1 = 0$, $F_2 = 0$ and by an elliptic cylinder $F_3 = 0$.

The equations describing plastic behaviour of structures can be simplified by using certain approximate yield criteria such as the maximum reduced stress criterion

$$\sup|\sigma_1 - (\sigma_1 + \sigma_2 + \sigma_3)/3| = \frac{2}{3}\sigma_0, \qquad i = 1, 2, 3. \tag{2.8}$$

In the space of principal stresses it represents a regular hexagonal prism circumscribing the Tresca criterion and having common symmetry planes. In plane stress the criterion becomes

$$\sup(|\sigma_1 - \frac{1}{2}\sigma_2|, |\sigma_2 - \frac{1}{2}\sigma_1|, \frac{1}{2}|\sigma_1 + \sigma_2|) = \sigma_0. \tag{2.9}$$

In plate analysis a yield criterion of maximum normal stress is also employed. For the case of plane stress it reduces to the first two of Eqs.(2.7) and represents two intersecting cones.

Comparison of Huber-Mises, Tresca, maximum reduced stress and maximum normal stress criteria for plane stress in the plane of principal stresses is shown in Fig. 2.2.

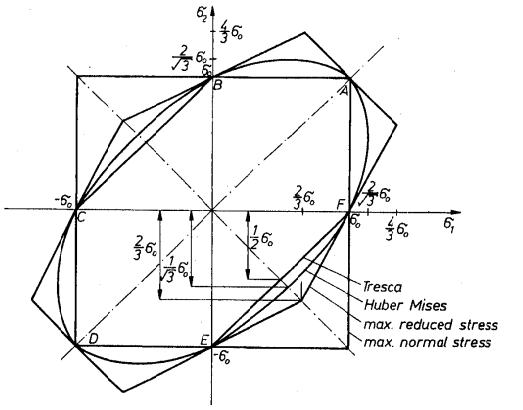

Fig. 2.2. Comparison of Huber-Mises, Tresca, maximum reduced stress and maximum normal stress yield criteria

2.1.3. Power of dissipation. The power of dissipation in plastic flow at a generic particle whose stress state is described by $\boldsymbol{\sigma}$ and the strain rate state by $\mathbf{V}$ is

$$d = \boldsymbol{\sigma} \cdot \mathbf{V}. \tag{2.10}$$

This power is assumed to be fully dissipated in the form of heat during plastic flow and is regarded positive.

The constitutive equation of plastic solid relates the stress tensor $\boldsymbol{\sigma}$ only to the tensor of the plastic strain rates $\mathbf{V}$, (2.1), and it is homogeneous of order zero; thus

a) the power of dissipation is a single valued function of the strain rate

$$d = d(\mathbf{V}), \tag{2.11}$$

b) the dissipation rate function $d(\mathbf{V})$ is homogeneous of the order one with respect to the strain rates

$$d(\alpha \mathbf{V}) = \alpha d(\mathbf{V}), \qquad \alpha > 0$$

or

$$\frac{\partial d}{\partial \mathbf{V}} \cdot \mathbf{V} = d. \tag{2.12}$$

The latter property expresses the inviscid nature of plastic flow.

2.1.4. Constitutive equation of limit analysis. The yield criterion predicts at what state of stress the plastic motion can take place. In order to answer the question what is the mechanism of motion at a particle stressed so that the yield criterion is satisfied it is necessary to know a flow rule, i.e. the constitutive relation governing plastic motion. Various theories of plasticity exist depending upon the form of the constitutive relation.

In limit analysis the associated flow rule is accepted in which the yield function (2.3) is taken as the plastic potential:

$$V_{ij} = \nu \frac{\partial F}{\partial \sigma_{ij}} = \nu \frac{\partial f}{\partial \sigma_{ij}}, \qquad \nu \geqslant 0. \tag{2.13}$$

This means that the strain rate vector $\mathbf{V}$ is directed along the outer normal to the surface $F = 0$, Fig. 2.3. Since the yield surface (2.3) is convex,

$$\frac{\partial f}{\partial \sigma_{ij}} \sigma_{ij} \geqslant 0, \tag{2.14}$$

and the power of dissipation (2.10) is nonnegative thus the scalar multiplier ν is nonnegative.

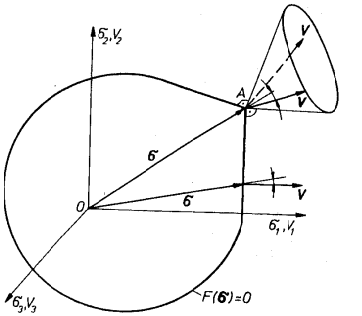

Fig. 2.3. Associated flow rule

Taking $f(\sigma_{ij})$ as a homogeneous function of order $n>0$ in stress it is found that

$$\nu = \frac{d}{nf} = \frac{d}{nc}. \tag{2.15}$$

When the yield surface has ridges and corners, as at A in Fig. 2.3, the gradient there is not uniquely defined. The plastic potential flow law at the singular points where k surfaces $F_k=0$ meet is then generalized to take the form

$$V_{ij} = \nu_k \frac{\partial F_k}{\partial \sigma_{ij}} \tag{2.16}$$

and all ν_k are nonnegative. The strain rate vector remains within the fan defined by the normals to the surfaces meeting at singular points. Such a situation takes place for the Tresca yield condition (2.7) on the ridges of the corresponding yield surface.

2.1.5. Description of limit analysis problem. In the theory of limit analysis an incipient motion of perfectly plastic structures and continua is studied. Its objective is to solve boundary value problems for equations governing plastic motion under a system of loads increasing quasistatically, starting from zero. The term quasistatic means that the loading process is so slow that all dynamic effects can be disregarded.

The classical presentation of the limit analysis theory concerns a system of loads increasing in proportion to a single parameter μ and is described as follows:

$$\mathbf{T}(\mathbf{x},t) = \mu(t)\, \mathbf{P}(\mathbf{x}), \tag{2.17}$$

where $\mathbf{P}(\mathbf{x})$ denotes a reference load distribution. For definiteness and clarity the analysis will be restricted to this type of loading only.

The limit analysis theory for a case of a finite number of loading parameters, i.e. $\mathbf{T}(\mathbf{x},t)=\mu_l(t)\,\mathbf{P}_l(\mathbf{x})$ can be generalized immediately, [29], [43].

Dealing with incipient plastic flow we assume that strains $\boldsymbol{\varepsilon}$ remain very small. Hence, strains $\boldsymbol{\varepsilon}$ and displacements $\mathbf{u}$ obey the small strain tensor definition

$$\varepsilon_{ij}=\frac{1}{2}(u_{i,j}+u_{j,i}). \tag{2.18}$$

Displacements $\mathbf{u}$ and their velocities $\dot{\mathbf{u}}$ are proportional to each other; thus strain rates $\dot{\boldsymbol{\varepsilon}}$ are

$$\dot{\varepsilon}_{ij}=V_{ij}=\frac{1}{2}(\dot{u}_{i,j}+\dot{u}_{j,i}). \tag{2.19}$$

As a rule for most metallic materials no plastic volume changes are admitted and therefore the strain rates are subjected to the incompressibility requirement,

$$V_{ii}=0. \tag{2.20}$$

The complete solution of limit analysis problem consists in specifying:

– the ultimate load (collapse load) i.e. the value μ_u of the load multiplier at which plastic motion can commence,

– the stress field $\boldsymbol{\sigma}(\mathbf{x})$ associated with the load multiplier μ_u and satisfying:

a) the equilibrium equations

$$\sigma_{ij,i}=0, \tag{2.21}$$

b) the prescribed stress boundary conditions,

c) a yield condition $F(\boldsymbol{\sigma})\leqslant 0$.

– a mechanism of plastic motion, i.e. a velocity field $\dot{\mathbf{u}}(\mathbf{x})$ of incipient plastic motion under the load $\mu_u\mathbf{P}$, satisfying the prescribed kinematical boundary conditions,

– the flow law specifying the mechanism of plastic motion at a material particle stressed to the yielding. The associated flow law (2.13) is employed. The requirement regarding nonnegativeness of the flow multiplier v must be verified. If $v=0$ the region stressed to the collapse behaves in the overall motion as a rigid body. The plastic motion ceases whenever $F(\boldsymbol{\sigma})<0$.

2.1.6. Uniqueness of solution. The solution of a limit analysis problem specifies the stress field and the collapse mechanism at the ultimate load.

The problem of uniqueness in the theory of limit analysis consists in answering the question whether a stress field $\sigma_{ij}(\mathbf{x})$ and a strain rate field

$V_{ij}(\mathbf{x})$ associated with an incipient plastic motion of a structure subjected to the collapse load $\mathbf{T}=\mu_u\mathbf{P}(\mathbf{x})$, are unique.

Consider an isotropic rigid-plastic body of volume V and surface S, subjected to surface traction $\mathbf{T}=\mu_u\mathbf{P}$ over area S_P and to prescribed velocities $\dot{\mathbf{u}}$ over area S_u, $S=S_P\cup S_u$. Moreover, since the surface does not vary in time, thus $\dot{S}_P=\dot{S}_u=0$.

The principle of virtual power states that

$$\int_S \mathbf{T}\cdot\dot{\mathbf{u}}\,dS=\int_V \boldsymbol{\sigma}\cdot\mathbf{V}\,dV, \tag{2.22}$$

where $\boldsymbol{\sigma}$ denotes any stress field in equilibrium with the tractions $\mathbf{T}$ and strain rate field $\mathbf{V}$ is derived from a velocity field $\dot{\mathbf{u}}$ satisfying the prescribed kinematical restraints. No connection whatsoever between $\boldsymbol{\sigma}$ and $\mathbf{V}$ is required.

Let us suppose for the moment that there exist two different complete solutions, in the sense of Sec. 2.1.5, satisfying the same boundary conditions and corresponding to the same ultimate load intensity μ_u, namely

$$\boldsymbol{\sigma}',\ \dot{\mathbf{u}}',\ \mathbf{V}' \quad \text{and} \quad \boldsymbol{\sigma}'',\ \dot{\mathbf{u}}'',\ \mathbf{V}'' \quad \text{for} \quad \mu_u\mathbf{P}. \tag{2.23}$$

To answer the question of uniqueness of the stress field we apply the principle (2.22) consecutively to the fields specified in (2.23) and obtain

$$\int_S \mathbf{T}\cdot\dot{\mathbf{u}}'\,dS=\int_V \boldsymbol{\sigma}'\cdot\mathbf{V}'\,dV=\int_V \boldsymbol{\sigma}''\cdot\mathbf{V}'\,dV \;\Rightarrow\; \int_V (\boldsymbol{\sigma}'-\boldsymbol{\sigma}'')\cdot\mathbf{V}'\,dV=0,$$
$$\int_S \mathbf{T}\cdot\dot{\mathbf{u}}''\,dS=\int_V \boldsymbol{\sigma}'\cdot\mathbf{V}''\,dV=\int_V \boldsymbol{\sigma}''\cdot\mathbf{V}''\,dV \;\Rightarrow\; \int_V (\boldsymbol{\sigma}'-\boldsymbol{\sigma}'')\cdot\mathbf{V}''\,dV=0. \tag{2.24}$$

In view of the convexity of the yield surface, both integrands are nonnegative and therefore they vanish identically to satisfy the integral conditions (2.24) and so the difference of the integrands must vanish too.

$$(\boldsymbol{\sigma}'-\boldsymbol{\sigma}'')\cdot(\mathbf{V}'-\mathbf{V}'')=0. \tag{2.25}$$

The uniqueness theorem for rigid plastic solids states that for strictly convex yield loci the stress fields of two complete solutions are identical except, possibly, in the common rigid regions. In fact, due to the required vanishing of the integrand in (2.25),

$$\boldsymbol{\sigma}'=\boldsymbol{\sigma}'' \quad \text{if} \quad \mathbf{V}'\neq\mathbf{0},\ \ \mathbf{V}''\neq\mathbf{0}$$
or
$$\boldsymbol{\sigma}'\neq\boldsymbol{\sigma}'' \quad \text{if} \quad \mathbf{V}'=\mathbf{0},\ \ \mathbf{V}''=\mathbf{0} \tag{2.26}$$

For yield loci containing planes the integrand of (2.25) vanishes identically when the stress fields belong to the same plane. Uniqueness can be established by employing a different procedure, [40].

Therefore in a rigid plastic structure which is at collapse under the specified surface loads and for the prescribed surface velocities the stress field is unique in the deforming region. The collapse mode, although not uniquely defined, must be compatible with the stress field, i.e. be associated with the stress profile on the yield surface.

2.1.7. Discontinuities. A perfectly plastic material admits some discontinuities in the field variables. In a real material it is rapid changes in the quantity in question across a narrow region that are observed rather than sudden jumps. Discontinuities admitted by the mathematical model appear to be very useful in developing approximate solutions, [58]. Across a discontinuity line Γ a jump in a quantity G is denoted as

$$[G] = G^+ - G^-. \tag{2.27}$$

By considering a narrow zone across which the examined quantity suffers a rapid change a pertinent information is obtained.

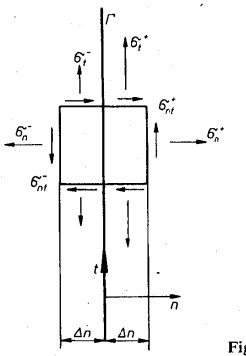

Fig. 2.4. Stress discontinuity line Γ

Let us consider the situation shown in Fig. 2.4 and examine the stress discontinuities admitted by the equilibrium equations (2.21) in plane stress. Since $\partial\sigma_t/\partial n$ does not enter the equilibrium requirements suitable integration yields the jump in the normal stress σ_t acting on the section perpendicular to a line Γ,

$$\lim_{\Delta n \Rightarrow 0} \int_{-\Delta n}^{\Delta n} \frac{\partial \sigma_t}{\partial n} dn = [\sigma_t], \tag{2.28}$$

while the remaining stress components are continuous across Γ. The magnitude of the jump (2.28) depends on the type of yield criterion.

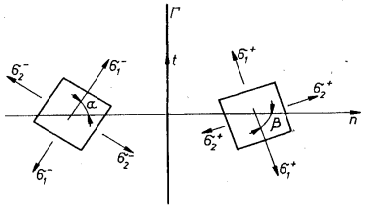

Fig. 2.5. Change in the principal stress directions across stress discontinuity line

The continuity of σ_n and σ_{nt} leads to an appropriate relation between the principal stresses on both sides of the discontinuity line, Fig. 2.5,

$$\begin{aligned} \sigma_1^- \cos^2\alpha + \sigma_2^- \sin^2\alpha &= \sigma_1^+ \cos^2\beta + \sigma_2^+ \sin^2\beta \\ (\sigma_1^- - \sigma_2^-)\sin 2\alpha &= (\sigma_1^+ - \sigma_2^+)\sin 2\beta. \end{aligned} \tag{2.29}$$

The discontinuities admitted by the kinematical relation (2.19) for plane situation, are

$$\lim_{\Delta n \Rightarrow 0} \int_{-\Delta n}^{\Delta n} \frac{\partial u_t}{\partial t} dn = 0, \qquad \lim_{\Delta n \Rightarrow 0} \int_{-\Delta n}^{\Delta n} \left(\frac{\partial \dot{u}_n}{\partial t} + \frac{\partial \dot{u}_t}{\partial n} \right) dn = [\dot{u}_t]$$

and (2.30)

$$\lim_{\Delta n \Rightarrow 0} \int_{-\Delta n}^{\Delta n} \frac{\partial u_n}{\partial n} dn = [\dot{u}_n].$$

On the discontinuity lines of velocity fields (2.30) the following amount of the energy is dissipated:

$$d_\Gamma = \lim_{\Delta n \Rightarrow 0} \int_{-\Delta n}^{\Delta n} \sigma_{ij} V_{ij} \, dn = \sigma_{nt} [\dot{u}_t] + \sigma_n [\dot{u}_n]. \tag{2.31}$$

The above integral components of the deformation localized in yielding bands can be represented in generalized variables of the plate theory. Thus, curvatures and deformations of the reference plane will be represented by discontinuities in slopes and in-plane displacements, respectively, [28], [29]. Because of the continuity condition for deflections, a slope tangential to the band must be continuous.

On the other hand, in the absence of membrane forces (as is the case within this book) displacement jumps in the reference plane are irrelevant. Therefore, the only meaningful generalized variable is the curvature normal to the band of localized deformation, Fig. 2.6, which, when integrated across the band width, gives a discontinuity in slope:

$$\lim_{\Delta n \to 0} \int_{-\Delta n}^{\Delta n} \frac{\partial^2 \dot{W}}{\partial n^2} dn = \left[\frac{\partial \dot{W}}{\partial n}\right] \equiv \Phi_n . \tag{2.32}$$

The band of the localized deformation (yield line) represented as a discontinuity line can be considered as a simple plastic hinge.

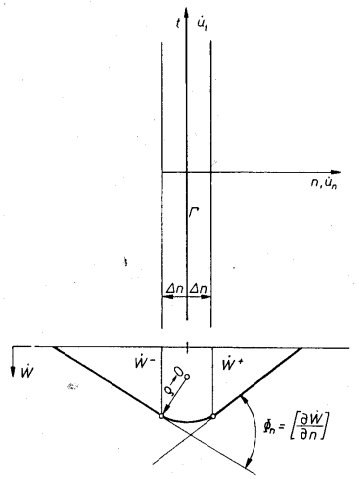

Fig. 2.6. Plastic hinge

For completeness let us write down the expression for the dissipation per unit length of the hinge line defined in (2.32),

$$d_\Gamma = M_n \cdot \Phi_n , \tag{2.33}$$

where M_n is the normal moment across the slope discontinuity line.

Whenever kinematical discontinuity lines appear the expression for internal dissipation contains line integrals

$$D_{\text{int}} = \int_V \sigma_{ij} V_{ij} \, dV + \sum_l \int_\Gamma d_\Gamma \, dl, \tag{2.34}$$

where dl is a line element of Γ and summation is extended over all the discontinuity lines.

2.2. Generalized variables

In the mechanics of thin plates and shells the equations of equilibrium are expressed in terms of stress resultants, namely membrane forces N_{ij}, moments M_{ij} and shear forces S_i, $i,j=1,2$. For thin structures $(H/A \ll 1)$ the above magnitudes are defined as follows:

$$M_{ij} = \int_{-H}^{H} \sigma_{ij} z dz, \quad N_{ij} = \int_{-H}^{H} \sigma_{ij} \, dz, \quad S_i = \int_{-H}^{H} \sigma_{zi} \, dz, \tag{2.35}$$

where $2H$ is a thickness of the structure. These magnitudes are further referred to as the generalized stresses Q_k, $k=1,..,n$.

Since internal actions enter the equilibrium and boundary conditions in the form of generalized stresses it is necessary to express also the yield criteria in terms of generalized stresses.

The yield condition expressed in terms of generalized stresses is called an interaction condition,

$$F(\boldsymbol{\sigma}) = 0 \quad \Rightarrow \quad \mathscr{F}(\mathbf{M}, \mathbf{N}, \mathbf{S}) \equiv \mathscr{F}(\mathbf{Q}) = 0$$

or (2.36)

$$f(\boldsymbol{\sigma}) - c = 0 \quad \Rightarrow \quad f(\mathbf{Q}) - \mathbf{C} = 0$$

where $\mathbf{C}$ is a vector of structural constants. For the bending of plates such constants represent, for instance ultimate moments per unit length of cross section.

In Fig. 2.7a,b the stress distributions at collapse for a homogeneous and reinforced plates are shown; below the resulting ultimate moments are specified, respectively.

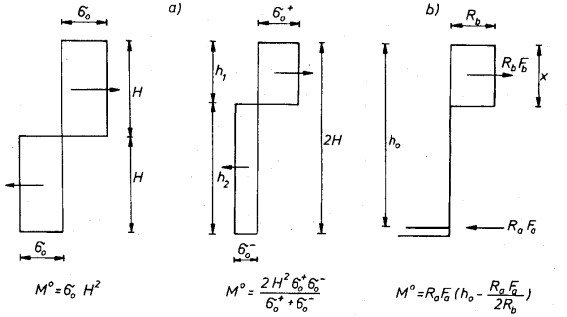

Fig. 2.7. Stress distributions at collapse for (a) homogeneous, (b) reinforced cross-sections

The interaction condition (2.36) is visualized in the n-dimensional space of generalized stresses in the form of a closed interaction surface.

Generalized strain rates $\dot{\mathbf{q}}$ are associated with the generalized stresses $\mathbf{Q}$ by the requirement that the dissipation remains invariant under the transformation of variables,

$$D = \int_V \boldsymbol{\sigma} \cdot \mathbf{V}\, dV = \int_A \mathbf{Q} \cdot \dot{\mathbf{q}}\, dA\,. \tag{2.37}$$

For example, since the power of dissipation for thin structures is

$$d = M_{ij}\dot{K}_{ij} + N_{ij}\dot{\lambda}_{ij} + S_i\dot{\gamma}, \tag{2.38}$$

where the rates of the curvature $\dot{K}_{ij}$, velocities of elongations $\dot{\lambda}_{ij}$ and rates of shear strain $\dot{\gamma}_i$ are generalized strain rates associated with generalized stresses M_{ij}, N_{ij}, and S_i.

The interaction function $\mathscr{F}(\mathbf{Q})$ constitutes a potential for the generalized strain rates. This means that the associated flow rule applies also in the case of generalized variables

$$\dot{\mathbf{q}} = \nu \frac{\partial \mathscr{F}}{\partial \mathbf{Q}}, \qquad \nu \geqslant 0\,. \tag{2.39}$$

In general, the interaction surface (2.36) has singularities where the normal to the surface $\mathscr{F}=0$ is not uniquely specified. Then

$$\dot{\mathbf{q}} = \nu_i \frac{\partial \mathscr{F}_i}{\partial \mathbf{Q}}, \qquad \nu_i \geqslant 0\,. \tag{2.40}$$

Derivation of the yield conditions in terms of generalized stresses is an essential part of the theory of plastic structures, [62], [74].

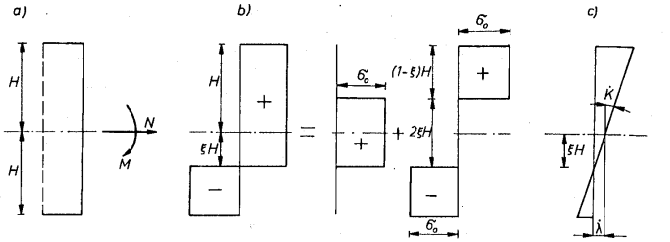

Fig. 2.8. Bending and stretching of beam: (a) generalized stresses, (b) stress distribution at collapse, (c) generalized strain rates

A simple example of combined bending and stretching of a beam will illustrate the transformation procedure. The beam is of rectangular cross-section $2H \times B$. The stress distribution at collapse is specified to within a parameter $\xi = Z/H$, Fig. 2.8b. The resulting bending moment and axial load are

$$M = \sigma_0 BH^2\,(1-\xi^2), \qquad N = 2\sigma_0 BH\xi, \tag{2.41}$$

where σ_0 denotes the yield stress of the material in uniaxial tension or compression; positive directions of the generalized stresses M and N are shown in Fig. 2.8a. The ultimate moment M^0 and axial load N^0 of the cross-section is readily calculated as:

$$M^0 = BH^2\sigma_0, \qquad N^0 = 2BH\sigma_0\,. \tag{2.42}$$

Elimination of ξ from (2.41) results in the expression

$$\mathscr{F} = \frac{M}{M^0} + \left(\frac{N}{N^0}\right)^2 - 1 = 0\,. \tag{2.43}$$

An analogous parabola corresponds to the negative bending moment. The interaction curve (2.43) as a result of the transformation of the yield criterion $F = \sigma \pm \sigma_0 = 0$ into $\mathscr{F}(M,N)=0$ is shown in Fig. 2.9.

In the considered example, under the condition that plane sections remain plane, the velocity distribution is

$$\dot{\varepsilon} = \dot{\lambda} + z\dot{K}, \tag{2.44}$$

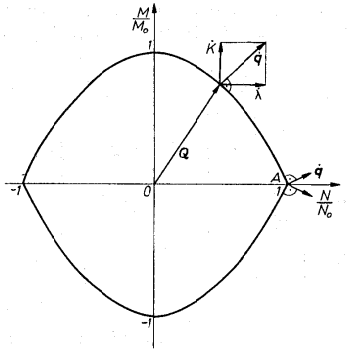

Fig. 2.9. Interaction curve for bending and stretching of beam with rectangular cross-section

where $\dot{\lambda}$ denotes the rate of axial elongation of the beam and $\dot{K}$ is the rate of curvature, Fig. 2.8c. Inserting (2.44) into (2.37), we obtain the power of dissipation per unit length of beam:

$$d = B\int_{-H}^{H} \sigma\cdot\dot{\varepsilon}\,dz = N\cdot\dot{\lambda} + M\cdot\dot{K}. \tag{2.45}$$

Hence, the generalized strains for the considered problem are $\dot{\lambda}$ and $\dot{K}$. For the mechanism shown in Fig. 2.8c we find

$$\frac{\dot{\lambda}}{\dot{K}} = \xi \mathrm{H} = \frac{2M^0}{(N^0)^2}N. \tag{2.46}$$

On applying (2.39) to (2.43) the associated flow law takes the form

$$\dot{\lambda} = \nu\frac{2N}{(N^0)^2}, \qquad \dot{K} = \nu\frac{1}{M^0}. \tag{2.47}$$

Elimination of ν from (2.47) leads to the second equation of (2.46).

2.3. Intersections and projections of interaction surface

When certain stress resultants are neglected or when additional kinematical restraints are imposed, $\mathscr{F}(\mathbf{Q})=0$ can be simplified in the sense that its respective projections or intersection are used, [69].

If Q_i, $i=k+1,..,n$, vanish, the interaction locus constitutes an intersection of the general interaction surface with the planes $Q_i=0$. The corresponding $\dot{q}_i$ do not necessarily vanish and are to be keept in the kinematical relations.

Such a situation occurs in the case of the beam described in the preceding section when $N=\pm N^0$, $M=0$, and the rate of curvature $\dot{K}$ does not have to disappear (point A in Fig. 2.9).

When $\dot{q}_i=0$, $i=r+1,..,m$, additional kinematical restraints are imposed. Therefore the corresponding Q_i become reactions. They can be eliminated from $\mathscr{F}(Q_i)=0$, $i=1,..,m$, since the above restraints give $(m\text{-}r)$ relations between the m stress resultants. In geometrical terms $\dot{q}_i=0$, $i=\mathrm{r}+1,..,m$ means that an orthogonal projection of $\mathscr{F}(\mathbf{Q})=0$ onto the subspace of r-dimensions is then used. The boundary of such a projection constitutes then the appropriate interaction locus in the r-dimensional space. Nevertheless the reactions Q_i, $i=r+1,..,m$ enter the equilibrium equations.

An example of such a situation is furnished by the thin plate theory. The Kirchhoff-Love hypothesis ($\dot{\gamma}_i \equiv 0$) means that the generalized strains corresponding to transversal forces S_i are absent and, therefore, the latter should not influence the interaction condition $\mathscr{F}(M_{ij}, N_{ij})=0$.

2.4. Admissible states

Set of generalized stresses Q_i and generalized strain rates $\dot{q}_i$ in a structure are known as fields of the generalized stresses and strain rates, respectively.

In the limit analysis of structures it is convenient to use a notion of a statically admissible stress field $\mathbf{Q}^0(\mathrm{x})$ and a kinematically admissible field of displacement velocities $\dot{\mathbf{u}}^*(\mathbf{x})$.

2.4.1. A statically admissible stress field $\mathbf{Q}^0$ satisfies:

a) the equilibrium requirements within the body

$$L_{ij}\,Q_j = \mu_s\,P_i, \tag{2.48}$$

where L is a differential operator,

b) the prescribed stress boundary conditions,

c) does not violate the interaction condition. The value of $\mathscr{F}(\mathbf{Q})$ computed for $\mathbf{Q}^0=\mathbf{Q}^0(\mathbf{x})$ gives a stress profile which remains within the interaction surface, i.e. $\mathscr{F}(\mathbf{Q})\leqslant 0$ throughout the body, Fig. 2.10, line OBC.

To evaluate μ_s we use the property that at every point of the structure a statically admissible generalized stress can be written as follows:

$$\mathbf{Q}^0(\mathbf{x}) = \mu_s\,\xi(\mathbf{x}). \tag{2.49}$$

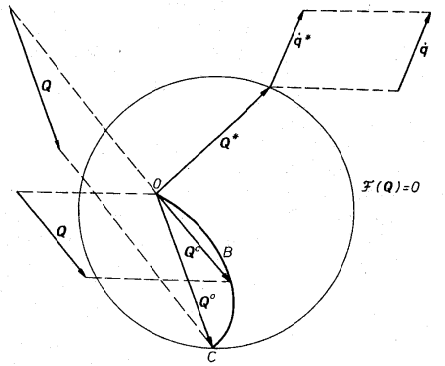

Fig. 2.10. Admissible states: statically admissible stress field $\mathbf{Q}^0$ and kinematically admissible strain field $\dot{\mathbf{q}}^*$ with associated stress field $\mathbf{Q}^*$

Let us assume that the interaction condition $f(\mathbf{Q})-\mathbf{C}=0$ is a homogeneous function of degree n in the generalized stresses. The requirement that at each section of the structure stresses remain within the interaction surface, e.i. $f(\mathbf{Q}^0)\leqslant\mathbf{C}$, yields the inequality $\mu_s^n\, g(\mathbf{x})\leqslant\mathbf{C}$, where $g(\mathbf{x})=f(\xi(\mathbf{x}))$. The statically admissible load multiplier is therefore defined as

$$\mu_s^n = \min \frac{\mathbf{C}}{g(\mathbf{x})}. \tag{2.50}$$

For a selected statically admissible stress field $\mathbf{Q}^0$ the relation (2.50) allows to calculate a multiplier specifying the load intensity at which the interaction surface is not violated. Practically speaking, μ_s is computed by requiring that the yield condition be satisfied at least at one point of the structure.

2.4.2. A kinematically admissible velocity field $\dot{\mathbf{u}}^*$ satisfies:

a) the prescribed velocity constraints on the surface of a structure as well as the required continuity conditions and kinematical constraints within the structure,

b) leads to a strain rate field $\dot{\mathbf{q}}^*=\dot{\mathbf{q}}^*(\dot{\mathbf{u}}^*)\not\equiv 0$ satisfying the continuity requirements of internal constraints imposed by the associated flow rule and chosen interaction condition,

c) the requirement that the rate of external work D_{ext} done by the actual loads on the assumed velocity field is positive,

$$D_{\text{ext}} = \mu_s \int_S \mathbf{P}\cdot\dot{\mathbf{u}}^*\, dS > 0. \tag{2.51}$$

Once a velocity field $\dot{\mathbf{u}}^*$ is chosen, the associated stress field $\mathbf{Q}^*$ is specified by the plastic potential flow law as shown in Fig. 2.10, since, to commence plastic motion, the yield condition must be satisfied. The stresses $\mathbf{Q}^*$ do not have to satisfy the differential equations of equilibrium (2.48). The rate of internal work D_{int} is fully specified by the velocity field $\dot{\mathbf{u}}^*$ since the strain rates are functions of them,

$$D_{\text{int}} = \int_V \mathbf{Q}^*\cdot\dot{\mathbf{q}}^*\, dV = \int_V d(\dot{\mathbf{q}}^*)\, dV. \tag{2.52}$$

Kinematically admissible velocity field $\dot{\mathbf{u}}^*$ is associated with the kinematically admissible load multiplier μ_k defined as

$$\mu_k = \int_V d(\dot{\mathbf{q}}^*)\, dV \Big/ \int_S \mathbf{P}\cdot\dot{\mathbf{u}}^*\, dS. \tag{2.53}$$

2.5. Bounding theorems

The solution of a limit analysis problem specifies the stress field and the collapse mechanism under the ultimate load. Complete solutions are usually difficult to obtain due either to nonlinearity of yield conditions or to a large number of domains governed by different sets of field equations for piece-wise continuous yield loci. The quantity of the greatest interest for the stress analysts is the ultimate load. This quantity can be bounded from below and from above with the help of two extremum principles of the limit analysis theory.

In the bounding theorems the notions of a statically admissible stress field $\mathbf{Q}^0$ and of a kinematically admissible velocity field $\dot{\mathbf{u}}^*$ are employed. With these fields are associated the statically admissible load multiplier μ_s and the kinematically admissible load multiplier μ_k, respectively.

For a given problem there virtually exists an infinite number of statically and kinematically admissible states. Each of them corresponds to a certain value of the load multiplier specifying the intensity of loading. Two fundamental theorems of perfect plasticity allow to arrange these values so as to bound the load intensity corresponding to the complete solution.

2.5.1. The lower bound theorem states that any statically admissible load multiplier μ_s is smaller than or equal to the ultimate load multiplier μ_u.

To prove the theorem the principle of virtual work and the property of convexity of the yield surface are used, [18], [56], [59]. Let $\mathbf{Q}$, $\dot{\mathbf{u}}$, $\dot{\mathbf{q}}$ and μ_u represent the complete solution of the boundary value problem for incipient plastic flow, whilst $\mathbf{Q}^0$ and μ_s correspond to a statically admissible field. Hence $(\mathbf{Q}-\mathbf{Q}^0)$ is in equilibrium and satisfies the stress boundary conditions whereas $\dot{\mathbf{u}}$ satisfies the kinematical constraints. Therefore the principle of virtual work applied to these fields takes the form

$$(\mu_u - \mu_s)\int_S \mathbf{P}\cdot\dot{\mathbf{u}}\,dS = \int_V (\mathbf{Q}-\mathbf{Q}^0)\cdot\dot{\mathbf{q}}\,dV. \tag{2.54}$$

The integral on the left-hand side is positive by virtue of (2.51) since $\dot{\mathbf{u}}$ is kinematically admissible. The second integral is nonnegative since its integrand is nonnegative in view of the convexity of the interaction surface and an associated flow rule, Fig. 2.11. Hence

$$\mu_u - \mu_s \geqslant 0 \tag{2.55}$$

as stated in the theorem.

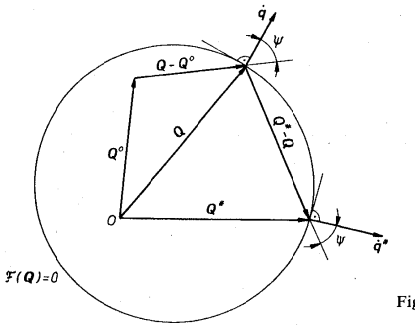

Fig. 2.11. Illustration of bounding theorems

2.5.2. The upper bound theorem states that any kinematically admissible load multiplier μ_k is larger than or equal to the ultimate load multiplier μ_u.

To prove this theorem consider two solutions as above: $\mathbf{Q}$, $\dot{\mathbf{u}}$, $\dot{\mathbf{q}}$ and μ_u represent the complete solution of the problem whilst $\dot{\mathbf{u}}^*$, $\dot{\mathbf{q}}^*$, $\mathbf{Q}^*$ and μ_k characterize the kinematical solution. The stress field $\mathbf{Q}^*$ and the kinematically admissible load multiplier μ_k are associated with $\dot{\mathbf{u}}^*$, $\dot{\mathbf{q}}^*$ via the flow law in which the plastic potential is accepted. Rewriting (2.53), we obtain

$$\mu_k\int_S \mathbf{P}\cdot\dot{\mathbf{u}}^*\,dS = \int_V \mathbf{Q}^*\cdot\dot{\mathbf{q}}^*\,dV. \tag{2.56}$$

For the stress field $\mathbf{Q}$, load $\mu_u\mathbf{P}$ and kinematically admissible velocity fields $\dot{\mathbf{u}}^*$, $\dot{\mathbf{q}}^*$ the virtual power principle holds true,

$$\mu_u\int_S \mathbf{P}\cdot\dot{\mathbf{u}}^*\,dS = \int_V \mathbf{Q}\cdot\dot{\mathbf{q}}^*\,dV. \tag{2.57}$$

Subtracting (2.57) from (2.56) we get

$$(\mu_k - \mu_u)\int_S \mathbf{P}\cdot\dot{\mathbf{u}}^*\,dS = \int_V (\mathbf{Q}^* - \mathbf{Q})\cdot\dot{\mathbf{q}}^*\,dV. \tag{2.58}$$

The integrand on the left-hand side is positive by virtue of (2.51). The integrand on the right-hand side is nonnegative due to the convexity of the interaction surface, Fig. 2.11. Hence

$$\mu_k - \mu_u \geqslant 0 \tag{2.59}$$

The two fundamental theorems can thus be combined to bound the collapse load multiplier,

$$\mu_s \leqslant \mu_u \leqslant \mu_k. \tag{2.60}$$

2.5.3. Important corollaries of the theorems

a) The collapse load multiplier $\mu_u(\mathscr{F}^*)$ furnished by the exact solution obtained for $\mathscr{F}^*=0$ circumscribing the actual interaction locus $\mathscr{F}=0$ is an upper bound on the collapse load multiplier $\mu_u(\mathscr{F})$ for the original locus $\mathscr{F}=0$.

b) The collapse load multiplier $\mu_u(\mathscr{F}^0)$ furnished by the exact solution obtained for $\mathscr{F}^0=0$ inscribed in the actual interaction surface $\mathscr{F}=0$ is a lower bound on the collapse load multiplier $\mu_u(\mathscr{F})$ for the original locus $\mathscr{F}=0$.

This can be summarized as follows:

$$\mu_u(\mathscr{F}^0) \leqslant \mu_u(\mathscr{F}) \leqslant \mu_u(\mathscr{F}^*). \tag{2.61}$$

The bounding theorems also hold true if certain stress and strain rate discontinuities are admitted.

CHAPTER 3

PLATE EQUATIONS

3.1 Basic relations

A plate element in the Cartesian coordinate system is shown in Fig. 3.1, in which the adopted sign convention can also be seen. We shall consider bending of transversely loaded thin plates under the assumption that straight normals remain straight and that changes in geometry in plastic flexure are negligible.

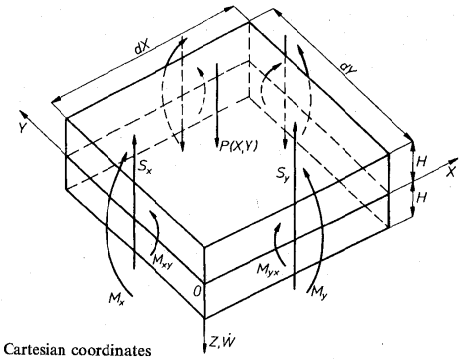

Fig. 3.1. Plate element in Cartesian coordinates

It follows from these assumptions that the deformation of the plate is entirely defined by the displacement $W(X,Y)$ normal to the middle surface.

The displacement rates in the directions of the coordinate axes are

$$\dot{U}_x = -Z\frac{\partial \dot{W}}{\partial X}, \qquad \dot{U}_y = -Z\frac{\partial \dot{W}}{\partial Y}, \qquad \dot{U}_z = \dot{W}(X,Y). \tag{3.1}$$

Therefore the strain rate tensor is

$$V_{ij} = -Z\dot{W}_{ij}, \qquad i,j = X, Y, Z. \tag{3.2}$$

The total power of dissipation (2.10) per unit area across the thickness of the plate is given by

$$d = \int_{-H}^{H} \sigma_{ij} V_{ij}\, dZ =$$

$$= -\frac{\partial^2 \dot{W}}{\partial X^2}\int_{-H}^{H} \sigma_x Z dZ + \left(-\frac{\partial^2 \dot{W}}{\partial Y^2}\right)\int_{-H}^{H} \sigma_y Z dZ + \left(-2\frac{\partial^2 \dot{W}}{\partial X \partial Y}\right)\int_{-H}^{H} \tau_{xy} Z dZ \equiv$$

$$\equiv M_x \dot{K}_x + M_y \dot{K}_x + M_{xy}\dot{K}_{xy}, \tag{3.3}$$

where $2H$ is the plate thickness, Fig. 3.1. Moments per unit length are defined by

$$M_{ij} = \int_{-H}^{H} \sigma_{ij} Z dZ, \qquad i,j = X, Y \tag{3.4}$$

and the curvature rates of the middle surface are

$$\dot{K}_x = -\frac{\partial^2 \dot{W}}{\partial X^2}, \qquad \dot{K}_y = -\frac{\partial^2 \dot{W}}{\partial Y^2}, \qquad \dot{K}_{xy} = -\frac{\partial^2 \dot{W}}{\partial X \partial Y}. \tag{3.5}$$

For the bending of thin plate the generalized variables are the moments and the curvature rates defined by Eqs.(3.4) and (3.5).

The stress state in the plate under bending is described by the moments M_{ij} and shear forces S_i. All the relevant equations will be written down in terms of the dimensionless variables defined as follows:

$$x = \frac{X}{L}, \quad y = \frac{Y}{L}, z = \frac{Z}{L}, \quad \dot{w} = \frac{H\dot{W}}{L^2}, \quad \dot{\kappa}_x = H\dot{K}_x, \quad \dot{\kappa}_y = H\dot{K}_y, \quad \dot{\kappa}_{xy} = H\dot{K}_{xy},$$

$$m_x = \frac{M_x}{M^0}, \quad m_y = \frac{M_y}{M^0}, \quad m_{xy} = \frac{M_{xy}}{M^0}, \quad s_x = \frac{S_x L}{M^0}, \quad s_y = \frac{S_y L}{M^0},$$

$$p = \frac{PL^2}{M^0}, \quad \bar{p} = \frac{\bar{P}L}{M^0}, \quad q = \frac{Q}{M^0} \tag{3.6}$$

where $P(X,Y)$, $\bar{P}(X,Y)$ denote the distributed pressure and the line load, respectively, and Q stands for the point loading. L denotes a reference length and M^0 is the unit ultimate moment

$$M^0 = 2\int_0^H \sigma_0 Z dZ = \sigma_0 H^2. \tag{3.7}$$

In terms of variables (3.6) the power of dissipation per unit area of the plate becomes

$$d = \frac{M^0}{H}(m_x \dot{\kappa}_x + m_y \dot{\kappa}_y + m_{xy} \dot{\kappa}_{xy}). \tag{3.8}$$

The system of equations governing plastic flexure of plates consists of the equilibrium equations, the curvature-deflection rate relations (3.5) and the plastic potential flow law associated with an interaction condition.

The equilibrium equations are

$$\frac{\partial m_x}{\partial x} + \frac{\partial m_{xy}}{\partial y} = s_x, \qquad \frac{\partial m_{xy}}{\partial x} + \frac{\partial m_y}{\partial y} = s_y, \tag{3.9}$$

$$\frac{\partial s_x}{\partial x} + \frac{\partial s_y}{\partial y} = -p. \tag{3.10}$$

At incipient plastic motion the moments satisfy the interaction condition

$$\mathscr{F}(m_x, m_y, m_{xy}) = f(m_x, m_y, m_{xy}) - 1 = 0. \tag{3.11}$$

The influence of transverse shear on yielding is here neglected. The stresses and the deformation rates are related by a flow rule. The associated flow law states that in the considered case the curvature rates (3.5) are related to the interaction equation (3.11) through the normality rule.

$$(\dot{\kappa}_x, \dot{\kappa}_y, \dot{\kappa}_{xy}) = \nu\left(\frac{\partial \mathscr{F}}{\partial m_x}, \frac{\partial \mathscr{F}}{\partial m_y}, \frac{\partial \mathscr{F}}{\partial m_{xy}}\right), \qquad \nu \geqslant 0. \tag{3.12}$$

A system of ten equations (3.5) and (3.9) through (3.12) is obtained in ten unknowns, namely three moments, two shear forces, the deflection rate, three curvatures and the flow multiplier ν. In plastically deforming regions where $\nu > 0$ they reduce to the following set of four equations, consisting of (3.11) and

$$\frac{\partial^2 m_x}{\partial x^2} + 2\frac{\partial^2 m_{xy}}{\partial x \partial y} + \frac{\partial^2 m_y}{\partial y^2} + p = 0, \tag{3.13}$$

$$\frac{\dfrac{\partial^2 \dot{w}}{\partial x^2}}{\dfrac{\partial \mathscr{F}}{\partial m_x}} = 2\frac{\dfrac{\partial^2 \dot{w}}{\partial x \partial y}}{\dfrac{\partial \mathscr{F}}{\partial m_{xy}}} = \frac{\dfrac{\partial^2 \dot{w}}{\partial y^2}}{\dfrac{\partial \mathscr{F}}{\partial m_y}}. \tag{3.14}$$

After this system is solved it remains to check whether $\nu > 0$ in the plastic zones.

3.2. Interaction surface for isotropic plates

For thin plate in bending, in which the membrane forces $\mathbf{N} = 0$ and the influence of shear forces on yielding can be neglected, the strain rate tensor components, according to the Kirchhoff-Love assumption (3.2), are in proportion to the distance of a considered layer from the middle surface. Thus the rate of curvature vector has the same direction for each layer of the cross-section. Hence, when a yield condition is symmetric with respect to the centre of the coordinate system, the stress state of the cross-section is independent of z-coordinate. Bending and ultimate moments according to (3.4) and (3.7) are as follows:

$$M_{ij} = \int_{-H}^{H} \sigma_{ij}(X,Y)\, Z dZ = \sigma_{ij}(X,Y) H^2, \quad M^0 = \sigma_0 H^2, \quad i,j = X,Y \tag{3.15}$$

and in the dimensionless variables (3.6) one obtains

$$m_{ij} = \frac{M_{ij}}{M^0} = \frac{\sigma_{ij}}{\sigma_0}, \tag{3.16}$$

which means that for the relevant case the interaction surfaces are of identical form as the yield condition in plane stress,

$$f\left(\frac{\sigma_{ij}}{\sigma_0}\right) \equiv f(m_{ij}) = 1. \tag{3.17}$$

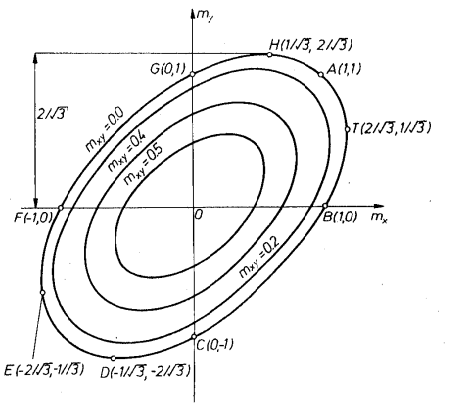

Fig. 3.2. Interaction surface for Huber-Mises plates

The Huber-Mises interaction condition for plates has therefore the same form as the Huber-Mises yield criterion in plane stress, (2.5)

$$\mathscr{f} = m_x^2 + m_y^2 - m_x m_y + 3m_{xy}^2 = 1. \tag{3.18}$$

The ellipsoid (3.18) is shown in Fig. 3.2 by a set of level curves.

The plastic potential flow law results in the following dimensionless curvature rates:

$$\begin{aligned} \dot{\kappa}_x &= \nu(2m_x - m_y), \\ \dot{\kappa}_y &= \nu(2m_y - m_x), \\ \dot{\kappa}_{xy} &= 6\nu m_{xy}, \quad \nu \geq 0. \end{aligned} \tag{3.19}$$

The Tresca interaction condition for plates has the following dimensionless form:

$$\mathscr{f} = \sup(|m_1|, |m_2|, |m_1 - m_2|) = 1. \tag{3.20}$$

The condition (3.20) when transformed into the space of m_x, m_y, m_{xy} consists of two elliptic cones and an elliptic cylinder. The surface is visualized in Fig. 3.3. Singular zones for the flow law can be noticed.

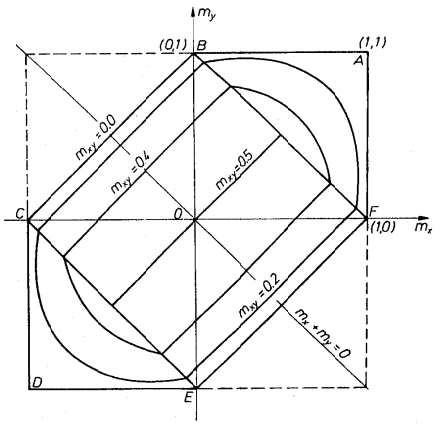

Fig. 3.3. Interaction surface for Tresca plates

The maximum principal moment interaction condition has the form

$$\begin{aligned} \mathscr{F}_1 &= m_x + m_y - m_x m_y + m_{xy}^2 - 1 = 0, \\ \mathscr{F}_2 &= -m_x - m_x - m_x m_y + m_{xy}^2 - 1 = 0. \end{aligned} \tag{3.21}$$

The interaction locus consists therefore of two coaxial elliptic cones intersecting on the plane $m_x + m_y = 0$. The cones defined by (3.21) are the same as in the case of the Tresca condition, dashed lines in Fig. 3.3. The only difference is that now they define the entire interaction surface.

For reinforced concrete plates the interaction condition depends on the amount and arrangement of reinforcement. In the case of isotropic reinforcement of different intensity at the top and bottom surface of the slab the interaction condition has the form

$$\begin{aligned} \mathscr{F}_1 &= m_x + m_y - m_x m_y + m_{xy}^2 - 1 = 0, \\ \mathscr{F}_2 &= -\Lambda' m_x - \Lambda' m_y - m_x m_y + m_{xy}^2 - (\Lambda')^2 = 0, \end{aligned} \tag{3.22}$$

where $\Lambda' = \dfrac{M_x^{0\,\text{top}}}{M_x^{0\,\text{bottom}}} = \dfrac{M_y^{0\,\text{top}}}{M_y^{0\,\text{bottom}}}$ is the top steel coefficient.

This surface is shown in Fig. 3.4. The rectangle $ABCD$ at $m_{xy} = 0$ represents the Johansen condition.

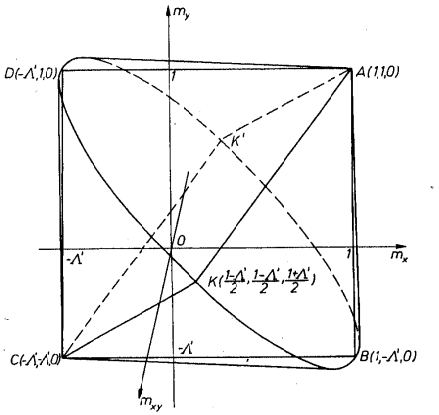

Fig. 3.4. Interaction surface for reinforced slabs

The maximum reduced stress yield condition (2.9) for plates takes the following form:

$$\sup\left(|m_1 - \frac{1}{2}m_2|,\ |m_2 - \frac{1}{2}m_1|,\ \frac{1}{2}|m_1 + m_2|\right) - 1 = 0. \quad (3.23)$$

It represents two truncated cones in the space of bending and twisting moments. The advantages of such an interaction surface for bounding procedure in the limit analysis of plates was pointed out in [74].

3.3. Analysis of plate equations

The equations of plastic bending involve, in the case of regular interaction loci, one algebraic equation (3.11). By a suitable choice of variables this equation can be made identically satisfied and the obtained system of partial differential equations can eventually be identified as to its type, [20], [73], [78]. Denote

$$2\omega = m_1 + m_2, \qquad 2\psi = m_2 - m_1, \quad (3.24)$$

where m_1, m_2 are the principal moments. The interaction condition can therefore be written in the form

$$\mathscr{F}(m_{ij}) = \psi - \varphi(\omega) \quad (3.25)$$

representing a closed convex curve in the plane of invariants (3.24).

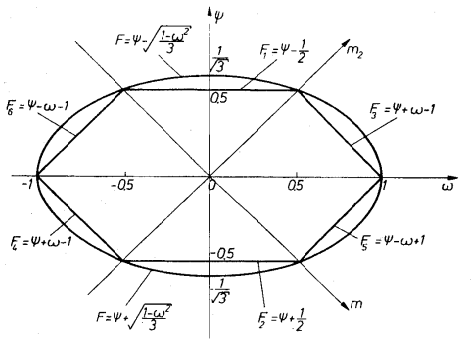

Fig. 3.5. Huber-Mises and Tresca interaction curves in the plane of invariants ω, ψ

The Huber-Mises and the Tresca interaction conditions in the new coordinates ω and ψ take the following forms:

Huber-Mises

$$\mathscr{F} = \psi \pm \sqrt{\frac{1-\omega^2}{3}}, \quad (3.26)$$

Tresca

$$\mathscr{F}_{1,2} = \psi \mp \frac{1}{2}, \quad \mathscr{F}_{3,4} = \psi + \omega \mp 1, \quad \mathscr{F}_{5,6} = \psi - \omega \pm 1, \quad (3.27)$$

They are visualized in Fig. 3.5.

Referring the stress state to the coordinate system rotated with respect to the principal lines so that the x-axis makes an angle θ with the positive direction of the second trajectory, Fig. 3.6, the stress state can be defined in terms of ω, ψ and θ, namely

$$m_x = \omega + \psi\cos 2\theta, \quad m_y = \omega - \psi\cos 2\theta, \quad m_{xy} = \psi\sin 2\theta. \quad (3.28)$$

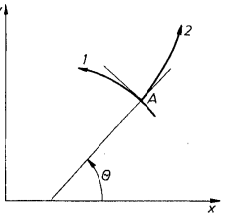

Fig. 3.6. Principal bending moment and curvature trajectories

The following set of quasi-linear partial differential equations is obtained combining the equilibrium equations (3.9-3.10), (3.28) and the interaction condition (3.25)

$$(1 + \varphi'\cos 2\theta)\,\omega_{,x} - 2\varphi\sin 2\theta\,\theta_{,x} + \varphi'\sin 2\theta\,\omega_{,y} + 2\varphi\cos 2\theta\,\theta_{,y} - \phi_{,y} = p_x,$$
$$\varphi'\sin 2\theta\,\omega_{,x} + 2\varphi\cos 2\theta\,\theta_{,x} + (1 - \varphi'\cos 2\theta) + 2\varphi\sin 2\theta\,\theta_{,y} + \phi_{,x} = p_y, \quad (3.29)$$

whereas the relations concerning kinematics (3.5), (3.27), (3.28) and the flow law result in

$$2\dot{w}_{,xx} = \nu(\varphi' - \cos 2\theta), \quad 2\dot{w}_{,yy} = \nu(\varphi' + \cos 2\theta),$$
$$2\dot{w}_{,xy} = -\nu\sin 2\theta. \quad (3.30)$$

in the above relations

$$\varphi' = \frac{\partial \varphi}{\partial \omega}, \quad p_x = -\frac{1}{2}\int p dx, \quad p_y = -\frac{1}{2}\int p dy \tag{3.31}$$

and ϕ is a shear potential chosen so as to satisfy identically the vertical equilibrium condition (3.10),

$$s_x = \phi_{,y} + p_x, \quad s_y = -\phi_{,x} + p_y. \tag{3.32}$$

Equations (3.29) and (3.30) involve five unknowns, namely ϕ, θ, $\dot{w}$, ω and v. A prerequisite for the solution of a boundary value problem as a system of quasi-linear partial differential equations is the determination of the type of the system. This is done here by referring the system of equations to the principal lines of moments and curvatures, thus putting $\theta = 0$.

By eliminating v from (3.30) we obtain the equation, specifying the displacement velocity $\dot{w}$ in terms of the interaction function, (3.25),

$$(1 + \varphi')\dot{w}_{,xx} + (1 - \varphi')\dot{w}_{,yy} = 0. \tag{3.33}$$

The type of equation is disclosed by examining the characteristic determinant of the system composed of (3.33) and of the differentials $d(\dot{w}_{,x})$, $d(\dot{w}_{,y})$, namely

$$\begin{vmatrix} dx & dy & 0 \\ 0 & dx & dy \\ 1+\varphi' & 0 & 1-\varphi' \end{vmatrix} = 0 \tag{3.34}$$

which results in the following equation for the characteristic directions

$$\left(\frac{dy}{dx}\right)^2 = \frac{\varphi' - 1}{\varphi' + 1}. \tag{3.35}$$

Depending upon the actual value of φ', Eq.(3.33) is either elliptic or hyperbolic or parabolic, the following variation of the interaction condition with the mean moment ω. If the right-hand side of (3.35) is negative no real characteristic direction exists and the set is elliptic. When the right-hand side is zero the equation is parabolic, when it is positive the set of equations is hyperbolic.

It can be further observed that the discriminant of the second fundamental form of the deflection velocity is

$$\dot{w}_{,xx}\dot{w}_{,yy} - (\dot{w}_{,xy})^2 = \frac{v^2}{4}(\varphi'^2 - 1). \tag{3.36}$$

Hence the deflection velocity can be either of positive or negative or zero Gaussian curvature. The deflected shape depends on the interaction condition.

We shall return to the system of equations consisting of (3.29) and (3.30). Since the deflected surface has been discussed above we eliminate $\dot{w}$ from (3.30) on computing higher order derivatives. The relations are obtained which, combined with (3.29), make a complete set of equations for ω, θ, ψ and $\Delta = \ln v$

$$\begin{aligned} &\varphi''\omega_{,x} - 2\sin 2\theta\ \theta_{,x} + (\varphi' + \cos 2\theta)\Delta_{,x} + 2\cos 2\theta_{,y} + \sin 2\theta\ \Delta_{,y} = 0, \\ &\varphi''\omega_{,y} + 2\cos 2\theta\ \theta_{,x} + \sin 2\theta\ \Delta_{,x} + 2\sin 2\theta\ \theta_{,y} + (\varphi' - \cos 2\theta)\Delta_{,y} = 0. \end{aligned} \tag{3.37}$$

In the case of a system of quasi-linear partial differential equations

$$A_{ij}\xi_{j,x} + B_{ij}\xi_{j,y} = C_i, \qquad i,j = 1,2,\ldots,n \tag{3.38}$$

for n unknown functions $\xi(x,y)$ the type of the set (3.38) is established by considering the eigenvalue problem for the following matrix

$$|B_{ij} - \lambda A_{ij}| = 0, \tag{3.39}$$

where $\lambda = dy/dx$.

For the considered system of equations (3.29) and (3.37), appropriately simplified by referring it to the principal directions as coordinate axes, the characteristic determinant becomes

$$\begin{vmatrix} -\lambda(1+\varphi') & \varphi & -1 & 0 \\ 1-\varphi' & -\lambda\varphi & -\lambda & 0 \\ -\lambda\varphi'' & 1 & 0 & -\lambda(1+\varphi') \\ \varphi'' & -\lambda & 0 & -(1-\varphi') \end{vmatrix} = 0 \tag{3.40}$$

The requirement that the determinant (3.40) vanish yields the following equation for the characteristic directions:

$$\lambda^4(1+\varphi')^2 - 2\lambda^2(2\varphi\varphi'' + \varphi'^2 - 1) + (1-\varphi')^2 = 0. \tag{3.41}$$

The system is hyperbolic, thus it possesses four characteristics provided the roots of (3.41), considered as a quadratic equation in λ^2, are real and positive. Computation shows that the roots are real if

$$4\varphi\varphi''(\varphi\varphi'' + \varphi'^2 - 1) \geqslant 0. \tag{3.42}$$

Since the interaction curve (3.25) is convex it is either $\varphi\varphi'' < 0$ when $\varphi(\omega)$ is nonlinear in the mean moment ω, or $\varphi\varphi'' = 0$. A necessary condition for a nonlinear interaction condition to result in real roots is therefore

$$\varphi''\varphi + \varphi'^2 - 1 \leqslant 0. \tag{3.43}$$

However, both roots λ_1^2 and λ_2^2 of (3.41) are related as follows:

$$\lambda_1^2\lambda_2^2 = \frac{(1-\varphi')^2}{(1+\varphi')^2}, \qquad \lambda_1^2+\lambda_2^2 = \frac{2(2\varphi\varphi''+\varphi'^2-1)}{(1+\varphi')^2}. \tag{3.44}$$

These relations result from the properties of quadratic algebraic equations. The first one indicates that both roots are of the same sign, the second one states that the necessary condition for the roots to be positive is

$$2\varphi\varphi'' + \varphi'^2 - 1 \geqslant 0. \tag{3.45}$$

The requirements (3.43), (3.45) and $\varphi\varphi' < 0$ can never be satisfied simultaneously. Hence there is no real characteristic direction and the considered system of four equations in ω, θ, ϕ and Δ is elliptic whenever $\varphi(\omega)$ is non-linear. If, however, the interaction condition (3.25) is linear in the mean moment ω, thus

$$\varphi = a\omega + b, \tag{3.46}$$

the two roots of (3.41) coincide and the characteristic directions are

$$\left(\frac{dy}{dx}\right)^2 = \frac{a-1}{a+1}. \tag{3.47}$$

Hence the equations (3.29) and (3.37) are elliptic if $|a|<1$, hyperbolic for $|a|>1$ and parabolic with a quadruple characteristic at $a=1$. Characteristics coincide then with one family of the principal directions.

For piecewise continuous interaction conditions stress régimes exist where φ is not uniquely defined. The stress state satisfies then simultaneously two interaction equations

$$\psi = \varphi_1(\omega), \qquad \psi = \varphi_2(\omega) \tag{3.48}$$

so that $\omega=\omega_0$ and $\psi=\psi_0$ are fixed. The relations (3.29) become a pair of equations for θ and ϕ

$$\begin{aligned} -2\psi_0\sin2\theta\,\theta_{,x} + 2\psi_0\cos2\theta\,\theta_{,y} - \phi_{,y} &= p_x, \\ 2\psi_0\cos2\theta\,\theta_{,x} + 2\psi_0\sin2\theta\,\theta_{,y} + \phi_{,x} &= p_y \end{aligned} \tag{3.49}$$

with the characteristic determinant

$$\begin{vmatrix} \cos2\theta+\lambda\sin2\theta & 1 \\ \sin2\theta-\lambda\cos2\theta & \lambda \end{vmatrix} = 0 \tag{3.50}$$

Hence, if $\psi_0=0$ the characteristic direction is not defined and any curve may be considered as a characteristic in the zone of isotropic bending where $m_1=m_2$.

If $\psi_0\neq0$ the system (3.49) is always hyperbolic the characteristics being

$$\lambda_1 = \frac{dy}{dx} = \tan\theta, \qquad \lambda_2 = \frac{dy}{dx} = \operatorname{cotan}\theta, \tag{3.51}$$

i.e. they coincide with the trajectories of principal moments. For a corner point where (3.48) hold the kinematical relations (3.30) take the form

$$\begin{aligned} 2\dot{w}_{,xx} &= \nu_1(\varphi_1' - \cos2\theta) + \nu_2(\varphi_2' - \cos2\theta), \\ 2\dot{w}_{,yy} &= \nu_1(\varphi_1' + \cos2\theta) + \nu_2(\varphi_2' + \cos2\theta), \\ 2\dot{w}_{,xy} &= -(\nu_1+\nu_2)\sin2\theta. \end{aligned} \tag{3.52}$$

Elimination of ν_1 and ν_2 yields the following equation for the deflection velocity

$$\dot{w}_{,xx} - 2\operatorname{cotan}2\theta\,\dot{w}_{,xy} - \dot{w}_{,yy} = 0. \tag{3.53}$$

Eq. (3.53) is hyperbolic, with characteristics given by (3.51). Hence principal directions of moments and curvatures coincide also for singular stress régimes. The deflected surfaces has a saddle form.

3.4. Discontinuities

The preceding discussion has shown that in plate problems non-elliptic equations may occur and therefore certain discontinuities in the field variables may appear. Distinct analytical solutions can be matched along certain characteristics.

Discontinuities be present both in the derivatives and the field quantities themselves. We shall consider variations of the field quantities across a narrow strip $2\Delta n$ adjacent to a stationary discontinuity line Γ.

Equilibrium equations (3.9) and (3.10) admit the following jumps.

$$[p]\Delta n + [s_n] = 0, \qquad [m_n] = [s_n]\Delta n, \qquad [m_{nt}] = 0. \tag{3.54}$$

If there is no line load on Γ then $[p]$ in (3.54) is finite and the shear s_n is continuous across the discontinuity line as $\Delta n \Rightarrow 0$,

$$[s_n] = 0 \quad \text{on } \Gamma. \tag{3.55}$$

The equilibrium requirements do not impose any restriction on s_t and m_t. These quantities are thus not necessarily continuous across Γ.

In the plate theory only two stress conditions can be prescribed on a plate boundary. If, therefore, we consider a stress discontinuity line as a boundary

line between two parts of a plate then instead of (3.54) only the following two continuity requirements can be imposed:

$$[m_n] = 0, \qquad \left[s_t + \frac{\partial m_{nt}}{\partial n}\right] = 0. \tag{3.56}$$

Eq. (3.56) results in a nodal force of magnitude $\pm m_{nt}$ at the ends of the discontinuity line and, specifically, whenever Γ meets the plate boundary.

Consider discontinuities admitted by the kinematical relations. A discontinuity in the displacement rate $\dot{w}$ is excluded a priori in a theory not accounting for the transverse shear deformation. Hence

$$[\dot{w}] = 0 \tag{3.57}$$

and also

$$[\dot{w}_{,t}] = 0 \qquad [\dot{w}_{,tt}] = 0 \tag{3.58}$$

if continuity in $\dot{w}$ is required.

For a stationary discontinuity line the normal derivative of the deflection velocity may be discontinuous,

$$[\dot{w}_{,n}] \neq 0. \tag{3.59}$$

The discontinuity in $\dot{w}_{,n}$ involves indefinitely large values of the second derivative in a narrow region. It value becomes infinite in the limit

$$\lim_{\Delta n \Rightarrow 0} (\dot{w}_{,nn}) \Rightarrow \infty \tag{3.60}$$

whereas it is possible for $\dot{w}_{,nt}$ and $\dot{w}_{,tt}$ to remain finite. In this case

$$\lim_{\Delta n \Rightarrow 0} \left(\frac{2\dot{w}_{,nt}}{\dot{w}_{,nn} - \dot{w}_{,tt}}\right) \tag{3.61}$$

tends to zero on Γ and the normal and tangential directions to Γ are accordingly directions of principal curvature rates. Thus putting $\theta = 0$, the kinematical relations (3.30) become

$$2\dot{w}_{,tt} = v(\varphi' - 1), \quad 2\dot{w}_{,nn} = v(\varphi' + 1), \quad v \neq 0 \tag{3.62}$$

According to (3.60) and in view of the second equation of (3.62)

$$\lim_{\Delta n \Rightarrow 0} \int \frac{v(\varphi' + 1)}{2} dn \equiv [\dot{w}_{,n}] \neq 0 \tag{3.63}$$

so that v assumes indefinitely large value if φ' remains finite.

The condition of isotropy requires the principal curvature rate directions to coincide with the principal stress directions, Fig. 3.6. Thus on crossing the trajectory corresponding to $\theta = 0$ the moment field suffer a jump. It value

$$[m_t] = 2[\omega] \tag{3.64}$$

is found by using the definitions (3.24), when $m_t = m_1$ and $m_n = m_2$, and the first condition of (3.56).

3.5. Bounds on the collapse load

Complete solutions in the limit analysis of plates can effectively be obtained only for a narrow class of interaction criteria and boundary conditions. It is therefore often necessary to use the bounding theorems to establish bounds on the collapse load.

The upper bound on the collapse load multiplier (2.53) takes, for a transversely loaded plate, the form

$$\mu_k = \frac{D_{\text{int}}}{D_{\text{ext}}} = \int_A M_{ij} \dot{K}_{ij} \, dA \; / \int_A P_0 \, \dot{W} \, dA, \tag{3.65}$$

where P_0 specifies the spatial distribution of load so that $P = \mu P_0$. In terms of the dimensionless quantities defined in (3.6) the kinematically admissible load multiplier becomes

$$\mu_k = \iint m_{ij} \dot{\kappa}_{ij} \, dxdy \; / \iint p_0 \, \dot{w} \, dxdy. \tag{3.66}$$

The rate of internal energy dissipation represented by the numerator of (3.66) can be expressed in terms of kinematical variables. To this end we replace $\dot{\kappa}_{ij}$ by their values furnished by the associated flow law. The integrand becomes then $(v \frac{\partial f}{\partial m_{ij}} m_{ij})$. For the interaction conditions which are homogeneous of degree n in the stress variables, i.e. $\frac{\partial f}{\partial m_{ij}} m_{ij} = n f(m_{ij})$ and $f(m_{ij}) = 1$, we obtain the kinematically admissible load multiplier in the form

$$\mu_k = n \iint v \, dxdy \; / \iint p_0 \, \dot{w} \, dxdy. \tag{3.67}$$

Eq.(3.67) indicates that the magnitude of μ_k differs for the same admissible velocity field depending upon the interaction condition. In the case of Huber-Mises condition (3.18) which is quadratic in bending moments, $n = 2$, we have

$$v = \frac{1}{\sqrt{3}} \sqrt{\dot{\kappa}_x^2 + \dot{\kappa}_x \dot{\kappa}_y + \dot{\kappa}_y^2 + \frac{1}{4}\dot{\kappa}_{xy}^2} \tag{3.68}$$

and therefore, remembering the displacement-curvature relations (3.5), (3.67) takes the form

$$\mu_k = \frac{\frac{2}{\sqrt{3}} \iint \sqrt{\dot{w}_{,xx}^2 + \dot{w}_{,xx}\dot{w}_{,yy} + \dot{w}_{,yy}^2 + \dot{w}_{,xy}^2}\, dxdy}{\iint p_0 \dot{w}\, dxdy}. \tag{3.69}$$

For the Tresca condition the rate of internal energy dissipation, if expressed in terms of the principal curvatures $\dot{\kappa}_{11}$, $\dot{\kappa}_{22}$, takes the following form:

$$\iint v\, dxdy = \frac{1}{2} \iint (|\dot{\kappa}_{11}| + |\dot{\kappa}_{22}| + |\dot{\kappa}_{11} + \dot{\kappa}_{22}|)\, dxdy. \tag{3.70}$$

An analogous relation applies for the maximum principal moment condition:

$$\iint v\, dxdy = \frac{1}{2} \iint (|\dot{\kappa}_{11}| + |\dot{\kappa}_{22}|)\, dxdy. \tag{3.71}$$

For discontinuous velocity fields, energy is dissipated on the discontinuity lines as well. For plates in bending it is only slope discontinuities of the deflected surface that are allowed for, as shown in (2.32), so that the contribution of a system of hinge lines is

$$D_\Gamma = M^0 L \sum \int_l m_n \cdot \Phi_n\, dl. \tag{3.72}$$

Explicit form of the internal dissipation across the hinge line is

$$D_\Gamma = \alpha M^0 L \sum \int_l \Phi_n\, dl = \alpha M^0 L \sum \int_l \left(\sqrt{[\dot{w}_{,x}]^2 + [\dot{w}_{,y}]^2} \right) dl, \tag{3.73}$$

where $[\dot{w}_{,x}]$, $[\dot{w}_{,y}]$ denote the jumps in partial derivates of the displacement rate across a hinge line. The multiplier α takes the value $\alpha = 1$ for the Tresca condition and $\alpha = 2/\sqrt{3}$ for the Huber-Mises condition. The collapse load multiplier in the presence of slope discontinuities is defined as follows:

$$\mu_k = \frac{D_C + D_\Gamma}{D_{\text{ext}}}, \tag{3.74}$$

where D_C denotes the energy dissipation rate in continuously deforming zone, i.e. where $\dot{w}$ is twice continuously differentiable, (3.8).

Lower bound to the collapse load can be obtained by selecting the bending moment field $M_{ij}^0(X,Y,C_i)$ in equilibrium with external load and containing a number of parameters C_i. A bound is obtained on putting the moment field into the interaction condition and choosing the magnitudes of the parameters so as not to violate the interaction condition. The best bound in the considered class is

$$\mu_s^n = \frac{1}{\max f(m_{ij}^0)} \tag{3.75}$$

for the interaction condition homogeneous of degree n in the moments, i.e. $f(\mu_s m_{ij}^0) = \mu_s^n f(m_{ij}^0)$.

For the Huber-Mises interaction condition the load multiplier amounts to

$$\mu_s^2 = \frac{1}{\max\left((m_x^0)^2 - m_x^0 m_y^0 + (m_y^0)^2 + 3(m_{xy}^0)^2\right)}. \tag{3.76}$$

The exact collapse load multiplier μ_u corresponding to the complete solution lies within the range (2.60).

CHAPTER 4

CIRCULAR PLATES

4.1. Equations

In rotationally symmetric loading and support conditions plastic bending of circular and annular plates is governed by ordinary differential equations. The net of principal lines of moments and curvatures defines a system of polar coordinates on the plate middle surface. A plate element and the coordinate system R, θ are shown in Fig. 4.1 where the adopted notation and the sign convention for the stress resultants as well as for the deflection velocity are also specified.

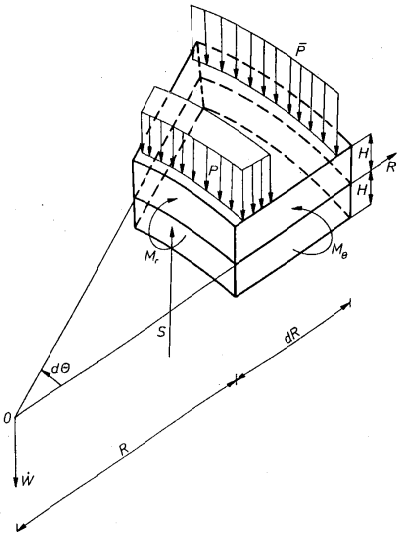

Fig. 4.1. Rotationally symmetric plate element in polar coordinates

We shall consider plates subjected to loading distributed over the middle plane. Dimensionless variables are defined as follows

$$r = \frac{R}{L}, \qquad \dot{w} = \frac{H\dot{W}}{L^2},$$

$$m_r = \frac{M_r}{M^0}, \quad m_\theta = \frac{M_\theta}{M^0}, \quad s_r = s = \frac{SL}{M^0}, \quad s_\theta = 0, \tag{4.1}$$

$$p = \frac{PL^2}{M^0}, \quad \bar{p}_i = \frac{\bar{P}_i L}{M^0}, \quad q = \frac{Q}{M^0},$$

where P, $\bar{P}_i$ denote the distributed pressure and line load, respectively, Q is a concentrated load and L stands for the plate radius.

The dissipation rate per unit area of the middle surface becomes

$$d = \frac{M^0}{H}(m_r\dot{\kappa}_r + m_\theta\dot{\kappa}_\theta) \tag{4.2}$$

where

$$\dot{\kappa}_r = H\dot{K}_r, \quad \dot{\kappa}_\theta = H\dot{K}_\theta, \tag{4.3}$$

and $\dot{K}_r$, $\dot{K}_\theta$ stand for the curvature rates of the plate middle surface.

The kinematical relations are

$$\dot{\kappa}_r = -\dot{w}'', \quad \dot{\kappa}_\theta = -\frac{\dot{w}'}{r}, \tag{4.4}$$

where prime denotes differentiation with respect to r.

In terms of the dimensionless variables (4.1) the equilibrium equations become

$$(rm_r)' - m_\theta - rs = 0, \qquad (rs)' + rp = 0 \tag{4.5}$$

or, in another form

$$rm_r' + m_r - m_\theta = rs$$

$$rs = -\int p(r)\,dr - \bar{p}_i \cdot r_i - \frac{q}{2\pi}.$$

The equations (4.4) and (4.5) are supplemented by the interaction condition

$$\mathscr{F}(m_r, m_\theta) = 0 \tag{4.6}$$

and the plastic potential flow law

$$(\dot{\kappa}_r, \dot{\kappa}_\theta) = \left(v\frac{\partial \mathscr{F}}{\partial m_r}, v\frac{\partial \mathscr{F}}{\partial m_\theta}\right), \qquad v \geqslant 0 \tag{4.7}$$

subject to appropriate generalizations in the case of singular stress régimes corresponding to the intersection of two or more interaction loci.

In the considered case of bending without membrane forces the circular plate equations split into two systems. Eqs. (4.5) and the interaction condition written in the form $m_\vartheta = \vartheta(m_r)$ reduce to the following single equation

$$(rm_r)' - \vartheta(m_r) + \int prdr + C = 0. \tag{4.8}$$

The problem thus becomes statically determinate provided the stress boundary conditions are prescribed.

Stress fields in plastic bending can have some discontinuities. Under the requirements $[m_r] = 0$ and $[p] = 0$ the equations (4.5) yield the following relation on a circumferential line of stress discontinuity

$$[rm_r'] - [m_\theta] = 0. \tag{4.9}$$

A circular hinge line forms in a plate when the slope of the deflected surface $\dot{w}$ suffers a discontinuity $[\dot{w}'] \neq 0$, and $\dot{w}'' = -\dot{\kappa}_r = -v\frac{\partial \mathscr{F}}{\partial m_r}$ is there indefinitely large. Then circumferential hinge corresponds to the points of the interaction curve at which

$$\dot{\kappa}_r = -\dot{w}'' \Rightarrow \infty, \tag{4.10}$$

thus

$$\frac{dm_r}{dm_\theta} = -\frac{\dfrac{\partial \mathscr{F}}{\partial m_\theta}}{\dfrac{\partial \mathscr{F}}{\partial m_r}} = 0. \tag{4.11}$$

The deflection velocity is governed by the equation

$$r\dot{w}'' + \dot{w}'\frac{dm_\theta}{dm_r} = 0 \tag{4.12}$$

which follows from (4.4) and (4.7) by elimination of v. When $\dot{w}$ is established it is necessary to check whether the flow multiplier v is nonnegative.

4.2. General solution for piece-wise linear interaction surface

The problem of plastic flexure of a circular plate can easily be solved for an arbitrary piece-wise linear interaction condition. We take a interaction equation, linear with respect to m_r and m_θ,

$$m_\theta = (1 - \alpha)m_r + \beta, \tag{4.13}$$

where α and β are constants relevant to each face of the polygon.

Equilibrium requirements (4.5), when combined with (4.13), yield the following equation for the radial moment:

$$rm_r' + \alpha m_r = \beta - \int prdr + C, \tag{4.14}$$

C being the integration constant of the vertical equilibrium equation. The solution of (4.14) for $\alpha \neq 0$ is

$$m_r = \frac{1}{\alpha}(\beta + C) + \frac{D}{r^\alpha} - \frac{1}{\alpha}\int prdr + \frac{1}{\alpha r^\alpha}\int pr^{(\alpha+1)}\,dr \tag{4.15}$$

and for $\alpha = 0$ takes the form

$$m_r = (\beta + C)\ln r - \int\left(\frac{1}{r}\int prdr\right)dr + D. \tag{4.16}$$

The radial moment in a plate at collapse consists of a combination of (4.15) or (4.16) satisfying the boundary conditions as well as the imposed continuity requirements. We observe that the constant C changes only at the jumps of the transverse shear, whereas D changes with the stress profile.

The deflection rate field is described by (4.4), (4.7) and (4.13) so that

$$-\dot{w}' = vr, \qquad -\dot{w}'' = v(\alpha - 1), \qquad v \geqslant 0. \tag{4.17}$$

Hence

$$r\dot{w}'' - \dot{w}'(\alpha - 1) = 0 \tag{4.18}$$

so for $\alpha \neq 0$ we obtain

$$\dot{w} = Ar^\alpha + B \tag{4.19}$$

and for $\alpha = 0$ we get

$$\dot{w} = A\ln r + B. \tag{4.20}$$

The deflection rate thus obtained is kinematically admissible if $v > 0$, hence if

$$v r^{2-\alpha} = -\alpha A > 0, \quad \alpha \neq 0,$$
$$v r^2 = -A > 0, \quad \alpha = 0. \tag{4.21}$$

4.3. Maximum reduced stress interaction surface

In terms of principal moments the condition has the form given in (3.23). Hence, for a rotationally symmetric deformation the maximum reduced stress interaction curve is described by

$$\max\left(|m_r - \frac{1}{2}m_\theta|, \quad |m_\theta - \frac{1}{2}m_r|, \quad \frac{1}{2}|m_r + m_\theta|\right) = 1. \tag{4.22}$$

The respective hexagon is shown in Fig. 4.2.

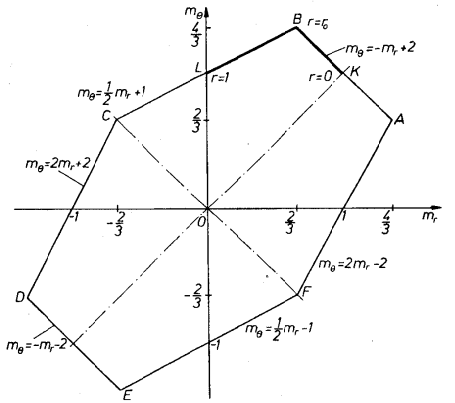

Fig. 4.2. Maximum reduced stress interaction curve for rotationally symmetric plates

The general solution (4.15) will be used in solving the limit analysis problem for isotropic, simply supported circular plate. The loading and boundary conditions have the following dimensionless form

$$p = \text{constant}, \quad 0 \leqslant r \leqslant 1, \tag{4.23}$$
$$m_r(0) = m_\theta(0) = 1, \; m_r(1) = 0, \; \dot{w}(1) = 0, \; \dot{w}(0) = \dot{w}_0.$$

Consider the stress profile *KBL*, Fig. 4.2, allowing to satisfy the boundary conditions. Two stress states are involved:

$$AB: \quad m_\theta = -m_r + 2, \quad \alpha = 2, \quad \beta = 2,$$
$$BC: \quad m_\theta = \frac{1}{2}m_r + 1, \quad \alpha = \frac{1}{2}, \quad \beta = 1. \tag{4.24}$$

For the stress régimes (4.24) the solution given in (4.15) results in

$$m_r = \begin{cases} 1 - \dfrac{pr^2}{8}, & 0 \leq r \leq r_0, \\ \dfrac{1 - r^{-1/2}}{1 - r_0^{-1/2}}\left(\dfrac{2}{3} - \dfrac{p}{5}\left(1 - r_0^2\right)\right) + \dfrac{p}{5}(1 - r^2), & r_0 \leq r \leq 1. \end{cases} \tag{4.25}$$

where r_0 defines the radius of a circle across which the stress régime changes (point B, $m_r = 2/3$, see Fig. 4.2). The radial moment at B is subjected to the continuity requirement $[m_r] = 0$ and $[m_r'] = 0$ since there is no jump in shears. Hence

$$6r_0^{5/2} - 15r_0^2 + 4 = 0, \qquad p = \frac{8}{3r_0^2} \tag{4.26}$$

leading to the result

$$r_0 = 0.624, \qquad p = 6.852. \tag{4.27}$$

The deflection velocity (4.19) becomes

$$\dot{w} = \begin{cases} A_1 r^2 + B_1, & 0 \leq r \leq r_0, \\ A_2 r^{1/2} + B_2, & r_0 \leq r \leq 1. \end{cases} \tag{4.28}$$

The requirements $[\dot{w}(r_0)] = 0$, $[\dot{w}'(r_0)] = 0$ together with (4.23) allow to compute the constants

$$A_1 = \frac{\dot{w}_0}{r_0^{3/2}(3r_0^{1/2} - 4)}, \quad B_1 = \dot{w}_0, \quad A_2 = \frac{4\dot{w}_0}{3r_0^{1/2} - 4}, \quad B_2 = -A_2. \tag{4.29}$$

No hinge line occurs in the velocity field (4.28).

It can be verified that (4.21) holds good because for $0 \leq r_0 \leq 1$ both A_1 and A_2 are negative. The flow multiplier v is therefore found to be positive and the solution is complete.

For a clamped plate a hinge circle forms at the fixed boundary. Only for the stress points A and D of the interaction hexagon of Fig. 4.2, where $-1/2 \leq dm_r/dm_\theta \leq 1$, the slope discontinuity may be admitted. Therefore the clamped edge belongs either to the stress régime A or D, the boundary moment being $m_r = \pm 4/3$, respectively.

At the plate centre $w'(0) = 0$, the curvatures are finite and no singularity in slope appears.

4.4. Tresca plates

4.4.1. Simple examples. For circular plates the Tresca condition has the form

$$\mathcal{F} = \max(|m_r|, |m_\theta|, |m_r - m_\theta|) - 1 = 0, \tag{4.30}$$

shown in Fig. 4.3. Each of the straight sides of the interaction hexagon (4.30) defines a different stress profile and results in a different form of equations (4.8) and (4.12) specifying the stress field and the deformation mode of the plate, respectively.

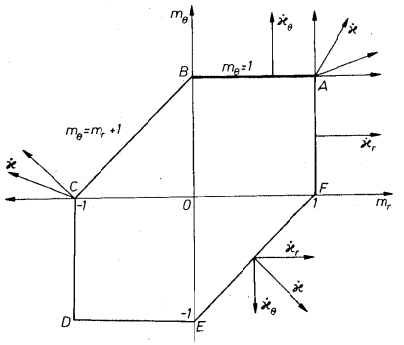

Fig. 4.3. Interaction curve for rotationally symmetric Tresca plates

Let us consider a simply supported plate subjected to linearly varying pressure

$$p(r) = p_0 r, \qquad 0 \leq r \leq 1 \tag{4.31}$$

and to the stress boundary conditions

$$m_r(0) = 1, \qquad m_r(1) = 0. \tag{4.32}$$

Assuming the entire plate to yield, we take the stress profile tracing the side AB of hexagon, i.e. $m_\theta = 1$, and $\alpha = 1$, $\beta = 1$. This assumption will be proved a posteriori. Eq.(4.15), satisfying the first boundary condition (4.32), becomes

$$m_r = 1 - p_0 \frac{r^3}{12}. \tag{4.33}$$

Using the second condition (4.32) the collapse load is obtained

$$p_0 = 12. \tag{4.34}$$

The bending moments and the collapse load are obtained using the equilibrium and the stress boundary conditions. The solution thus obtained can only be said to be statically admissible and further analysis regarding kinematical admissibility is needed.

To find the mechanism of plastic motion we put $\alpha = 1$ in Eqs. (4.18) and (4.19), hence

$$\dot{w}'' = 0 \text{ and } \dot{w} = Ar + B. \tag{4.35}$$

The first equation (4.35) can be directly obtained by inspecting Fig. 4.3 since for the stress profile AB $\dot{\kappa}_r = -\dot{w}'' = 0$.

The kinematical boundary conditions are

$$\dot{w}(0) = \dot{w}_0, \qquad \dot{w}(1) = 0 \tag{4.36}$$

hence it follows from (4.35) that

$$\dot{w} = \dot{w}_0 (1 - r). \tag{4.37}$$

The profile AB is therefore both statically and kinematically admissible and represents the complete solution.

It can be seen that first of (4.21) is verified because $A = -\dot{w}_0$ in (4.35) is negative. The flow multiplier v is therefore found to be positive and for the stress régime AB is

$$v = \dot{\kappa}_\theta = -\frac{\dot{w}'}{r} = \frac{\dot{w}_0}{r} > 0 \tag{4.38}$$

and the solution is thus complete. Let us note that $v \Rightarrow \infty$ for $r = 0$. This means that in the centre of plate a point plastic hinge occurs.

Solution for piece-wise continuous interaction conditions may involve several different stress régimes, i.e. the stress profile may belong to more than one side of the polygon (4.30).

As an example a clamped plate under uniform pressure p = constant will be considered to illustrate such a situation. Since a negative moment is

expected to appear at the clamped boundary we assume that the stress profile involves the régimes AB and BC, Fig. 4.3.

According to (4.18) with the stress régime BC, $m_\theta = m_r + 1$, $\alpha = 0$, the following displacement velocity is associated

$$r\dot{w}'' + \dot{w}' = 0 \tag{4.39}$$

and therefore

$$\dot{w} = A \ln r + B. \tag{4.40}$$

The velocity field corresponding to neither the stress profile AB nor BC can satisfy conditions of both zero slope and zero velocity at clamped edge. Hence a hinge circle must be admitted. According to (4.10) such a hinge can form for the stress profile CD where $m_r = -1$. The stress profile for the solution runs over AB and BC and the stress conditions at the centre and the edge of the plate are established as follows:

$$m_r(0) = 1, \qquad m_r(1) = -1. \tag{4.41}$$

The stress profile changes at $r = \rho$, where

$$[m_r(\rho)] = 0, \quad m_r(\rho) = 0, \quad [m_r'(\rho)] = 0 \tag{4.42}$$

since there is no jumps in shear forces at the corner B.

The integration yields

$$m_r = \begin{cases} 1 - \dfrac{pr^2}{6}, & 0 \le r \le \rho, \\ -1 + \dfrac{\ln r}{\ln \rho}\left(1 - \dfrac{p}{4}(1-\rho^2)\right) + \dfrac{p}{4}(1-r^2), & \rho \le r \le 1. \end{cases} \tag{4.43}$$

The continuity of m_r' at the radius ρ where stress profile changes furnishes the following equation, [23]:

$$3 - 5\rho^2 + 2\rho^2 \ln \rho = 0 \tag{4.44}$$

whose solution is $\rho = 0.730$. The dimensionless collapse load is

$$p = \frac{6}{\rho^2} = 11.26. \tag{4.45}$$

The deflection velocity is obtained in the form

$$\frac{\dot{w}}{\dot{w}_0} = \begin{cases} 1 - \dfrac{r}{\rho(1-\ln\rho)}, & 0 \le r \le \rho, \\ \dfrac{\ln r}{\ln \rho - 1}, & \rho \le r \le 1 \end{cases} \tag{4.46}$$

for the following kinematical boundary conditions:

$$\dot{w}(0) = \dot{w}_0, \quad \dot{w}(1) = 0, \quad [\dot{w}(\rho)] = 0, \quad [\dot{w}'(\rho)] = 0 \tag{4.47}$$

as no slope discontinuity is admitted at the corner B where

$$\frac{dm_r}{dm_\theta} \neq 0. \tag{4.48}$$

It can be checked that in both zones $v > 0$, and therefore the solution is statically and as well as kinematically admissible. The slope discontinuity at the clamped edge is $[\dot{w}'(1)] = (\ln\rho - 1)^{-1}$.

Discontinuous stress fields can also form in rigid-perfectly plastic plates. Such is the case in an annular plate. To find the stress profile it is necessary to consider both the stress and velocity equations. Examples can be found in [19], [45] and [72].

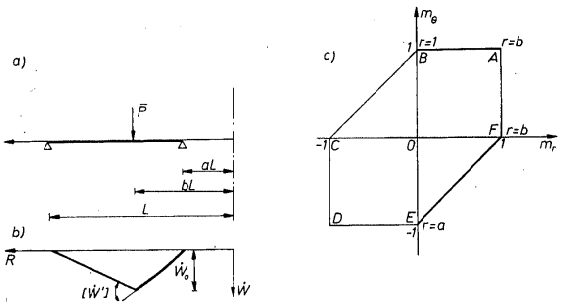

Fig. 4.4. Annular plate: (a) support and load pattern, (b) deflection rates, (c) stress profile

Consider an annular plate subjected to a ring force as shown in Fig. 4.4. The boundary conditions are

$$m_r(a) = 0, \quad m_r(1) = 0, \quad \dot{w}(a) = 0, \quad \dot{w}(1) = 0. \tag{4.49}$$

To establish the stress profile we suppose that $\dot{w} > 0$ for $a \leqslant r \leqslant 1$. In order to get a non-trivial solution satisfying the kinematical boundary

conditions in (4.49), velocity field $\dot{w}$ must have the extremum within the range. Hence $\dot{w}'$ and, according to (4.4), also $\dot{\kappa}_\theta$ must change sign in this region. Since $\dot{w}>0$ it is $\dot{w}'(a)>0$ and $\dot{w}'(a)<0$ and respectively $\dot{\kappa}_\theta(1)<0$ and $\dot{\kappa}_\theta(1)>0$.

The signs of m_θ and $\dot{\kappa}_\theta$ must be the same to yield positive rate of the energy dissipation. Therefore the stress profile of the régime AB ($m_\theta=1, \alpha=1$) occurs at the outer boundary, and of the régime FE ($m_\theta=m_r-1, \alpha=0$) at the inner one. The stress profile cannot run over ABC since then m_θ would be positive throughout.

However, a transition from the velocity field $\dot{w}=A_1 r+B_1$ in the zone AB to $\dot{w}=A_2 \ln r+B_2$ in EF such as to preserve slope continuity and to satisfy the boundary conditions is impossible. Therefore hinge circles should develop at the stress state satisfying (4.10), hence at A and F. Either two hinges form or m_θ is discontinuous. The second possibility is permitted in the considered case since there is a sudden change in the shear force across $r = b$.

In general the zone represented by the stress régime AF can move only as a rigid body since the flow law gives there $\dot{\kappa}_\theta=0$ hence $\dot{w}'=0$, whereas $\dot{\kappa}_r=-\dot{w}''\geq 0$.

At the stress discontinuity on $r=b$ the following condition must be satisfied

$$b[m_r'] - [m_\theta] - b[s] = 0, \tag{4.50}$$

obtained from the equilibrium requirement under the assumption of continuity of m_r. The jump in m_θ must be such as to pass from one side of the interaction hexagon to another, for both parts of the plate are at yield.

Denoting by t the reaction at the plate inner edge the shear force is found to be

$$rs = \begin{cases} ta, & a \leqslant r \leqslant b, \\ ta - \bar{p}b, & b \leqslant r \leqslant 1. \end{cases} \tag{4.51}$$

The bending moments satisfying (4.49) are eventually found to be

$$\begin{aligned} &m_r = (ta - 1)\ln\frac{r}{a}, \quad m_\theta = m_r - 1, \quad a \leqslant r \leqslant b, \\ &m_r = \left(1 - \frac{1}{r}\right)(1 + ta - \bar{p}b), \quad m_\theta = 1, \quad b \leqslant r \leqslant 1. \end{aligned} \tag{4.52}$$

The conditions $m_r(b^+)=1$ and $m_r(b^-)=1$ allow to evaluate the collapse load $\bar{p}$ and the reaction t

$$\bar{p}b = \frac{1}{\ln\frac{b}{a}} + \frac{2-b}{1-a}, \quad ta = 1 + \frac{1}{\ln\frac{b}{a}}. \tag{4.53}$$

The discontinuity $[m_\theta]=1$ is accompanied by the discontinuity in m_r' across the load application line.

The deflection rate, compatible with the stress profile is as follows:

$$\begin{aligned} \dot{w} &= \dot{w}_0 \frac{\ln\frac{r}{a}}{\ln\frac{b}{a}}, \quad \text{for} \quad a \leqslant r \leqslant b, \\ \dot{w} &= \dot{w}_0 \frac{1-r}{1-b}, \quad \text{for} \quad b \leqslant r \leqslant 1. \end{aligned} \tag{4.54}$$

It suffers a jump in a slope discontinuity at $r=b$. The result is depicted in Fig. 4.4.

4.4.2. General solution for Tresca plates. Each of the straight lines of the interaction hexagon (4.30) defines a distinct stress profile and results in a different analytical solution.

Consider first the stress profile AB, Fig. 4.3. The interaction equation and the flow law give the following set

$$\mathscr{F} = m_\theta - 1 = 0, \quad \dot{\kappa}_r = 0, \quad \dot{\kappa}_\theta = v. \tag{4.55}$$

From Eq.(4.15) for $\alpha=1, \beta=1$ we obtain following moment field:

$$m_\theta = 1, \quad m_r = 1 + C_1 + \frac{D_1}{r} - \int p\rho d\rho + \frac{1}{r}\int p\rho^2\, d\rho. \tag{4.56}$$

The radial moment depends on the actual loading distribution and on the boundary conditions, whereas the circumferential moment is constant along the radius.

The deflection velocity for the considered stress profile must satisfy the requirement $\dot{\kappa}_r=0$. Hence it follows from (4.4) that $\dot{w}''=0$ and therefore

$$\dot{w} = A_1 r + B_2. \tag{4.57}$$

Furthermore, the condition $\dot{\kappa}_\theta = v$ results in the following expression for the flow vector multiplier:

$$v = -\frac{\dot{w}'}{r} = -\frac{A_1}{r}. \tag{4.58}$$

The deflection velocity field is therefore admissible and plastic flow can effectively take place only if $A_1<0$. Since $v \Rightarrow \infty$ when $r \Rightarrow 0$ there is a slope

discontinuity at $r=0$ as only on the hinge lines the flow multiplier is unbounded.

The results regarding stress field and displacement velocities associated with the stress profiles on the interaction hexagon are summarized in Table 4.1. We note that the stress profiles FA and CD can support a rigid body motion only as $v=0$ is associated with such profiles.

Table 4.1

Moments and collapse modes for circular Tresca plates

Stress profile	m_r	m_θ	$\dot{w}$	v
AB	$1+C_1+\frac{D_1}{r}-\int prdr+\frac{1}{r}\int pr^2dr$	1	A_1r+B_1	$-\frac{A_1}{r}$
BC	$\left(1+C_2-\int prdr+\frac{pr^2}{2}\right)\ln r-\frac{1}{2}\int prdr+D_2$	m_r+1	$A_2\ln r+B_2$	$-\frac{A_2}{r^2}$
CD	-1	$-1-C_3+\int prdr$	const	0
DE	$-1+C_4+\frac{D_4}{r}-\int prdr+\frac{1}{r}\int pr^2dr$	-1	A_4r+B_4	$-\frac{A_4}{r}$
EF	$\left(-1+C_5-\int prdr+\frac{pr^2}{2}\right)\ln r-\frac{1}{2}\int prdr+D_5$	m_r-1	$A_5\ln r+B_5$	$-\frac{A_5}{r^2}$
FA	1	$1-C_6-\int prdr$	const	0

It is seen that $\dot{w}'\neq 0$ at the plate boundary r = constant. None of the velocity fields can non-trivially satisfy both conditions $\dot{w}=0$ and $\dot{w}'=0$. Therefore at a clamped edge $[\dot{w}]\neq 0$ must appear and a hinge line must develop. It is seen in Fig. 4.3 that the stress profile accompanied by plastic motion must necessarily reach the stress point A, C, D or F in order to allow a hinge line to form. The boundary conditions can therefore be written as

$$\begin{aligned} &\dot{w}=0, \quad m_r=0, \quad \text{hinged plate,} \\ &\dot{w}=0, \quad m_r=\pm 1, \quad \text{clamped plate.} \end{aligned} \tag{4.59}$$

One concludes that the stress state at a simply supported boundary maps onto the points B and E of the interaction hexagon, Fig. 4.3, whereas a clamped edge corresponds to the stress state represented by the points A, C, D, or F.

Step-wise loading of Tresca plates. To expose certain specific features of point loaded plates we shall first consider a simply supported plate loaded over the central part

$$p=\begin{cases}\text{constant}, & 0\leqslant r\leqslant a,\\ 0 & a\leqslant r\leqslant 1.\end{cases} \tag{4.60}$$

The solution is required to satisfy the conditions

$$m_r(0)=m_\theta(0)=1, \quad [m_r(a)]=0, \quad [s(a)]=0, \quad m_r(1)=0, \tag{4.61}$$

following from the isotropy condition and the requirement of continuity of the radial moment and shear, respectively. The last expression represents the stress boundary condition.

The stress profile is associated with the side AB of the interaction hexagon of Fig. 4.3, since the requirements (4.61) can then be met. The stress field is found from Table 4.1 to be

$$m_\theta=1, \quad m_r=\begin{cases}1+C_1+\frac{D_1}{r}-\frac{pr^2}{6}, & 0\leqslant r\leqslant a,\\ 1+C_2+\frac{D_2}{r}, & a\leqslant r\leqslant 1.\end{cases} \tag{4.62}$$

Since $m_r(0)$ is finite, and is at most unity, it follows that $C_1=0$ and $D_1=0$. The continuity of shear and radial moment across $r=a$ yields $C_2=pa^2/2$, $D_2=pa^3/3$. In order to satisfy the boundary condition $m_r(1)=0$ the load must be

$$p=\frac{6}{3a^2-2a^3}. \tag{4.63}$$

The five conditions (4.61) allow to determine the integration constants and the statically admissible collapse load intensity (4.63). The moments are

$$\mathrm{m}_\theta=1, \quad m_r=\begin{cases}1-\frac{r^2}{3a^2-2a^3}, & 0\leqslant r\leqslant a,\\ 1-\frac{3r-2a}{r(3-2a)}, & a\leqslant r\leqslant 1.\end{cases} \tag{4.64}$$

With the moments (4.64) and the collapse load (4.63) it is readily checked that $0\leqslant m_r\leqslant 1$ for $0\leqslant r\leqslant 1$.

The velocity field is conical as in (4.37), independently of the loaded area. It is readily proved that $v>0$ in plastically deforming zones.

Therefore the solution obtained is both statically and kinematically admissible. The result is plotted in Fig. 4.5.

The result (4.64) allows to get the solution for a plate subjected to a point load at the centre. Let $Q = \pi a^2 L^2 P$ denote the total load acting on the plate. The dimensionless ultimate load is found from (4.63),

$$q = \frac{6\pi}{3 - 2a}. \tag{4.65}$$

If $a \Rightarrow 0$ the collapse load is obtained for a point loaded plate

$$q = 2\pi, \quad m_\theta = 1, \quad m_r = 0. \tag{4.66}$$

The result is independent of the plate dimensions.

Through an analogous procedure the solution is obtained for a clamped plate. According to (4.59) the clamped boundary must be associated with a hinge line. Under downward directed loading (4.60) it is reasonable to expect $m_r = -1$ at $r = 1$. Hence the stress profile coincides now with the side AB and BC of the interaction hexagon of Fig. 4.3.

The results contained in Table 4.1 for the respective profile have to be matched at a certain radius r_0.

The stress régime must be such as to satisfy the continuity requirements of the radial moment, the shear force and the slope. Continuity of the slope is required by the stress régime B.

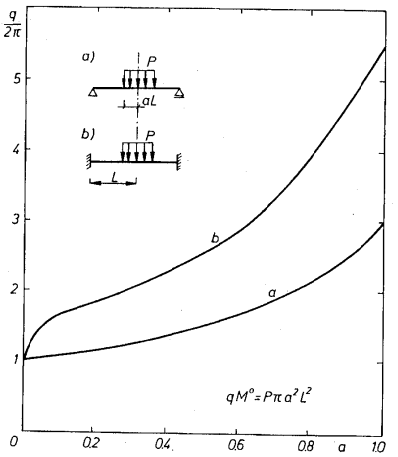

Fig. 4.5. Total collapse load for step-wise loaded circular plate: (*a*) simply supported, (*b*) clamped

In Fig. 4.5 comparison of the collapse load for simply supported and for clamped plates is given for the loading case (4.60). Singularity of the plate behaviour under centrally applied concentrated load is noticed. The collapse load in such a case for a Tresca plate is independent of the edge fixity, $q = 2\pi$.

4.5. General solution for Johansen plates

The Johansen yield condition has been found to lead to relatively simple solutions and, at the same time, to a good approximation of the behaviour of reinforced concrete slabs, [48], [49].

Table 4.2

Moments and collapse modes for circular Johansen plates

Stress profile	m_r	m_θ	$\dot{w}$	v
AB	$1+C_1+\frac{D_1}{r}-\int prdr+\frac{1}{r}\int pr^2dr$	1	A_1r+B_1	$-\frac{A_1}{r}$
BCD	-1	$-1-C_2+\int prdr$	const	0
DEF	$-1+C_3+\frac{D_3}{r}-\int prdr+\frac{1}{r}\int pr^2dr$	-1	A_3r+B_3	$-\frac{A_3}{r}$
FA	1	$1-C_4+\int prdr$	const	0

The general solution for this condition is given in Table 4.2. Its form is the same as in Table 4.1, provided the stress profiles BC and EF are ignored and the ranges of variation of m_r and m_θ are different, Fig. 4.6.

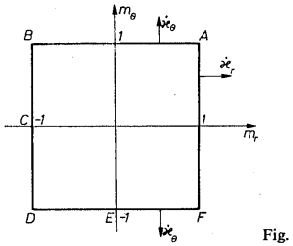

Fig. 4.6. Interaction curve for Johansen plates

As an example, let us analyse a uniformly loaded annular plate with arbitrary supports at both edges. The whole plate is assumed to yield under its ultimate load. Suitable stress profiles will be associated with certain selected forms of the deflection rates surfaces. Let us assume two collapse modes, Fig. 4.7a,b, with one and two ring hinge lines, respectively.

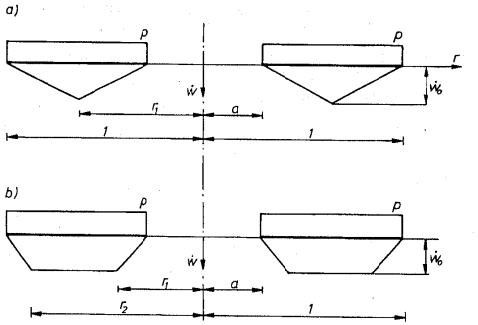

Fig. 4.7. Two collapse modes for Johansen annular plate

Mechanism a (Fig. 4.7a): For $a \leqslant r \leqslant r_1$ the deflected surface has a negative hoop curvature $\dot{\kappa}_\theta < 0$ hence the tip of moment vector can only touch the side *DEF* of the interaction square (Fig. 4.6 and Table 4.2).

$$m_\theta = -1, \quad m_r = -1 + C_3 + \frac{D_3}{r} - \frac{pr^2}{6}, \quad s = \frac{C_3}{r} - \frac{pr}{2}, \tag{4.67}$$

$$\dot{w} = A_3 r + B_3.$$

For $r_1 \leqslant r \leqslant 1$ the hoop curvature is positive $\dot{\kappa}_\theta > 0$, thus the profile *AB* is valid,

$$m_\theta = 1, \quad m_r = 1 + C_1 + \frac{D_1}{r} - \frac{pr^2}{6}, \quad s = \frac{C_1}{r} - \frac{pr}{2}, \tag{4.68}$$

$$\dot{w} = A_1 r + B_1.$$

At $r = r_1$ the hoop moment suffers jump, $[m_\theta] \neq 0$, which, according to the considerations of Section 3.4, is admissible. Eqs.(4.67) and (4.68) must be supplemented with the following boundary and continuity conditions:

$$m_r(a) = m_r^i, \quad m_r(r_1) = 1, \quad [m_r(r_1)] = 0, \quad [s(r_1)] = 0, \quad m_r(1) = m_r^o, \tag{4.69}$$

$$\dot{w}(a) = 0, \quad \dot{w}(r_1) = \dot{w}_0, \quad [\dot{w}(r_1)] = 0, \quad \dot{w}(1) = 0.$$

It follows that only 9 conditions are present to determine 10 constants appearing in (4.67) and (4.68). Thus the mechanism a cannot be associated with the assumed moment field.

Mechanism b (Fig. 4.7b): For $a \leqslant r \leqslant r_1$, the hoop curvature $\dot{\kappa}_\theta < 0$ which corresponds to the profile *DEF* of the interaction curve.
Thus:

$$m_\theta = -1, \quad m_r = -1 + C_3 + \frac{D_3}{r} - \frac{pr^2}{6}, \quad s = \frac{C_3}{r} - \frac{pr}{2}, \tag{4.70}$$

$$\dot{w} = A_3 r + B_3.$$

For $r_1 \leqslant r \leqslant r_2$, $\dot{\kappa}_\theta = 0$, profile *FA*

$$m_\theta = 1 - C_4 + \frac{pr^2}{2}, \quad m_r = 1, \quad s = \frac{C_4}{r} - \frac{pr}{2}, \tag{4.71}$$

$$\dot{w} = \text{constant}.$$

For $r_2 \leqslant r \leqslant 1$, $\dot{\kappa}_\theta > 0$ profile *AB*.

$$m_\theta = 1, \quad m_r = 1 + C_1 + \frac{D_1}{r} - \frac{pr^2}{6}, \quad s = \frac{C_1}{r} - \frac{pr}{2}, \tag{4.72}$$

$$\dot{w} = A_1 r + B_1.$$

The following boundary and compatibility conditions must be satisfied:

$$m_r(a) = m_r^i, \; m_r(r_1) = 1, \; m_\theta(r_1) = -1, \; m_\theta(r_2) = 1, \; m_r(r_2) = 1, \; m_r(1) = m_r^o,$$
$$[s(r_1)] = 0, \quad [s(r_2)] = 0, \tag{4.73}$$
$$\dot{w}(a) = 0, \quad \dot{w}(r_1) = \dot{w}_0, \quad \dot{w}(r_2) = \dot{w}_0, \quad \dot{w}(1) = 0,$$

where m_r^i and m_r^o denote the radial bending moments at the inner and the outer edge, respectively. In this case the number of equations and unknowns coincide. The constants can be obtained from the conditions (4.73) and are:

$$A_1 = -B_1 = -\frac{\dot{w}_0}{1-r}, \quad A_3 = -\frac{B_3}{a} = \frac{\dot{w}_0}{a-r_1}, \tag{4.74}$$

$$C = C_1 = C_3 = C_4 = \frac{pr_2^2}{2} = 2 + \frac{pr_1^2}{2}, \quad D_1 = -\frac{pr_2^3}{3}, \quad D_3 = -\frac{pr_1^3}{3}.$$

On inserting the constants into the equations (4.70 - 4.72) and rearrangement, the bending moments and the deflection rates take the form:

for $a \leqslant r \leqslant r_1$

$$m_\theta = -1, \quad m_r = -1 + \frac{p}{6r}(3r_2^2 r - 2r_1^3 - r^3), \quad \dot{w} = \dot{w}_0 \frac{r-a}{r_1 - a},$$

$$v = -\frac{A_3}{r} = \frac{\dot{w}_0}{r(r_1 - a)} > 0$$

for $r_1 \leqslant r \leqslant r_2$

$$m_\theta = 1 - \frac{p}{2}(r_2^2 - r^2), \quad m_r = 1, \quad \dot{w} = \dot{w}_0, \quad v = 0 \qquad (4.75)$$

for $r_2 \leqslant r \leqslant 1$

$$m_\theta = 1, \quad m_r = 1 + \frac{p}{6r}(3r_2^2 r - 2r_2^3 - r^3), \quad \dot{w} = \dot{w}_0 \frac{1-r}{1-r_2},$$

$$v = -\frac{A_1}{r} = \frac{w_0}{r(1-r_2)} > 0.$$

The shear force is

$$s = \frac{p}{2r}(r_2^2 - r^2) \qquad (4.76)$$

and the ultimate load amounts to

$$p = \frac{4}{r_2^2 - r_1^2}. \qquad (4.77)$$

The obtained solution satisfies all the conditions necessary for the complete solution hence the mechanism b is fully acceptable. The radial yield hinges and the deflection rates depend solely on the support conditions and can be arrived at from the following system of equations:

$$m_r^i = -1 + \frac{p}{6a}(3r_2^2 a - 2r_1^3 - a^3),$$

$$m_r^o = 1 + \frac{p}{6}(3r_2^2 - 2r_2^3 - 1). \qquad (4.78)$$

For simply loading conditions, closed-form solutions to the rotationally symmetric Johansen plates can be obtained. Ready formulae for the collapse loads, internal actions and deflection rates are given in Tables 4.3 - 4.6 for a number of particular examples.

Table 4.3

Load-carrying capacity for Johansen circular and annular plates under uniform load

Simply Supported	Load-carrying capacity p	Load-carrying capacity total load	clamped	Load-carrying capacity p	Load-carrying capacity total load
	6	6π		12	12π
	$\frac{6\pi}{3\alpha+\pi}$	$\frac{6\pi}{3\alpha+\pi}(\pi+\alpha)$		$\frac{12\pi}{3\alpha+\pi}$	$\frac{12}{3\alpha+\pi}(\pi+\alpha)$
	$\frac{6}{(1-\alpha)(2\alpha+1)}$	$\frac{6\pi(1+\alpha)}{(2\alpha+1)}$		$\frac{6(2-\alpha)}{(1-\alpha)^2(2\alpha+1)}$	$\frac{6\pi(2-\alpha)(1+\alpha)}{(1-\alpha)(2\alpha+1)}$
	$\frac{6}{(1-\alpha)(2+\alpha)}$	$\frac{6\pi(1+\alpha)}{(2+\alpha)}$		$\frac{6}{(1-\alpha)^2(2+\alpha)}$	$\frac{6\pi(1+\alpha)}{(1-\alpha)(2+\alpha)}$

Table 4.4

Bending moments and deflection rates for Johansen circular and annular plates under uniform load

Simply Supported	Bending moments and deflection rates	[0,1]	clamped	Bending moments and deflection rates	[0,1]
	r			r	
	m_r	$1-r^2$		m_r	$1-2r^2$
	m_θ	1		m_θ	1
	$\dot{w}$	$\dot{w}_0(1-r)$		$\dot{w}$	$\dot{w}_0(1-r)$

Table 4.4, contd

[89]

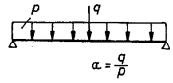 $\alpha = \frac{q}{p}$	r	[0, 1]	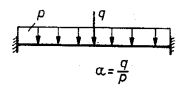 $\alpha = \frac{q}{p}$	r	[0, 1]
	$-m_r$	$1-\frac{3\alpha+\pi r^2}{3\alpha+\pi}$		m_r	$1-2\frac{3\alpha+\pi r^2}{3\alpha+\pi}$
	m_θ	1		m_θ	1
	$\dot{w}$	$\dot{w}_0(1-r)$		$\dot{w}$	$\dot{w}_0(1-r)$
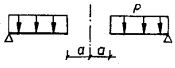	r	[a, 1]	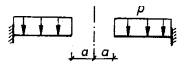	r	[a, 1]
	m_r	$\frac{p}{6}\left((1-r^2)-(1+a)a\frac{1-r}{r}\right)$		m_r	$\frac{a-r}{r(1-a)}+\frac{p}{6}\left((1-r^2)-(1+a)a\frac{1-r}{r}\right)$
	m_θ	1		m_θ	1
	$\dot{w}$	$\dot{w}_0\frac{1-r}{1-a}$		$\dot{w}$	$\dot{w}_0\frac{1-r}{1-a}$
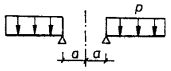	r	[a, 1]		r	[a, 1]
	m_r	$\frac{p}{6}\left((1-r^2)-\frac{(1+a)a(1-r)}{r}\right)$		m_r	$\frac{a(1-r)}{r}+\frac{p}{6}\left((1-r^2)-\frac{(1+a)a(1-r)}{r}\right)$
	m_θ	-1		m_θ	-1
	$\dot{w}$	$\dot{w}_0\frac{r-a}{1-a}$		$\dot{w}$	$\dot{w}_0\frac{r-a}{1-a}$

Table 4.5

Load-carrying capacity for Johansen circular and annular plates under ring loads

[69]

Simply Supported	Load-carrying capacity		clamped	Load-carrying capacity	
	$\bar{p}$	total load		$\bar{p}$	total load
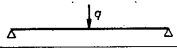		2π			4π
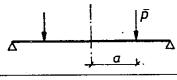	$\frac{1}{a(1-a)}$	$\frac{2\pi}{1-a}$	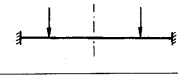	$\frac{2}{a(1-a)}$	$\frac{4\pi}{(1-a)}$
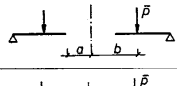	$\frac{1-a}{b(1-b)}$	$\frac{2\pi(1-a)}{(1-b)}$	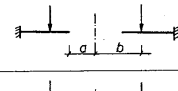	$\frac{2-a}{(1-b)b}$	$\frac{2\pi(2-a)}{(1-b)}$
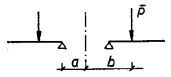	$\frac{(1-a)}{b(b-a)}$	$\frac{2\pi(1-a)}{(b-a)}$		$\frac{1}{(b-a)b}$	$\frac{2\pi}{(b-a)}$
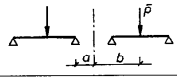	$\frac{1}{b}\left(1+\frac{b}{b-a}+\frac{1}{1-b}\right)$	$2\pi\left(1+\frac{b}{b-a}+\frac{1}{1-b}\right)$	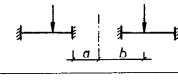	$\frac{2}{b-a}+\frac{2}{(1-b)}$	$2\pi\left(\frac{2b}{b-a}+\frac{2}{1-b}\right)$
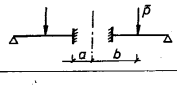	$\frac{2}{b-a}+\frac{1}{b(1-b)}$	$2\pi\left(\frac{2b}{b-a}+\frac{1}{1-b}\right)$	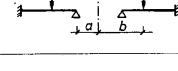	$\frac{1}{b}\left(1+\frac{b}{b-a}+\frac{2}{1-b}\right)$	$2\pi\left(1+\frac{b}{b-a}+\frac{2}{1-b}\right)$

Table 4.6

Bending moments and deflection rates for Johansen circular and annular plates under ring loads

Simply Supported	Bending moments and deflection rates		clamped	Bending moments and deflection rates	
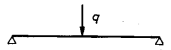	r	[0,1]	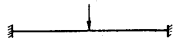	r	[0,1]
	m_r	0		m_r	-1
	m_θ	1		m_θ	1
	$\dot{w}$	$\dot{w}_0(1-r)$		$\dot{w}$	$\dot{w}_0(1-r)$
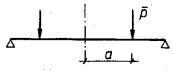	r	[0, a] [a, 1]	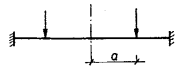	r	[0, a] [a, 1]
	m_r	1 $\quad \frac{a}{r}\cdot\frac{1-r}{1-a}$		m_r	1 $\quad 1-\frac{2}{1-a}\left(1-\frac{a}{r}\right)$
	m_θ	1 $\quad$ 1		m_θ	1 $\quad$ 1
	$\dot{w}$	$\dot{w}_0 \quad \frac{\dot{w}_0}{1-a}(1-r)$		$\dot{w}$	$\dot{w}_0 \quad \frac{\dot{w}_0}{(1-a)}(1-r)$
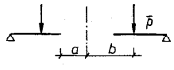	r	[a, b] [b, 1]	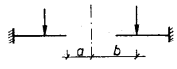	r	[a, b] [b, 1]
	m_r	$1-\frac{a}{r} \quad \frac{b-a}{1-b}\cdot\frac{1-r}{r}$		m_r	$1-\frac{a}{r} \quad 1+\frac{2b}{1-b}\cdot\frac{a}{r}\cdot\frac{1-r}{r}$
	m_θ	1 $\quad$ 1		m_θ	1 $\quad$ 1
	$\dot{w}$	$\dot{w}_0\frac{1-r}{1-a}$		$\dot{w}$	$\dot{w}_0\frac{1-r}{1-a}$

[70]

Table 4.6, contd

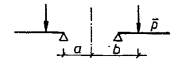	r	[a, b] [b, 1]	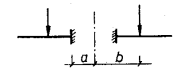	r	[a, b] [b, 1]
	m_r	$\frac{1-b}{b-a}\cdot\frac{r-a}{r} \quad \frac{1-r}{r}$		m_r	$\frac{1}{b-a}\cdot\frac{r-a}{r}-1 \quad \frac{1-r}{r}$
	m_θ	$-1 \quad -1$		m_θ	$-1 \quad -1$
	$\dot{w}$	$\dot{w}_0(r-a)$		$\dot{w}$	$\dot{w}_0(r-a)$
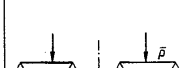	r	[a, b] [b, 1]	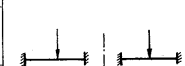	r	[a, b] [b, 1]
	m_r	$1-\frac{a}{b-a}\cdot\frac{b-r}{r} \quad \frac{b}{1-b}\cdot\frac{1-r}{r}$		m_r	$1-\frac{2a}{b-a}\cdot\frac{b-r}{r} \quad -1+\frac{2b}{1-b}\cdot\frac{1-r}{r}$
	m_θ	$-1 \quad 1$		m_θ	$-1 \quad 1$
	$\dot{w}$	$\dot{w}_0\frac{r-a}{b-a} \quad \dot{w}\frac{1-r}{1-b}$		$\dot{w}$	$\dot{w}\frac{r-a}{b-a} \quad \dot{w}\frac{1-r}{1-b}$
	r	[a, b] [b, 1]		r	[a, b] [b, 1]
	m_r	$1-\frac{2a}{b-a}\cdot\frac{b-r}{r} \quad \frac{b}{1-b}\cdot\frac{1-r}{r}$		m_r	$1-\frac{a}{b-a}\cdot\frac{b-r}{r} \quad -1+\frac{2b}{1-b}\cdot\frac{1-r}{r}$
	m_θ	$-1 \quad 1$		m_θ	$-1 \quad 1$
	$\dot{w}$	$\dot{w}_0\frac{r-a}{b-a} \quad \dot{w}_0\frac{1-r}{1-b}$		$\dot{w}$	$\dot{w}_0\frac{r-a}{b-a} \quad \dot{w}_0\frac{1-r}{1-b}$

[71]

4.6. Beam analogy for Johansen plates

The equilibrium equation for a beam subjected to a transverse load ${}^{b}p(r)$ and a distributed bending moment m are as follows:

$$\frac{d^{b}m}{dr} = {}^{b}s + m, \quad \frac{d^{b}s}{dr} = -{}^{b}p(r), \tag{4.79}$$

where ${}^{b}m$ and ${}^{b}s$ are the dimensionless bending moment and shear force, respectively. m stands for the bending moment uniformly applied to the whole length of beam and having opposite sing to that generated by the external load.

Comparison of the equations (4.79) and the equilibrium equations (4.5) for plates reveals that they are identical provided rm is treated as the bending moment ${}^{b}m$, the hoop moment m_{θ} as the distributed moment m, rs as the shear force ${}^{b}s$ and the load $rp(r)$ as the load ${}^{b}p(r)$ of the beam.

The above analogy, [51], enables the plate to be replaced by a substitute beam, provided the circumferential moment is constant, $m_{\theta} = \text{const}$. This is the case when, for instance, the stress profile coincides with the sides AB and DE of the Tresca yield hexagon, Fig. 4.3, or with the sides AB and DEF of Johansen yield square, Fig. 4.6.

To conclude, the substitute beam pattern of Fig. 4.8a applies to the annular or circular Johansen plates supported at outer edge, whereas the beam pattern of Fig. 4.8b is suitable for annular plates supported at inner edge. The collapse load can in both cases be calculated with the use of the boundary condition at the supported edge.

In a similar manner other substitute beam patterns may be adopted for plates with different support conditions such as supported along an arbitrarily situated ring or along both edges. The sense of an additional moment m depends in each case on the collapse mechanism of the plate. More detailed information on the subject can be found in [51].

To illustrate the procedure, consider an annular plate simply supported at outer edge and subjected to a load shown in Fig. 4.9a. The substitute beam pattern is depicted in Fig. 4.9b. The bending moment for the beam is

for $a \leqslant r \leqslant b$

$${}^{b}m = m(r-a) - \frac{pa(r-a)^2}{2} - \frac{pa(r-a)^3}{6} = r m_r(r), \tag{4.80}$$

$b \leqslant r \leqslant 1$

$${}^{b}m = m(r-a) - \frac{pa(r-a)^2}{2} - \frac{pa(r-a)^3}{6} - \bar{p}b(r-b) = r m_r(r). \tag{4.81}$$

Fig. 4.8. Substitute beam pattern for annular plate: (a) supported at outer edge, (b) supported at inner edge

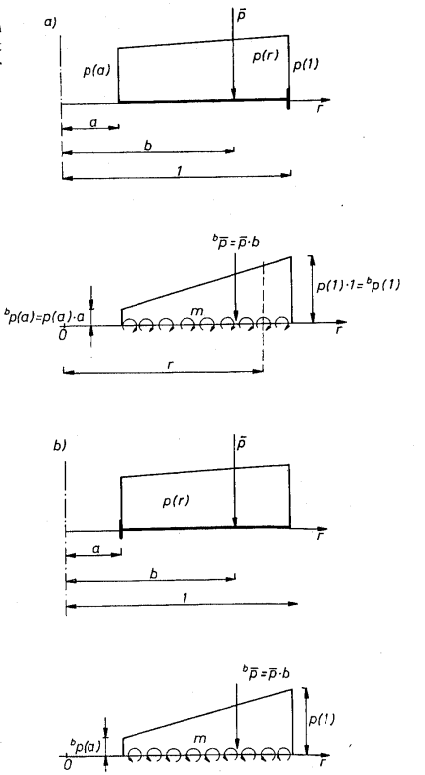

Since the bending moment at simple support must vanish, the following collapse load is obtained:

$$p = \frac{6\left(1 - \bar{p}b\,\dfrac{1-b}{1-a}\right)}{(1-a)(2a+1)}, \tag{4.82}$$

under the assumption that $m = 1$.

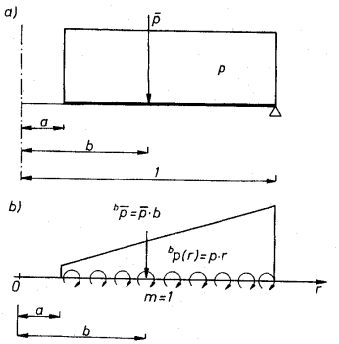

Fig. 4.9. Annular plate simply supported at outer edge: (a) support and load pattern of plate, (b) substitute beam pattern

When $\bar{p} = 0$ the above formula applies to the annular plate supporting a uniformly distributed load. The same result can be obtained in a different way, Table 4.3. It is worth of note that the beam method furnishes the generalized stress fields with no necessity to find the integration constants in the expressions given in Table 4.2.

4.7. Huber-Mises plates

Under rotationally symmetric conditions the Huber-Mises interaction condition is

$$m_r^2 - m_r m_\theta + m_\theta^2 - 1 = 0 \tag{4.83}$$

and represents an ellipse, Fig. 4.10.

Using this relation in the equilibrium requirements (4.5) the following nonlinear equation governing the bending moments at collapse is obtained:

$$\frac{dm_r}{dr} = \frac{1}{r}\left(\frac{1}{2}\left(-m_r \pm \sqrt{4 - 3m_r^2}\right) - \int p\rho d\rho + C\right). \tag{4.84}$$

This equation, in general, must be integrated numerically. Hinge circles can form for the stress states satisfying (4.11). It is found that $m_r = 2m_\theta$ must hold

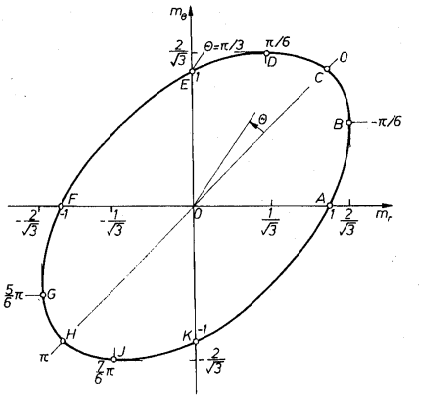

Fig. 4.10. Huber-Mises interaction ellipse for rotationally symmetric plates

for a hinge to form. The respective stress magnitudes are $m_r = \pm 2/\sqrt{3}$, $m_\theta = \pm 1/\sqrt{3}$, points B and G in Fig. 4.10.

The plastic potential flow law leads to the following components of the flow vector:

$$\dot{\kappa}_r = \nu(2m_r - m_\theta), \quad \dot{\kappa}_\theta = \nu(2m_\theta - m_r). \tag{4.85}$$

Contrary to the situation for the piece-wise interaction conditions, in the case of the Huber-Mises interaction condition the deflection velocity is uniquely coupled with the stress field,

$$r\dot{w}''(2m_\theta - m_r) - \dot{w}'(2m_r - m_\theta) = 0 \tag{4.86}$$

Let us change variables so as to satisfy the interaction condition identically,

$$m_r = \frac{2}{\sqrt{3}}\cos\left(\theta + \frac{\pi}{6}\right), \quad m_\theta = \frac{2}{\sqrt{3}}\cos\left(\theta - \frac{\pi}{6}\right). \tag{4.87}$$

At collapse the stress profile traces an arc of the ellipse, Fig. 4.10. Equations of equilibrium expressed in terms of the variable used in (4.87) take the form

$$r\frac{d\theta}{dr} = \frac{\varphi - \sin\theta}{\sin\left(\theta - \frac{\pi}{6}\right)}, \quad \varphi = -\frac{\sqrt{3}}{2}rs = \frac{\sqrt{3}}{2}\int p\rho d\rho, \tag{4.88}$$

the interaction condition being satisfied. When the range of θ is known, i.e. the stress profile is specified by the stress boundary conditions, this equation can be integrated for θ, and the collapse load can be evaluated.

The velocity field is governed by (4.86), which in view of (4.87) can be written as

$$r\dot{w}'' + \frac{\sin\left(\theta - \frac{\pi}{6}\right)}{\sin\left(\theta + \frac{\pi}{6}\right)}\dot{w}' = 0. \tag{4.89}$$

It can be concluded that the deflected surface is of a positive Gaussian curvature within the ranges $-\pi/6 \leqslant \theta \leqslant \pi/6$ and $5\pi/6 \leqslant \theta \leqslant 7\pi/6$, a negative curvature elsewhere, except the stress states where either $\dot{\kappa}_\theta$ or $\dot{\kappa}_r$ vanishes.

For the stress states represented by $\theta = n\pi \pm \pi/6$ either circles of contraflexure occur or the surface is developable. A plate deflects into a cone if $\dot{\kappa}_r = 0$, hence for the stress states represented in Fig. 4.10 by the points D and J we have:

$$m_r = \pm\frac{1}{\sqrt{3}}, \quad m_\theta = \pm\frac{2}{\sqrt{3}}, \quad \theta = n\pi + \frac{\pi}{6}. \tag{4.90}$$

As an example consider a simply supported plate loaded by a central concentrated load Q, [11], [24]. For the stress field the following form of (4.88) is obtained

$$\frac{1}{r}dr = \frac{1}{2}\frac{\sqrt{3}\sin\theta + \cos\theta}{\varphi - \sin\theta}d\theta, \quad \varphi = \frac{\sqrt{3}}{4\pi}q, \tag{4.91}$$

where q is defined in (4.1). Eventually the collapse load is found to be

$$q = 2\pi. \tag{4.92}$$

This load is associated with the stress field $m_r = 0, m_\theta = 1$ within $0 < r \leqslant 1$ with singularity at $r=0$. The stress state is represented by point E in Fig. 4.10, $\theta = \pi/3$.

From (4.89) it follows for the stress state $\theta = \pi/3$ that the deflection rate is

$$\dot{w} = \dot{w}_0(1 - \sqrt{r}), \quad \text{for } 0 \leqslant r \leqslant 1. \tag{4.93}$$

Collapse load for a downward loaded clamped plate is associated with the stress point G, Fig. 4.10, and its value is

$$q = \frac{4\pi}{\sqrt{3}}. \tag{4.94}$$

The stress field also has a singularity at $r=0$.

4.7.1. Numerical solutions, step-wise loading. For plates subjected to distributed loads numerical integration of Eq. (4.84) is needed. The results of a systematic search for the load-carrying capacity of circular and annular plates are given in [92]. A set of bending moment fields and collapse mechanisms for various loading and boundary conditions is given there. Previously available results [14], [24] were checked and supplemented.

We consider plates with the interaction surface (4.83) shown in Fig. 4.10. Equation (4.84) specifying the radial moment becomes

$$\frac{dm_r}{dr} = \frac{1}{r}\left(\frac{1}{2}\left(-m_r \pm \sqrt{4 - 3m_r^2}\right) + rs\right), \tag{4.95}$$

where

$$rs = -\mu\left\{\sum_1^{k-1}\int_{c_j}^{c_{j+1}} p_j(\rho)\,\rho d\rho + \int_{c_k}^{r} p_k(\rho)\,\rho d\rho + \sum_1^{l}\bar{p}_i b_i - \beta\frac{p^T}{2\pi}\right\}, \tag{4.96}$$

in which μ denotes the collapse load multiplier and μp^T stands for the total load acting on the plate in yielding, hence

$$p^T = 2\pi\left\{\sum_1^{m}\int_{c_j}^{c_{j+1}} p_j(\rho)\,\rho d\rho + \sum_1^{n}\bar{p}_i b_i\right\}. \tag{4.97}$$

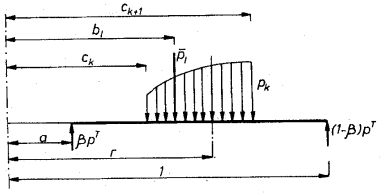

Fig. 4.11. Radial section of annular plate under step-wise loading

In Eq. (4.96) β denotes a parameter specifying the reaction at an inner support. The notation employed is defined in Fig. 4.11 representing a radial section of an annular plate under step-wise loading.

For statically determinate situations, $\beta = 0$ or $\beta = 1$, Eq. (4.95) can be integrated for the appropriate stress boundary conditions. Otherwise, the integration of Eq. (4.95) is accompanied by solving the equation governing the displacement velocity.

For the Huber-Mises interaction condition Eq. (4.12) takes the form

$$2r\dot{w}'' + \left(1 \mp \frac{3m_r}{\sqrt{4 - 3m_r^2}}\right) = 0 \tag{4.98}$$

since

$$m_\theta = \frac{1}{2}\left(m_r \pm \sqrt{4 - 3m_r^2}\right). \tag{4.99}$$

Its solution is

$$\dot{w} = C_1 \int_a^r \exp\left[\int_a^\rho \frac{1}{2t}\left(\pm \frac{3m_r}{\sqrt{4 - 3m_r^2}} - 1\right) dt\right] d\rho + C_2 \tag{4.100}$$

whereas C_1 and C_2 are to be determined from the kinematical boundary conditions. For statically indeterminate situations a missing condition for evaluating the reaction β entering Eq. (4.96) is that of changing the sign of circumferential curvature of the deflection velocity (4.100). Requiring

$$\dot{\kappa}_\theta = 0 \quad \text{thus} \quad \dot{w}' = 0, \tag{4.101}$$

one obtains $r = r^*$ such that $\dot{w}(r^*) = \dot{w}_0$ and

$$m_r(r^*) = \pm \frac{2}{\sqrt{3}}, \quad \frac{dm_r}{dr}\Big|_{r\,=\,r^*} = 0 \tag{4.102}$$

hence r^* is obtained from the equation

$$sr \mp \frac{1}{\sqrt{3}} = 0, \tag{4.103}$$

which specifies the radius for which the stress profile changes from the upper part of the interaction ellipse in Fig. 4.10 to the lower part *BAKJHG*.

A computer program was developed to yield numerical solutions to Eqs. (4.95) and (4.100). The flow chart and details of the program concerning the Huber-Mises interaction condition can be found in [85] and for an arbitrary nonlinear interaction condition in [90].

The load-carrying capacities for several cases of loading are given in Table 4.7. Moreover, Tables 4.8 and 4.9 contain the bending moments obtained from (4.84) and the deflection rates resulting from (4.86) for simply supported and clamped plates, respectively. In Fig. 4.12a characteristic diagrams of bending moments are shown.

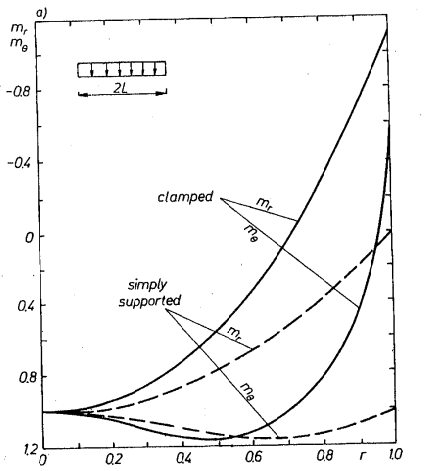

Fig. 4.12a. Characteristic diagrams for Huber-Mises circular plates – moment distribution

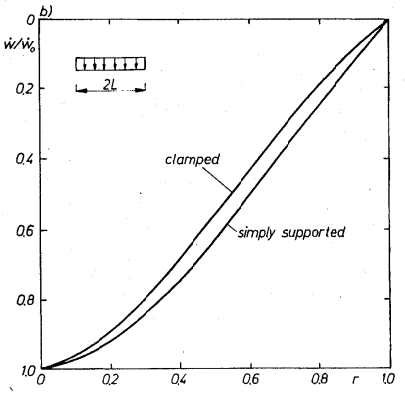

Fig. 4.12b. Characteristic diagrams for Huber-Mises circular plates — deflection rates

The deflection rates associated with the moments presented earlier are shown in Fig. 4.12b. It should be remarked that the deflected surface changes its Gaussian curvature at a certain radius. As it was already stated the contraflexure radii correspond to the stres state represented by point D on the interaction curve of Fig. 4.10.

The collapse loads for plates loaded at a part of their surface are given in Table 4.10. In all the cases considered the stress profile runs over the part $CDEFG$ of the interaction locus in Fig. 4.10.

For plates loaded by the ring of forces bending moment distributions are similar except that in the zone $0 \leqslant r \leqslant a$ a uniform flexure takes place, Fig. 4.13a. The respective deflection rates are given in Fig. 4.13b. A broken line shows the velocity field for a plate point-loaded at the centre.

The load-carrying capacities of annular plates are collected in Table 4.11. As an example of bending moment distribution in plates with openings the case of simply supported plate is presented in Fig. 4.14a where the bending moments are plotted. The stress profile coincides then with the line CDE in such a way as to meet the stress boundary conditions. All the points of the respective part of the Huber-Mises ellipse are attained twice.

If a plate is furnished with a rigid central boss the stress profile contains the point B of the interaction locus of Fig. 4.10 and runs up to the point E or G depending upon the boundary conditions at the outer circumference.

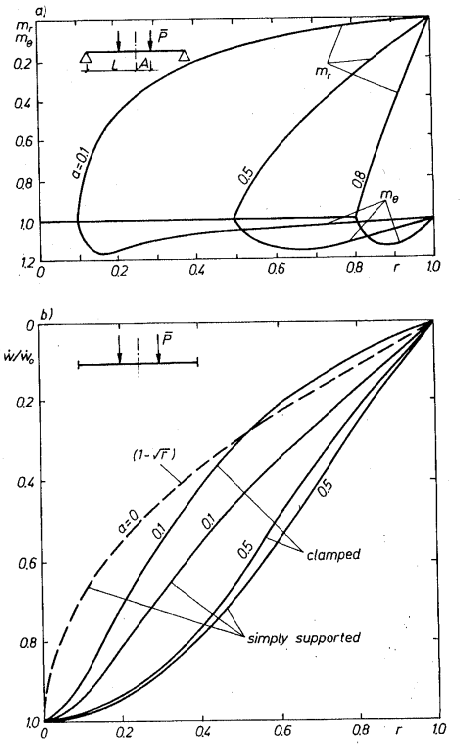

Fig. 4.13. Huber-Mises circular plates loaded by ring forces: (a) moment distribution, (b) deflection rates

For annular plates, supported or clamped at the inner circumference the corresponding stress profiles run over the part $CBAKJHG$ of the interaction curve in Fig. 4.10. The load-carrying capacities are given in Table 4.12. The examples of bending moments are shown in Fig. 4.14b. Further examples of moment fields can be found in [8], [14], [66].

To complete the presentation of annular plates we show a few results concerning statically indeterminate cases. Annular plates supported at both boundaries and uniformly loaded over the entire surface have the load-carrying capacities as given in Table 4.13.

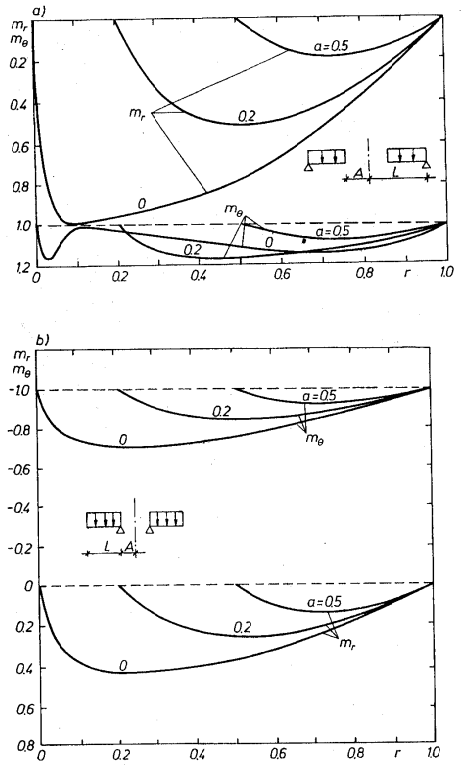

Fig. 4.14. Moment distribution in Huber-Mises plates simply supported (a) at outer edge, (b) at inner edge

The stress profile for such structures at collapse runs over a large part of the interaction curve (4.83) and involves both Eqs. (4.95). The stress régime changes at $r = r^*$, following from Eq. (4.103) and corresponding to the stress point B in Fig. 4.10. A dimensionless parameter β specifying the reaction is given in Table 4.13. Some typical bending moment distributions are shown in Fig. 4.15. More results regarding computational details as well as bending moment diagrams are given in [85], [92].

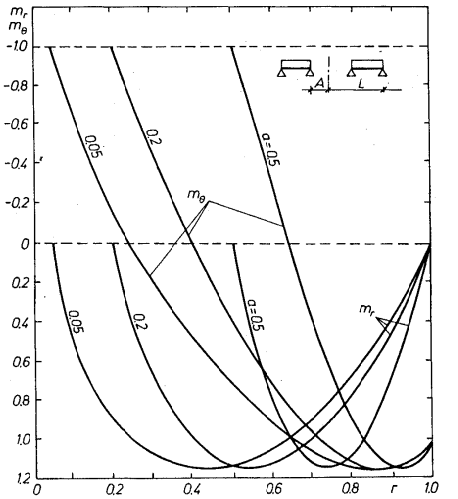

Fig. 4.15. Moment distribution in annular plate simply supported at both boundaries

Table 4.7

Load-carrying capacities for Huber-Mises circular plates

Load pattern	Load-carrying capacity			
	Simply supported		clamped	
	μ	total load	μ	total load
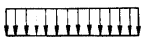	6.517	20.472	12.551	39.431
	13.074	13.691	24.316	25.463
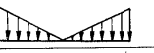	12.848	26.907	25.454	53.309
	9.322	14.643	17.515	27.511
	21.189	33.283	42.687	67.053

Bending moments and deflection rates for simply supported circular plates from Table 4.7

Loading		Bending moments and							
	r	0.000	0.050	0.100	0.150	0.20	0.25	0.30	0.35
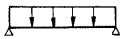 $\mu = 6.517$	m_r	1.000	0.998	0.992	0.981	0.967	0.947	0.924	0.896
	m_θ	1.000	1.002	1.008	1.017	1.030	1.045	1.061	1.078
	$\dot{w}/\dot{w}_0$	1.000	0.991	0.978	0.955	0.924	0.886	0.841	0.792
 $\mu = 13.074$	m_r	1.000	0.995	0.984	0.966	0.940	0.908	0.869	0.825
	m_θ	1.000	1.004	1.015	1.031	1.051	1.072	1.093	1.112
	$\dot{w}/\dot{w}_0$	1.000	0.989	0.972	0.945	0.909	0.865	0.816	0.762
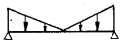 $\mu = 12.848$	m_r	1.000	1.000	0.999	0.998	0.993	0.987	0.977	0.963
	m_θ	1.000	1.000	1.001	1.003	1.007	1.013	1.022	1.034
	$\dot{w}/\dot{w}_0$	1.000	0.993	0.983	0.965	0.940	0.909	0.870	0.826
 $\mu = 9.322$	m_r	1.000	0.997	0.988	0.974	0.953	0.926	0.894	0.855
	m_θ	1.000	1.003	1.011	1.025	1.041	1.060	1.080	1.100
	$\dot{w}/\dot{w}_0$	1.000	0.990	0.975	0.949	0.915	0.873	0.826	0.773
 $\mu = 21.189$	m_r	1.000	1.000	1.000	0.999	0.999	0.997	0.993	0.987
	m_θ	1.000	1.000	1.000	1.001	1.001	1.003	1.008	1.013
	$\dot{w}/\dot{w}_0$	1.000	0.994	0.985	0.969	0.947	0.919	0.884	0.844

Bending moments and deflection rates for clamped circular plates from Table 4.7

Loading		Bending moments and							
	r	0.000	0.050	0.100	0.150	0.20	0.25	0.30	0.35
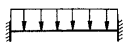 $\mu = 12.551$	m_r	1.000	0.996	0.984	0.964	0.935	0.898	0.850	0.793
	m_θ	1.000	1.004	1.015	1.033	1.054	1.078	1.102	1.123
	$\dot{w}/\dot{w}_0$	1.000	0.988	0.970	0.939	0.899	0.852	0.798	0.740
 $\mu = 24.316$	m_r	1.000	0.992	0.971	0.935	0.886	0.824	0.749	0.661
	m_θ	1.000	1.008	1.027	1.054	1.084	1.113	1.136	1.150
	$\dot{w}/\dot{w}_0$	1.000	0.984	0.960	0.923	0.874	0.819	0.758	0.696
 $\mu = 25.454$	m_r	1.000	1.000	0.998	0.994	0.986	0.973	0.953	0.925
	m_θ	1.000	1.000	1.002	1.006	1.013	1.025	1.041	1.061
	$\dot{w}/\dot{w}_0$	1.000	0.992	0.979	0.958	0.928	0.890	0.846	0.795
 $\mu = 17.515$	m_r	1.000	0.994	0.978	0.950	0.910	0.858	0.794	0.717
	m_θ	1.000	1.006	1.021	1.044	1.071	1.098	1.123	1.142
	$\dot{w}/\dot{w}_0$	1.000	0.986	0.964	0.930	0.885	0.832	0.774	0.712
 $\mu = 42.687$	m_r	1.000	1.000	1.000	0.999	0.997	0.993	0.986	0.973
	m_θ	1.000	1.000	1.000	1.001	1.003	1.007	1.014	1.025
	$\dot{w}/\dot{w}_0$	1.000	0.993	0.983	0.965	0.940	0.908	0.869	0.823

Table 4.8

deflection rates												
0.40	0.45	0.50	0.55	0.60	0.65	0.70	0.75	0.80	0.85	0.90	0.95	1.00
0.862	0.823	0.779	0.730	0.675	0.613	0.546	0.472	0.392	0.304	0.210	0.115	0.000
1.096	1.112	1.127	1.139	1.148	1.153	1.154	1.148	1.136	1.116	1.088	1.052	1.000
0.738	0.681	0.621	0.559	0.497	0.433	0.370	0.306	0.243	0.181	0.119	0.059	0.000
0.776	0.722	0.663	0.602	0.537	0.469	0.401	0.331	0.261	0.193	0.126	0.061	0.000
1.129	1.141	1.150	1.154	1.154	1.148	1.138	1.124	1.105	1.082	1.057	1.029	1.000
0.705	0.646	0.586	0.525	0.464	0.403	0.342	0.282	0.224	0.166	0.109	0.054	0.000
0.944	0.920	0.889	0.851	0.805	0.749	0.683	0.605	0.515	0.410	0.219	0.154	0.000
1.048	1.064	1.083	1.101	1.120	1.136	1.148	1.154	1.153	1.140	1.113	1.068	1.000
0.777	0.722	0.664	0.602	0.537	0.471	0.404	0.335	0.267	0.199	0.132	0.065	0.000
0.810	0.760	0.705	0.645	0.580	0.511	0.440	0.366	0.291	0.216	0.141	0.069	0.000
1.118	1.133	1.145	1.152	1.155	1.152	1.145	1.131	1.113	1.090	1.063	1.033	1.000
0.717	0.658	0.598	0.537	0.475	0.413	0.351	0.290	0.230	0.170	0.112	0.056	0.000
0.977	0.963	0.944	0.917	0.882	0.836	0.776	0.704	0.612	0.499	0.362	0.197	0.000
1.021	1.033	1.048	1.066	1.086	1.108	1.128	1.145	1.154	1.151	1.131	1.084	1.000
0.798	0.745	0.689	0.628	0.564	0.497	0.427	0.356	0.284	0.212	0.141	0.070	0.000

Table 4.9

deflection rates												
0.40	0.45	0.50	0.55	0.60	0.65	0.70	0.75	0.80	0.85	0.90	0.95	1.00
0.725	0.646	0.555	0.452	0.336	0.206	0.063	−0.095	−0.269	−0.459	−0.668	−0.898	−1.155
1.141	1.152	1.154	1.146	1.125	1.087	1.030	0.949	0.838	0.688	0.482	0.180	−0.576
0.679	0.616	0.553	0.490	0.428	0.367	0.307	0.250	0.194	0.141	0.091	0.044	0.000
0.562	0.453	0.334	0.206	0.071	−0.071	−0.218	−0.369	−0.552	−0.678	−0.835	−0.993	−1.155
1.155	1.146	1.124	1.087	1.036	0.963	0.873	0.764	0.631	0.471	0.274	0.015	−0.576
0.632	0.568	0.505	0.443	0.383	0.326	0.271	0.218	0.168	0.121	0.077	0.037	0.000
0.887	0.838	0.775	0.696	0.599	0.482	0.342	0.177	−0.016	−0.241	−0.501	−0.803	−1.155
1.084	1.107	1.129	1.146	1.154	1.150	1.126	1.077	0.992	0.857	0.650	0.317	−0.576
0.739	0.678	0.616	0.551	0.485	0.419	0.354	0.289	0.227	0.166	0.107	0.052	0.000
0.628	0.526	0.413	0.289	0.154	0.011	−0.141	−0.300	−0.464	−0.632	−0.803	−0.977	−1.155
1.153	1.153	1.140	1.113	1.068	1.005	0.922	0.816	0.684	0.521	0.317	0.045	−0.576
0.650	0.585	0.522	0.459	0.399	0.339	0.283	0.228	0.177	0.127	0.081	0.039	0.000
0.954	0.926	0.885	0.831	0.757	0.661	0.538	0.381	0.186	−0.057	−0.352	−0.714	−1.155
1.041	1.061	1.085	1.110	1.134	1.150	1.154	1.135	1.080	0.971	0.776	0.429	−0.576
0.772	0.715	0.654	0.590	0.523	0.455	0.386	0.317	0.250	0.183	0.119	0.058	0.000

Table 4.10

Collapse loads for Huber-Mises circular plates under various loads

Loading		Collapse load										
	a	0.00	0.10	0.20	0.30	0.40	0.50	0.60	0.70	0.80	0.90	1.00
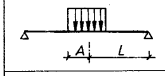	μ	—	226.500	61.687	29.875	18.375	12.969	10.016	8.281	7.258	6.703	6.517
	p^T	2π	7.115	7.751	8.446	9.236	10.185	11.327	12.747	14.592	17.056	20.473
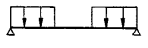	μ	6.517	6.680	7.188	8.156	9.766	12.547	17.656	28.531	58.750	216.189	—
	p^T	20.473	20.775	21.678	23.316	25.771	29.562	35.498	45.711	66.442	129.044	—
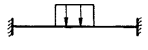	μ	—	349.437	100.594	50.625	32.141	23.266	18.367	15.484	13.766	12.844	12.551
	p^T	$4\pi/\sqrt{3}$	10.997	12.640	14.313	16.155	18.272	20.772	23.835	27.677	32.683	39.429
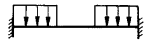	μ	12.551	12.898	14.004	16.031	19.453	25.312	36.094	59.094	123.250	459.606	—
	p^T	39.429	40.113	42.233	45.829	51.334	59.698	72.569	94.678	138.388	274.340	—
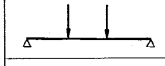	μ	—	11.766	6.648	5.055	4.398	4.195	4.336	4.906	6.375	11.219	—
	p^T	2π	7.392	8.354	9.528	11.053	13.178	16.346	21.577	32.043	63.440	—
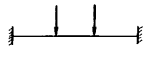	μ	—	18.676	11.262	8.971	8.109	7.984	8.492	9.875	13.152	23.680	—
	p^T	$4\pi/\sqrt{3}$	11.734	14.152	16.909	20.375	25.082	32.013	43.431	66.107	133.903	—

[98]

Table 4.11

Collapse loads for Huber-Mises annular plates

Loading		Collapse load										
	a	0.00	0.10	0.20	0.30	0.40	0.50	0.60	0.70	0.80	0.90	0.95
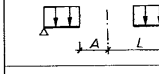	μ	6.515	6.270	5.984	5.875	5.984	6.359	7.109	8.594	11.750	21.625	41.557
	p^T	20.468	17.924	18.046	16.795	16.167	14.982	14.293	13.769	13.288	13.907	12.729
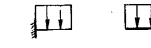	μ	12.550	12.352	12.504	13.355	15.164	18.492	24.781	38.125	74.813	262.250	984.058
	p^T	39.426	38.416	37.910	38.178	40.015	43.569	49.824	61.082	84.609	156.533	301.422
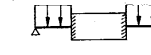	μ	6.516	6.700	7.270	8.326	10.112	13.178	18.853	30.979	65.005	244.231	949.211
	p^T	20.470	20.838	21.926	23.802	26.685	31.049	37.906	49.566	73.518	145.782	290.748
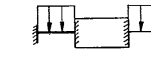	μ	12.551	12.933	14.106	16.257	19.870	26.044	37.437	61.764	129.893	488.600	1899.054
	p^T	39.429	40.224	42.542	46.476	52.435	61.364	75.271	98.959	146.905	291.647	581.690
	μ	—	11.931	6.828	5.256	4.634	4.478	4.692	5.394	7.123	12.743	24.225
	p^T	—	7.496	8.580	9.907	11.646	14.068	17.688	23.724	35.804	72.060	144.599
	μ	—	18.961	11.517	9.232	8.395	8.315	8.893	10.399	13.929	25.221	48.220
	p^T	—	11.913	14.427	17.402	21.098	26.122	33.523	45.737	70.014	142.621	287.827

[81]

Table 4.12

Collapse loads for Huber-Mises annular plates supported at inner edge

[88]

Loading and support conditions	Collapse load											
	a	0.05	0.1	0.2	0.3	0.4	0.5	0.6	0.7	0.8	0.9	0.95
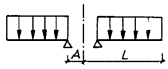	μ	2.620	2.763	3.061	3.417	3.891	4.555	5.531	7.211	10.547	20.625	40.503
	p^T	8.209	8.593	9.232	9.769	10.268	10.732	11.121	11.554	11.928	12.311	12.406
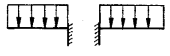	μ	3.025	3.437	4.359	5.619	7.484	10.531	16.039	27.758	60.859	236.875	935.722
	p^T	9.481	10.690	13.146	16.064	19.750	24.813	32.248	44.474	68.830	141.339	286.616
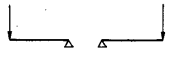	μ	1	1	1	1	1	1	1	1	1	1	1
	p^T	2π	2π	2π	2π	2π	2π	2π	2π	2π	2π	2π
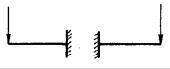	μ	1.112	1.193	1.366	1.577	1.854	2.238	2.815	3.776	5.698	11.469	23.015
	p^T	6.986	7.496	8.580	9.907	11.647	14.065	17.689	23.725	35.802	72.062	144.606

Table 4.13

Collapse loads for Huber-Mises annular plates supported at both boundaries

[68]

Loading and support conditions	Collapse load										
	a	0.05	0.1	0.2	0.3	0.4	0.5	0.6	0.7	0.8	0.9
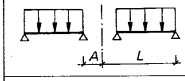	μ	13.812	15.252	18.692	23.531	30.881	42.833	64.767	111.651	243.712	946.630
	p^T	43.283	47.436	56.692	67.272	81.493	100.923	130.222	178.889	275.632	565.046
	β	0.268	0.293	0.333	0.366	0.393	0.418	0.438	0.456	0.473	0.487
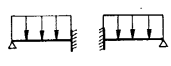	μ	15.263	17.434	22.424	29.280	39.653	56.581	87.543	153.961	343.071	1359.593
	p^T	47.829	54.223	67.629	83.707	104.642	133.316	176.016	246.678	388.004	811.545
	β	0.298	0.333	0.368	0.427	0.460	0.489	0.513	0.535	0.554	0.571
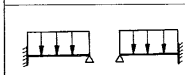	μ	21.174	23.184	28.023	34.999	45.635	63.229	95.040	163.617	356.662	1382.386
	p^T	66.353	72.106	84.515	100.057	120.428	148.980	191.089	262.149	403.375	825.150
	β	0.182	0.206	0.245	0.277	0.304	0.328	0.350	0.368	0.385	0.401
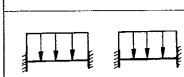	μ	22.947	25.900	32.709	42.174	56.381	79.916	122.846	214.653	475.674	1873.782
	p^T	71.910	80.554	98.648	120.569	148.786	188.298	246.997	343.920	537.975	1118.465
	β	0.219	0.242	0.293	0.334	0.368	0.397	0.423	0.446	0.466	0.484

CHAPTER 5

BOUNDING TECHNIQUES

5.1. Upper bound

An upper bound to the collapse load is obtained from (3.65). The rate of external work at collapse is not smaller than the rate of internal work done on a considered collapse mode. In selecting admissible fields we are guided by elastic solutions, by experimental observations or by the complete solutions of similar loading cases dealt with under different interaction conditions. The computational side of the problem should be kept as simple as possible in order not to loose the essential advantages of bounding techniques.

5.1.1 Continuous deformation mode. We consider a simply supported, circular, uniformly loaded plate. We shall seek an upper bound to the collapse load in the case of Huber-Mises interaction condition, assuming a continuous velocity field satisfying the conditions

$$\dot{w}(0) = \dot{w}_0, \ \dot{w}'(0) = 0 \tag{5.1}$$

in the polar coordinate system. A velocity field

$$\dot{w} = \dot{w}_0 (1 - r^2) \tag{5.2}$$

satisfies the kinematical requirements (5.1) and is twice continuously differentiable so that no hinge appears. Once the velocity field is assumed both the internal and external rates of work can be computed. Expressing (3.69) in terms of polar coordinates one obtains

$$\mu_k = \frac{2}{\sqrt{3}} \frac{\int_0^1 \sqrt{\dot{w}''^2 + \frac{1}{r}\dot{w}'\dot{w}'' + \frac{1}{r^2}\dot{w}'^2}\, rdr}{\int_0^1 \dot{w} r dr} = \frac{2}{\sqrt{3}} \frac{2\sqrt{3}\int_0^1 rdr}{\int_0^1 (1-r^2) rdr} = 8. \tag{5.3}$$

It is worthwhile to remark that for the considered collapse mode (5.2) the

curvatures are $\dot{w}'' = \dot{w}'/r = -2\dot{w}_0$. Therefore the associated stress state on the interaction condition is represented by the point C: $m_r = m_\theta = 1$ on the yield curve of Fig. 4.10.

Evidently this moment field does not satisfy the stress boundary condition $m_r(1) = 0$, and therefore it is not statically admissible. The collapse load multiplier $\mu_k = 8$ obtained in (5.3) is larger than the respective one corresponding to the exact solution $\mu_u = 6.517$, Table 4.7.

Since a choice of the collapse mode is arbitrary, except that the kinematical admissibility conditions must be satisfied, we take the velocity field

$$\dot{w} = \dot{w}_0 (1 - r). \tag{5.4}$$

Hence $\dot{w}'' = 0$, $\dot{w}'/r = -\dot{w}_0/r$ and Eq. (5.3) gives in this case a better upper bound

$$\mu_k = \frac{2}{\sqrt{3}} \frac{\int_0^1 dr}{\int_0^1 (1-r) rdr} = \frac{12}{\sqrt{3}} = 6.928. \tag{5.5}$$

The associated stress field is found from the plastic potential flow law. For the collapse mode (5.4) $\dot{\kappa}_r = -\dot{w}'' = 0$, $\dot{\kappa}_\theta = -\dot{w}'/r = \dot{w}_0/r$ and therefore the corresponding stress state is represented on the interaction ellipse of Fig. 4.10 by the point D: $m_r = 1/\sqrt{3}$, $m_\theta = 2/\sqrt{3}$ and the stress boundary conditions cannot be met.

The computational procedure is similar for any other interaction surface, except that the internal dissipation is expressed by a different formula.

Let us assume that the collapse velocity field (5.2) applies to a Tresca plate. Eq. (3.70) represents then the rate of internal work. The kinematically admissible load multiplier can be calculated directly from (3.66) and becomes

$$\mu_k = \frac{\int_0^1 (m_r\dot{\kappa}_r + m_\theta\dot{\kappa}_\theta) rdr}{\int_0^1 \dot{w}_0 (1-r^2) rdr} = \frac{4\int_0^1 rdr}{\int_0^1 (1-r^2) rdr} = 8 \tag{5.6}$$

since $\dot{\kappa}_r = \dot{\kappa}_\theta = 2\dot{w}_0$ and therefore the corresponding stress régime is $m_r = m_\theta = 1$ throughout the plate, the same as in the case of a Huber-Mises

plate. The strain rate vector falls within the fan admitted by the generalized plastic potential flow law for the point A of the interaction hexagon of Fig. 4.3.

Consequently we apply the collapse mechanism (5.4) to a Tresca plate. Since $\dot{\kappa}_r = 0$ and $\dot{\kappa}_\theta = \dot{w}_0/r$ the kinematically admissible load multiplier can be calculated from (3.67) with (3.70) and becomes

$$\mu_k = \frac{\frac{1}{2}\int_0^1 (|\dot{\kappa}_r| + |\dot{\kappa}_\theta| + |\dot{\kappa}_r + \dot{\kappa}_\theta|)\, r dr}{\int_0^1 (1-r)\, r dr} = 6. \tag{5.7}$$

The corresponding moment field represented on the interaction polygon of Fig. 4.3 by the line AB,

$$m_r = 1 - r^2, \quad m_\theta = 1, \tag{5.8}$$

satisfies the stress boundary conditions: $m_r(0) = 1$, $m_r(1) = 0$ and the equilibrium equations (4.5). Then the load multiplier (5.7) corresponds to the exact solution for Tresca plate,

$$\mu_u = 6. \tag{5.9}$$

5.1.2. Collapse mode with discontinuities. An application of the limit analysis theorems to the collapse load evaluation when the exact solution is not known will be made for a rectangular plate.

The plate is uniformly loaded and simply supported on the periphery. The supports allow the corners to lift under downward pressure $p = \mu$. A plate quarter is shown in Fig. 5.1.

We consider a kinematically admissible velocity field generated by planes rotating about certain lines and intersecting along hinge lines, i.e. the lines of sudden change of slope.

No energy is dissipated outside the hinges since $\dot{\kappa}_{ij} = 0$ in flat zones. The yield line pattern, specified to within a single parameter ξ, is shown in Fig. 5.1a. The best upper bound will be obtained requiring that $d\mu/d\xi = 0$. Dimensionless deflection velocities in the respective zones *1*, *2* and *3* in the figure are

$$\dot{w}_1 = \dot{w}_0 (1-x), \; \dot{w}_2 = \dot{w}_0 \left(1 - \frac{x+y}{1+\xi}\right), \; \dot{w}_3 = \dot{w}_0 (1-y). \tag{5.10}$$

The velocity field is referred to the coordinate system marked in Fig. 5.1. The kinematical boundary conditions

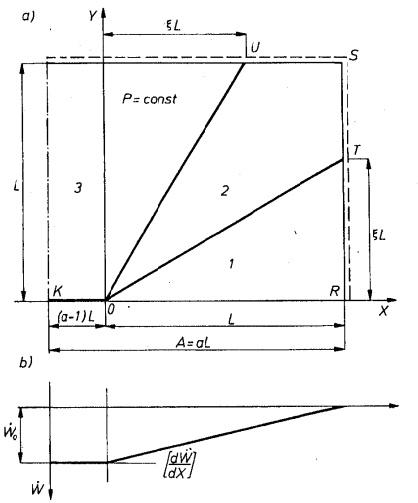

Fig. 5.1. Simply supported and uniformly loaded rectangular plate: (a) yield line pattern, (b) deflection rate

$$\dot{w} = 0 \text{ for } (a-1) \leqslant x \leqslant \xi, \; y = 1,$$
$$\dot{w} = 0 \text{ for } 0 \leqslant y \leqslant \xi, \; x = 1, \tag{5.11}$$

are satisfied by (5.10). The corner zone *UST* lifts up as it is not restrained against upward movement.

Across the line separating the zone *1* and *2* the following discontinuities in slope occur

$$\left[\frac{\partial \dot{w}}{\partial x}\right] = \frac{\dot{w}_0}{1+\xi}, \quad \left[\frac{\partial \dot{w}}{\partial y}\right] = \frac{\dot{w}_0 \xi}{1+\xi}. \tag{5.12}$$

The total rotations about the hinge lines and the lengths of respective hinges are

$$\Phi_{OT} = \Phi_{OU} = \dot{w}_0 \frac{\sqrt{1+\xi^2}}{1+\xi}, \quad \Phi_{OK} = \dot{w}_0, \tag{5.13}$$

$$l_{OT} = l_{OU} = \sqrt{1+\xi^2}, \quad l_{OK} = a-1. \tag{5.14}$$

5.2. Lower bound

In order to find a lower bound on the collapse load a stress field has to be found in equilibrium with the external loads and such that the interaction condition is not violated.

We consider a Huber-Mises plate of the preceding section. The stress boundary conditions are

$$m_r(1) = 0, \quad s(0) = 0 \Rightarrow m_r'(0) = 0. \tag{5.21}$$

As suggested by the elastic solution the stress field is assumed in the form

$$m_r = \mu m_r^0 = \mu\alpha(1-r^2), \quad m_\vartheta = \mu m_\vartheta^0 = \mu\alpha(1-\beta r^2). \tag{5.22}$$

It satisfies the requirements (5.21), [56]. Equilibrium equations (4.5), when putting $\mu=p$, result in the following relation between the multipliers α and β:

$$2\alpha(3-\beta) = 1 \tag{5.23}$$

for the entire range of $0 \leqslant r \leqslant 1$. The stress field (5.22), now specified to within a single multiplier, must be substituted into the interaction condition. The most stressed section has then to be found and the requirement that the stress vector for this region stays within the interaction surface furnishes a lower bound multiplier.

The condition (3.75) becomes in the case of the Huber-Mises interaction surface

$$\mu_s = \frac{1}{\max\sqrt{(m_r^0)^2 - m_r^0 m_\vartheta^0 + (m_\vartheta^0)^2}} = \\ = \frac{1}{\alpha}\frac{1}{\max\sqrt{1-r^2(1+\beta)+r^4(1-\beta+\beta^2)}}. \tag{5.24}$$

The denominator attains its maximum value at $r = 1$ and $r = 0$ for $\beta = 0$. Hence from (5.23)

$$\mu = \frac{1}{\alpha} = 6 \tag{5.25}$$

and the associated statically admissible stress field is

$$m_r = 1 - r^2, \quad m_\vartheta = 1. \tag{5.26}$$

The corresponding stress profile is therefore that of the solution for a Tresca plate and lies within the Huber-Mises ellipse, touching it in the stress points corresponding to the plate centre and the plate boundary. This is marked by the straight line AB in Fig. 5.3.

The collapse load for a Huber-Mises plate is therefore contained within the limits given by (5.5) and (5.25)

$$6 \leqslant \mu_u \leqslant \frac{2}{\sqrt{3}}6 = 6.928. \tag{5.27}$$

The correct value corresponding to the complete solution is $\mu_u = 6.517$, Table 4.7. To bound the collapse load for a rectangular plate of Fig. 5.1 from below we select the following stress field referred to the X,Y – coordinate system with the origin at the plate centre, point K,

$$m_x = 1 - \frac{x^2}{a^2}, \quad m_y = 1 - y^2, \quad m_{xy} = Cxy. \tag{5.28}$$

The stress field (5.28) satisfies the stress boundary conditions

$$m_x(a,y) = 0, \quad m_y(x,1) = 0. \tag{5.29}$$

To be statically admissible the stress field (5.28) must satisfy the equilibrium equation (3.13). For $\mu = p =$ constant it is necessary that

$$C = 1 + \frac{1}{a^2} - \frac{\mu}{2}. \tag{5.30}$$

In order to find a statically admissible load multiplier μ_s the stress field (5.28) under the condition (5.29) has to be substituted into a chosen interaction condition. For the Huber-Mises condition (3.18) we obtain the following inequality

$$m_x^2 + m_x m_y + m_y^2 + 3m_{xy}^2 = \\ = 1 - \frac{x^2}{a^2} + \frac{x^4}{a^4} - y^2 + y^4 + x^2y^2\left(3\left(1 + \frac{1}{a^2} - \frac{\mu}{2}\right)^2 - \frac{1}{a^2}\right) \leqslant 1. \tag{5.31}$$

The equality sign is valid for $x = y = 0$ and at the corner $S(a,1)$, providing that in the latter case the expression in the square bracket vanishes. This requirement leads to the best lower bound possible within the considered class of stress field (5.28). The result

$$\mu_s = 2\left(1 + \frac{1}{a^2} + \frac{1}{a\sqrt{3}}\right) \tag{5.32}$$

is plotted in Fig. 5.2, curve b.

The assumed distribution of moments (5.28) produces yielding at isolated points only, namely at the plate centre K and at the corners S, Fig. 5.1. The computed load-carrying capacity obviously underestimates the real one.

A better estimate can be obtained using power series expressions for the moments.

Several solutions regarding lower bounds can be found in [81], [93].

5.3. Bounding through inscribed and circumscribed interaction loci

Another bounding procedure employs exact solutions for the interaction surfaces inscribing and circumscribing the actual interaction surfaces, as specified in (2.61).

Since the Tresca hexagon lies inside the Huber-Mises ellipse the exact solution for the Tresca plate represents a lower bound to the collapse load for a Huber-Mises plate. Similarly, the exact solution for the maximum reduced stress interaction condition which circumscribes the Huber-Mises curve gives an upper bound for a Huber-Mises plate, Fig. 5.3.

Consider for example a simply supported circular plate under uniform pressure. According to (5.8) and (4.27) the collapse load associated with any interaction condition between the Tresca interaction condition and that of maximum reduced stress is necessarily contained within the bounds

$$6 \leqslant \mu_u \leqslant 6.852. \tag{5.33}$$

The collapse load for a Huber-Mises plate falls well into the range in the case of simply supported plate, solid lines AB in Fig. 5.3.

The stress profiles for exact solutions of a clamped plate indicate the solid lines ABC in Fig. 5.3.

5.4. Remarks on mathematical programming techniques

For plates of arbitrary shape the analytical solutions can be obtained only for a few special cases of loading and support conditions. That is why the numerical methods remain to be an effective tool for solving problems of limit analysis for plates.

The correspondence between the static and kinematic theorems of limit analysis and the duality theorems of the mathematical programming provides useful methods to obtain numerical solutions of the limit analysis, [4], [5]. Depending on linearity or nonlinearity of an interaction condition, either linear or nonlinear mathematical programming is to be used.

The first attempt at posing a limite analysis plate problem in mathematical programming form was made in [37]. in which the finite difference method of discretization of the plate was used. This procedure was extended in [4].

Recently the finite difference method of discretization has been used to a lesser extent.

The most common method today is the finite element method. An important advantage of that method is not only its flexibility with regard to the boundary conditions but a possibility to obtain truly admissible stress or displacement rate fields as well.

Mathematical programming with the use of the FEM of discretization to obtain upper and lower bounds of limit analysis of plates was first employed by Hodge and Belytschko, [21], [22].

Since that time many authors have been applying mathematical programming to the limit analysis of structures discretized by finite elements. Some of these works were related to plates in bending.

Strictly speaking, a problem of limit analysis formulated for a plate of arbitrary shape and loading is always a nonlinear programming problem. The reason is the nonlinearity of the yield condition with respect to the bending and twisting moments (recall that even the Tresca condition becomes linear in terms of principal moments).

However, the majority of numerical results was obtained by means of the linear programming approach, [1], [2], [6], [10], [46]. Adopting a piecewise linear approximation of the yield surface one obtains a mathematical programming problem that has many constraints and unknowns but still remains linear. Since computer packages exist that solve very large linear programming problems, the ultimate loads of plates can be efficiently found in that way.

On the other hand, the efficiency of existing nonlinear programming solvers diminishes rapidly with increasing dimension of the problem. This is probably why the pioneering work of Hodge and Belytschko has not found many followers, [5], [7], [60].

CHAPTER 6

NONHOMOGENEOUS AND ORTHOTROPIC PLATES

6.1. Nonhomogeneous plates

In nonhomogeneous plates the ultimate moment varies with the coordinates of the middle surface. The variation results either from the variable thickness of a plate or from variation of the material yield point, non-uniform reinforcement etc.

For a rotationally symmetric plastic nonhomogeneity the interaction condition takes the form

$$f(m_r, m_\theta) - m_0(r) = 0. \tag{6.1}$$

The interaction locus varies in size, stepwise or continuously. The equilibrium equations (4.5) and the flow law (4.7) remain unchanged.

As an example let us consider a circular, simply supported and uniformly loaded plate made of a Tresca material composed of two concentric annuli of different mechanical properties, Fig. 6.1.

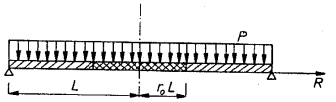

Fig. 6.1. Circular plate composed of two concentric parts with different ultimate moments

The jump in mechanical properties may be caused by a jump in plate thickness or by a change of material properties. Depending on the values of nonhomogeneity and division parameters there exist two solutions for a plate with a stronger central part and four solutions for a plate with a weak internal part, as it was obtained in [35].

Analyse a plate with a stronger central part, so that the Tresca condition is

$$f = \sup(|m_r|, |m_\theta|, |m_r - m_\theta|) = \begin{cases} 1, & 0 \leqslant r \leqslant r_0, \\ \eta, & r_0 \leqslant r \leqslant 1. \end{cases} \tag{6.2}$$

and $\eta < 1$ as shown in Fig. 6.2. The boundary and continuity requirements are

$$m_r(1) = 0, \quad [m_r(r_0)] = 0, \quad m_r(0) = m_\theta(0), \tag{6.3}$$
$$\dot{w}(0) = \dot{w}_0, \quad \dot{w}(1) = 0.$$

Two solutions are possible, corresponding to total or partial yielding, depending on the degree η of plastic nonhomogeneity.

In the first case of the total yielding we assume that the stress profile corresponds to sides $A'B'$ and AB in Fig. 6.2a, solid lines.

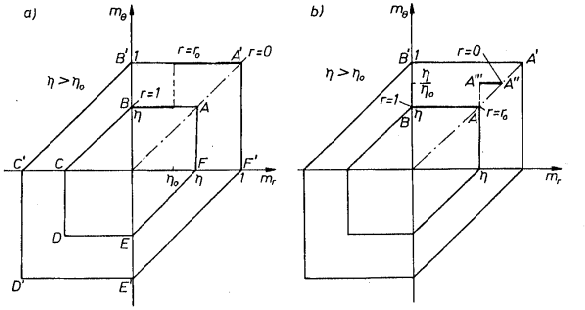

Fig. 6.2. Stress profiles for nonhomogeneous simply supported circular plate with a stronger central part: (a) total yielding, (b) partial yielding

There is an admissible jump in m_θ at r_0, namely $[m_\theta(r)] = 1-\eta$. Integrating the equilibrium equations (4.5) and taking into account the conditions (6.3) we obtain

$$m_r(1) = -r^2(\eta + r_0(1-\eta)) + \begin{cases} 1, & 0 \leqslant r \leqslant r_0, \\ \eta + \dfrac{r_0}{r}(1-\eta), & r_0 \leqslant r \leqslant 1 \end{cases} \tag{6.4}$$

and the limit load is found to be

$$p = 6(\eta + r_0(1-\eta)). \tag{6.5}$$

Since $\dot{\kappa}_r = 0$ is satisfied throughout the stress profile the deflected surface is a cone

$$\dot{w} = \dot{w}(1-r) \tag{6.6}$$

as for a homogeneous plate.

The solution applies if $m_r \leqslant \eta$ within the zone $r_0 \leqslant r \leqslant 1$. Since m_r is a monotonically decreasing function of r, therefore (6.4) is valid if

$$\eta \gtrless \eta_0(r_0) = \frac{1-r_0^3}{1+r_0^2-r_0^3}. \tag{6.7}$$

The other case is such that the central part remains rigid and a hinge forms at $r = r_0$ for the radial moment $m_r(r_0) = \eta$. It is found that in this case

$$p = \frac{6\eta}{1-r_0^3}, \tag{6.8}$$

$$m_r = \eta + \frac{\eta}{1-r_0^3}\left(\frac{r_0^3}{r} - r^2\right), \quad m_\theta = \eta, \quad r_0 \leqslant r \leqslant 1, \tag{6.9}$$

$$\dot{w} = \dot{w}_0 \begin{cases} 1, & 0 \leqslant r \leqslant r_0, \\ \dfrac{1-r}{1-r_0}, & r_0 \leqslant r \leqslant 1. \end{cases} \tag{6.10}$$

The stress field has to be extended in to the rigid zone in order to ensure statical admissibility of the solution. For instance, the solution can take the form, for fixed r_0,

$$m_r = \frac{\eta}{\eta_0}(1 - r(\eta_0 + r_0(1-\eta_0))), \quad m_\theta = \frac{\eta}{\eta_0}, \quad 0 \leqslant r \leqslant r_0. \tag{6.11}$$

An extension is indicated in Fig. 6.2b with the solid line $A''A'''$. The ranges of validity of (6.5) and (6.8) are shown in Fig. 6.3. For various positions of the thickness variation two considered cases of total and partial collapse are discerned.

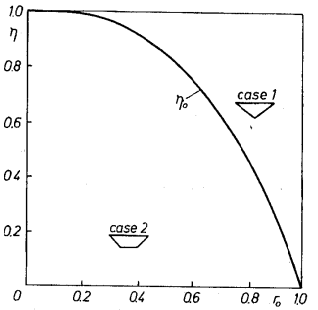

Fig. 6.3. The ranges of validity of the solutions for nonhomogeneous circular plate with a stronger central part

If the central part is weaker there are four solutions. Complete analysis is given in [35] and the set of them is represented in Fig. 6.4. As can be seen for the cases 2, 3 and 4 the stress profile involves the stress régimes BC and $B'C'$ therefore the outer ring can serve as clamping.

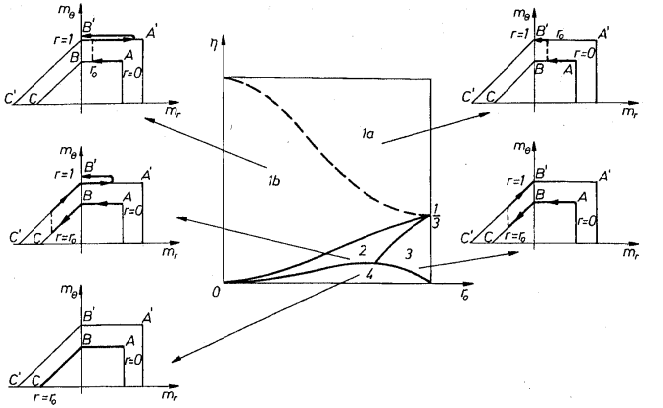

Fig. 6.4. The ranges of validity of the solutions for a nonhomogeneous circular plate with a weaker central part

The solution of the circular plate made of a Johansen material as an example of continuous change of the interaction surface (6.1) was obtained in [94].

6.2. Orthotropic plates

Two types of anisotropy of materials can be distinguished: an innate anisotropy caused, for instance, by plastic working of metallic materials and a structural anisotropy generated by a reinforcement of an isotropy matrix with bars or fibres embedded in specific directions. The material constants for such materials depend upon the direction in the physical space. Suitable yield conditions have to allow for this property. To describe anisotropic bodies, the Huber-Mises yield condition, [17], [54] is usually generalized or its linearization is used in form similar to that of the Tresca yield condition.

In what follows some examples of rotationally symmetric orthotropic plates will be presented. In such plates two mutually perpendicuar directions of anisotropy can be distinguished that coincide with the principal directions of the bending moments M_r, M_θ and their ultimate values M_r^0, M_θ^0.

The negative and the positive ultimate moments are assumed to have the same moduli, which means the yield surface remains symmetric with respect to the origin of the coordinate axes.

The system of basic equations, except the yield condition, is the same as the system for isotropic plates. Thus the equilibrium equations (4.5), the kinematical relationships (4.4), the associated flow law (4.7) and the compatibility conditions (4.9) remain unchanged.

6.2.1. Orthotropic plates with nonlinear yield conditions. The Huber-Mises yield condition for rotationally symmetric plates can be generalized as follows:

$$\mathscr{F} = A_r m_r^2 + 2A_{r\theta} m_r m_\theta + A_\theta m_\theta^2 - 1 . \tag{6.12}$$

The coefficients A_r, A_θ, $A_{r\theta}$ are constants which depend on the plastic properties of the orthotropic material. To make the yield curve represented by (6.12) closed and convex, two inequalities must be satisfied,

$$A_r A_\theta - A_{r\theta}^2 > 0 \quad \text{and} \quad A_r + A_\theta > 0 \tag{6.13}$$

which means that A_r and A_θ have to be positive. For isotropic plates we have $A_r = A_\theta = 1$, $A_{r\theta} = -1/2$.

Let us analyse a yield condition (6.12), in which $A_r = 1$, $A_\theta = c^2$ and $A_{r\theta} = -b$, then

$$\mathscr{F} = m_r^2 - 2bm_r m_\theta + c^2 m_\theta^2 - 1 = 0 \quad \text{for} \quad c > b . \tag{6.14}$$

This form of eq. (6.12) describes a certain family of curves in a more convenient manner, Fig. 6.5. Parameter c appears to be a reciprocal of the orthotropy coefficient,

$$\Lambda = \frac{1}{c} = \frac{M_\theta^0}{M_r^0} . \tag{6.15}$$

Nonlinearity of the yield condition leads, similarly as in the case of isotropic plates, to the necessity of employing numerical methods of solution, at least for arbitrary loading conditions.

Analytically solved specific plates are few; two examples are shown below, after [70].

Consider a circular simply supported plate subjected to a central concentrated force. The method of solution is similar to that used for an isotropic plate in [24].

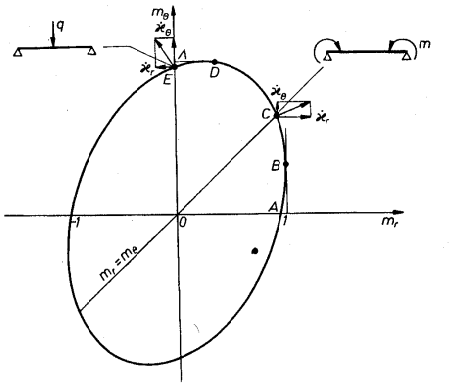

Fig. 6.5. Generalization of Huber-Mises ellipse to the orthotropic case

The collapse load

$$q = \frac{2\pi}{c} \tag{6.16}$$

is associated with the bending moment state represented by the point E of the yield curve, Fig. 6.5, at which

$$m_r = 0 , \quad m_\theta = \frac{1}{c} \quad \text{for} \quad 0 < r \leqslant 1 . \tag{6.17}$$

At $r = 0$ a singularity occurs. The deflection rate field (4.12), on account of (6.17), is described by

$$r\dot{w}'' + \frac{b}{c^2}\dot{w}' = 0 . \tag{6.18}$$

After integration, the deflection rate function takes the form

$$\dot{w} = \dot{w}_0 \left(1 - r^{1-\frac{b}{c^2}}\right) . \tag{6.19}$$

In order to satisfy the edge condition $\dot{w}(0) = \dot{w}_0$, the parameters b and c must be such that $c^2 > b$. This inequality is, for $c < 1$, stronger than $c > b$ which ensures that the the yield surface (6.14) is closed and convex.

The Gaussian curvature of the deflection rate surface is, remembering (6.17),

$$\dot{\kappa}_r \cdot \dot{\kappa}_\theta = \nu^2 \frac{\partial \mathscr{F}}{\partial m_r} \cdot \frac{\partial \mathscr{F}}{\partial m_\theta} = -4\nu^2 b. \tag{6.20}$$

For $b > 0$ the Gaussian curvature is negative, as was the case for an isotropic plate, and has at the its centre a singularity of the type $\dot{w}'(0) \Rightarrow \infty$.

Another example of an analytical solution is furnished by a circular simply supported plate subjected to applied bending moments m around the circumference.

Integration of the equilibrium equation in the presence of the boundary conditions

$$m_r(0) = m_\theta(0), \quad \text{and} \quad m_r(1) = m \tag{6.21}$$

leads to the following distribution of moments

$$m_r = m_\theta = \frac{1}{\sqrt{1-2b+c^2}} = m \tag{6.22}$$

which corresponds to the point C on the yield surface, Fig. 6.5. Integration of (4.12) results, in turn, in the deflection rate function of the form

$$\dot{w} = \dot{w}_0 \left(1 - r^{\frac{1-2b+c^2}{c^2-b}}\right). \tag{6.23}$$

Since $1-2b+c^2 > 0$, the inequality $c^2 - b > 0$ must be also satisfied. The Gaussian curvature is found to be

$$\dot{\kappa}_r \cdot \dot{\kappa}_\theta = 4(1-b)(c^2-b)m^2. \tag{6.24}$$

From the above expression it follows that two cases of an orthotropic plate can take place: first, when $b < 1$ the Gaussian curvature is positive and no singularity at the centre occurs since $\dot{w}'(0) = 0$ and, second, when $b > 1$ when the curvature is negative and the singularity at the centre does occur since $\dot{w}'(0) \Rightarrow \infty$.

The two examples discussed above show that the orthotropy affects the whole behaviour of the plates considered. Before we proceed to other numerical examples, let us analyse the stress profile that can develop in a simply supported plate under uniformly distributed load. Due to the boundary conditions

$$m_r(0) = m_\theta(0) \quad \text{and} \quad m_r(1) = 0 \tag{6.25}$$

the bending moments at the centre are

$$m_r(0) = m_\theta(0) = \frac{1}{\sqrt{1-2b+c^2}} \tag{6.26}$$

and are represented by the point B in Fig. 6.6. The moment profile runs over the portion BC of the yield curve which, for orthotropy, is no longer symmetrical with respect to the diagonal $m_r = m_\theta$. Two cases can take place.

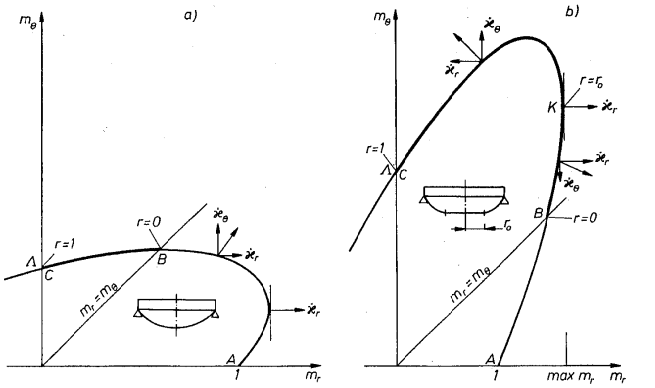

Fig. 6.6. Two variants of collapse for circular simply supported orthotropic plate obeying nonlinear interaction curve

The first one, shown in Fig. 6.6a, does not differ qualitatively from that for isotropic plate. The other, Fig. 6.6b, occurs when $m_r' > 0$ in the central part of the plate. There exists the point K at which the moment m_r attains maximum, $\max m_r = c/\sqrt{c^2-b^2}$ and $\dot{\kappa}_\theta = 0$; this means that a ring hinge can develop at a circle $r = r_0 \neq 0$.

From the flow law it follows that the sings of the curvatures are: $\dot{\kappa}_\theta < 0$ for $0 \leqslant r \leqslant r_0$ and $\dot{\kappa}_\theta > 0$ for $r_0 < r \leqslant 1$. At the centre, symmetry requires that either the deflected surface is smooth, $\dot{w}'(0) = 0$, or a plastic hinge can develop. For the part BC a hinge can form at $r = r_0 \neq 0$ and therefore for the part BK associated with $0 \leqslant r \leqslant r_0$ the curvature $\dot{\kappa}_\theta = 0$. To simultaneously satisfy the flow law, this part of the plate can only move as a rigid body, $v = 0$.

The conclusion is that it is orthotropy of the plate that is the reason for a rigid central portion of the plate to form at certain values of the parameters b and c. Such a specific behaviour is not observed for the isotropic Huber-Mises plates.

In general, the numerical methods of solution are the same in the case of the orthotropic and isotropic rotationally symmetric plates, [90]. However, particular solutions differ appreciably.

Let us illustrate these differences with the help of a circular simply supported plate by assuming a number of sets of parameters b and c. The diagrams of the hoop and radial bending moments are shown in Figs. 6.7, 6.8, 6.9. The distributions for isotropic plates are drawn in dashed lines.

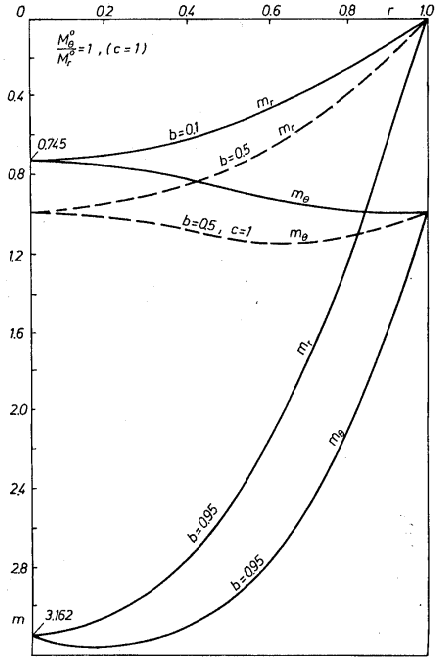

Fig. 6.7. Distribution of moments in circular simply supported orthotropic plate for parameters $c = 1$ and $b = 0.1$ and 0.95

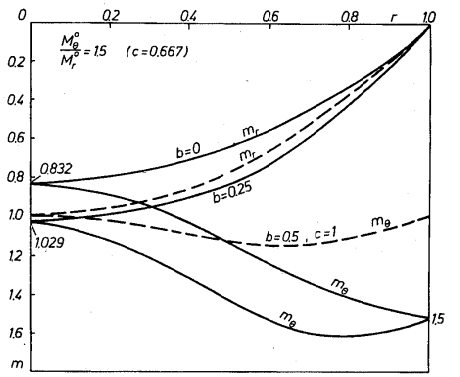

Fig. 6.8. Distribution of moments in circular simply supported orthotropic plate for parameters $c = 0.667$ and $b = 0$ and 0.25

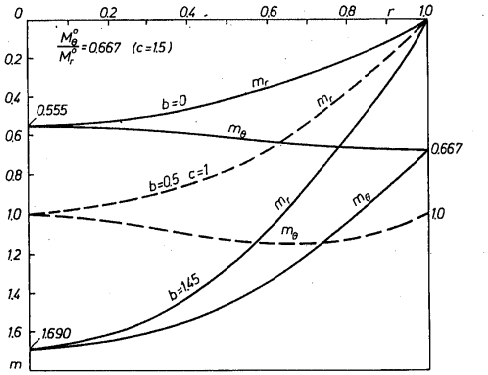

Fig. 6.9. Distribution of moments in circular simply supported orthotropic plate for parameters $c = 1$ and $b = 0$ and 1.45

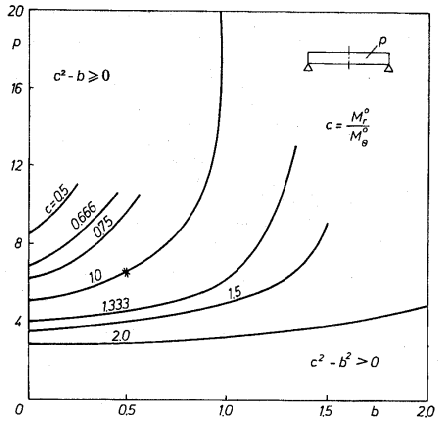

Fig. 6.10. Collapse load for uniformly loaded circular simply supported orthotropic plate

The influence of orthotropy on the ultimate load is depicted in Fig. 6.10. A star corresponds to the isotropic case. Increase in the circumferential ultimate bending moment is seen to remarkably enhance the collapse load.

6.2.2. Orthotropic plates with piece-wise linear yield conditions. Two types of linearization of the yield condition are usually employed for orthotropic plates: a nonsymmetric one [42], [67], Fig. 6.11a and a symmetric one [68], Fig. 6.11b with respect to the diagonal $m_r = m_\theta$.

Respective equations and curvature rate components of the deflected middle surface for both types of linearization are given in Tables 6.1 and 6.2.

The solutions for orthotropic plates are found to differ from those for isotropic ones not only quantitatively but also qualitatively. This will be demonstrated on an example of simply supported circular plate under uniform pressure p.

The generalized stress field and the deflection rate surface have to satisfy the following boundary conditions:

$$m_r(0) = m_\theta(0), \quad m_r(1) = 0, \tag{6.27}$$

$$\dot{w}(0) = \dot{w}_0, \quad \dot{w}(1) = 0. \tag{6.28}$$

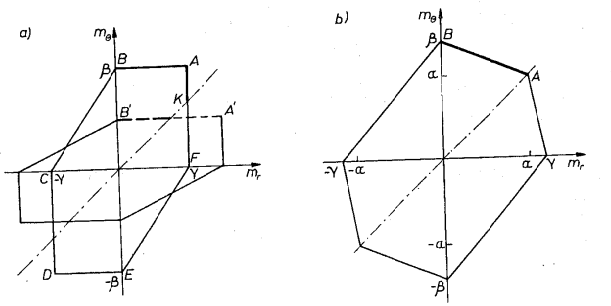

Fig. 6.11. Stress profile for orthotropic simply supported circular plate obeying: (a) asymmetrical, (b) symmetrical piece-wise interaction curve

Let us employ the yield surface shown in Fig. 6.11a and consider two specific cases: $\beta > \gamma$ and $\beta < \gamma$. For the former the boundry conditions (6.27) indicate that it is KAB that is a statically admissible stress profile. It is worth noting that at KA the curvature rate components are $\dot{\kappa}_\theta = 0$, $\dot{\kappa}_r \neq 0$ which means that the central part of the plate can only move as a rigid body. For the point A a sudden change in the hoop component $\dot{\kappa}_\theta$ occurs: as a result a ring hinge is formed at $r = r_A$. This radius can be calculated from

$$m_r(r_A) = \gamma \quad \text{and} \quad m_r'(r_A) = 0 \tag{6.29}$$

which follow from the continuity requirement $[m_r(r_A)] = 0$ and the equation (4.9).

Integrating the equilibrium equation (4.5) and the deflection rate equation (4.12) or making use of the general solutions (4.15) and (4.19) in the presence of the boundary conditions (6.27) and (6.28), the following moment distributions are arrived at:

for $0 \leqslant r \leqslant r_A$

$$\begin{aligned} m_r &= \gamma, \\ m_\theta &= \gamma + \frac{pr^2}{2}, \\ \dot{w} &= \dot{w}_0, \end{aligned} \tag{6.30}$$

for $r_A \leqslant r \leqslant 1$

$$\begin{aligned} m_r &= \beta - \frac{p}{6r}(2r_A^3 + r^3), \\ m_\theta &= \beta, \\ \dot{w} &= \dot{w}_0\left(\frac{1-r}{1-r_A}\right), \end{aligned} \tag{6.31}$$

the ultimate load is

$$p = \frac{2(\beta-\gamma)}{r_A^2}, \tag{6.32}$$

in which r_A is a relevant root of the equation

$$3r_A^2\beta - (\beta-\gamma)(1+2r_A^3) = 0. \tag{6.33}$$

The radius r_A as a function of β is shown in Fig. 6.12. The parameter γ is taken as unity, in other words the reference ultimate moment is M_r^0.

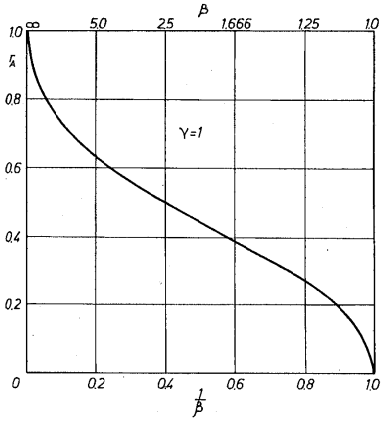

Fig.6.12. Hinge circle radius r_A against the ratio of orthotropy β

For the other specific case, $\beta < \gamma$, the stress profile is represented by the dashed line AB, Fig. 6.11a, similarly as for an isotropic plate. Also similar is the deflection rate surface and the internal actions field:

$$\begin{aligned} m_r &= \beta(1-r^2), \\ m_\theta &= \beta, \\ \dot{w} &= \dot{w}_0(1-r), \\ p &= 6\beta. \end{aligned} \tag{6.34}$$

The moment distributions, the ultimate load and the deflection rates for various orthotropy coefficients β (when $\gamma = 1$) are shown diagrammatically in Figs. 6.13, 6.14, 6.15, respectively.

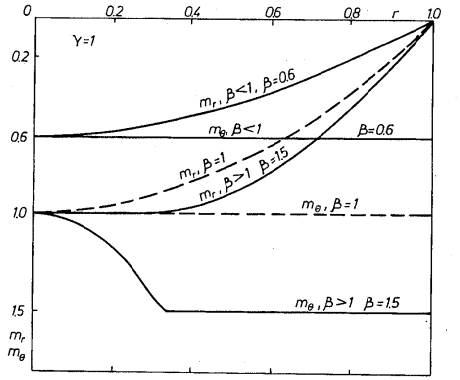

Fig. 6.13. Moment distribution in simply supported orthotropic circular plate obeying interaction curve shown in Fig. 6.11a

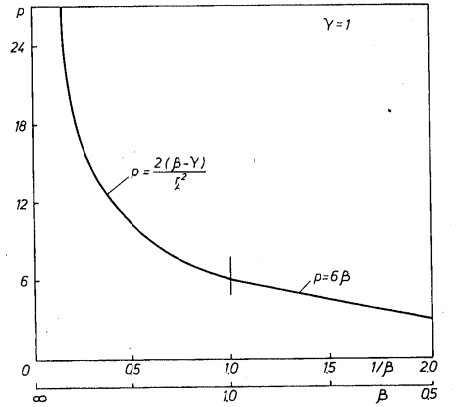

Fig. 6.14. Collapse load for uniformly loaded simply supported orthotropic plate obeying interaction curve shown in Fig. 6.11a

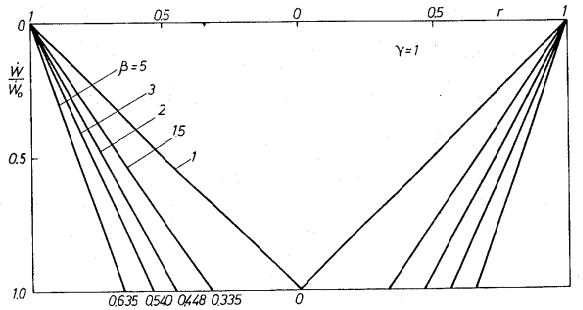

Fig. 6.15. Deflection rates for simply supported orthotropic circular plate obeying interaction curve shown in Fig. 6.11a

A considerable number of solutions for plates with various boundary conditions and load patterns are given in [42].

The yield surface shown in Fig. 6.11b lead to somewhat simpler solutions. The boundary conditions (6.27) restrict the stress profile to the line AB, Table 6.2.

Making use, as before, of the solutions (4.15) and (4.17) and remembering the boundary conditions (6.27) and (6.28), the following moment distribution and the deflection rate surface is obtained:

$$m_r = \alpha(1-r^2), \tag{6.35}$$

$$m_\theta = \alpha\left(1-\left(1-\frac{\beta}{\alpha}\right)r^2\right),$$

$$\dot{w} = \dot{w}_0\left(1-r^{\frac{\beta}{\alpha}}\right), \tag{6.36}$$

associated with the ultimate load

$$p = 2(2\alpha + \beta). \tag{6.37}$$

Its magnitude does not depend upon the ultimate radial bending moment ($m_r^0=\gamma$). The radial bending moment has the same distribution as for the isotropic plate. The hoop moment, which was kept constant in the isotropic Tresca plate, does have depend on r. Both bending moment diagrams for various rations β/α are shown in Fig. 6.16.

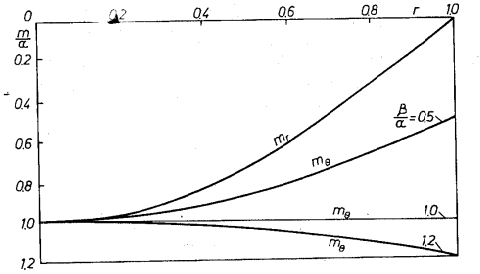

Fig. 6.16. Moment distribution in simply supported orthotropic circular plate obeying interaction curve shown in Fig. 6.11a

Return to the deflection rate function (6.36). From the analysis of its derivative

$$\dot{w}' = -\dot{w}_0\frac{\beta}{\alpha}r^{\frac{\beta}{\alpha}-1} \tag{6.38}$$

it follows that, depending on β/α, this function can have either negative or positive Gaussian curvature. Moreover, for $\beta/\alpha > 1$ the deflection rate surface remains smooth at the centre. This simply means that no plastic hinge form there, contrary to the case of the isotropic Tresca plate.

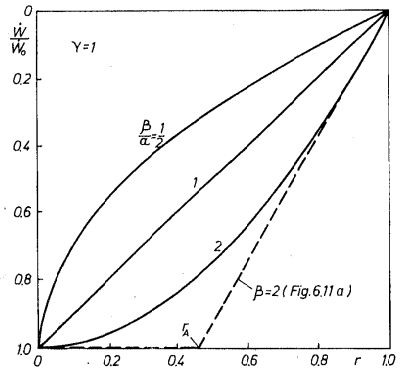

Fig. 6.17. Deflection rates for simply supported orthotropic circular plate obeying interaction curve shown in Fig. 6.11a

Table 6.1

Modified Tresca interaction curve and flow law for orthotropic circular plates

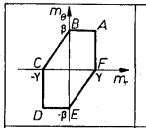	stress profile	$\dot{\varkappa}_r : \dot{\varkappa}_\theta$
AB	$m_\theta = \beta$, $0 < m_r < \gamma$	0:1
BC	$m_\theta = \beta + \frac{\beta}{\gamma} m_r$, $-\gamma < m_r < 0$	$-\frac{\beta}{\gamma}$:1
CD	$-\beta < m_\theta < 0$, $m_r = -\gamma$	-1:0
DE	$m_\theta = -\beta$, $-\alpha < m_r < 0$	0:-1
EF	$m_\theta = \frac{\beta}{\gamma} m_r - \beta$, $0 < m_r < \gamma$	$\frac{\beta}{\gamma}$:-1
FA	$0 < m_\theta < \beta$, $m_r = \gamma$	1:0

Table 6.2

Symmetric interaction curve and flow law for orthotropic circular plate

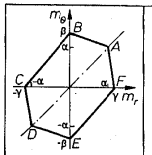	stress profile	$\dot{\varkappa}_r : \dot{\varkappa}_\theta$
AB	$m_\theta = (1 - \frac{\beta}{\alpha}) m_r + \beta$, $0 < m_r < \alpha$	$\beta - \alpha : \alpha$
BC	$m_\theta = \frac{\beta}{\gamma} m_r + \beta$, $-\gamma < m_r < 0$	$-\beta : \gamma$
CD	$m_\theta = \frac{\alpha}{\alpha - \gamma} m_r - \frac{\alpha \cdot \gamma}{\gamma - \alpha}$, $-\gamma < m_r < -\alpha$	$-\alpha : -(\gamma - \alpha)$
DE	$m_\theta = (1 - \frac{\beta}{\alpha}) m_r - \beta$, $-\alpha < m_r < 0$	$-(\beta - \alpha) : -\alpha$
EF	$m_\theta = \frac{\beta}{\gamma} m_r - \beta$, $0 < m_r < \gamma$	$\beta : -\gamma$
FA	$m_\theta = \frac{\alpha}{\alpha - \gamma} m_r + \frac{\alpha \cdot \gamma}{\gamma - \alpha}$	$\alpha : \gamma - \alpha$

For $\beta/\alpha < 1$ a singularity $\dot{w}'(0) \Rightarrow \infty$ does exist. As readily seen in Fig. 6.17, the deflected surface of the orthotropic plate obeying the yield curve of Fig. 6.11b is completely different from that found for the isotropic plate. For the sake of comparison, the deflected surface for the orthotropic plate obeying the yield curve of Fig. 6.11a is given with dashed line. The above solution is valid for all the ratios β/α provided the yield surface remains convex.

CHAPTER 7

YIELD LINE THEORY

7.1. Assumptions

The yield line method for the evaluation of the collapse load for plates foreshadowed the development of consistent theories of plastic plates and shells. Due to an ingenious simplification of the fissuration pattern of reinforced concrete slabs and profiting from the principle of virtual work the yield line theory became a method of rapid estimation of collapse load of plates under complicated boundary conditions and loading patterns, [30], [32], [39].

Regarded from the viewpoint of the present theory of plastic structures the yield line method provides for upper bounds on the collapse loads.

The collapse mechanism is assumed to consist of flat portions, finite or infinitesimal, joined by plastic hinge lines.

These hinges, or yield lines can be considered as narrow bonds of the plate in which strains are dramatically larger than those in the neighbouring regions. The generalized strain rates (the curvature rates) concentrated along the yield lines are understood as the following limits:

$$\dot{\overset{*}{\kappa}}_{ij} = \lim_{\Delta n \Rightarrow 0} \int_0^{\Delta n} \dot{\kappa}_{ij}\, dn\,. \tag{7.1}$$

On the other hand, in view of Chapter 3.4, a yield line constitutes a line of discontinuity in the curvature rate along which a jump in the normal derivative is admissible, (3.59),

$$\left[\frac{d\dot{w}}{dn}\right] = \Phi_n = \dot{\overset{*}{\kappa}}_n \neq 0\,. \tag{7.2}$$

This means that a concentrated curvature rate $\dot{\overset{*}{\kappa}}_n$ at the yield line is equal to the vector of mutual rotation of two adjacent undeformed, plane portions of the plate. The remaining components of the concentrated curvature rate are:

$$\dot{\overset{*}{\kappa}}_{nt} = \left[\frac{d\dot{w}}{dt}\right] = 0 \quad \text{and} \quad \dot{\overset{*}{\kappa}}_t = 0 \tag{7.3}$$

which results from the continuity of the deflection rate surface $[\dot{w}] = 0$. From the fact that $\dot{\overset{*}{\kappa}}_{nt}$ vanishes it follows that each yield line is a trajectory of the principal curvature rate. Vanishing of both curvature rate components, $\dot{\overset{*}{\kappa}}_{nt}$, $\dot{\overset{*}{\kappa}}_t$, means that the yield condition at the yield line is a projection of the respective yield conditions on the axis m_n (Chapter 2.3). Assuming in Figs. 3.2, 3.3, and 3.4 that $m_x = m_n$, $m_y = m_t$, $m_{xy} = m_{nt}$, the bending moment normal to the yield line attains, for the Tresca and the Johansen yield conditions, the values

$$m_n = \pm\, m_0 \tag{7.4}$$

whereas, for the Huber-Mises yield condition, it amounts to

$$m_n = \pm\, \frac{2}{\sqrt{3}}\, m_0\,, \tag{7.5}$$

where $m_n = \pm\, \dfrac{M_n}{M^0}$ and M^0 is the reference ultimate bending moment.

The power of dissipation in the yield line theory is concentrated in all the yield line and can be calculated from the formula

$$D = M^0\, L \sum_i m_{ni}\, \Phi_{ni}\, l_i\,, \tag{7.6}$$

where L is a reference length and l_i is a nondimensional length of the i-th yield line.

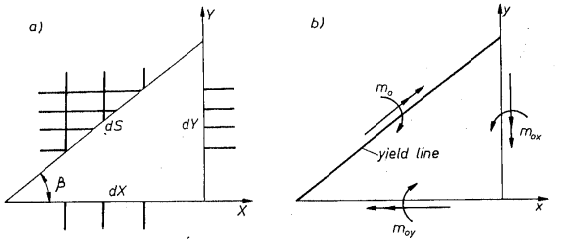

Fig. 7.1. Moments along the yield line: (a) orthotropic reinforcement, (b) ultimate moment along the yield line and its components in the direction of reinforcement

For orthotropic plates we assume, after [30], that the ultimate bending moment along the yield line can be expressed by means of two ultimate moments in the directions of orthotropy, Fig. 7.1,

$$m_n = m_{no} = m_{ox} \sin^2\beta + m_{oy} \cos^2\beta, \tag{7.7}$$

$$m'_n = -m'_{no} = -(m'_{ox} \sin^2\beta + m'_{oy} \cos^2\beta). \tag{7.8}$$

where (m_{ox}, m_{oy}) and (m'_{ox}, m'_{oy}) are dimensionless sagging and hogging ultimate bending moments par unit length in the directions x and y, m_{no} and m'_{no} are the dimensionless ultimate moments along the positive (for sagging) and the negative (for hogging) yield line, respectively.

The relationships (7.7), (7.8) are equivalent to the assumption that the bending capacity is exhausted when the maximum bending moment surface (7.9), (7.10) is reached. This conclusion is due to [48] and [62]. In [48] it was assumed that the yield line coincides with the trajectory of the principal curvature and that the maximum bending moment yield condition is relevant and relations (7.7) and (7.8) were obtained. In [62] it was started from (7.7) and (7.8) and it was obtained the following equations as a result:

$$(m_x - m_{ox})(m_y - m_{oy}) - m_{xy}^2 = 0, \tag{7.9}$$

$$(m_x + m'_{ox})(m_y + m'_{oy}) - m_{xy}^2 = 0. \tag{7.10}$$

Assumptions of the yield line theory can be set up as follows:

- plastic deformations in a plate concentrate in the yield lines,
- the yield lines, constituting a yield pattern, divide the plate into a collection of plane, rigid elements,
- the yield pattern corresponds to a kinematically admissible mechanism of instantaneous motion. The yield pattern does not change with the motion, thus the classical yield line theory describes an incipient plastic motion only and cannot account for the changes in geometry without appropriate modification,
- the bending moment across the yield line attains the ultimate value m_n, which depends on the amount of reinforcement and the properties of the matrix in which the reinforcing bars are embedded.

Under such assumptions the collapse load multiplier is computed with the use of the principle of virtual work,

$$\mu_Y \iint p_0 \dot{w}\, dxdy = \sum_i m_{ni}\, \Phi_{ni}\, l_i, \tag{7.11}$$

where the right-hand side summation is performed over all the yield lines of respective lengths l_i. In general, the yield line pattern of the collapse mode is specified to within a number of parameters η_j, $j = 1, 2, \ldots, n$. The best bound on the collapse load will be obtained when

$$\mu = \min \mu_Y(\eta_j). \tag{7.12}$$

7.2. Discrete yield line pattern

A collapse mechanism of a plate consisting of a finite number of plane portions separated by yield lines is termed a discrete yield line pattern. Such collapse modes can be conveniently described with the help of vectors corresponding to rotations of particular rigid portions. Such a rotation vector coincides with the axis of rotation of the portion under consideration and is equal to

$$\Phi = \frac{\dot{w}}{h}, \tag{7.13}$$

where $\dot{w}$ is a deflection rate of a generic point of the rigid element and h denotes its distance from the rotation axis.

As a result of ignoring the in-plane deflection rate components and requiring continuity of the deflection rates, the yield line pattern and the associated rotation vectors have to satisfy the following conditions:

a) the rotation vectors lie in the rotation axes,
b) the rotation vectors remain in the middle plane of plate,
c) the rotation vectors of rigid regions neighbouring the supports coincide with these supported edges,
d) the vectors of mutual rotation of adjacent portions are the differences of the rotations of particular portions involved and coincide with the separating yield line,
e) a yield line runs through the point of intersection of the rotation axes of adjacent portions.

Satisfaction of the above conditions amounts to saying that the hodograph of the rotation vectors (the rotation rate diagram) must be closed, Fig. 7.2. Before using the expressions (7.11) and (7.12), the moduli of rotation vectors (within an accuracy of one of them taken as a virtual quantity) are adopted as parameters of the assumed collapse mode. When the support conditions do not determine the yield line pattern in a unique manner (point supports etc.), some additional parameters must be employed describing the directions of rotation axes. Then the hodograph is constructed to determine the kinematically admissible collapse mechanism. Some collapse modes together with the corresponding rotation rate diagrams are shown in Fig. 7.2.

A yield line OA shown in Fig. 7.2d will be used as an example to give a number of useful formulae for the calculations of the power dissipated in the yield line. A relative rotation of the adjacent rigid parts 1 and 2 is

$$\Phi_n = \Phi_{12} = \Phi_1 \cos\alpha_1 - (-\Phi_2 \cos\alpha_2) = \Phi_1 \cos\alpha_1 + \Phi_2 \cos\alpha_2. \tag{7.14}$$

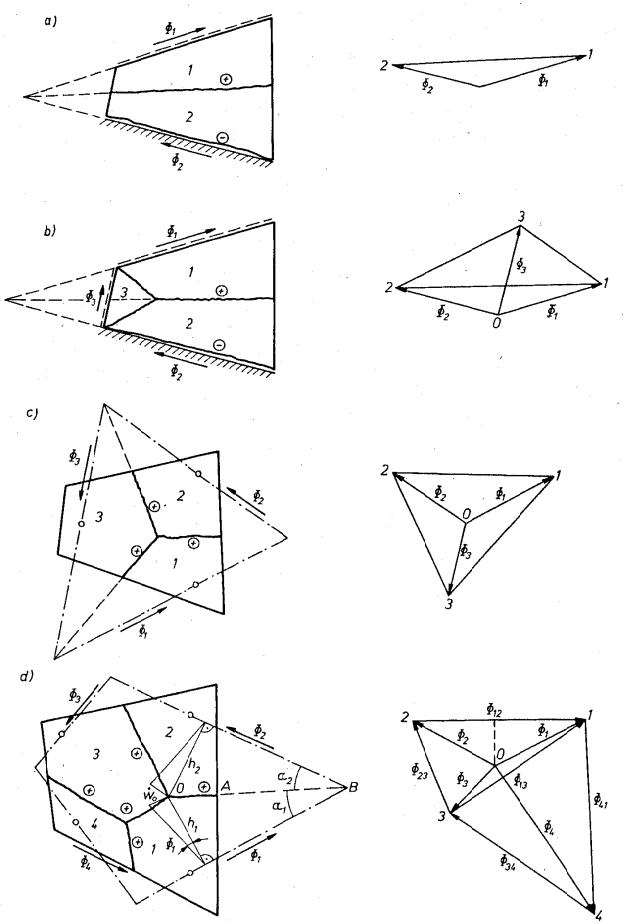

Fig. 7.2. Yield line patterns and rotation rate diagrams for four examples of plates

According to the condition d), the rotations of parts 1 and 2 are related to each other by the equality

$$\Phi_1 \sin\alpha_1 = \Phi_2 \sin\alpha_2 \tag{7.15}$$

and are equal to:

$$\Phi_1 = \frac{\dot{w}_0}{h_1} = \frac{\dot{w}_0}{l_{OB}\sin\alpha_1}, \qquad \Phi_2 = \frac{\dot{w}_0}{h_2} = \frac{\dot{w}_0}{l_{OB}\sin\alpha_2}, \tag{7.16}$$

where $\dot{w}_0$ denotes the deflection rate of the point O. Making use of (7.14) and (7.16) the power of dissipation in the yield line OA can be eventually calculated from the formula

$$d_{OA} = m_n \Phi_{12} l_{OA} = m_n \dot{w}_0 \frac{l_{OA}}{l_{OB}} (\cot\alpha_1 + \cot\alpha_2). \tag{7.17}$$

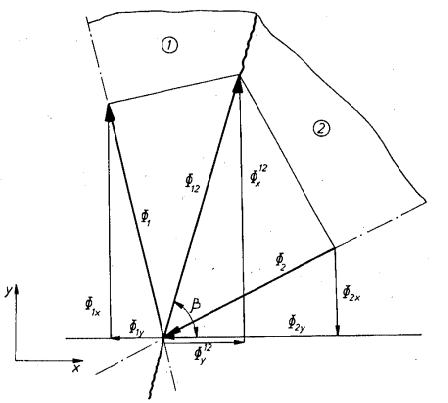

Fig. 7.3. Rotation vector of two adjacent plane portions about the yield line and its components

For a plate with the orthotropy directions x and y, Fig. 7.3, it appears convenient to use the relevant components

$$\begin{aligned} \Phi_x^{12} &= \Phi_{1x} - \Phi_{2x} = \Phi_{12}\sin\beta, \\ \Phi_y^{12} &= \Phi_{1y} - \Phi_{2y} = \Phi_{12}\cos\beta, \\ l_x &= l\cos\beta, \quad l_y = l\sin\beta. \end{aligned} \tag{7.18}$$

The power of dissipation in the yield line 12 with the length l and with the ultimate bending moment components shown in (7.9) is given by

$$d_{12} = (m_{ox} \sin^2\beta + m_{oy} \cos^2\beta)\Phi_{12} l. \tag{7.19}$$

Finally, remembering (7.18) and (7.19), the power of dissipation in an arbitrary yield line ij amounts to

$$\begin{aligned} d_{ij} &= (m_{ox} \Phi_x^{ij} l_y + m_{oy} \Phi_y^{ij} l_x) \quad \text{for} \quad \Phi_{ij} > 0, \\ d_{ij} &= -(m'_{ox} \Phi_x^{ij} l_y + m'_{oy} \Phi_y^{ij} l_x) \quad \text{for} \quad \Phi_{ij} < 0 \end{aligned} \tag{7.20}$$

for sagging and hogging, respectively.

When all the rigid portions are surrounded by the positive yield lines the overall dissipation is a sum of the expressions for each part.

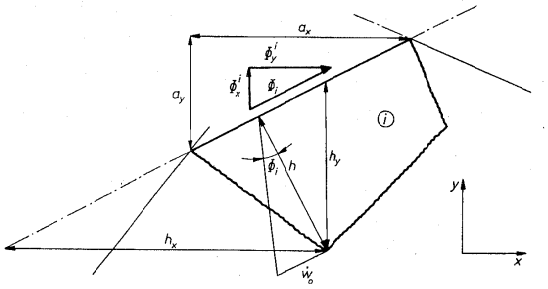

Fig. 7.4. Rotation vector of the i-th plane portion about the supported edge and its components

In the case of portion adjacent to a simply supported edge, Fig. 7.4, the power of dissipation is equal to

$$d_i = m_{ox} \Phi_x^i a_y + m_{oy} \Phi_y^i a_x, \tag{7.21}$$

where $\Phi_x^i = \dot{w}_0/h_x$, $\Phi_y^i = \dot{w}_0/h_y$ are the projections of the rotation vector Φ_i and the remaining notation is shown in Fig. 7.4. When the considered portion of the plate is clamped, the expression (7.21) must be supplemented by a term corresponding to the hogging action at the support, and eventually becomes

$$d_i = (m_{ox} + m'_{ox}) \Phi_x^i a_y + (m_{oy} + m'_{oy}) \Phi_y^i a_x. \tag{7.22}$$

Consider, as an example, a hinged rectangular plate under uniformly distributed pressure. Let the plate be orthotropic in the sense of Fig. 7.1. Due

to the double symmetry of support and loading conditions an admissible yield pattern is specified in the considered case to within a single parameter η.

Requiring the flat portions 1, 2, 3, 4 to rotate with respect to the supports, the yield line pattern, shown in heavy lines in Fig. 7.5, is obtained. The corresponding diagram of rotations is also given in the figure. The vectors Φ_1, Φ_2, Φ_3, Φ_4 represent plastic rotations with respect to the supports. Similarly, the relative rotations of the parts 1,...4 are represented by the respective vectors Φ_{12} etc.

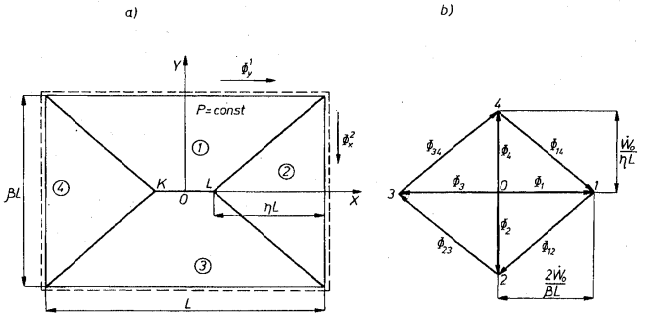

Fig. 7.5. Simply supported and uniformly loaded rectangular plate: (a) yield line pattern, (b) rotation rate diagram

The following dimensionless quantities will be employed:

$$\mu_Y = p = \frac{PL^2}{M^0}, \quad m_{oy} = \frac{M_{oy}}{M^0} = 1, \quad m_{ox} = \frac{M_{ox}}{M^0} = \Lambda, \quad \dot{w}_0 = \frac{\dot{W}_0}{L} \tag{7.23}$$

whereas L is the reference length, M_{0y} the reference ultimate moment and $\dot{W}_0$ denotes the vertical displacement rate on KL. Rotations with respect to the supports and the respective lengths of the supports are:

$$\begin{aligned} \Phi_2 = \Phi_4 = \Phi_x^2 = \frac{\dot{w}_0}{\eta}, \quad a_y = \beta, \\ \Phi_1 = \Phi_3 = \Phi_y^1 = \frac{2\dot{w}_0}{\beta}, \quad a_x = 1. \end{aligned} \tag{7.24}$$

According to (7.21) the total rate of internal work for the whole plate is in the dimensionless form

$$\frac{D_{\text{int}}}{M^0 L} = 2(m_{ox}\,\Phi_x^2\beta + m_{oy}\,\Phi_y^1) = 2\dot{w}_0\left(\frac{\beta}{\eta}\,\Lambda + \frac{2}{\beta}\right). \tag{7.25}$$

The rate of external work is

$$\frac{D_{\text{int}}}{M^0 L} = \mu_Y \frac{1}{6}\,\beta(3-2\eta)\,\dot{w}_0. \tag{7.26}$$

The balance equation (7.9) yields the collapse load multiplier in terms of a single parameter η specifying the yield pattern,

$$\mu_Y = p = \frac{12}{\eta\beta^2}\,\frac{2\eta + \beta^2\Lambda}{3 - 2\eta}. \tag{7.27}$$

The lowest multiplier is obtained by imposing the requirement $d\mu_Y/d\eta = 0$. Eventually the following value of the collapse load is obtained from the yield line theory

$$\mu = \frac{6\Lambda}{\eta^2}, \quad \eta = \frac{1}{2}\beta^2\Lambda\left(-1 + \sqrt{1 + \frac{3}{\beta^2\Lambda}}\right) \tag{7.28}$$

for $\beta^2\Lambda \leqslant 1$. Otherwise the yield pattern changes so that the line KL is parallel to the Y-axis in Fig. 7.5.

In Table 7.1 the resulting formulae for the collapse load of rectangular plates with various fixity conditions are collected. Most of the notation is explained in the inserted figures and

$$M^0 = M_{oy}, \quad \Lambda = \frac{M_{ox}}{M_{oy}}, \quad \Lambda_i' = \frac{M_{oi}'}{M_{oi}}, \quad \Lambda_i'' = \frac{M_{oi}''}{M_{oi}}, \quad i = x,y. \tag{7.29}$$

In the above notation primes refer to the yield moments in negative bending. In Table 7.2 the numerical values are given for several values of the parameter $\mathscr{A}$ combining the plate aspect ratio, orthotropy and layered structure, [86]. Mixed boundary conditions can easily be accounted for in the yield line theory.

We consider a square plate, clamped on two side and supported in the corner as shown in Fig. 7.6. The plate is isotropic but endowed with different ultimate moments M^0 for positive and $\Lambda' M^0$ for negative flexure so that dimensionless ultimate moments are

$$m_0' = \Lambda' m_0, \quad m_0 = 1 \tag{7.30}$$

and therefore Λ' defines the degree of fixity. Under the point load $Q = qM^0$ applied in the centre, the simplest yield pattern is shown in Fig. 7.6. Flat elements 1, 2, 3 of the plate at failure rotate about the supports and about an

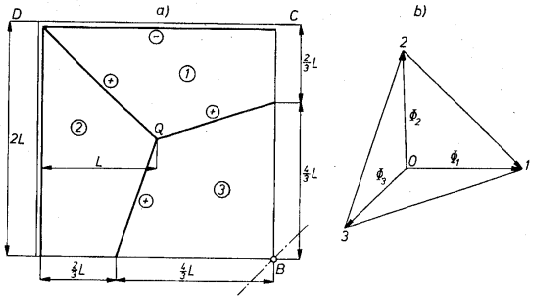

Fig. 7.6. Square plate with mixed boundary conditions: (a) yield line pattern, (b) rotation rate diagram

axis passing through the point support. Due to symmetry, and at the prescribed deflection rate $\dot{w}_0$ of the point of load application the rotations are

$$\Phi_1 = \Phi_2 = \dot{w}_0, \quad \Phi_3 = \frac{\dot{w}_0}{\sqrt{2}}, \quad l_{AD} = l_{DC} = 2. \tag{7.31}$$

The vectors of rotation coinciding with the positive and negative yield lines are, respectively,

$$\Phi_{12} = \Phi_1\cos 45° + \Phi_2\cos 45° = \sqrt{2}\,w_0, \quad l_{12} = \sqrt{2}, \tag{7.32}$$

$$\Phi_{13} = \Phi_{23} = \Phi_1\cos\alpha_1 + \Phi_3\cos\alpha_2 = \dot{w}_0\sqrt{\frac{5}{2}}, \quad l_{13} = l_{23} = \frac{\sqrt{10}}{3},$$

where $\cos\alpha_1 = 3/\sqrt{10}$, $\cos\alpha_2 = 2/\sqrt{5}$. The relation (7.9) leads to

$$q\dot{w}_0 = \Phi_{12}l_{12} + 2\Phi_{13}l_{13} + 2\Phi_1 l_{DC}\,\Lambda' \tag{7.33}$$

and the collapse load is

$$q = 4\left(\frac{4}{3} + \Lambda'\right). \tag{7.34}$$

As another example of plates with mixed boundary conditions we consider a corner plate under uniformly distributed pressure. Particular edges

are clamped, hinged and free as shown in Fig. 7.7. The following dimensionless quantities will be employed:

$$\mu_Y = p = \frac{PL^2}{M^0}, \quad M_{oy} = M^0, \quad \Lambda = \frac{M_{ox}}{M_{oy}}, \quad \Lambda' = \frac{M'_{oy}}{M_{oy}}. \tag{7.35}$$

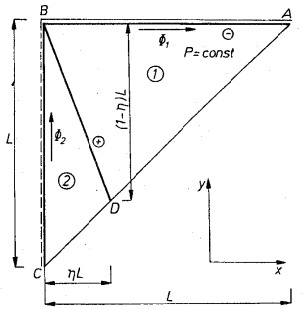

Fig. 7.7. Yield line pattern in uniformly loaded corner plate with mixed boundary conditions

The rotations of the flat parts with respect to the support are

$$\Phi_1 = \frac{\dot{w}_0}{1-\eta}, \quad \Phi_2 = \frac{\dot{w}_0}{\eta}, \tag{7.36}$$

and the projections of the vector Φ_{12} and the length of the yield line 12 on the axes x, y are, on account of (7.18)

$$\begin{aligned} \Phi_x^{12} &= \Phi_2, & l_y^{12} &= 1-\eta, \\ \Phi_y^{12} &= \Phi_1, & l_x^{12} &= \eta, \\ \Phi_y^{AB} &= \Phi_1, & l_x^{AB} &= 1. \end{aligned} \tag{7.37}$$

According to (7.20) the internal energy rate is

$$\frac{D_{\text{int}}}{M^0 L} = \Lambda \Phi_x^{12} l_y^{12} + \Phi_y^{12} l_x^{12} + \Lambda'_y \Phi_y^{AB} l_x^{AB} = \Lambda \Phi_2 (1-\eta) + (\eta + \Lambda'_y) \Phi_1 \tag{7.38}$$

and the external energy rate

$$\frac{D_{\text{ext}}}{M^0 L} = \frac{1}{6} \dot{w}_0 \mu_Y. \tag{7.39}$$

From (7.9) the collapse load follows,

$$\mu_Y = \frac{6}{\eta(1-\eta)} (\Lambda(1-\eta)^2 + \eta^2 + \Lambda'_y \eta). \tag{7.40}$$

The best upper bound is found from the condition $d\mu_Y/d\eta = 0$ and the respective value of the governing parameter is

$$\eta = \frac{\sqrt{\Lambda}}{\sqrt{\Lambda} + \sqrt{1+\Lambda'_y}}. \tag{7.41}$$

Thus the lowest upper bound within the considered class of collapse modes is

$$\mu = 6(\Lambda'_y + 2\sqrt{\Lambda(1+\Lambda'_y)}). \tag{7.42}$$

The examples presented make it clear that the yield patterns depend on the aspect ratio and on the orthotropy.

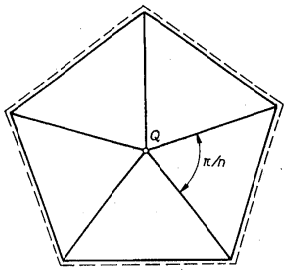

Fig. 7.8. Yield line pattern in polygonal simply supported plate under point load

Let us now consider an isotropic plate in the shape of a regular n-sided polygon loaded at the centre. An admissible discrete yield pattern is shown in Fig. 7.8. A straight-forward computation using (7.9) and (7.17) provides the collapse load associated with the considered mode of deformation

$$q = 2n \tan \frac{\pi}{n}. \tag{7.43}$$

Two observations can be made in connection with this example when $n \Rightarrow \infty$. First, the collapse load is then $q = 2\pi$. Even more interesting is the conclusion that as n increases the hinge lines approach each other to form eventually a continuous field when the plate boundary is curvilinear, [30], [41], [72].

The problem of continuous modes of deformation and curvilinear hinges will now be studied.

Table 7.1

Collapse loads for rectangular plates with various boundary conditions, orthotropy and layered structures

$$\mathcal{P}=\frac{6}{3-2\xi},\quad \xi=\mathcal{A}^2(-1+\sqrt{1+3/\mathcal{A}^2}),\quad \lambda_i=\sqrt{1+\Lambda_i'}+\sqrt{1+\Lambda_i''},\quad i=x,\ y,\ \beta=\frac{B}{A}$$

I $\quad \mathcal{A}=\beta\sqrt{\Lambda}\,\dfrac{\lambda_x}{\lambda_y}$

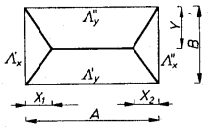

$$\frac{PB^2}{M_{oy}}=\mathcal{P}\lambda_y^2,\qquad \frac{X_1}{A}=\xi\frac{\sqrt{1+\Lambda_x'}}{\lambda_x},\quad \frac{X_2}{A}=\xi\frac{\sqrt{1+\Lambda_x''}}{\lambda_x}$$

$$\beta\leqslant\frac{\lambda_y}{\lambda_x\sqrt{\Lambda}},\qquad \xi=\frac{X_1+X_2}{A},\qquad \frac{Y}{B}=\frac{\sqrt{1+\Lambda_y''}}{\lambda_y}$$

II $\quad \mathcal{A}=\beta\sqrt{\Lambda}\,\dfrac{\lambda_y}{\lambda_x}$

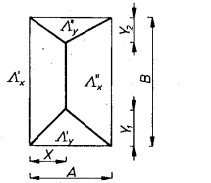

$$\frac{PB^2}{M_{oy}}=\mathcal{P}\lambda_x^2\Lambda\beta^2,\qquad \frac{Y_1}{B}=\xi\frac{\sqrt{1+\Lambda_y'}}{\lambda_y},\quad \frac{Y_2}{B}=\xi\frac{\sqrt{1+\Lambda_y''}}{\lambda_y}$$

$$\beta\geqslant\frac{\lambda_y}{\lambda_x\sqrt{\Lambda}},\qquad \xi=\frac{Y_1+Y_2}{B},\qquad \frac{X}{A}=\frac{\sqrt{1+\Lambda_x''}}{\lambda_x}$$

III $\quad \mathcal{A}=\beta\sqrt{\Lambda}\,\dfrac{\sqrt{1+\Lambda_x'}}{\lambda_y}$

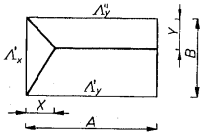

$$\frac{PB^2}{M_{oy}}=\mathcal{P}\lambda_y^2,\qquad \frac{Y}{B}=\frac{\sqrt{1+\Lambda_y''}}{\lambda_y}$$

$$\beta<\frac{\lambda_y}{\sqrt{\Lambda(1+\Lambda_x')}},\qquad \xi=\frac{X}{B}$$

$$\text{for}\ \frac{\lambda_y}{\sqrt{\Lambda(3+\Lambda_x')}}\leqslant\beta\leqslant\frac{\lambda_y}{\sqrt{\Lambda(1+\Lambda_x')}},\ \frac{PB^2}{M_{oy}}=\min(\square,\square)$$

IV $\quad \mathcal{A}=\dfrac{1}{\beta\sqrt{\Lambda}}\,\dfrac{\lambda_y}{\sqrt{3+\Lambda_x'}}$

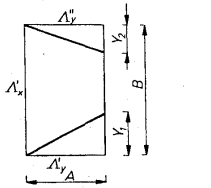

$$\frac{Y_1}{B}=\xi\frac{\sqrt{1+\Lambda_y'}}{\lambda_y},\qquad \frac{Y_2}{B}=\xi\frac{\sqrt{1+\Lambda_y'}}{\lambda_y}$$

$$\frac{PB^2}{M_{oy}}=\mathcal{P}\beta^2\Lambda(\Lambda_x'+2\xi)$$

$$\beta>\frac{\lambda_y}{\sqrt{\Lambda(3+\Lambda_x')}},\qquad \xi=\frac{Y_1+Y_2}{B}$$

Table 7.2

Parameters $\mathcal{A}$, ξ, and $\mathcal{P}$

$$\xi=\mathcal{A}\left(-1+\sqrt{1+\frac{3}{\mathcal{A}^2}}\right),\qquad \mathcal{P}=\frac{6}{3-2\xi}$$

$\mathcal{A}$	ξ	$\mathcal{P}$	$\mathcal{A}$	ξ	$\mathcal{P}$	$\mathcal{A}$	ξ	$\mathcal{P}$
0.00	0.00	2.000	0.51	0.661	3.575	0.76	0.860	4.687
0.01	0.017	2.023	0.52	0.670	3.614	0.77	0.867	4.737
0.02	0.034	2.047	0.53	0.679	3.655	0.78	0.873	4.787
0.03	0.051	2.070	0.54	0.688	3.695	0.79	0.880	4.837
0.04	0.068	2.095	0.55	0.697	3.737	0.80	0.886	4.888
0.05	0.084	2.119	0.56	0.706	3.777	0.81	0.893	4.840
0.06	0.100	2.143	0.57	0.714	3.819	0.82	0.899	4.992
0.07	0.116	2.168	0.58	0.723	3.861	0.83	0.905	5.044
0.08	0.132	2.193	0.59	0.731	3.904	0.84	0.911	5.097
0.09	0.148	2.219	0.60	0.740	3.946	0.85	0.917	5.150
0.10	0.163	2.245	0.61	0.748	3.990	0.86	0.923	5.204
0.11	0.179	2.271	0.62	0.756	4.033	0.87	0.929	5.258
0.12	0.194	2.297	0.63	0.764	4.077	0.88	0.935	5.312
0.13	0.209	2.324	0.64	0.772	4.122	0.89	0.941	5.367
0.14	0.224	2.351	0.65	0.780	4.167	0.90	0.947	5.422
0.15	0.238	2.378	0.66	0.778	4.212	0.91	0.952	5.478
0.16	0.253	2.405	0.67	0.795	4.258	0.92	0.958	5.534
0.17	0.267	2.433	0.68	0.803	4.304	0.93	0.963	5.591
0.18	0.281	2.461	0.69	0.810	4.350	0.94	0.969	5.648
0.19	0.295	2.490	0.70	0.818	4.397	0.95	0.974	5.706
0.20	0.309	2.518	0.71	0.825	4.444	0.96	0.979	5.764
0.21	0.322	2.547	0.72	0.832	4.492	0.97	0.985	5.882
0.22	0.336	2.577	0.73	0.839	4.540	0.98	0.990	5.881
0.23	0.349	2.606	0.74	0.846	4.589	0.99	0.995	5.940
0.24	0.362	2.636	0.75	0.853	4.637	1.00	1.00	6.00
0.25	0.375	2.667						
0.26	0.388	2.697						
0.27	0.400	2.728						
0.28	0.413	2.760						
0.29	0.425	2.791						
0.30	0.437	2.823						
0.31	0.449	2.855						
0.32	0.461	2.888						
0.33	0.473	2.921						
0.34	0.485	2.954						
0.35	0.496	2.988						
0.36	0.507	3.022						
0.37	0.518	3.056						
0.38	0.529	3.091						
0.39	0.540	3.126						
0.40	0.551	3.161						
0.41	0.562	3.197						
0.42	0.572	3.233						
0.43	0.582	3.270						
0.44	0.593	3.307						
0.45	0.603	3.444						
0.46	0.613	3.381						
0.47	0.623	3.419						
0.48	0.632	3.457						
0.49	0.642	3.496						
0.50	0.651	3.535						

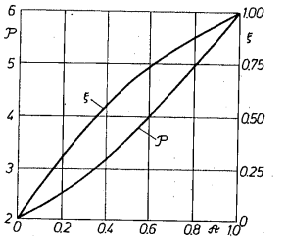

7.3. Yield line field

A continuous field of straight yield lines is generated when the plate boundary is smoothly curved. Such a field can also occur in the case of partial collapse when a plastically deforming region extends only on a portion of the plate. Fields of yield lines form fans developed either from a point or from an envelope. Since the normal moment on a hinge line takes the value of ultimate moment, the circumferential moment stays constant in a yield line for isotropic plates. We recognize therefore the situation specific for the maximum principal moment condition at parabolic stress régimes which will be studied in Chapter 8.

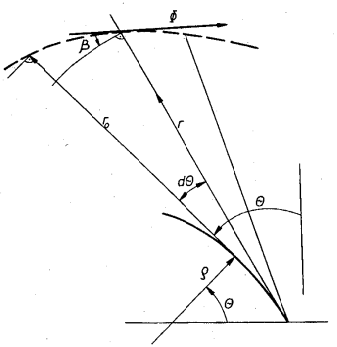

Fig. 7.9. Yield line fan developed from an envelope

The main problem connected with fans consists in the computation of the rate of internal work for such a collapse mode. Let us consider a fan developed from an envelope as shown in Fig. 7.9. Equation of the deflected surface passing through the plate boundary $r_0 = r_0(\theta)$ is

$$\dot{w} = \dot{w}_0(\theta)\left(1 - \frac{r}{r_0(\theta)}\right), \tag{7.44}$$

where $\dot{w}_0(\theta)$ denotes the deflection rate on the envelope line

$$\dot{w}_0(\theta) = C_0 \exp\left[-\int \frac{\rho}{r_0} d\theta\right] \tag{7.45}$$

whereas C_0 is an arbitrary constant, [28]. Dimensionless curvature rates are expressed as follows:

$$\dot{\kappa}_r = \dot{\kappa}_{r\theta} = 0,$$
$$\dot{\kappa}_\theta = \frac{1}{r r_0}\left(1 + \frac{(r_0'+\rho)(2r_0'+\rho)}{r_0^2} - \frac{r_0''+\rho'}{r_0}\right)\dot{w}_0(\theta), \tag{7.46}$$

where prime denotes differentiation with respect to θ.

In view of (7.46) the rate of internal work, due to the fact that the considered yield lines are straight, consists solely of contributions due to the ultimate moment on the curvature rate $\dot{\kappa}_\theta$. For an isotropic plate with the ultimate moment M^0 the rate of work in an infinitesimal plate segment is

$$\frac{1}{M^0 L} dD_{\text{int}} = m_0\left(\int_0^{r_0} \dot{\kappa}_\theta \, r dr\right) d\theta =$$
$$= m_0\left(1 + \frac{(r_0'+\rho)(2r_0'+\rho)}{r_0^2} - \frac{r_0''+\rho'}{r_0}\right)\dot{w}_0(\theta)\, d\theta. \tag{7.47}$$

The rate of work on the envelope where a ridge of the deflected surface can form if the envelope belongs to the plate, is not considered at the moment. When $\rho = 0$ and $\dot{w}_0$ is constant we obtain from (7.47) the known expression for the rate of internal work of a polar fan

$$\frac{1}{M^0 L} dD_{\text{int}} = m_0\left(1 + 2\left(\frac{r_0'}{r_0}\right)^2 - \frac{r_0''}{r_0}\right)\dot{w}_0 \, d\theta. \tag{7.48}$$

Hence for a point loaded plate simply supported along a convex boundary $r_0(\theta)$, the yield line theory furnishes the collapse load

$$q = \int_0^{2\pi}\left(1 + 2\left(\frac{r_0'}{r_0}\right)^2 - \frac{r_0''}{r_0}\right) d\theta. \tag{7.49}$$

Whenever integration prescribed in (7.49) is performed on closed smooth boundary the expression specifying the collapse load is simplified to become

$$q = \int_0^{2\pi}\left(1 + \left(\frac{r_0'}{r_0}\right)^2\right) d\theta. \tag{7.50}$$

This can easily be verified remarking that

$$\frac{r_0 r_0'' - r_0'^2}{r_0^2} = d\left(\frac{r_0'}{r_0}\right) \tag{7.51}$$

which, if integrated, vanishes for a closed smooth contour. When the integration is not carried out over a closed curve the expression (7.51) represents the work in the two limiting positive yield lines corresponding to $\theta = \theta_1$ and $\theta = \theta_2$.

Thus the total work of a polar fan with limiting positive yield lines consists of (7.48) and (7.51)

$$\frac{D_{\text{int}}}{M^0 L} = \int_{\theta_1}^{\theta_2} \left(1 + \left(\frac{r_0'}{r_0}\right)^2\right) d\theta . \tag{7.52}$$

This question will reappear when complete solutions are studied.

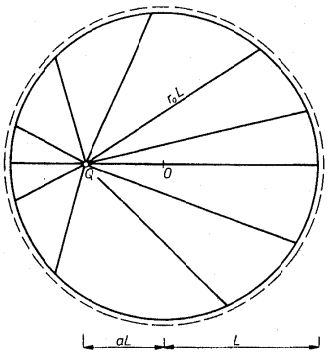

Fig. 7.10. Collapse mode for simply supported circular plate under eccentrically applied point load

As an example we consider a circular plate loaded by an eccentrically applied concentrated force as shown in Fig. 7.10. In the polar coordinate system with the origin at the point of loading the boundary is given by

$$r_0 = a\cos\theta + \sqrt{1 - a^2 \sin^2\theta} . \tag{7.53}$$

The collapse load is obtained from (5.50) to become

$$q = \frac{2\pi}{\sqrt{1-a^2}} . \tag{7.54}$$

It can be pointed out that no restriction is imposed on the angle which the yield line forms with the normal to the contour. The collapse load (7.54) increases infinitely with increasing a to 1. This being unreasonable it is expected that another local mechanism will form, possibly with negative hinge lines so as to give finite value of the collapse load. The energy is then dissipated along such a negative hinge.

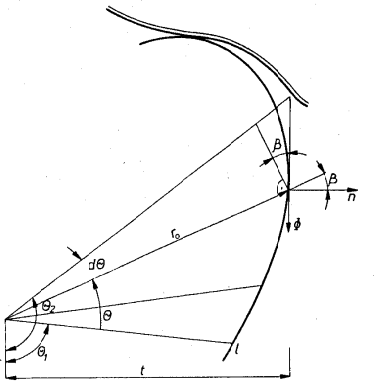

Fig. 7.11. Yield line fan bounded by a negative yield line $r_0 = r_0(\theta)$

In order to derive the expression for the rate of work on a curved negative yield line, which necessarily must appear in clamped plates, we consider the situation shown in Fig. 7.11. The yield line fan is bounded by a curve $r_0 = r_0(\theta)$. Let the plate be isotropic both in negative and positive flexure, with the ultimate moments m_0' and m_0, respectively. For an infinitesimal segment the rate of work done by the negative ultimate moment is

$$\frac{1}{M^0 L} dD_{\text{int}} = m_0' \Phi\, dl = m_0' \frac{\dot{w}_0}{t} \frac{r_0 d\theta}{\cos\beta} = m_0' \dot{w}_0 \left(1 + \left(\frac{r_0'}{r_0}\right)^2\right) d\theta \tag{7.55}$$

since $\Phi = \dfrac{\dot{w}_0}{t}$, $t = r_0 \cos\beta$, $\tan^2\beta = (r_0'/r_0)^2$.

The contributions (7.48) and (7.55) result in the following expression for the rate of energy dissipated in a polar fan of yield lines

$$\frac{1}{M^0 L} dD_{\text{int}} = m_0 \left(1 + 2\left(\frac{r_0'}{r_0}\right)^2 - \frac{r_0''}{r_0}\right) \dot{w}_0\, d\theta + m_0' \left(1 + \left(\frac{r_0'}{r_0}\right)^2\right) \dot{w}_0\, d\theta . \tag{7.56}$$

The load carried by the fan shown in Fig. 7.11 is

$$q = \int_{\theta_1}^{\theta_2} \left(1 + \Lambda' + (2+\Lambda')\left(\frac{r_0'}{r_0}\right)^2 - \frac{r_0''}{r_0}\right) d\theta, \tag{7.57}$$

where $\Lambda' = m_0'/m_0$ and $m_0 = 1$. When the integration is performed over a closed contour $r_0(\theta)$ the collapse load becomes

$$q = (1+\Lambda') \int_0^{2\pi} \left(1 + \left(\frac{r_0'}{r_0}\right)^2\right) d\theta. \tag{7.58}$$

The equation of the negative hinge $r_0(\theta)$ appearing in (7.55) remains yet unspecified. It is neither obvious nor reasonable to expect that identifying $r_0(\theta)$ with the plate clamped boundary the lowest collapse load will be obtained. Hence a variational problem arises: to find $r_0(\theta)$ such that the functional (7.57) takes the minimum value,

$$q = \int_{\theta_1}^{\theta_2} \varphi\,(\theta, r_0, r_0', r_0'') \Rightarrow \min. \tag{7.59}$$

The Euler equation yields

$$\frac{2(1+\Lambda')}{r_0^3}(r_0'^2 - r_0'' r_0) = 0 \tag{7.60}$$

and its solution is a logarithmic spiral

$$r_0 = A \exp[C\,\theta]. \tag{7.61}$$

Expressing the integration constant C in terms of the angle β, Fig. 7.11, the negative hinge line is obtained in the form

$$r_0 = A \exp[\theta \tan\beta]. \tag{7.62}$$

The value of the collapse load (7.57) with (7.62) becomes

$$q = (1+\Lambda')(1 + \tan^2\beta)(\theta_2 - \theta_1). \tag{7.63}$$

For a clamped point loaded plate the negative yield line should form a closed curve. Such a curve is necessarily a circle, Fig. 7.12. No requirement is imposed as to the magnitude of its radius but is usually argued that the circle should touch the clamped boundary. The collapse load for such a point loaded plate isotropic both in positive and negative flexure, is

$$q = 4\pi. \tag{7.64}$$

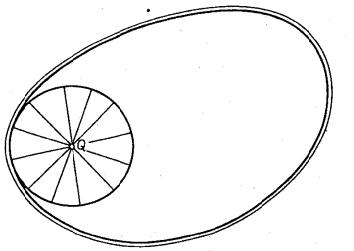

Fig. 7.12. Collapse mode of a point loaded clamped plate

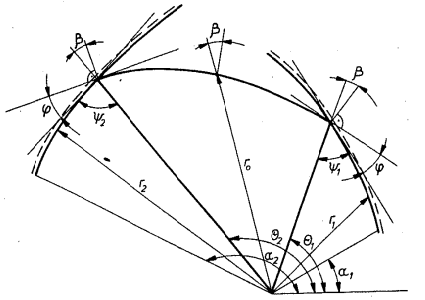

Fig. 7.13. Polar yield line fan bounded by a negative yield line and contained within two simply supported edges

Let us consider a not infrequent case of a polar fan bounded by a negative yield line as specified in (7.61) and contained within two simply supported edges, Fig. 7.13. The collapse load according to (7.52) and (7.63) consists of the following contributions

$$q = \int_{\alpha_1}^{\theta_1} \left(1+\left(\frac{r_0'}{r_0}\right)^2\right) d\theta + (1+\Lambda')(1+\tan^2\beta)(\theta_2-\theta_1) + \int_{\theta_2}^{\alpha_2} \left(1+\left(\frac{r_0'}{r_0}\right)^2\right) d\theta. \tag{7.65}$$

The expression (7.65) reaches its minimum for the following relations between the angles $\beta, \psi_1, \psi_2, \varphi$ and the coefficient of negative bending Λ', Fig. 7.13, [39]

$$\frac{\Lambda'}{1+\Lambda'}\cos^2\beta = \sin^2\beta, \quad \operatorname{cotan}\psi_1 + \operatorname{cotan}\psi_2 = 2\Lambda'\operatorname{cotan}\varphi, \tag{7.66}$$

$$C = \tan\beta = \sqrt{\frac{1}{1+\Lambda'}\left(\frac{\Lambda'}{\tan^2\varphi} - 1\right)}.$$

Although the question of continuous fans and the associated rate of work seems to be somewhat simpler when complete solutions are considered in the next chapter let us for completeness return to an arbitrary fan patterns, Fig. 7.9, in order to compute the rate of energy dissipated in an infinitesimal strip bounded by two arbitrary curved hinges r_1 and r_2, Fig. 7.14.

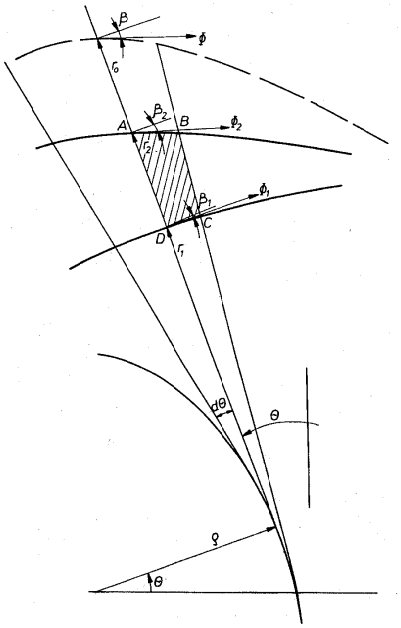

Fig. 7.14. Infinitesimal strip bounded by two arbitrarily curved hinges

The rotations on the yield lines r_1 and r_2 are

$$\Phi_i = \Phi\cos(\beta-\beta_i), \quad i = 1, 2, \tag{7.67}$$

where Φ is the rotation with respect to the boundary line. The rotation Φ was obtained from the continuity condition of rotation on the line separating two adjacent infinitesimal portions,

$$\Phi = \frac{\dot{w}_0(\theta)}{r_0\cos\beta}, \tag{7.68}$$

where $\dot{w}_0(\theta)$ is given in (7.45). The rate of internal work (7.55) at the hinge r_i is

$$\frac{1}{M^0L}dD^i_{\text{int}} = m_{oi}\Phi_i dl_i = m_{oi}\Phi_i\frac{r_i d\theta}{\cos\beta_i} =$$

$$= m_{oi}\left(\frac{r_i}{r_0} + \frac{(r_0'+\rho)(r_i'+\rho)}{r_0^2}\right)\dot{w}_0(\theta)\,d\theta. \tag{7.69}$$

Eventually, from (7.47) and (7.69) one arrives at a formula for the total dissipation in the region $ABCD$, Fig. 7.14,

$$\frac{1}{M^0L}dD_{\text{int}} = \left\{m_0\frac{r_2-r_1}{r_0}\left(1 + \frac{(r_0'+\rho)(2r_0'+\rho)}{r_0^2} - \frac{r_0''+\rho'}{r_0}\right) + \right.$$

$$+ m_{01}\left(\frac{r_1}{r_0} + \frac{(r_0'+\rho)(r_1'+\rho)}{r_0^2}\right) - m_{02}\left.\left(\frac{r_2}{r_0} + \frac{(r_0'+\rho)(r_2'+\rho)}{r_0^2}\right)\right\}\dot{w}_0(\theta)\,d\theta, \tag{7.70}$$

where m_{01}, m_{02} equal either m_0 or $-m_0'$, depending upon the sign of the total curvature at the respective hinge.

The most important case is that of $r_2 = r_0$. Then $m_{02} = -m_0'$ when the zone considered is adjacent to a rigid region or to a hinged support if $m_0' = 0$. Equation (7.70) can be rearranged to yield

$$\frac{1}{M^0L}dD_{\text{int}} = \left\{(1\mp\Lambda')\left(1 + \frac{r_0'+\rho}{r_0}\right)^2\right) +$$

$$+ \left(1 - \frac{r_1}{r_0}\right)\left(\frac{\rho}{r_0}\frac{r_0'+\rho}{r_0}\right) - \left(\left(1 - \frac{r_1}{r_0}\right)\left(\frac{r_0'+\rho}{r_0}\right)\right)'\Bigg\}\dot{w}_0(\theta)\,d\theta. \tag{7.71}$$

We can see that for $r_1 = 0$, $\rho = 0$ and consequently $\dot{w}_0 = C_0$ we obtain the equation (7.56). If the curvature of the envelope $\rho = 0$, but $r_1 \neq 0$, Eq. (7.71) after integration gives

$$\frac{D_{\text{int}}}{M^0 L} = C_0(1+\Lambda')\int_{\theta_1}^{\theta_2}\left(1+\left(\frac{r_0'}{r_0}\right)^2\right)d\theta - C_0\left[\left(1-\frac{r_1}{r_0}\right)\frac{r_0'}{r_0}\right]_{\theta=\theta_1}^{\theta=\theta_2}. \quad (7.72)$$

It is interesting to observe that dissipation is not influenced by the equations of the internal yield lines but only by the coordinates of their origins and ends, [28].

As an example we consider a circular simply supported plate loaded by two equal point loads applied with an eccentricity on the plate diameter, Fig. 7.15a, [93].

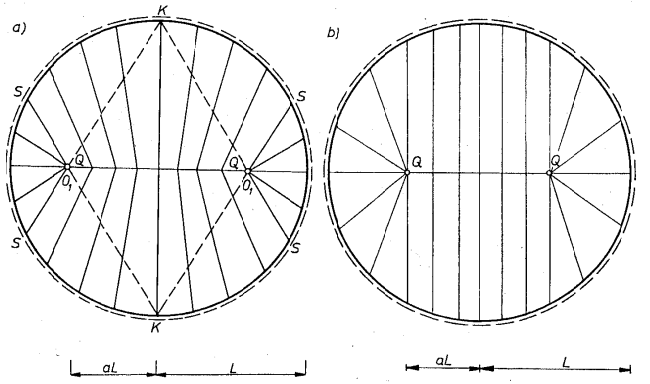

Fig. 7.15. Deflected surface for simply supported circular plate loaded by two equal point loads: (a) consisting of conical elements, (b) consisting of conical and cylindrical elements

We assume that the deflected surface consists of conical elements. The zones SO_1S are cones with vertices at the points of load application whereas the zone SO_1O_1S corresponds to a cone with the vertex K on the plate boundary. The expressions (7.47) and (7.72) furnish the rate of internal work in the zones SO_1S and SO_1O_1S, respectively.

Hence for a two point loaded plate, Fig. 7.15a, the collapse load is

$$2q = 2\frac{2}{\sqrt{1-a^2}}\left(\arctan\frac{\sqrt{1-a^2}}{a} + \frac{2a}{\sqrt{1-a^2}}\right). \quad (7.73)$$

A special case of a continuous field of yield lines is when the envelope degenerates into an infinitely distant point. Straight yield lines become parallel and the plate segment undergoes cylindrical bending, Fig. 7.16. As obtained in [28] the formula for dissipation in an infinitesimal strip takes the form

$$\frac{1}{M^0 L}\,dD_{\text{int}} = m_0(z_2 - z_1)(-z_0'') + m_{01}(1 + z_0'z_1') - m_{02}(1 + z_0'z_2'))\,C ds, \quad (7.74)$$

where $(\cdot)' = d/ds'\,C$ denotes a constant rotation of the generatrices and the z_0, z_1, z_2 are shown in Fig. 7.16. In the case of $z_2 = z_0$, $m_{01} = m_0 = 1$ and $m_{02} = -\Lambda'$ we obtain, similarly to (7.72),

$$\frac{D_{\text{int}}}{M^0 L} = C(1+\Lambda')\int_{s_1}^{s_2}(1 + z_0'^2)\,ds - C\left[z_0'(z_0 - z_1)\right]_{s=s_1}^{s=s_2}. \quad (7.75)$$

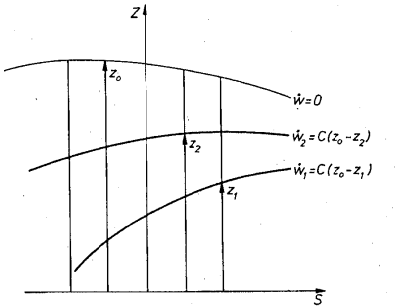

Fig. 7.16. Pattern with parallel yield lines

If the considered region does not meet an undeformed zone the deflection $\dot{w}_i$ at the line l_i must be prescribed, whereas the boundary line $z = z_0$ is unknown and fictitious, namely

$$z_0 = z_i + \frac{\dot{w}_i}{C}. \quad (7.76)$$

As an example we consider the plate subjected to two point loads as in the previous example. The deflected surface now consists of straight yield lines corresponding to cylindrical bending. Thus we assume the collapse mode shown in Fig. 7.15b. Two cones are joined by the cylindrical surface. Using (7.75) and (7.76) for $\Lambda' = 0$ we obtain the collapse load

$$2q = 2\frac{2}{\sqrt{1-a^2}}\left(\pi + \ln\left|\frac{a+1}{a-1}\right|\right). \tag{7.77}$$

More examples using an arbitrary field line can be found in [28].

7.4. Partial collapse modes

A partial collapse mode is associated with the appearance of a negative yield line. Such lines can touch a simply supported boundary if an angle that a straight positive yield line makes with the contour attains a critical value. To illustrate the point we shall consider the case of a plate strip loaded in the vicinity of its simply supported boundary. The geometry of a simply supported edge appears to have no influence on the angle the negative yield line makes with the boundary curve.

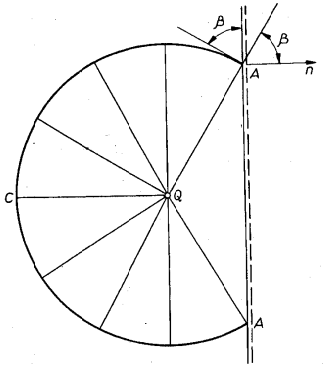

Fig. 7.17. Partial collapse of plate under point load in the vicinity of simply supported edge

The considered plate is equipped with the positive ultimate moment $m_0 = 1$ and the negative one $m_0' = \Lambda'$. The yield pattern under the concentrated force $Q = qM^0$ is shown in Fig. 7.17. Since the plate is isotropic and there is an axis of symmetry both in positive and negative bending, the circumferential hinge in negative bending is a circle. From (7.11) the dimensionless collapse load is found to be

$$q = 2\tan\beta + 2(1+\Lambda')(\pi-\beta). \tag{7.78}$$

The lowest value is obtained when

$$\tan\beta = \sqrt{\Lambda'}. \tag{7.79}$$

For $\Lambda' = 1$ the positive yield line makes therefore an angle $\beta = \pi/4$ with a hinged boundary and so does the negative one.

We note that $\beta = \pi/4$ corresponds to the passage from parabolic to hyperbolic stress régimes in the general theory of bending of plates with the maximum principal moment yield condition discussed in the next Chapter.

The collapse load is

$$q = 2(\sqrt{\Lambda'} + (1+\Lambda')(\pi - \arctan\sqrt{\Lambda'})). \tag{7.80}$$

For a curvilinear boundary $\tan\beta = r_0'/r_0$, hence the limiting condition (7.79) becomes

$$\left(\frac{r_0'}{r_0}\right)^2 = \Lambda'. \tag{7.81}$$

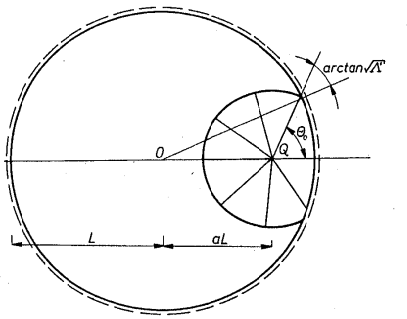

Fig. 7.18. Partial collapse of circular simply supported plate

We can now check the range of validity of the solution (7.54) concerning the circular plate shown in Fig. 7.18. Eq.(7.81) gives the following relation between the position of loading and the critical angle θ_0:

$$\sin\theta_0 = \frac{1}{a}\sqrt{\frac{\Lambda'}{1+\Lambda'}}. \tag{7.82}$$

The smallest eccentricity a at which the partial collapse occurs is that associated with $\max(\sin\theta_0)$, hence for $a = \sqrt{\frac{\Lambda'}{1+\Lambda'}}$. Eq. (7.54)

applies therefore in the range $0 \leqslant a \leqslant \sqrt{\frac{\Lambda'}{1+\Lambda'}}$. For $\sqrt{\frac{\Lambda'}{1+\Lambda'}} \leqslant a \leqslant 1$ the collapse pattern is shown in Fig. 7.18.

The collapse load consists of the contributions furnished by two continuous fields and by the hinge where the deflected surface has a ridge. The collapse load using (7.52) and (7.53) is

$$q = 2\left\{(1+\Lambda')(\pi-\theta_0) + \int_0^{\theta_0} \frac{d\theta}{1-a^2\sin^2\theta}\right\} =$$

$$= 2(1+\Lambda')(\pi-\theta_0) + \frac{2}{\sqrt{1-a^2}} \arctan\left(\sqrt{1-a^2}\,\tan\theta_0\right), \qquad (7.83)$$

where θ_0 is defined in (7.82).

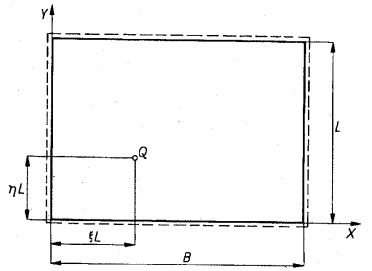

Fig. 7.19. Simply supported rectangular plate under point load

Let us finally consider a rectangular plate shown in Fig. 7.19 subjected to a concentrated force Q at an arbitrary position. Depending upon the position of the load different collapse mechanisms of partial or total collapse will lead to the best estimate of the load carrying capacity. The plate is isotropic but has different ultimate moments in positive and in negative flexure M^0 and $M_0' = \Lambda' M^0$, respectively.

As many as five different collapse mechanisms may appear, Table 7.3. The problem was systematically studied in [33], [61], and [88].

A set of level curves of the collapse load is shown in Fig. 7.20 for a square plate of equal ultimate moments in positive and negative bending. Fig. 7.21 shows the level curves of constant load-carrying capacity $q = Q/M^0$ for the plate aspect ratio $\beta = B/L = 1.5$. A large number of such diagrams can be found in [88].

Table 7.3

Collapse modes for simply supported rectangular plate under point load at arbitrary position

$$\beta=\frac{B}{L};\quad \Lambda'=\frac{M_0'}{M^0};\quad \xi=\frac{X}{L};\quad \eta=\frac{Y}{L};\quad q=\frac{Q}{M^0};$$

Mechanism I

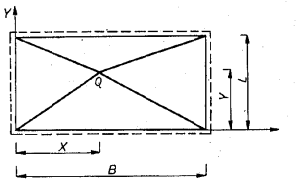

$$q=\beta\left(\frac{1}{\xi(\beta-\xi)}+\frac{1}{\eta(1-\eta)}\right)$$

Mechanism II

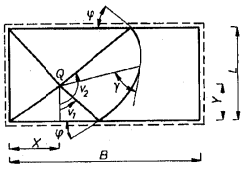

$$q=\frac{1}{\xi}+\frac{\xi}{\eta(1-\eta)}+\frac{\Lambda'}{\tan^2\varphi}(2\tan\varphi+(1+\tan^2\varphi)(\pi-2\varphi))$$

$$\eta=\frac{1-c\cdot\tan\varphi}{2\cdot e^{c(\pi-2\varphi)}};\quad c=\text{cotany};\quad c=\sqrt{\frac{1}{1+\Lambda'}\left(\frac{\Lambda'}{\tan^2\varphi}-1\right)}$$

for $\varphi \leqslant \arctan\sqrt{\Lambda'}$

Mechanism III

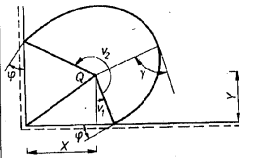

$$q=k+\frac{1}{k}+\frac{\Lambda'}{\tan^2\varphi_0}(2\tan\varphi+(1+\tan^2\varphi)(1.5\pi-2\varphi))$$

$$k=\frac{1+c\cdot\tan\varphi}{1-c\cdot\tan\varphi}e^{c(1.5\pi-2\varphi)};\quad k=\frac{X}{Y};$$

$$c=\sqrt{\frac{1}{1+\Lambda'}\left(\frac{\Lambda'}{\tan^2\varphi}-1\right)};\quad c=\text{cotany}$$

for $\varphi \leqslant \arctan\sqrt{\Lambda'}$

Mechanism IV

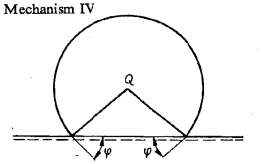

$$q=2\sqrt{\Lambda'}+(1+\Lambda')(\pi-\arctan\sqrt{\Lambda'})$$

for $\varphi=\arctan\sqrt{\Lambda'}$

Mechanism V

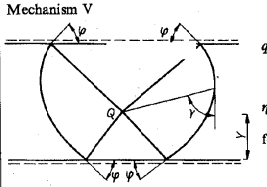

$$q=\frac{2\sqrt{\Lambda'}}{\tan^2\varphi}(2\tan\varphi+(1+\tan^2\varphi)(\pi-2\varphi)$$

$$\eta=\frac{1-c\cdot\tan\varphi}{2e^{c(\pi-2\varphi)}};\quad c=\sqrt{\frac{1}{1+\Lambda'}\left(\frac{\Lambda'}{\tan^2\varphi}-1\right)};\quad c=\text{cotany}$$

for $\varphi \leqslant \arctan\sqrt{\Lambda'}$

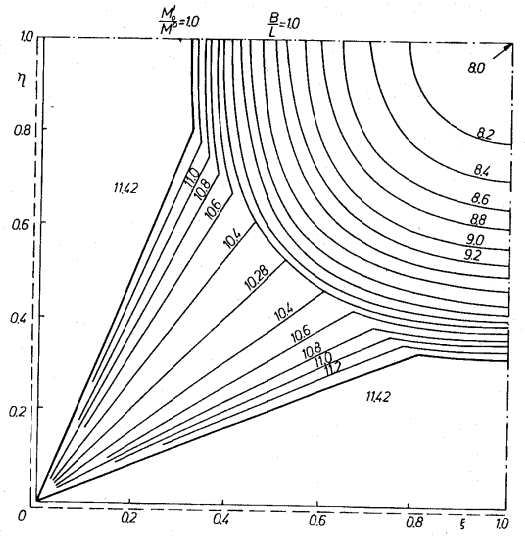

Fig. 7.20. Contour map of load-carrying capacity for a square plate under point load

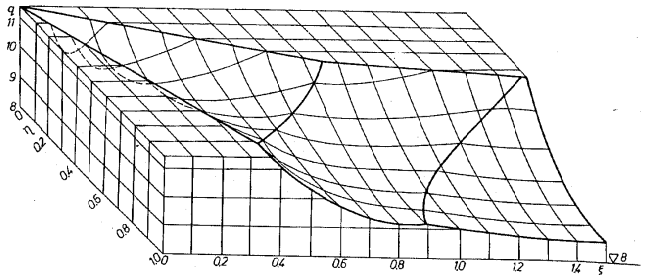

Fig. 7.21. Level curves of a constant load carrying-capacity for rectangular simply supported plate under point load

CHAPTER 8

COMPLETE SOLUTIONS

8.1. Equations of plastic flexure for the maximum principal moment interaction surface

The discussion of properties of plate equations in Chapter 3 has shown that for certain interaction surfaces the governing equations are either parabolic or hyperbolic. This fact allows to develop a method of generating complete solutions for a broader class of plates than rotationally symmetric ones.

Such a circumstance occurs in the case of the maximum principal moment interaction surface (3.21). In terms of the invariants (3.24) the interaction condition takes the form

$$\mathscr{F} = \psi \pm \omega \pm 1 = 0 \tag{8.1}$$

and in the plane of principal moments defines a square shown in Fig. 8.1. For the stress régimes corresponding to the sides of square (8.1) the representation (3.25) leads to

$$\varphi(\omega) = \pm\omega \pm 1, \quad \varphi' = \pm 1. \tag{8.2}$$

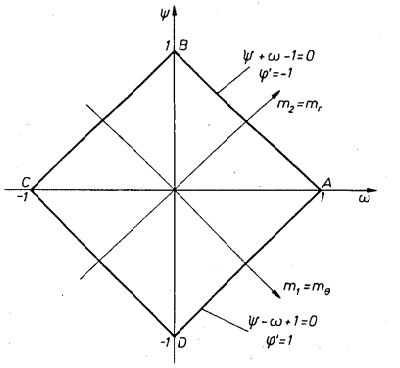

Fig. 8.1. Maximum principal moment interaction curve in the plane of the moment invariants

For definiteness we consider the side AD of the interaction square in Fig. 8.1. It follows from (3.36) that the deflected surface is then developable since

$$\dot{w}_{,xx}\,\dot{w}_{,yy} - (\dot{w}_{,xy})^2 = 0. \tag{8.3}$$

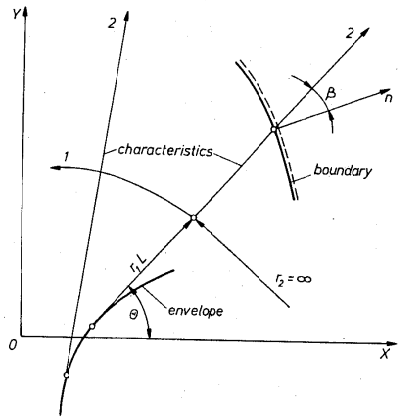

Fig. 8.2. Principal bending moment and curvature rate trajectories in the plate obeying maximum principal moment interaction curve

Finding a deflection velocity field at collapse consists therefore in deriving a developable surface passing through the plate boundary. The generatrix of the surface is a straight line marked in Fig. 8.2 as a characteristic. The velocity field has therefore the form

$$\dot{w} = A(\theta)\,r + B(\theta) \tag{8.4}$$

and the curvature rates in the system of coordinates r, θ are

$$\dot{\kappa}_\theta = \nu, \quad \dot{\kappa}_r = 0, \quad \dot{\kappa}_{r\theta} = 0. \tag{8.5}$$

Since the condition (8.1) is linear in the variable ω, thus it follows from (3.47) that the system of equations (3.29) and (3.37) is parabolic, except for the corners of the interaction square where simultaneously two yield equations are fulfilled and such a situation requires an additional analysis.

The characteristic direction is

$$\frac{dy}{dx} = \tan\theta \tag{8.6}$$

and the quadruple characteristic for the stress equations is a straight line. This can be seen directly from Eqs.(3.37) as one of them reduces under the condition of yielding (8.2) to the form

$$\theta_{,x}\cos\theta + \theta_{,y}\sin\theta = 0 \tag{8.7}$$

and therefore $d\theta = 0$. Hence the characteristic is a straight line. The characteristic coincides with the trajectory of $m_2 = m_r$, Fig. 8.2.

Choosing the net of trajectories as the system of orthogonal coordinates the following expressions are obtained for the variation of bending moments and shear forces along the characteristics

$$m_\theta = 1, \quad m_r = 1 + C(\theta) + \frac{D(\theta)}{r} + \frac{1}{r}\int p\rho^2\,d\rho - \int \rho p\,d\rho \tag{8.8}$$

$$s_\theta = 0, \quad rs_1 = C(\theta) - \int p\rho\,d\rho, \tag{8.9}$$

where $r = R/L$ stands for the dimensionless radius of curvature of the first trajectory, Fig. 8.2. The functions $C(\theta)$ and $D(\theta)$ are to be determined from the conditions available on the boundary, on the envelope of straight characteristics or elsewhere.

The load-carrying capacity of a parabolic régime is furnished by integrating the shear force along the curved trajectory. Different analytical solutions can be matched along the straight trajectories.

To complete the analysis of field equations associated with the interaction surface (8.1) it is necessary to study the singular stress régimes, namely the corner points A and C corresponding to vertices of the interaction cones (3.21) as well as the states B and D related to intersections of the cones.

For the states $m_1 = 1, m_2 = -1$ it is $\psi = \psi_0 = -1$, (point D in Fig. 8.1), and the field equations reduce to the set (3.49) and (3.53). The equations are hyperbolic and the characteristics coincide with the trajectories of principal moments, as given in (3.51).

The principal moments, shear forces and curvature rates are then

$$m_1 = -m_2 = 1, \quad s_1 = \frac{2}{r_2}, \quad s_2 = -\frac{2}{r_1}, \tag{8.10}$$

$$\dot{\kappa}_1 = \nu_1, \quad \dot{\kappa}_2 = -\nu_2, \quad \dot{\kappa}_{12} = 0, \quad \nu_1 > 0, \quad \nu_2 > 0. \tag{8.11}$$

Finally consider the states represented by $\psi_0 = 0$; then the corner points A and C of the interaction square of Fig. 8.1 are associated with the stress states

$$m_1 = m_2 = m_x = m_y = 1, \quad m_{xy} = 0, \quad s_x = s_y = 0, \tag{8.12}$$

independently of the orientation of trajectories. Such a stress zone is further referred to as isotropic. The curvature rates are

$$\dot{\kappa}_1 = v_1, \quad \dot{\kappa}_2 = v_2, \tag{8.13}$$

being arbitrary but nonnegative.

8.2. Matching the stress régimes

To match different analytical solutions on straight characteristics it is first necessary to establish admissible jumps across such lines. Across a straight trajectory 2, Fig. 8.2, the bending moment m_1 must be continuous but m_2 and s_2 do not have to since they are balanced on each side of the discontinuity line, similarly as σ_t in Fig. 2.4.

Consider situations when the external loading is continuous across a characteristic, $[p] = 0$. The magnitude of a jump depends on the stress régimes matched on the discontinuity line. Accordingly, the jumps to within the sign across the boundary line between the respective zones are:

parabolic – parabolic

$$[s_2] = \left[\frac{C}{r}\right], \quad [m_2] = [C] - \left[\frac{D}{r}\right], \tag{8.14}$$

parabolic – hyperbolic

$$r[s_2] = 2 + C, \quad [m_2] = 2 + C + \frac{D}{r}, \tag{8.15}$$

where C and D are established in the parabolic zone,

parabolic – isotropic

$$r[s_2] = C, \quad [m_2] = C + \frac{D}{r}, \tag{8.16}$$

isotropic – hyperbolic

$$r[s_2] = 2, \quad [m_2] = 2. \tag{8.17}$$

8.3. Point loaded plates

Let us apply the theory to point loaded plates. Consider a simply supported plate a quarter of which is shown in Fig. 8.3. The plate is subject to

the concentrated force Q at the origin of the polar coordinate system r, θ and its boundary is described in dimensionless variables, Fig. 8.3,

$$r = r_0(\theta). \tag{8.18}$$

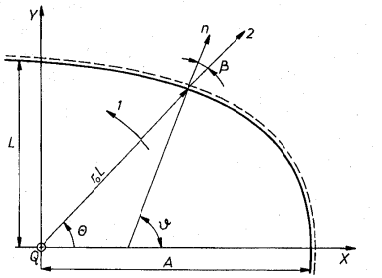

Fig. 8.3. A quarter of simply supported elliptic plate loaded at its centre

We consider a parabolic stress régime. Hence the deflected surface is a developable one passing through the boundary and through the point of load application, thus forming a cone. The characteristics are straight lines through the origin. They make an angle β with the normal to the boundary

$$\tan\beta = \frac{r_0'}{r_0}, \tag{8.19}$$

where prime denotes differentiation with respect to θ.

The boundary condition on a simply supported contour requires the normal moment to vanish, $m_n = 0$. Since $m_\theta = m_1 = \pm 1$ on the straight trajectory the following condition on the boundary is obtained:

$$m_n = m_r \cos^2\beta \pm \sin^2\beta = 0, \tag{8.20}$$

where $m_2 = m_r$. From (8.20) the stress boundary condition on m_r follows,

$$m_r = -\tan^2\beta = -\left(\frac{r_0'}{r_0}\right)^2 \geqslant -1. \tag{8.21}$$

The inequality sign comes from the requirement that the stress profile cannot go further than the hyperbolic point, thus e.g. the point D of the side AD in Fig. 8.1. The limitation $|\beta| \leqslant \pi/4$ follows from (8.21). It allows to find the extent of a parabolic zone.

Under a point load the expressions (8.8) and (8.9) for the stress field in a parabolic zone take the form

$$m_1 \equiv m_\theta = 1, \quad m_2 \equiv m_r = 1 + C(\theta) + \frac{D(\theta)}{r}, \tag{8.22}$$

$$s_\theta = 0, \quad rs_r = C(\theta), \tag{8.23}$$

where r denotes the dimensionless radius of the first curvature trajectory.

Since m_r remains bounded $D(\theta) = 0$ if $r = 0$ belongs to the plate, as it is the case in the considered example of load applied at the coordinate origin. Eventually parabolic stress fields in a point loaded plate under downward directed loading are of the form

$$m_\theta = 1, \quad m_r = -\tan^2\beta, \quad s_\theta = 0, \quad rs_r = -(1 + \tan^2\beta) \tag{8.24}$$

for $|\beta| \leqslant \pi/4$. The stress field is fully specified by the plate contour.

Once the radial shear force is known the load-carrying capacity q_p of a parabolic segment can be evaluated, namely

$$q_p = -\int s_r\, dt = -\int_{\theta_1}^{\theta_2} C(\theta)\, d\theta = \int_{\theta_1}^{\theta_2}\left(1 + \left(\frac{r_0'}{r_0}\right)^2\right) d\theta. \tag{8.25}$$

The deflected surface (8.4) for a parabolic segment is a part of a cone with vertex at the point of load application,

$$\dot{w} = \dot{w}_0\left(1 - \frac{r}{r_0}\right), \tag{8.26}$$

$\dot{w}_0$ being the deflection rate of the loaded point.

It is to be remarked that whenever the angle is not uniquely determined, i.e. when discontinuities in the boundary slope occur, the moment m_r suffers a jump

$$[m_r] = r[s_r] = \tan^2\beta^+ - \tan^2\beta^- = \text{constant}. \tag{8.27}$$

There is also a ridge on the deflection surface (8.26) along the straight trajectory passing through a corner point.

For a hyperbolic zone the stress field is given in (8.10) for a point loaded plate. If, moreover, the family of straight characteristics (3.51) forms a Hencky-Prandtl net, extensively studied in the plane plastic flow, then the load carried by a hyperbolic zone is

$$q_h = -\int s_r\, dt_\theta = 2\int_{\theta_1}^{\theta_2} d\theta = 2(\theta_2 - \theta_1) \tag{8.28}$$

since $s_r = s_2$ is given in (8.10) and r_1 is independent of θ when the deflected surface is a cone (8.26).

No load is carried by an isotropic region (8.12). Such a zone, if exists in a plate must be contained within other stress régimes.

As an example of the proposed technique of deriving complete solutions to limit analysis of slabs we consider an elliptic, simply supported plate loaded at the centre. Fig. 8.3 shows a quarter of the plate. The boundary curve in dimensionless variables is

$$r_0(\theta) = a(a^2\sin^2\theta + \cos^2\theta)^{-1/2}, \quad a = \frac{A}{L}. \tag{8.29}$$

In a parabolic region the bending moments specified by (8.24) are easily found once the boundary curve is specified, as it is the case in (8.29). One obtains

$$m_\theta = 1, \quad m_r = -\frac{(1-a^2)^2\tan^2\theta}{(1+a^2\tan^2\theta)^2}. \tag{8.30}$$

In view of (8.21) the solution applies for the plate aspect ratio

$$1 \leqslant a \leqslant 1 + \sqrt{2} \tag{8.31}$$

otherwise hyperbolic zones are present.

For the plate satisfying the requirement (8.31) the collapse load is found from (8.25)

$$q = 4\int_0^{2\pi}\left(1 + \left(\frac{r_0'}{r_0}\right)^2\right) d\theta = \frac{\pi}{a}(1+a^2). \tag{8.32}$$

The velocity field is specified in (8.26) in the shape of a cone.

8.4. Welded solutions

The possibilities of combining different analytical solutions in the complete one for a plate requires a study of a certain number of elementary solutions corresponding to various shapes of the contour.

We shall consider the plate boundaries $r_0(\theta)$ satisfying the requirements, Fig. 8.4,

$$r_0(0) = 1, \quad r_0'(0) \geqslant 0 \tag{8.33}$$

and $0 \leqslant \theta \leqslant \pi/4$. For definiteness, the analysis will be restricted to the case $m_\theta = 1$. Knowing the boundary of a segment the load carried in the limit state is established according to (8.25):

a) straight boundary:

$$r_0 = \frac{1}{\cos\theta}, \quad m_r = -\tan^2\theta \tag{8.34}$$

and the collapse load of a segment $0 \leqslant \theta \leqslant \theta_0$ is

$$q_p = \tan\theta_0, \quad \theta_0 < \frac{\pi}{4}, \tag{8.35}$$

b) circle:

$$r_0 = 1, \quad m_r = 0 \tag{8.36}$$

and a circular segment carries thus the load

$$q_p = \theta_0. \tag{8.37}$$

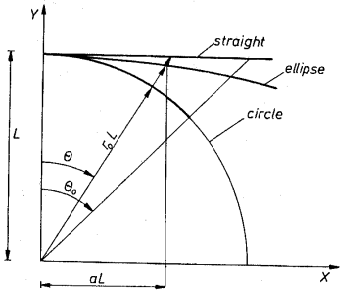

Fig. 8.4. Simply supported plate elements

There is no limitation on the value of θ_0 within the range $0 \leqslant \theta_0 \leqslant 2\pi$.

c) ellipse:

$$q_p = \frac{1}{2a}\left\{(1+a^2)\arctan\left(a^{-1}\tan\theta_0\right) + a(a^2-1)\frac{\tan\theta_0}{a^2+\tan^2\theta_0}\right\} \tag{8.38}$$

whereas the plate contour and radial moment are

$$r_0 = a(\sin^2\theta + a^2\cos^2\theta)^{-1/2}, \quad m_r = -\frac{(1-a^2)^2\tan^2\theta}{(a^2+\tan^2\theta)^2}, \tag{8.39}$$

d) logarithmic spiral

$$r_0 = \mathrm{e}^{\gamma\theta}, \quad m_r = -\gamma^2 \tag{8.40}$$

and the collapse load for the segment $0 \leqslant \theta \leqslant \theta_0$ is

$$q_p = (1+\gamma)^2\,\theta_0, \quad 0 \leqslant \theta_0 \leqslant \frac{\pi}{2}. \tag{8.41}$$

If $\gamma = 1$ the zone becomes hyperbolic, $m_\theta = 1, m_r = -1$ and the collapse load is then

$$q_h = 2\theta_0. \tag{8.42}$$

This result concerns a clamped plate as well.

Such elementary solutions for different loaded segments can be found in Table 8.1 and may be „welded" along straight characteristics, [47], [89].

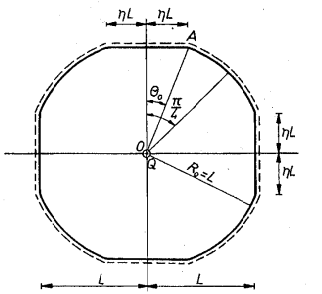

Fig. 8.5. Simply supported square plate with rounded corners

As an example of a welded solution we consider a plate as shown in Fig. 8.5, a square with rounded corners loaded at the centre. The load-carrying capacity is

$$q = 2\pi + 8(\eta - \arctan\eta). \tag{8.43}$$

The result follows from (8.35) and (8.37). The moments are $m_\theta = 1$ throughout and

$$m_r = \begin{cases} -\eta^2, & 0 \leqslant \theta \leqslant \theta_0 \\ 0, & \theta_0 \leqslant \theta \leqslant \dfrac{\pi}{4}. \end{cases} \tag{8.44}$$

There is a jump in the radial moment on the line AO as well as the remaining points where the tangent to the boundary line is not uniquely defined.

In Fig. 8.6 a plate is shown whose boundary is composed of straight lines and logarithmic spirals. The collapse load is, according to (8.35) and (8.41),

$$q = 4 + (1+\gamma^2)\pi, \quad \gamma = \tan\beta. \tag{8.45}$$

The bending moment $m_r = -\gamma^2$ is constant in the zone OBC and varies according to (8.34) in OAB.

Table 8.1

Elementary solutions for various segments of plates

Segment of plate	Collapse load, bending moments, shear forces, deflection rates
$q=\frac{Q}{M^0}$, $p=\frac{PL^2}{M^0}$, $\Lambda'=\frac{M_0'}{M^0}$, $r=\frac{R}{L}$	
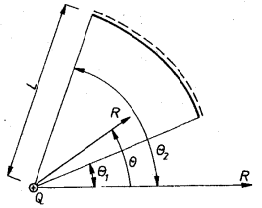	$q=\theta_2-\theta_1$ $m_\theta=1;\ s_\theta=0,\ s_r=-\frac{1}{r}$ $m_r=1$ for $r=0$ $m_r=0$ for $0<r\leqslant 1$ $\dot{w}=\dot{w}_0(1-r)$
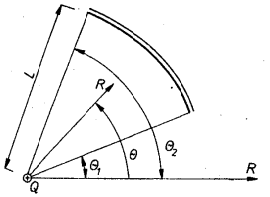	$q=(1+\Lambda')(\theta_2-\theta_1)$ $m_\theta=1;\ s_\theta=0,\ s_r=-\frac{1-\Lambda'}{r}$ $m_r=1$ for $r=0$ $m_r=1-\Lambda'$ for $0<r\leqslant 1$ $\dot{w}=\dot{w}_0(1-r)$
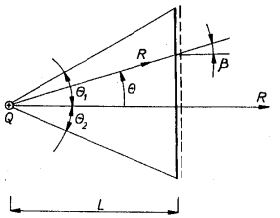	$q=\tan\theta_1+\tan\theta_2;\ \theta_1,\theta_2\leqslant\arctan\sqrt{\Lambda'}$ $m_\theta=1;\ s_\theta=0,\ s_r=-\frac{1}{r}(1+\tan^2\theta)$ $m_r=1$ for $r=0$ $m_r=-\tan^2\theta$ for $0<r\leqslant\frac{1}{\cos\theta}$ $\dot{w}=\dot{w}_0(1-r\cos\theta)$

Table 8.1, contd

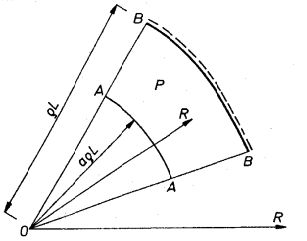	$p=\frac{6}{(\rho-a)^2\left(1+\frac{2a}{\rho}\right)}$ $m_\theta=m_r=1;\ s_\theta=s_r=0$ for AOA $m_\theta=1,\ m_r=1-\frac{p}{6}(r-a)^2\left(1+\frac{2a}{r}\right)$, $s_\theta=0,\ s_r=-\frac{p}{2}(\rho^2-a^2)$ for $AABB$ $\dot{w}=\dot{w}_0(1-r)$
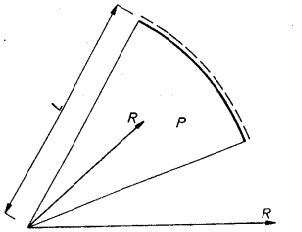	$p=6$ $m_\theta=1,\ m_r=1-r^2$ $s_\theta=0,\ s_r=-3r$ $\dot{w}=\dot{w}_0(1-r)$
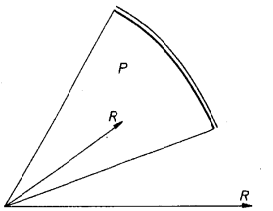	$p=6\,(1+\Lambda')$ $m_\theta=1,\ m_r=1-r^2\,(1+\Lambda')$ $s_\theta=0,\ s_r=-3r\,(1+\Lambda')$ $\dot{w}=\dot{w}_0\,(1-r)$
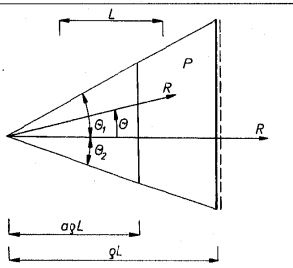	$p=\frac{6}{\rho^2(1-a)^2(1+2a)}\cdot\frac{1}{}$ $m_\theta=1,\ m_r=1-\frac{p}{6}\left(r-\frac{a\rho}{\cos\theta}\right)^2\left(1+\frac{2a\rho}{r\cos\theta}\right)$ $s_\theta=0,\ s_r=-\frac{p}{2}\left(r^2-\frac{a^2\rho^2}{\cos^2\theta}\right)$ $\theta_1,\ \theta_2\leqslant\arctan\sqrt{\Lambda'}$ $\dot{w}=\dot{w}_0\left(1-\frac{r}{\rho}\cos\theta\right)$

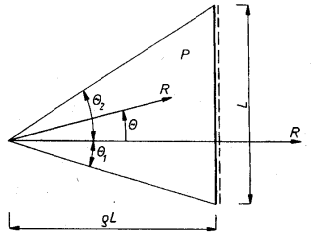

$$p=\frac{6}{\rho^2}$$

$$m_0=1,\ m_r=1-\frac{r^2}{\rho^2}$$

$$s_0=0,\ s_r=-3\frac{r}{\rho^2}$$

$$\theta_1,\ \theta_2\leqslant\arctan\sqrt{\Lambda'}$$

$$\dot{w}=\dot{w}_0\left(1-\frac{r}{\rho}\cos\theta\right)$$

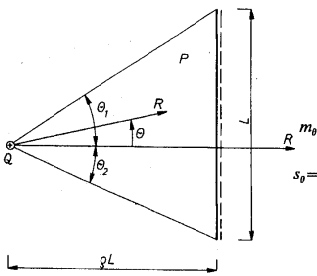

$$p=\frac{6\lambda}{\rho^2},\ q=\alpha p$$

$$\lambda=\frac{\rho^2 q_0}{6\alpha+\rho^2 q_0},\ q_0=\tan\theta_1+\tan\theta_2$$

$$m_0=1,\ m_r=\lambda\left(1-\frac{r^2}{\rho^2}\right)-(1-\lambda)\tan^2\theta$$

$$s_0=0,\ s_r=-3\lambda\frac{r}{\rho^2}-(1-\lambda)\frac{1}{r}(1+\tan^2\theta)$$

$$\theta_1,\ \theta_2\leqslant\arctan\sqrt{\Lambda'}$$

$$\dot{w}=\dot{w}_0\left(1-\frac{r}{\rho}\cos\theta\right)$$

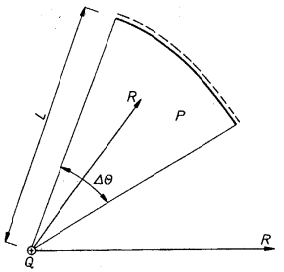

$$p=6\lambda,\ q=\alpha p$$

$$\lambda=\frac{\Delta\theta}{6\alpha+\Delta\theta}$$

$$m_0=1,\ m_r=\lambda\,(1-r^2)$$

$$s_0=0,\ s_r=-3r\lambda-\frac{1}{r}(1-\lambda)$$

$$\dot{w}=\dot{w}_0\,(1-r)$$

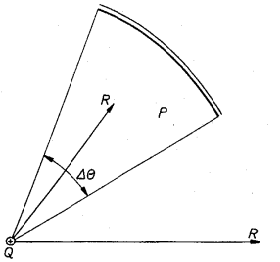

$$p=6\lambda\,(1+\Lambda'),\ q=\alpha p$$

$$\lambda=\frac{\Delta\theta}{6\alpha+\Delta\theta}$$

$$m_0=1,\ m_r=\Lambda'+(1+\Lambda')\,\lambda\,(1-r^2)$$

$$s_0=0,\ s_r=-3r\lambda(1+\Lambda')-\frac{1-\Lambda'}{r}(1-\lambda)$$

$$\dot{w}=\dot{w}_0\,(1-r)$$

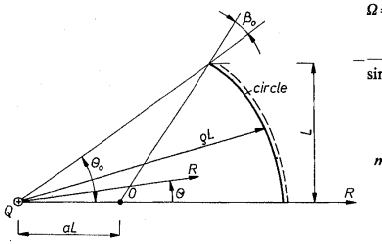

$$q=\sqrt{\frac{a^2+\Omega}{\Omega}}\arctan\left(\sqrt{\frac{\Omega}{a^2+\Omega}}\tan\theta_0\right)$$

$$\Omega=1+\operatorname{cotan}\theta_0(\operatorname{cotan}\theta_0-2a)$$

$$-\frac{\sin\beta_0}{\sin\theta_0\sin(\theta_0-\beta_0)}\leqslant a\leqslant\operatorname{cotan}\theta_0$$

$$\beta_0=\arctan\sqrt{\Lambda'}\leqslant\theta_0$$

$$m_0=1,\ m_r=-\frac{a^2\sin^2\theta}{a^2\cos^2\theta+\Omega}$$

$$s_0=0,\ s_r=-\frac{1}{r}\frac{1+(a-\operatorname{cotan}\theta_0)^2}{a\cos^2\theta+\Omega}$$

$$\dot{w}=\dot{w}_0\left(1-\frac{r}{\rho}\right)$$

$$\rho=a\cos\theta+\sqrt{a^2\cos^2\theta+\Omega}$$

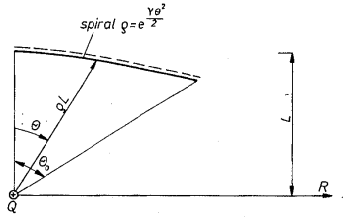

$$q=\theta_0\left(1+\frac{\gamma^2\theta_0^2}{3}\right)$$

$$\gamma\theta_0\leqslant\sqrt{\Lambda'}$$

$$m_0=1,\ m_r=-(\gamma\theta)^2$$

$$s_0=0,\ s_r=-\frac{1}{r}(1+(\gamma\theta)^2)$$

$$\dot{w}=\dot{w}_0\left(1-\frac{r}{\rho}\right)$$

$$\rho=\exp\left[\frac{\gamma\theta^2}{2}\right]$$

Table 8.1 contd

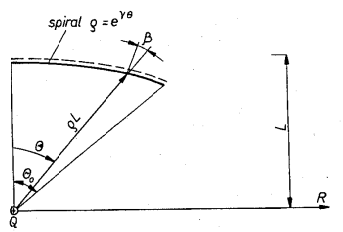

$$q=(1+\gamma^2)\theta_0$$

$$\gamma=\tan\beta\leqslant\sqrt{\Lambda'}$$

$$m_\theta=1,\ m_r=-\gamma^2$$

$$s_\theta=0,\ s_r=-\frac{1}{r}(1-\gamma^2)$$

$$\dot{w}=\dot{w}_0\left(1-\frac{r}{\rho}\right)$$

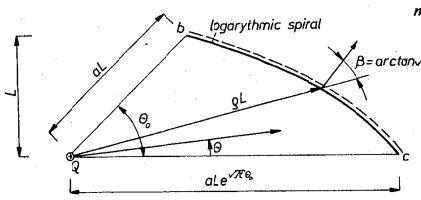

$$q=(1+\Lambda')\theta_0$$

$$m_\theta=1,\ m_r=-\Lambda'$$

$$s_\theta=0,\ s_r=-\frac{1+\Lambda'}{r}$$

$$m_r^{bc}=0,\ m_{rs}^{bc}=$$

$$=-\frac{1+\Lambda'}{2}\sin\left(2\arctan\sqrt{\Lambda'}\right)$$

$$s_n=-\frac{1+\Lambda'}{\rho}\cos\left(\arctan\sqrt{\Lambda'}\right)$$

$$\dot{w}=\dot{w}_0\left(1-\frac{r}{\rho}\right)$$

$$\rho=a\exp\left[\sqrt{\Lambda'}\,(\theta_0-\theta)\right]$$

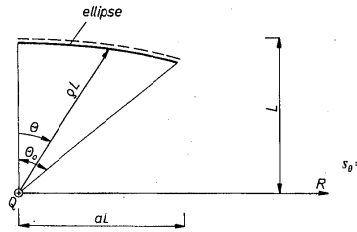

$$q=\frac{1}{2a}\left\{(1+a^2)\arctan\left(\frac{\tan\theta_0}{a}\right)\right\}+$$

$$a\,(a^2-1)\,\frac{\tan\theta_0}{a^2+\tan^2\theta_0}$$

$$1\leqslant a\leqslant\sqrt{\Lambda'}+\sqrt{1+\Lambda'}$$

$$m_\theta=1,\ m_r=-\frac{(1-a^2)^2\tan\theta}{(a^2+\tan^2\theta)^2}$$

$$s_\theta=0,\ s_r=\frac{1}{r}\,\frac{(1+\tan^2\theta)\,(a^4+\tan^2\theta)}{(a^2+\tan^2\theta)^2}$$

$$\dot{w}=\dot{w}\left(1-\frac{r}{\rho}\right)$$

$$\rho=a\,(\sin^2\theta+a^2\cos^2\theta)^{-1/2}$$

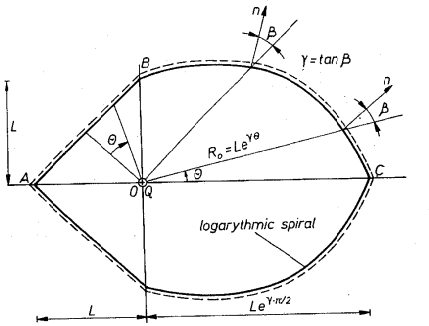

Fig. 8.6. Simply supported plate with boundary composed of straight lines and logarithmic spirals

To show the procedure of deriving complete solution combining parabolic and isotropic régimes let us consider a simply supported circular plates loaded by the point loads Q_1 and Q_2 as shown in Fig. 8.7, [91].

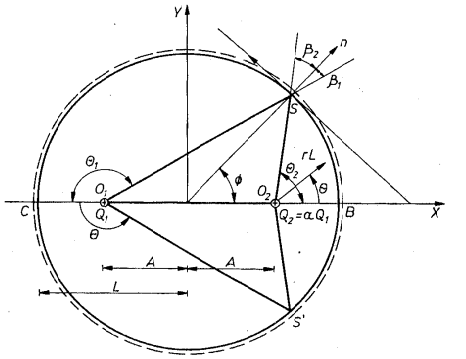

Fig. 8.7. Simply supported circular plate under two point loads

The complete solution consists of the parabolic zones $SCS'O_1$ and $S'BSO_2$, joined by the isotropic régimes $SO_1S'O_2$. In the isotropic zone of the plate the internal actions are:

$$m_x = m_y = m_r = m_\theta = 1, \quad s_x = s_y = s_r = s_\theta = 0. \tag{8.46}$$

In the parabolic zones $SCS'O_1$ and $S'BCO_2$ the bending moments and the shear forces expressed in polar coordinates with the origin at the point of loading, Fig. 8.7, are, respectively,

$$\begin{aligned} m_\theta &= 1, \quad m_r = -\frac{a^2 \sin^2\theta}{1-a^2\sin^2\theta}, \\ s_\theta &= 0, \quad s_r = -\frac{1}{r}\frac{1}{1-a^2\sin^2\theta}, \end{aligned} \tag{8.47}$$

where $a = A/L$.

Along the lines O_1S, O_2S, O_1S', O_2S' discontinuities in the radial moment appear, as can be seen when comparing (8.46) with (8.47). The collapse loads are found from (8.25)

$$\begin{aligned} q_1 &= \frac{2}{\sqrt{1-a^2}}\left(\pi - \arctan\left(\sqrt{1-a^2}\,\frac{\sin\phi}{a+\cos\phi}\right)\right), \\ q_2 &= \frac{2}{\sqrt{1-a^2}}\left(\gamma - \arctan\left(\sqrt{1-a^2}\,\frac{\sin\phi}{a-\cos\phi}\right)\right), \end{aligned} \tag{8.48}$$

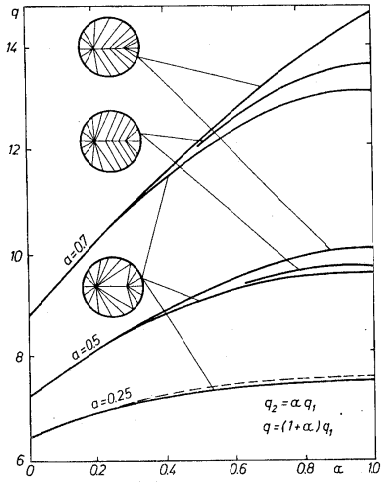

Fig. 8.8. Comparison of the exact and the yield line solutions for simply supported circular plate under two point loads

where $\gamma = 0$ if $\phi \leqslant \arccos a$ and $\gamma = \pi$ if $\phi > \arccos a$.

The solution is valid for the following range of load eccentricity

$$0 \leqslant a \leqslant k\frac{1}{\sqrt{2}}, \tag{8.49}$$

where $k = 1/\sin\theta_2$ for $\theta_2 < \pi/2$ and $k = 1$ for $\theta_2 \geqslant \pi/2$.

The angle ϕ specifying the meeting point S of two parabolic régimes is given by the equation

Table 8.2

Complete solution for circular plate under point loads

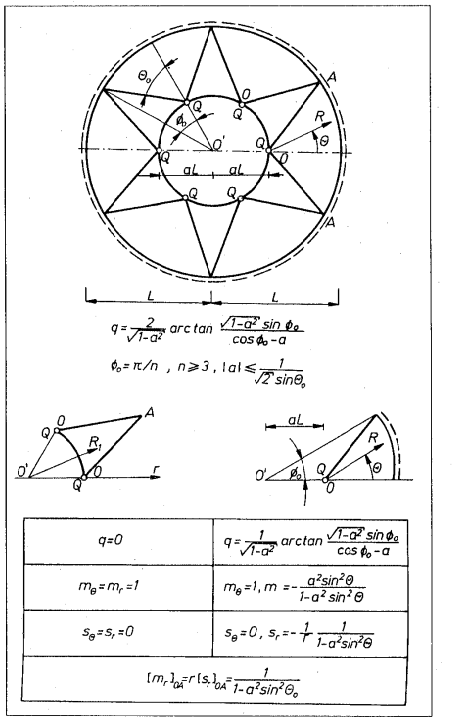

$q=0$	$q=\frac{1}{\sqrt{1-a^2}}\arctan\frac{\sqrt{1-a^2}\sin\phi_0}{\cos\phi_0-a}$
$m_\theta=m_r=1$	$m_\theta=1, m_r=-\frac{a^2\sin^2\theta}{1-a^2\sin^2\theta}$
$s_\theta=s_r=0$	$s_\theta=0, s_r=-\frac{1}{r}\frac{1}{1-a^2\sin^2\theta}$
$[m_r]_{QA}=r[s_r]_{QA}=\frac{1}{1-a^2\sin^2\theta_0}$	

$$\alpha = \frac{q_2}{q_1} = \frac{\gamma - \arctan\left(\sqrt{1-a^2}\,\frac{\sin\phi}{a-\cos\phi}\right)}{\pi - \arctan\left(\sqrt{1-a^2}\,\frac{\sin\phi}{a+\cos\phi}\right)}. \tag{8.50}$$

It is interesting to compare the obtained complete solution with that following from the yield line theory given in Chapter 7 for the ratio of the loads $\alpha = 1$, Figs. 7.15a and b.

We can observe that for the load ratio $0 < \alpha < 0.5$ the differences between the solutions are of the order of a few per cent only. The largest differences are obtained for $\alpha = 1$ at the largest admissible eccentricity for the studied complete solution involving parabolic and isotropic régimes. An illustration of this observation is given in Fig. 8.8.

An analogous procedure is applied to plates loaded by several point loads. A typical example is shown in Table 8.2. The central star-shaped region is isotropic, the rest of the plate belongs to parabolic régimes. A collection of tables can be found in the Appendix, [89].

8.5. Uniformly loaded plates

As an example of matching different parabolic régimes we consider a uniformly loaded plate shown in Fig. 8.9. Its boundary consists of straight lines and circular arcs. We assume, as will be justified later, that the solution

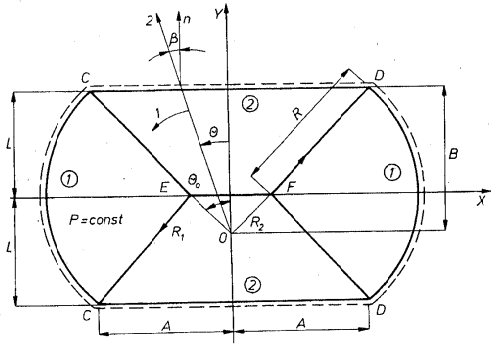

Fig. 8.9. Uniformly loaded simply supported plate

consists of two parabolic régimes associated respectively with curved and straight boundaries.

For uniformly distributed loading the stress field (8.8) and (8.9) becomes

$$m_1 = m_\theta = 1, \quad m_2 = m_r = 1 + C(\theta) + \frac{D(\theta)}{r} - \frac{pr^2}{6},$$
$$s_1 = s_\theta = 0, \quad rs_r = C(\theta) - \frac{pr^2}{2}, \tag{8.51}$$

where $p = PL^2/M^0$.

The solutions for the regions *1* and *2* are matched on *CE* and *DF* requiring the collapse pressure for both parts to be the same, $p_1 = p_2 = p$. In the zone *1* the stress boundary conditions are

$$m_r = 0 \text{ on } CC, \quad s_r = 0 \text{ and } m_r \leqslant 1 \text{ at } E \tag{8.52}$$

and the stress field (8.51), expressed in the polar coordinate system with the origin at E becomes

$$m_\theta = 1, \quad m_r = 1 - r^2\frac{L^2}{R^2}, \quad s_r = 3r\frac{L^2}{R^2}, \tag{8.53}$$

where $r = R_1/L$, Fig. 8.9. The collapse load of the zone *1* is found from (8.51) and (8.52),

$$p_1 = 6\frac{L^2}{R^2}. \tag{8.54}$$

In the zone *2* the boundary conditions are

$$m_r = -\tan^2\theta \text{ on } CD, \quad s_r = 0 \text{ and } m_r = 1 \text{ on } EF. \tag{8.55}$$

The stress (8.51) is easily established, [77], and the collapse load is found for the zone *2* to be

$$p_2 = \frac{6}{3 - 2\frac{L}{B}}. \tag{8.56}$$

Equating the results (8.54) and (8.56) the relation between the plate parameters is obtained,

$$\frac{R}{L} = \sqrt{3 + 2\left(\frac{L}{A}\right)^2\left(1 - \sqrt{1+2\left(\frac{A}{L}\right)^2}\right)}. \tag{8.57}$$

Eqs. (8.54) and (8.56) give the collapse load of the considered plate. Due to the parabolicity requirement (8.21) the solution holds for $0 \leqslant A/L \leqslant 2$.

There is a discontinuity in the shear force and in the radial moment across the trajectory *FD*. The jump is not constant as it was the case of point loaded plates, but obeys (8.14). The line *EF* corresponds to an isotropic régime.

The deflection velocity consists of conical parts corresponding to the curved boundary and of flat portions associated with the straight edges. A ridge runs along *CEFD*.

For an arbitrary boundary curve the analytical solutions are seldom possible as the envelope of straight trajectories is not known a priori. A suitable numerical procedure can, however, be developed for plates uniformly loaded over a part of the middle plane, [52].

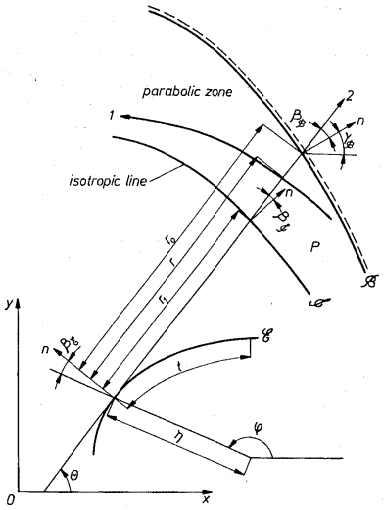

Fig. 8.10. Partially loaded fragment of simply supported plate

Let us consider a simply supported plate, a fragment of which is shown in Fig. 8.10. The non-loaded part carries no shearing forces and hence belongs to the isotropic régime.

The loaded part is assumed to be in a parabolic stress régime, thus the bending moments satisfy the condition (8.20). Let $\mathscr{B}$ and $\mathscr{J}$ be the boundaries of the plate and of the isotropic stress region, respectively. By $r_0(\theta)$ and $r_1(\theta)$ we denote the distance of these curves from the envelope $\mathscr{E}$ of straight trajectories, as measured along the second trajectory.

The boundary condition on a simply supported edge $\mathscr{B}$ is

$$m_r = -\tan^2\beta_{\mathscr{B}} \quad \text{on} \quad r = r_0(\theta), \tag{8.58}$$

where $\beta_{\mathscr{B}} = \theta - \gamma_{\mathscr{B}}$, Fig. 8.10. Along the line $\mathscr{J}$ separating the isotropic and parabolic stress zones

$$m_r = 1, \quad rs_r = 0 \quad \text{on} \quad r = r_1(\theta). \tag{8.59}$$

Application of the boundary conditions (8.58) and (8.59) to (8.8) allows to find constants $C(\theta)$ and $D(\theta)$ as well as to establish the following expression for the collapse load:

$$p = \frac{6(1+\tan^2\beta_{\mathscr{B}})}{(r_0-r_1)^2\left(1+2\,\dfrac{r_1}{r_0}\right)}. \tag{8.60}$$

The bending moment and the shear force along the straight trajectory are

$$m_r = 1 - \frac{p}{6}(r-r_1)^2\left(1+2\,\frac{r_1}{r}\right), \qquad rs_r = -\frac{p}{2}(r^2-r_1^2). \tag{8.61}$$

It is seen that m_r decreases monotonically with r and takes values ranging from 1 to $-\tan^2\beta_{\mathscr{B}}$. The condition for the parabolic type of equations is always satisfied if $\tan^2\beta_{\mathscr{B}} \leqslant 1$.

If t denotes the arc length of the envelope $\mathscr{E}$ measured from a certain point on $\mathscr{E}$ then

$$\tan\beta_{\mathscr{B}} = \frac{1}{r_0}\left(\frac{dr_0}{d\theta} - \frac{dt}{d\theta}\right). \tag{8.62}$$

Similarly

$$\tan\beta_{\mathscr{J}} = \frac{1}{r_1}\left(\frac{dr_1}{d\theta} - \frac{dt}{d\theta}\right). \tag{8.63}$$

Eq. (8.60) can be written as follows:

$$\frac{r_1}{r_0} = \frac{1}{2}\left(\frac{6(1-\tan^2\beta_{\alpha\alpha})}{p(r_0-r_1)^2} - 1\right) \tag{8.64}$$

whereas (8.62) and (8.63) lead to

$$\frac{d}{d\theta}(r_0 - r_1) = r_0 \tan\beta_{\alpha\alpha} - r_1 \tan\beta_{\beta\beta}. \tag{8.65}$$

The set (8.64) and (8.65) can be used to compute the envelope of straight trajectories numerically. An iterative technique to construct the net of trajectories, the envelope and to find the collapse load for plates of given boundary curve is described in [52].

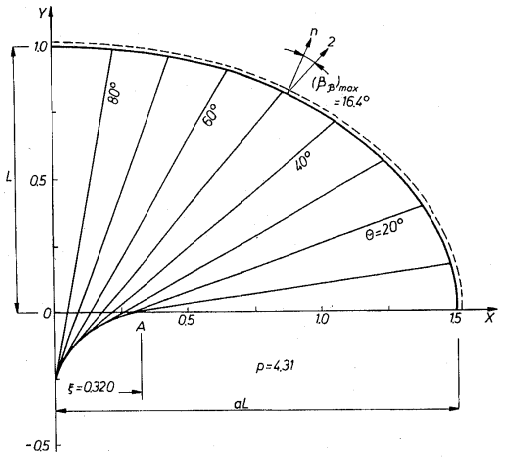

Fig. 8.11. Elliptic simply supported plate under uniform load

In Fig. 8.11 straight characteristics for a uniformly loaded elliptic plate of the aspect ratio $a = 1.5$ are shown. It is seen that the isotropic zone reduces to the line OA, which corresponds to a ridge of the deflection velocity $\dot{w}$.

The deflection velocity surface is developable, of the generatrix intersecting the boundary curve with $\beta_{\alpha\alpha}$ and tangent to the envelope.

Table 8.3

Collapse load for simply supported elliptic plate

a	1.0	1.1	1.2	1.3	1.4	1.5
p	6.0	5.48	5.08	4.76	4.52	4.31
ξ	0.0	0.053	0.113	0.178	0.247	0.320
a	1.6	1.8	2.0	2.2	2.4	2.6
p	4.14	3.89	3.70	3.56	3.45	3.37
ξ	0.397	0.557	0.726	0.901	1.081	1.265
a	2.8	3.0	3.2	3.4	3.52	
p	3.30	3.24	3.20	3.16	3.14	
ξ	1.451	1.640	1.830	2.022	2.137	

Table 8.3 gives the collapse load p and the ridge length ξ of the plate at collapse. For plates of $a > 3.52$ the parabolicity condition $(\beta_{\alpha\alpha})_{\max} \leqslant 45°$ is not satisfied and a hyperbolic régime appears. Thus the solutions are applicable to plates with the semi-axes aspect ratio $a \leqslant 3.52$.

Appendix

CATALOGUE OF COMPLETE SOLUTIONS FOR THE MAXIMUM PRINCIPAL MOMENT INTERACTION SURFACE

List of symbols

X, Y	– Cartesian coordinates
R, θ	– polar coordinates
L	– reference length
H	– plate thickness
M^0 , $M_0' = \Lambda' M^0$	– ultimate moments for positive and negative bending
Λ'	– coefficient
$M_x, M_y, M_{xy}, M_r, M_\theta, M_1, M_2$	– moments
$S_x, S_y, S_r, S_\theta, S_1, S_2$	– shear forces
$\dot{W}$	– deflection rates
$\dot{K}_x, \dot{K}_y, \dot{K}_{xy}, \dot{K}_r, \dot{K}_\theta, \dot{K}_1, \dot{K}_2$	– curvature rates
$P, \bar{P}, Q$	– collapse loads: distributed, line, concentrated, respectively
	– simply supported edge
	– clamped edge
	– free edge
	– column without restraint
	– yield line
	– downward-directed concentrated forces
	– line load

Dimensionless quantities

$$x = \frac{X}{L}, \quad y = \frac{Y}{L}, \quad r = \frac{R}{L}, \quad a = \frac{A}{L}, \quad b = \frac{B}{L}$$

$$m_x = \frac{M_x}{M^0}, \; m_y = \frac{M_y}{M^0}, \; m_{xy} = \frac{M_{xy}}{M^0}, \; m_r = \frac{M_r}{M^0}, \; m_\theta = \frac{M_\theta}{M^0}, \; m_1 = \frac{M_1}{M^0}, \; m_2 = \frac{M_2}{M^0},$$

$$s_x = \frac{S_x L}{M^0}, \; s_y = \frac{S_y L}{M^0}, \; s_r = \frac{S_r L}{M^0}, \; s_\theta = \frac{S_\theta L}{M^0}, \; s_1 = \frac{S_1 L}{M^0}, \; s_2 = \frac{S_2 L}{M^0}$$

$$\dot{w} = \frac{\dot{W}}{L},$$

$$\dot{\kappa}_x = H\dot{K}_y, \; \dot{\kappa}_y = H\dot{K}, \; \dot{\kappa}_{xy} = H\dot{K}_{xy}, \; \dot{\kappa}_r = H\dot{K}_r, \; \dot{\kappa}_\theta = H\dot{K}_\theta, \; \dot{\kappa}_1 = H\dot{K}_1, \; \dot{\kappa}_2 = H\dot{K}_2$$

$$p = \frac{PL^2}{M^0}, \quad \bar{p} = \frac{PL}{M^0}, \quad q = \frac{Q}{M^0}$$

List of solutions

No.	Pattern of plate	page	No.	Pattern of plate	page
15		193	22	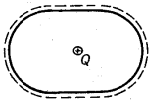	200
16	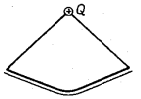	194	23	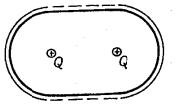	201
17	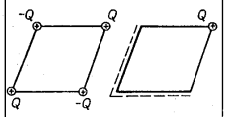	195	24	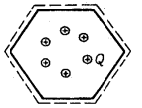	202
18	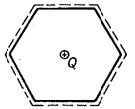	196	25	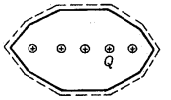	203
19	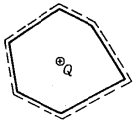	197	26	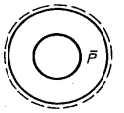	204
20	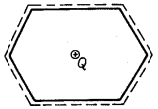	198	27	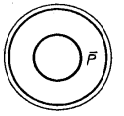	205
21	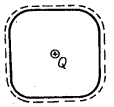	199	28	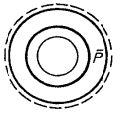	206

No.	Pattern of plate	page	No.	Pattern of plate	page
29	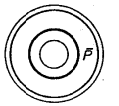	207	36	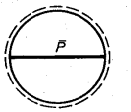	214
30	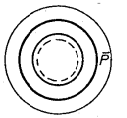	208	37		215
31	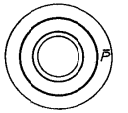	209	38	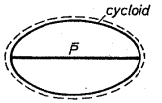	216
32	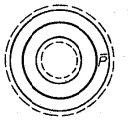	210	39	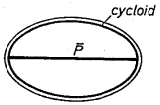	217
33	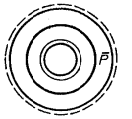	211	40	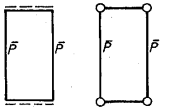	218
34	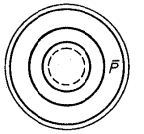	212	41	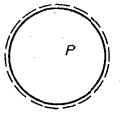	219
35	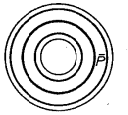	213	42	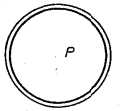	220

No.	Pattern of plate	page	No.	Pattern of plate	page
43	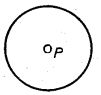	221	50		228
44		222	51	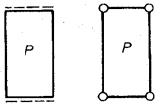	229
45		223	52	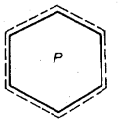	230
46		224	53		231
47	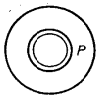	225	54	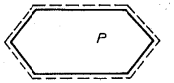	232
48	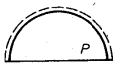	226	55	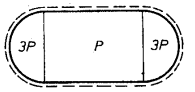	233
49		227	56	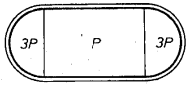	234

No.	Pattern of plate	page	No.	Pattern of plate	page
57	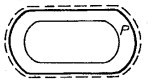	235 236	64	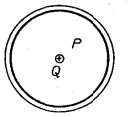	243
58		237	65		244
59	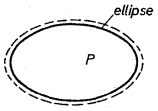	238	66	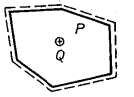	245
60	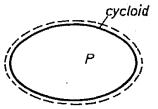	239	67	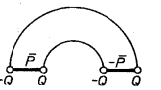	246
61	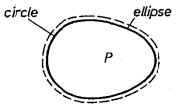	240			
62	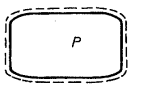	241			
63	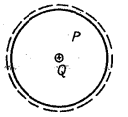	242			

PLATE 1

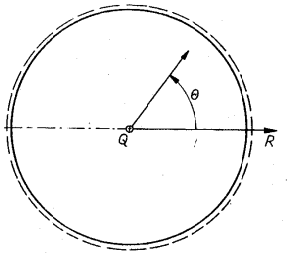

$q = 2\pi$

$m_\theta = 1;\ m_r = 0$
$s_\theta = 0;\ s_r = -\frac{1}{r}$
$\dot{w} = \dot{w}_0(1-r)$

PLATE 2

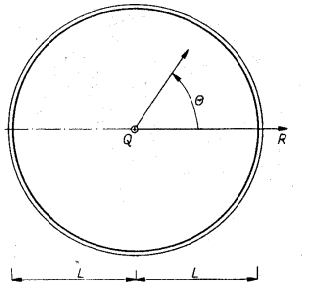

$q = 2\pi(1+\Lambda')$

$m_\theta = 1;\quad m_r = -\Lambda'$
$s_\theta = 0;\quad s_r = -\frac{1-\Lambda'}{r}$
$\dot{w} = \dot{w}_0(1-r)$

PLATE 3

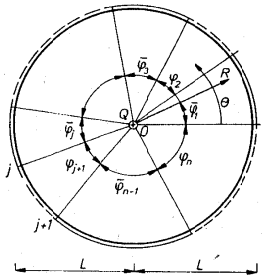

$$q = 2\pi * \Lambda' \Sigma \bar{\varphi}_j$$

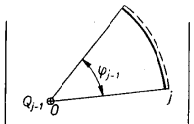	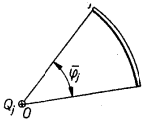
$q_{j-1} = \varphi_{j-1}$	$q_j = (1+\Lambda')\,\bar{\varphi}_j$
$m_\theta = 1$; $m_r = 0$	$m_\theta = 1$; $m_r = -\Lambda'$
$s_\vartheta = 0$; $s_r = -\frac{1}{r}$	$s_\theta = 0$ $s_r = -\frac{1+\Lambda'}{r}$
$(s_r)_j = \frac{1}{r}[m_r]_j = \frac{\Lambda'}{r}$	
$\dot{w} = \dot{w}_0(1-r)$	

PLATE 4

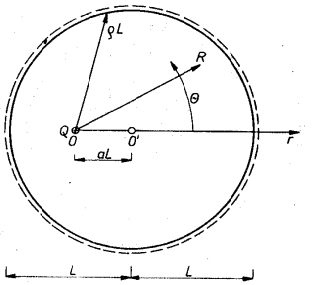

$$q = \frac{2\pi}{\sqrt{1-a^2}}\ ; \quad -\sqrt{\frac{\Lambda'}{1+\Lambda'}} \leqslant a \leqslant \sqrt{\frac{\Lambda'}{1+\Lambda'}}$$

$m_\theta = 1$; $m_r = -\frac{a^2\sin^2\Theta}{1-a^2\sin^2\Theta}$
$s_\theta = 0$; $s_r = -\frac{1}{r}\frac{1}{1-a^2\sin^2\Theta}$
$\dot{w} = \dot{w}_0(1-\frac{\varrho}{\bar{\varrho}})$; $\varrho = a\cos\Theta - \sqrt{1+a^2\sin^2\Theta}$

PLATE 5

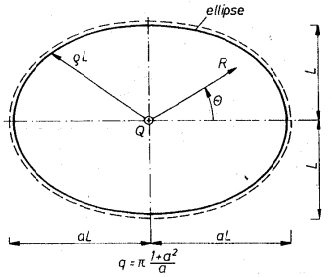

$$q = \pi\,\frac{1+a^2}{a}$$

$$1 \leqslant a \leqslant \sqrt{\Lambda^4+\sqrt{1+\Lambda^4}}$$

$m_\vartheta = 1\,;\quad m_r = -\dfrac{(1-a^2)^2\tan^2\vartheta}{(1+a^2\tan^2\vartheta)^2}$
$s_\vartheta = 0\,;\quad s_r = -\dfrac{1}{r}\,\dfrac{(1+\tan^2\vartheta)(1+a^4\tan^2\vartheta)}{(1+a^2\tan^2\vartheta)^2}$
$\dot w = \dot w_0\left(1-\dfrac{\varrho}{\varrho}\right)\,;\quad \varrho = \dfrac{a}{\sqrt{\cos^2\vartheta+a^2\sin^2\vartheta}}$

PLATE 6

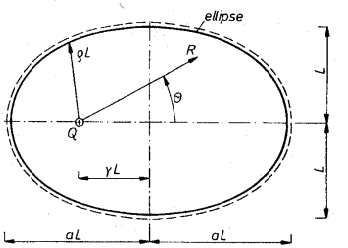

$$q = 2\pi a$$

$$1 \leqslant a \leqslant 1\Big/\sqrt{1-\frac{\Lambda^4}{(1+\Lambda)^2\sin^2\left(\arctan\left(\frac{1}{\sqrt{\Lambda^4}}\right)\right)}}$$

$m_\vartheta = 1\,;\quad m_r = -\dfrac{\gamma^2\sin^2\vartheta}{(a-\gamma\cos\vartheta)^2}\,;\quad \gamma = \sqrt{a^2-1}$
$s_\vartheta = 0\,;\quad s_r = -\dfrac{1}{r}\left(1+\dfrac{\gamma^2\sin^2\vartheta}{(a-\gamma\cos\vartheta)^2}\right)$
$\dot w = \dot w_0\left(1-\dfrac{\varrho}{\varrho}\right)\,;\quad \varrho = \dfrac{a^2-\gamma^2}{a-\gamma\cos\vartheta}$

PLATE 7

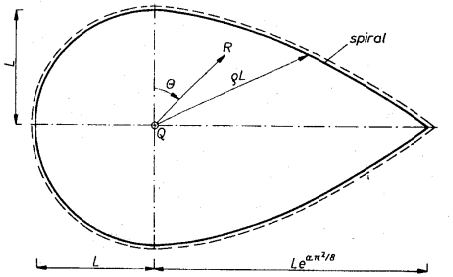

$$q = \pi\left(2+\frac{\alpha^2\pi^2}{12}\right)$$

$$0 \leqslant \alpha \leqslant \frac{2\sqrt{\Lambda}}{\pi}$$

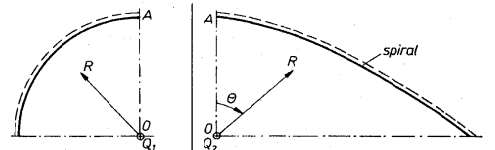

$q_1 = \frac{\pi}{2}$	$q_2 = \frac{\pi}{2}\left(1+\frac{\alpha^2\pi^2}{12}\right)$
$m_\vartheta = 1\ ;\ m_r = 0$	$m_\vartheta = 1\ ;\ m_r = -(\alpha\vartheta)^2$
$s_\vartheta = 0\ ;\ s_r = -\frac{1}{r}$	$s_\vartheta = 0 \quad s_r = -\frac{1}{r}\left(1+\alpha^2\vartheta^2\right)$
$[m_r]_{OA} = r\,[s_r] = \pm(\alpha\vartheta)^2$	
$\dot{w} = \dot{w}_0(1-r)$	$\dot{w} = \dot{w}_0\left(1-\frac{r}{\varrho}\right)\ ;\ \varrho = e^{\alpha\vartheta^2/2}$

PLATE 8

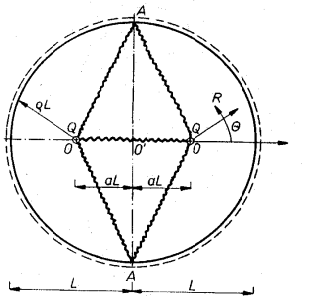

$$q = \frac{2}{\sqrt{1-a^2}}\left(\pi - \arctan\left(\frac{\sqrt{1-a^2}}{a}\right)\right)$$

$$|a| \leqslant \sqrt{\frac{\Lambda}{1+\Lambda}}$$

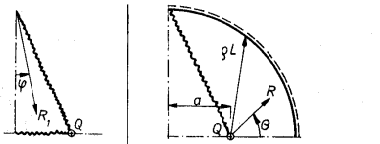

$q = 0$	$q = \frac{1}{\sqrt{1-a^2}}\left(\pi - \arctan\left(\frac{\sqrt{1-a^2}}{a}\right)\right)$
$m_r = m_\vartheta = 1$	$m_\vartheta = 1\ ;\ m_r = -\frac{a^2\sin^2\vartheta}{1-a^2\sin^2\vartheta}$
$s_\vartheta = s_r = 0$	$s_\vartheta = 0\ ;\ s_r = -\frac{1}{r}\frac{1}{1-a^2\sin^2\vartheta}$
$[s_r]_{OA} = \frac{1}{r}[m_r]_{OA} = \frac{1}{r}\frac{1}{1-a^2\sin^2\vartheta}$	
$\dot{w} = \dot{w}_0 r_1 \cos\varphi$	$\dot{w} = \dot{w}_0\left(1-\frac{r}{\varrho}\right)$ $\varrho = a\cos\vartheta + \sqrt{1-a^2\sin^2\vartheta}$

PLATE 9

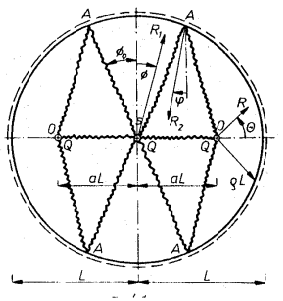

$$q = 4\,\phi_0$$

$$\phi_0 = \frac{1}{2\sqrt{1-a^2}}\arctan\left(\sqrt{1-a^2}\,\frac{\cos\phi_2}{\sin\phi_2 - a}\right);\quad |a| \le \sqrt{\frac{\Lambda}{1+\Lambda}}$$

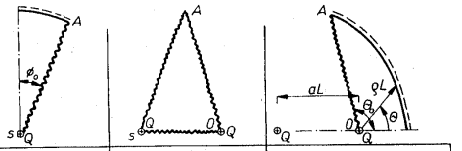

$q = \phi_0$	$q = 0$	$q = \frac{1}{\sqrt{1-a^2}}\arctan(\sqrt{1-a^2}\tan\theta_0)$
$m_\theta = 1\ ;\ m_r = 0$	$m_\theta = m_r = 1$	$m_\theta = 1;\ m_r = -\frac{a^2\sin^2\theta}{1-a^2\sin^2\theta}$
$s_\theta = 0\ ;\ s_r = -\frac{1}{r}$	$s_\theta = s_r = 0$	$s_\theta = 0;\ s_r = -\frac{1}{r}\frac{1}{(1-a^2\sin^2\theta)}$
$[m_r]_{SA} = r[s_r]_{SA} = -1\ ;\ [m_r]_{OA} = r[s_r]_{OA} = \frac{1}{1-a^2\sin^2\theta}$		
$\dot w = \dot w_0(1-r_1)$	$\dot w = \dot w_0 r_2\cos\varphi$	$\dot w = \dot w_0(1-\frac{r}{\varrho})$ $\varrho = a\cos\theta + \sqrt{1-a^2\sin^2\theta}$

PLATE 10

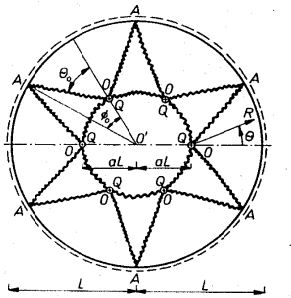

$$q = \frac{2}{\sqrt{1-a^2}}\arctan\frac{\sqrt{1-a^2}\sin\phi_0}{-a+\cos\phi_0}\ ;\quad \phi_0 = \frac{\pi}{n};\ n \ge 3$$

$$|a| \le \sqrt{\frac{\Lambda}{(1+\Lambda)\sin^2\theta_0}}$$

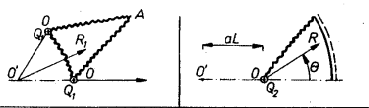

$q_1 = 0$	$q_2 = \frac{1}{\sqrt{1-a^2}}\arctan\frac{\sqrt{1-a^2}\sin\phi_0}{(-a+\cos\phi_0)}$
$m_\theta = m_r = 1$	$m_\theta = 1;\ m_r = -\frac{a^2\sin^2\theta}{1-a^2\sin^2\theta}$
$s_\theta = s_r = 0$	$s_\theta = 0;\ s_r = -\frac{1}{r}\frac{1}{1-a^2\sin^2\theta}$
$[m_r]_{OA} = r[s_r]_{OA} = \frac{1}{1-a^2\sin^2\theta}$	
$\dot w = \dot w_0 \quad 0 \le r_1 \le a$ $\dot w = \frac{\dot w_0}{1-a}(1-r_1)\ ;\ a \le r_1 \le 1$	$\dot w = \dot w_0(1-\frac{r}{\varrho})$ $\varrho = a\cos\theta + \sqrt{1-a^2\sin^2\theta}$

PLATE 11, [12]

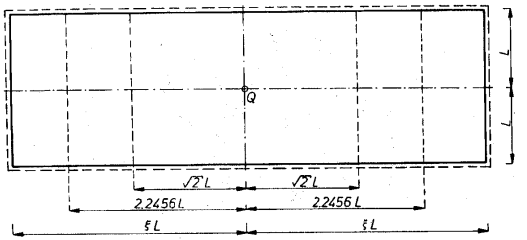

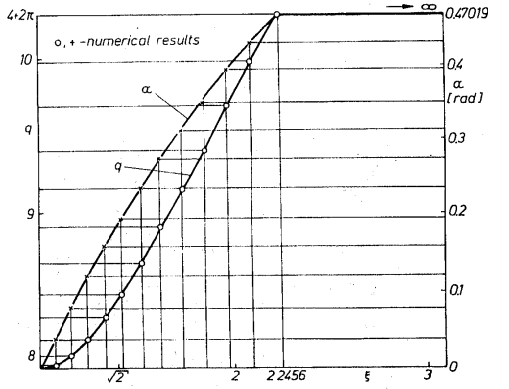

Details :
$1 \leqslant \xi \leqslant \sqrt{2}$ - plate 11a
$\sqrt{2} \leqslant \xi \leqslant 2.2456$ - plate 11b
$\xi \geqslant 2.2456$ - plate 11c

PLATE 11a

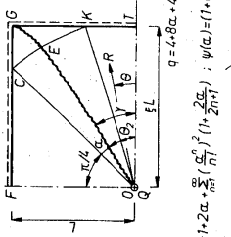

ξ	q
1	8
1.0901	8.0235
1.1636	8.0895
1.2506	8.1928
1.3416	8.3290

$$q = 4+8\alpha+4(1+2\psi(\alpha))/\xi \; ; \quad \psi(\alpha)=(1+\alpha)I_1+\sum_{n=1}^{\infty}\frac{\alpha_1^n}{n!}(\alpha+n+1)\,I_{n+1} \; ; \quad I_n = \sqrt{2}\int_0^{\alpha}\frac{y^n}{n!}\cos\left(\frac{\pi}{2}-\alpha+v\right)dv$$

$$\xi = 1+2\alpha+\sum_{n=1}^{\infty}\left(\frac{\alpha_1^n}{n!}\right)^2\left(1+\frac{2\alpha}{2n+1}\right) \; ; \quad \Lambda = 1$$

$q_1 = 1$	$q_2 = 2\alpha$	numerical solution	$q_2 = \tan\theta_2$
$m_\theta = 1 \; ; \; m_r = -\cot an^2\theta$	$m_\theta = 1 \; ; \; m_r = -1$	$m_\theta = 1 \; ; \; m_r = f(\theta)$	$m_\theta = 1 \; ; \; m_r = -\tan^2\theta$
$s_\theta = 0$ $s_r = -\frac{1}{r}(1+\cot an^2\theta)$	$s_\theta = 0 \; ; \; s_r = -\frac{2}{r}$	$s_\theta = 0 \; ; \; s_r = \frac{f(\theta)-1}{r}$	$s_\theta = 0 \; ;$ $s_r = -\frac{1}{r}(1+\tan^2\theta)$
$\dot{w} = \dot{w}_0(1-y)$	$\dot{w}$ - cone	$\chi(u,v) = 1+v+\sum_{n=1}^{\infty}\frac{u^n}{n!}\left[\frac{v^n}{n!}+\frac{v^{n+1}}{(n+1)!}\right]$	$\dot{w} = \dot{w}_0\left(1-\frac{r}{\xi}\right)$

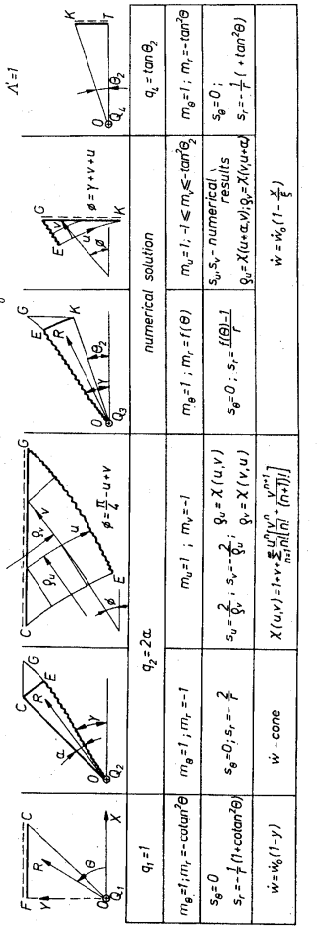

PLATE 11b

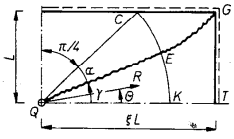

ξ	q	α [rad]	ξ	q	α [rad]
1.4367	8.4945	0.19635	1.8657	9.4015	0.35343
1.5363	8.6867	0.23562	1.9870	9.6804	0.39270
1.6408	8.9032	0.27489	2.1147	9.9775	0.43197
1.7505	9.1420	0.31416			

$$q = 4 + 8\alpha + 4(1 + 2\psi(\alpha))/\xi \quad ; \quad \sqrt{2} < \xi < 2.2456$$

$$\xi = 1 + 2\alpha + \sum_{n=1}^{\infty} \left(\frac{\alpha^n}{n!}\right)^2 \left(1 + \frac{2\alpha}{2n+1}\right) \quad ; \quad \psi(\alpha) = (1+\alpha)T_1 + \sum_{n=1}^{\infty} \frac{\alpha^n}{n!}(\alpha + n + 1)T_{n+1} \quad ; \quad T_n = \sqrt{2}^n \int_0^{\alpha} \frac{v^n}{n!} \cos\left(\frac{\pi}{4} - \alpha + v\right) dv$$

[188]

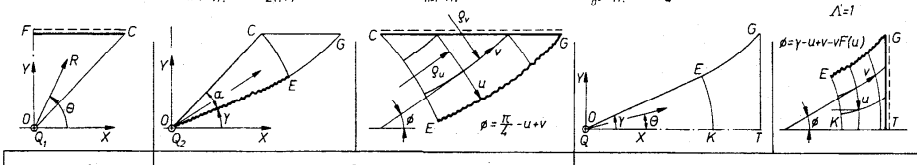

$q_1 = 1$	$q_2 = 2\alpha$		numerical solution	
$m_\theta = 1$; $m_r = -\cot an^2\theta$	$m_\theta = 1$; $m_r = -1$	$m_u = 1$; $m_v = -1$	$m_\theta = 1$; $m_r = f(\theta)$	$m_u = 1$; $\lvert m_r \rvert \leq 1$
$s_\theta = 0$ $s_r = -\frac{1}{r}(1 + \cot an^2\theta)$	$s_\theta = 0$; $s_r = -\frac{2}{r}$	$s_u = \frac{2}{q}$; $s_v = -\frac{2}{q}$; $q_u = \chi(u,v)$ $q_v = \chi(v,u)$	$s_\theta = 0$ $s_r = \frac{f(\theta) - 1}{r}$	s_u, s_v - numerical results $q_u = \chi(u+\alpha, v)$; $q_v = \chi(v, u+\alpha)$
$\dot{w} = \dot{w}_0(1 - y)$	$\dot{w}$ - cone	$\chi(u,v) = 1 + v + \sum_{n=1}^{\infty} \frac{u^n}{n!}\left[\frac{v^n}{n!} + \frac{v^{n+1}}{(n+1)!}\right]$	$\dot{w} = \dot{w}_0 \frac{\xi - x}{\xi}$	

PLATE 11c

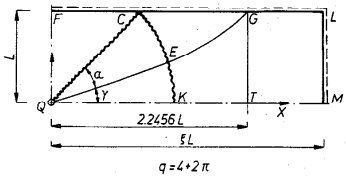

$$q = 4 + 2\pi$$

$$\alpha = 27° \qquad \xi \geq 2.2456$$

[688]

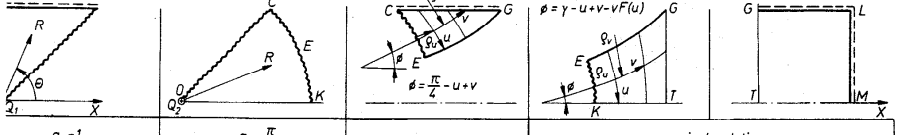

$q_1 = 1$	$q_2 = \frac{\pi}{2}$	——	numerical solution	
$m_\theta = 1$; $m_r = -\cot an^2\theta$	$m_\theta = 1$; $m_r = -1$	$m_u = 1$; $m_v = -1$	$0.925 \leq m_u \leq 1$ $-1 \leq m_v \leq 0$	$m_x = m_y = 0$; $m_{xy} = \frac{1}{2}\int_0^{\gamma} V(y)\,dy$ $m_1 = -m_2 = \lvert m_{xy} \rvert$
$_1 = 0$; $s_r = -\frac{1}{r}(1 + \cot an^2\theta)$	$s_\theta = 0$; $s_r = -\frac{2}{r}$	$s_u = \frac{2}{q_v}$; $s_v = -\frac{2}{q_u}$; $q_u = \chi(u,v)$ $q_v = \chi(v,u)$	s_u, s_v - numerical results $q_u = \chi(u+\alpha, v)$ $q_v = \chi(v, u+\alpha)$	$s_x = \frac{1}{2}V(y)$; $s_y = 0$ $[V(y)]_{GT} = 0$
——	——	$\chi(u,v) = 1 + v + \sum_{n=1}^{\infty} \frac{u^n}{n!}\left(\frac{v^n}{n!} + \frac{v^{n+1}}{(n+1)!}\right)$		
$\dot{w} = \dot{w}_0(1 - y)$	$\dot{w} = \dot{w}_0\left(1 - \frac{r}{\sqrt{2}}\right)$	$\dot{w} = 0$		

PLATE 13

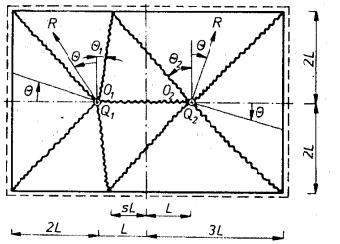

$q_2 = \alpha q_1$; $\alpha = \frac{5+s}{5-s}$

$q_1 = 5-s$; $q_2 = 5+s$

$\Theta_1 \leq \frac{\pi}{4}$ $\Theta_2 \leq \frac{\pi}{4}$

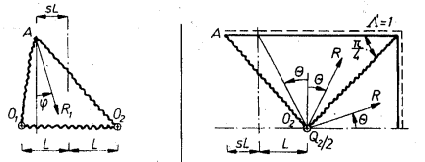

$q = 0$	$\frac{1}{2} q_2 = 2.5 + \frac{s}{2}$
$m_\theta = m_r = 1$	$m_\theta = 1$; $m_r = -\tan^2\Theta$
$s_\theta = s_r = 0$	$s_\theta = 0$; $s_r = -\frac{1}{r}(1+\tan^2\Theta)$
$[m_r]_{Q_1 A} = r\,[s_r]_{Q_1 A} = 1+\tan^2\Theta_2$	
$\dot{w} = \frac{\dot{w}_0}{2} r_1 \cos\varphi$	$\dot{w} = \dot{w}_0 (1 - \frac{1}{2} r \cos\Theta)$

PLATE 12, [84]

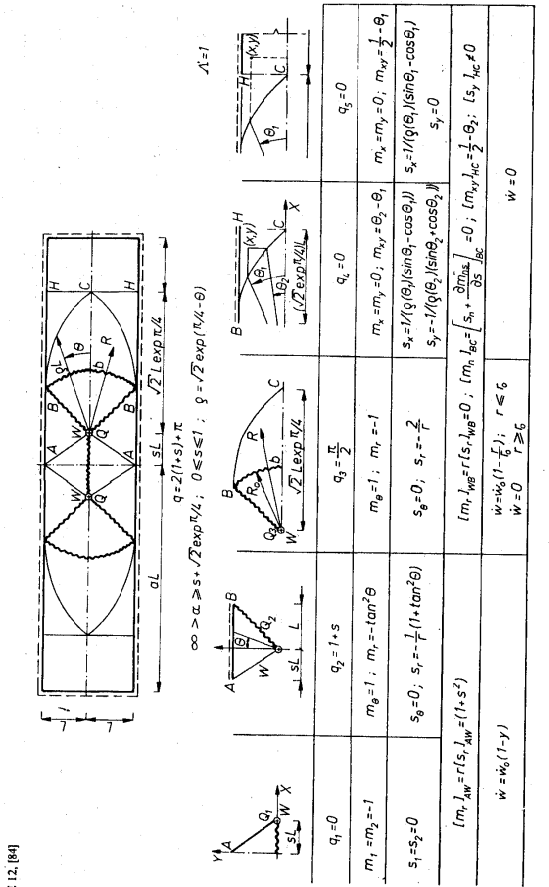

$q_1 = 0$	$q_2 = 1+s$	$q_0 = \frac{\pi}{2}$	$q_c = 0$	$q_s = 0$
$m_1 = m_2 = -1$	$m_\theta = 1$; $m_r = -\tan^2\Theta$	$m_\theta = 1$; $m_r = -1$	$m_x = m_y = 0$; $m_{xy} = \Theta_2 - \Theta_1$	$m_x = m_y = 0$; $m_{xy} = \frac{1}{2} - \Theta_1$
$s_1 = s_2 = 0$	$s_\theta = 0$; $s_r = -\frac{1}{r}(1+\tan^2\Theta)$	$s_\theta = 0$, $s_r = -\frac{2}{r}$	$s_x = 1/(g(\Theta_2)/\sin\Theta_2 - \cos\Theta_2))$; $s_y = -1/(g(\Theta_2)/\sin\Theta_2 + \cos\Theta_2))$	$s_x = 1/(g(\Theta_1)/(\sin\Theta_1 - \cos\Theta_1))$; $s_y = 0$
$[m_r]_{AW} = r[s_r]_{AW} = (1+s^2)$		$[m_r]_{WB} = r[s_r]_{WB} = 0$;	$[m_n]_{BC} = \left[s_n + \frac{\partial m_{ns}}{\partial s} \right]_{BC} = 0$;	$[m_x]_{HC} = \frac{1}{2} - \Theta_2$; $[s_y]_{HC} \neq 0$
$\dot{w} = \dot{w}_0 (1-y)$		$\dot{w} = \dot{w}_0 (1 - \frac{r}{r_0})$; $r \leq r_0$ $\dot{w} = 0$ $r \geq r_0$		$w = 0$

PLATE 14

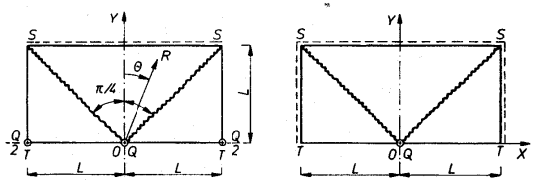

$$q = 2(q_1 + q_2) = 4$$

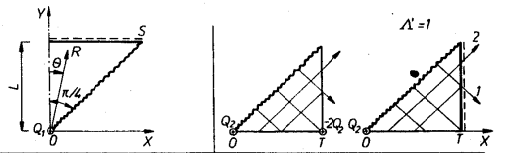

$q_1 = \tan\frac{\pi}{4} = 1$	$q_2 = 1$
$m_1 = m_\theta = 1\ ;\ m_2 = m_r = -\tan^2\Theta$	$m_1 = 1\ ;\ m_2 = -1$
$s_1 = s_\theta = 0\ ;\ s_2 = s_r = -\frac{1}{F}(1+\tan^2\Theta)$	$s_1 = s_2 = 0$
$[m_2]_{0S} = 0$ $\quad [s_2]_{0S} = \frac{2}{F}$	
$\dot{w} = \dot{w}_0(1-y)$	$\dot{w} = \dot{w}_0(1-x)$

PLATE 15, [48]

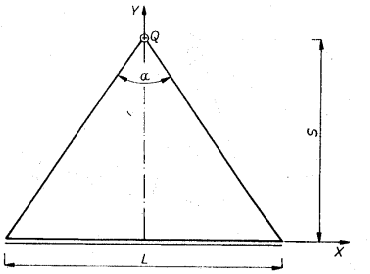

$$q = 2\Lambda' \tan\frac{\alpha}{2}$$

$$\alpha \leqslant 2\arctan\frac{1}{\sqrt{\Lambda'}} \leqslant \frac{\pi}{2}$$

$m_x = m_1 = \Lambda' \tan\frac{\alpha}{2}\ ;\ m_y = m_2 = -\Lambda'\ ;\ m_{xy} = 0$
$s_x = s_1 = 0\ ;\ s_y = s_2 = 0$
$\dot{w} = \frac{\dot{w}_0}{S} y$

PLATE 16, [48]

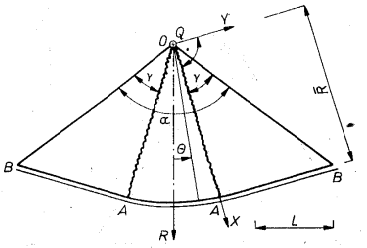

$$q = 2\sqrt{\Lambda'} + (1+\Lambda')(\alpha - 2\arctan\frac{1}{\sqrt{\Lambda'}})$$

$$\alpha \geq 2\arctan\frac{1}{\sqrt{\Lambda'}} \; ; \quad \gamma = \arctan\frac{1}{\sqrt{\Lambda'}}$$

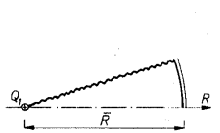

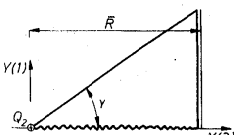

$q_1 = (\alpha - 2\gamma)(1+\Lambda')$	$q_2 = \sqrt{\Lambda'}$
$m_1 = m_\theta = 1$; $m_2 = m_r = -\Lambda'$	$m_1 = m_y = 1$; $m_2 = m_x = -\Lambda'$
$s_1 = s_\theta = 0$; $s_2 = s_r = -\frac{1+\Lambda'}{r}$	$s_1 = s_y = 0$; $s_2 = s_x = 0$
$[m_2]_{OA} = 0$; $[s_2]_{OA} = \frac{1+\Lambda'}{r}$	
$\dot{w} = \dot{w}_0(1 - \frac{r}{\bar{r}})$	$\dot{w} = \dot{w}_0(1 - \frac{x}{\bar{r}})$

PLATE 17, [48]

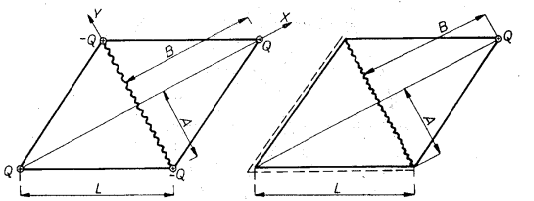

$$q = 2\frac{b}{a}$$

$$b \geq a \; , \quad \Lambda' = (\frac{b}{a})^2$$

$m_1 = m_y = 1$; $m_2 = m_x = -(\frac{b}{a})^2$; $m_{xy} = 0$
$s_1 = s_y = 0$; $s_2 = s_x = 0$
$\dot{w} = \dot{w}_0 \frac{x}{b}$

PLATE 18

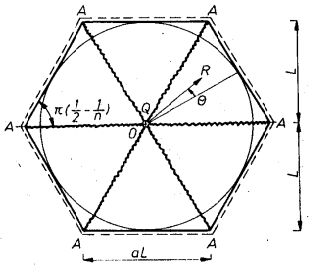

$$q = 2n\tan\frac{\pi}{2} = n\alpha$$

$n > 4$

n - number of polygon sides

$m_\theta = 1 \;;\; m_r = -\tan^2\Theta \;;\; \Theta \leqslant \arctan\sqrt{\Lambda}$
$s_\theta = 0 \;;\quad s_r = -\frac{1}{r}(1+\tan^2\Theta)$
$[m_r]_{OA} = r\,[s_r]_{OA} = 0$
$\dot{w} = \dot{w}_0(1 - r\cos\Theta)$

PLATE 19

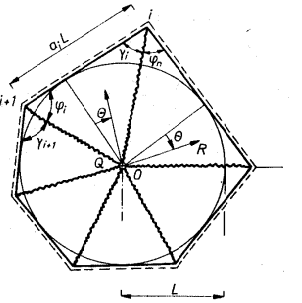

$$q = \sum_{i=1}^{n}(\operatorname{cotan}\gamma_i + \operatorname{cotan}\varphi_i) = \sum_{i=1}^{n} a_i$$

$$\varphi_i \geqslant \frac{\pi}{2} - \arctan\sqrt{\Lambda} \;;$$

$$\gamma_i \geqslant \frac{\pi}{2} - \arctan\sqrt{\Lambda}$$

n - number of corners

$m_\theta = 1 \;;\; m_r = -\tan^2\Theta;\; \Theta \leqslant \arctan\sqrt{\Lambda}$
$s_\theta = 0 \;;\; s_r = -\frac{1}{r}(1+\tan^2\Theta)$
$[m_r]_{0,i+1} = r\,[t_r]_{0,i+1} = \tan^2\gamma_{i+1} - \tan^2\varphi_i$
$\dot{w} = \dot{w}_0(1 - r\cos\Theta)$

PLATE 20

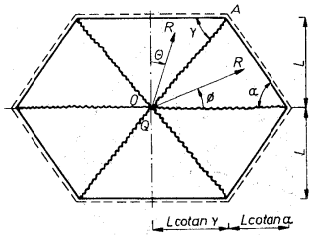

$$q = 4(\operatorname{cotan}\gamma + \operatorname{cotan}\alpha - \operatorname{cotan}(\alpha+\gamma))$$

$$\frac{\pi}{2} - \arctan\sqrt{\Lambda} \leqslant \alpha \leqslant \frac{\pi}{2} - \gamma + \arctan\sqrt{\Lambda};\quad \gamma \geqslant \frac{\pi}{2} - \arctan\sqrt{\Lambda}$$

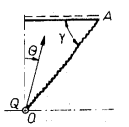

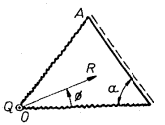

$q = \operatorname{cotan}\gamma$	$q = \operatorname{cotan}\alpha - \operatorname{cotan}(\gamma+\alpha)$
$m_\theta = 1;\ m_r = -\tan^2\Theta$	$m_\theta = 1;\ m_r = -\operatorname{cotan}^2(\alpha+\phi)$
$s_\theta = 0;\ s_r = -\frac{1}{r}(1+\tan^2\Theta)$	$s_\theta = 0;\ s_r = -\frac{1}{r}(1+\operatorname{cotan}^2(\alpha+\phi))$
$[m_r]_{OA} = r[s_r]_{OA} = \operatorname{cotan}^2(\alpha+\gamma) - \operatorname{cotan}^2\gamma$	
$\dot{w} = \dot{w}_0(1 - r\cos\Theta)$	$\dot{w} = \dot{w}_0\left(1 - r\frac{\sin(\alpha+\phi)}{\operatorname{cotan}\gamma\sin\alpha + \cos\alpha}\right)$

PLATE 21

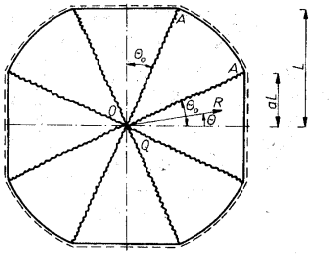

$$q = 2\pi + 8(a - \arctan\alpha)$$
$$0 \leqslant a \leqslant \sqrt{\Lambda}$$

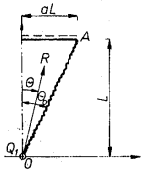

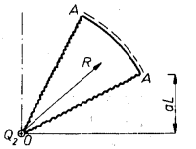

$q_1 = \tan\Theta_0$	$q_2 = \frac{\pi}{2} - 2\Theta_0$
$m_\theta = 1;\ m_r = -\tan^2\Theta$	$m_\theta = 1;\ m_r = 0$
$s_\theta = 0;\ s_r = -\frac{1}{r}(1+\tan^2\Theta)$	$s_\theta = 0;\ s_r = -\frac{1}{r}$
$[m_r]_{OA} = r[s_r]_{OA} = \pm\tan\Theta_0$	
$\dot{w} = \dot{w}_0(1 - r\cos\Theta)$	$\dot{w} = \dot{w}_0(1 - r)$

PLATE 22

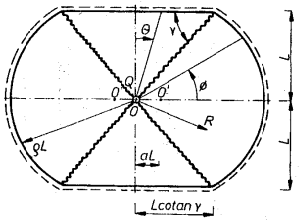

$$q = 4\left(\cot\gamma + \sqrt{1+\frac{a^2}{\Omega}}\arctan\frac{\tan\gamma}{\sqrt{1+\frac{a^2}{\Omega}}}\right)$$

$$\Omega = 1 + \cot\gamma(\cot\gamma - 2a)$$

$$-\frac{1}{\sin\gamma}\frac{\sin(\arctan\sqrt{\Lambda'})}{\sin(\gamma-\arctan\sqrt{\Lambda'})} \leqslant a \leqslant \cot\gamma\ ;\quad \gamma \geqslant \frac{\pi}{2} - \arctan\sqrt{\Lambda'}$$

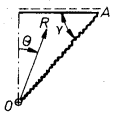

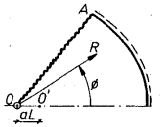

$q = \cot\gamma$	$q = \sqrt{1+\frac{a^2}{\Omega}}\arctan\frac{\tan\gamma}{\sqrt{1+\frac{a^2}{\Omega}}}$
$m_\theta = 1\ ;\quad m_r = -\tan^2\theta$	$m_\theta = 1\ ;\ m_r = -\frac{a^2\sin^2\phi}{a^2\cos^2\phi+\Omega}$
$s_\theta = 0\ ;\ s_r = -\frac{1}{r}(1+\tan^2\theta)$	$s_\theta = 0\ ;\ s_r = -\frac{1}{r}\left(\frac{a^2+\Omega}{a^2\cos^2\phi+\Omega}\right)$
$[m_r]_{OA} = r[s_r]_{OA} = -\cot\gamma + \frac{a^2\sin^2\gamma}{\Omega+a^2\cos^2\gamma}$	
$\dot w = \dot w_0(1-r\cos\theta)$	$\dot w = \dot w_0\left(1-\frac{r}{\varrho}\right)$ $\varrho = a\cos\phi + \sqrt{a^2\cos\phi+\Omega}$

PLATE 23

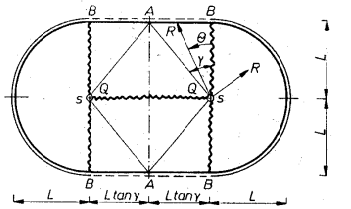

$$q = 2\tan\gamma + (1+\Lambda')\pi\ ;$$
$$\gamma \leqslant \arctan\sqrt{\Lambda'}$$

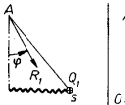

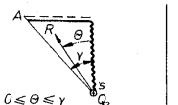

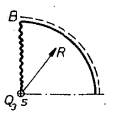

$q_1 = 0$	$q_2 = \tan\gamma$	$q_3 = (1+\Lambda')\frac{\pi}{4}$
$m_\theta = m_r = 1$	$m_\theta = 1\ ;\ m_r = -\tan^2\theta$	$m_\theta = 1\ ;\ m_r = -\Lambda'$
$s_\theta = s_r = 0$	$s_\theta = 0\ ;\ s_r = -\frac{1}{r}(1+\tan^2\theta)$	$s_\theta = 0\ ;\ s_r = -\frac{1+\Lambda'}{r}$
$[s_r]_{SA} = \frac{1}{r}[m_r]_{SA} = \frac{1}{r}(1+\tan^2\gamma)\ ;\ [s_r]_{SB} = \frac{1}{r}[m_r]_{SB} = -\frac{\Lambda'}{r}$		
$\dot w = \dot w_0 r_1\cos\varphi$	$\dot w = \dot w_0(1-r\cos\theta)$	$\dot w = \dot w_0(1-r)$

PLATE 24

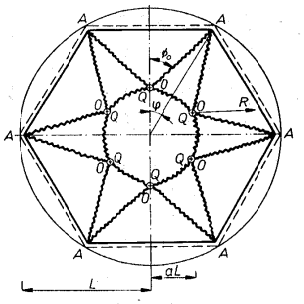

$$q = 2\tan\phi_o$$

$$\phi_o = \frac{\pi}{2} + \frac{\varphi}{2} - \operatorname{arctan}\left(\frac{1-a}{1+a}\cot\frac{\varphi}{2}\right);\quad \varphi = \frac{\pi}{n}$$

n - number of forces

$$\phi_o \leqslant \operatorname{arctan}\sqrt{\Lambda}$$

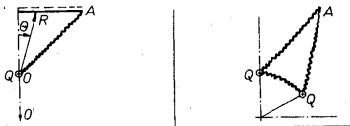

$q = \tan\phi_o$	$q = 0$
$m_\Theta = 1;\ m_r = -\tan^2\Theta$	$m_\Theta = m_r = 1$
$s_\Theta = 0;\ s_r = -\frac{1}{r}(1+\tan^2\Theta)$	$s_\Theta = s_r = 0$
$[m_\Theta]_{OA} = r\,[s_r]_{OA} = \pm(1+\tan\phi_o)$	
$\dot w = \dot w_o(1 - r\cos\Theta)$	$\dot w = \dot w_o \quad 0 \leqslant r_1 \leqslant a$ $\dot w = \frac{\dot w_o}{1-a}(1-r_1);\ a \leqslant r_1 \leqslant 1$

PLATE 25

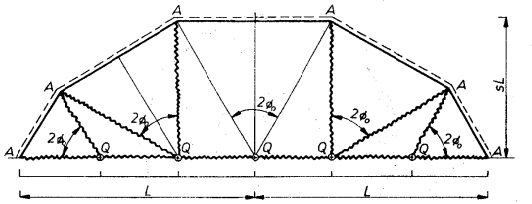

$$q = 4\tan\phi_o$$

$$\phi_o = \frac{\pi}{n+1} \leqslant \operatorname{arctan}\sqrt{\Lambda};\quad n\text{ - number of forces}$$

$$n \geqslant \text{entier}\left[\frac{\pi}{\operatorname{arctan}\sqrt{\Lambda}} - 1\right];\quad s = \frac{2}{n+1}\operatorname{cotan}\frac{\pi}{n+1}$$

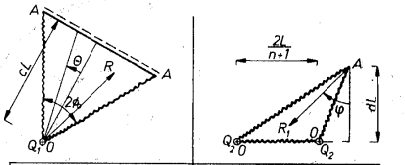

$q_1 = 2\tan\phi_o$	$q_2 = 0$
$m_\Theta = 1;\ m_r = -\tan^2\Theta$	$m_\Theta = m_r = 1$
$s_\Theta = 0;\ s_r = -\frac{1}{r}(1+\tan^2\Theta)$	$s_\Theta = s_r = 0$
$[m_r]_{OA} = r\,[s_r]_{OA} = 1+\tan^2\phi$	
$\dot w = \dot w_o(1 - \frac{\cos\Theta}{c}r)$	$\dot w = \dot w_o(1 - \frac{\cos\varphi}{d}r_1)$

PLATE 26

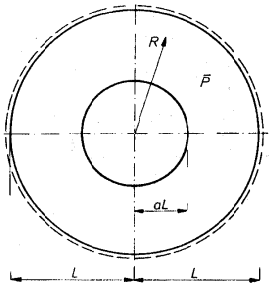

$$\bar{p} = \frac{1}{a(1-a)}$$

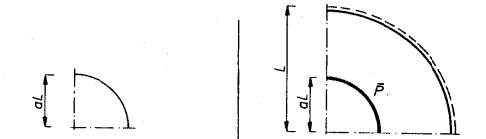

$m_\theta = m_r = 1$	$m_\theta = 1\,;\quad m_r = \frac{a}{r}\frac{1-r}{1-a}$
$s_\theta = s_r = 0$	$s_\theta = 0 \qquad s_r = -\frac{1}{(1-a)r}$
$(s_t)_{r=a} = -\frac{1}{a(1-a)}$	
$\dot{w} = \dot{w}_0 \qquad 0 \leq r \leq a$	$\dot{w} = \frac{\dot{w}_0}{1-a}(1-r)\,;\quad a \leq r \leq 1$

PLATE 27

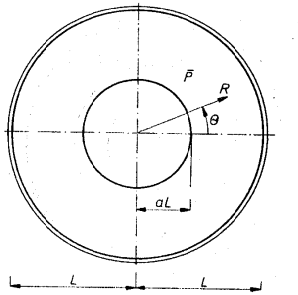

$$\bar{p} = \frac{1+\Lambda'}{a(1-a)}$$

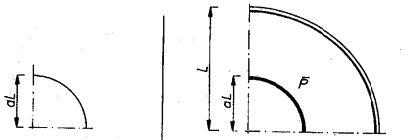

$m_\theta = m_r = 1$	$m_\theta = 1;\ m_r = 1 - \frac{1+\Lambda'}{1-a}\left(1-\frac{a}{r}\right)$
$s_\theta = s_r = 0$	$s_\theta = 0;\ s_r = -\frac{1+\Lambda}{(1-a)r}$
$(t_r)_{r=a} = -\frac{1+\Lambda'}{a(1-a)}$	
$\dot{w} = \dot{w}_0 \quad 0 \leq r \leq a$	$\dot{w} = \frac{\dot{w}_0}{1-a}(1-r);\quad a \leq r \leq 1$

PLATE 28

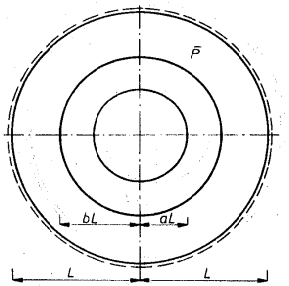

$$\bar{p} = \frac{1-a}{(1-b)b}$$

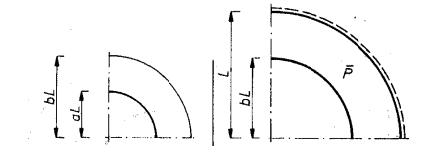

$m_\theta = 1\,; \quad m_r = 1 - \frac{a}{r}$	$m_\theta = 1\,; \quad m_r = \frac{b-a}{1-b}\,\frac{1-r}{r}$
$s_\theta = 0\,; \quad s_r = 0$	$s_\theta = 0\,; \quad s_r = -\frac{1-a}{(1-b)r}$
$[t_r]_{r=b} = \frac{1-a}{(1-b)b}$	
$\dot{w} = \dot{w}_0\,\frac{1-r}{1-a}$	

PLATE 29

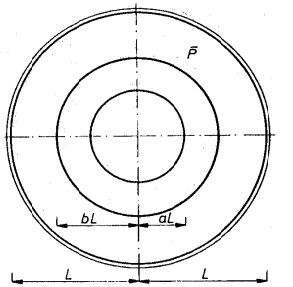

$$\bar{p} = \frac{1+\Lambda-a}{(1-b)b}$$

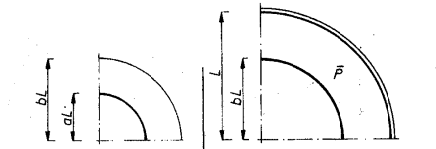

$m_\theta = 1\,; \quad m_r = 1 - \frac{a}{r}$	$m_\theta = 1\,; \quad m_r = -\Lambda' + \frac{b(1+\Lambda')-a}{1-b}\,\frac{1-r}{r}$
$s_\theta = 0\,; \quad s_r = 0$	$s_\theta = 0 \quad s_r = -\frac{1+\Lambda'-a}{(1-b)r}$
$[t_r]_{r=b} = \frac{1+\Lambda'-a}{(1-b)b}$	
$\dot{w} = \dot{w}_0\,\frac{1-r}{1-a}$	

PLATE 30

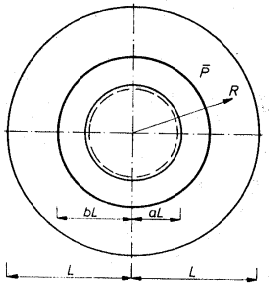

$$\bar{p} = \frac{\Lambda'(1-a)}{b(b-a)}$$

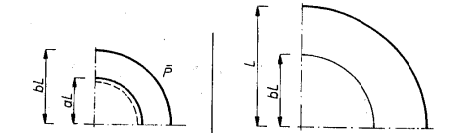

$m_\theta = -\Lambda'$; $m_r = \frac{\Lambda'(1-b)}{b-a}\frac{r-a}{r}$	$m_\theta = -\Lambda'$; $m_r = \Lambda'(\frac{1-r}{r})$
$s_\theta = 0$; $s_r = \frac{\Lambda'(1-a)}{r(b-a)}$	$s_\theta = 0$; $s_r = 0$
$(t_r)_{r=b} = \frac{\Lambda'(1-a)}{b(b-a)}$	
$\dot{w} = \dot{w}_0(r-a)$	

PLATE 31

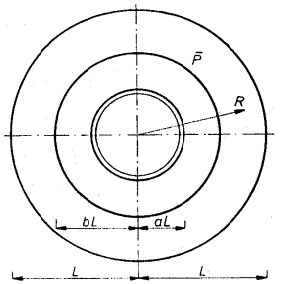

$$\bar{p} = \frac{\Lambda'}{(b-a)b}$$

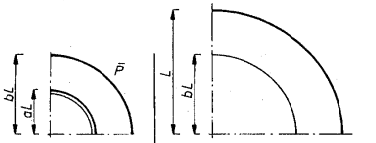

$m_\theta = -\Lambda'$; $m_r = -\Lambda'(1-\frac{1}{b-a}\frac{r-a}{r})$	$m_\theta = -\Lambda'$; $m_r = \Lambda'(\frac{1-r}{r})$
$s_\theta = 0$; $s_r = \frac{\Lambda'}{(b-a)r}$	$s_\theta = 0$; $s_r = 0$
$(t_r)_{r=b} = \frac{\Lambda'}{(b-a)b}$	
$\dot{w} = \dot{w}_0(r-a)$	

PLATE 32

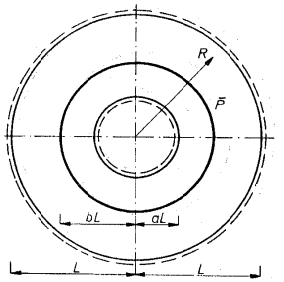

$$\bar{p} = \frac{1}{b}\,\frac{\Lambda'(1-b)(b-a)+(2b-b^2-a)}{(1-b)(b-a)}$$

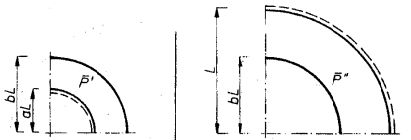

$\bar{p}' = \frac{1}{b}(\Lambda' + \frac{b}{b-a})$	$\bar{p}'' = \frac{1}{b(1-b)}$
$m_\theta = -\Lambda'$; $m_r = 1 - \frac{a}{b-a}\,\frac{b-r}{r}$	$m_\theta = 1$; $m_r = \frac{b}{1-b}\,(\frac{1-r}{r})$
$s_\theta = 0$; $s_r = \frac{1}{r}(\Lambda' + \frac{b}{b-a})$	$s_\theta = 0$; $s_r = -\frac{1}{r(1-b)}$
$(m_\theta)_{r=b} = -1 - \Lambda'$; $(s_r)_{r=b} = \frac{\Lambda'(1-b)(b-a)+(2b-b^2-a)}{b(1-b)(b-a)}$	
$\dot{w} = \dot{w}_0\,\frac{r-a}{b-a}$	$\dot{w} = \dot{w}_0\,\frac{1-r}{1-b}$

PLATE 33

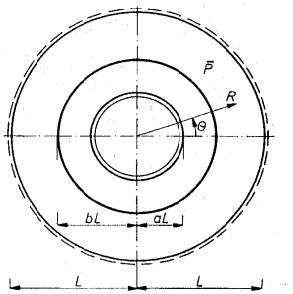

$$\bar{p} = \frac{1}{b}\,\frac{\Lambda' b(1-b)+(2b-b^2-a)}{(b-a)(1-b)}$$

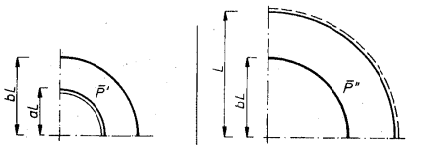

$\bar{p}' = \frac{1+\Lambda'}{b-a}$	$\bar{p}'' = \frac{1}{b(1-b)}$
$m_\theta = -\Lambda'$; $m_r = 1 - \frac{a(1+\Lambda')}{b-a}\,\frac{b-r}{r}$	$m_\theta = 1$; $m_r = \frac{b}{1-b}\,\frac{1-r}{r}$
$s_\theta = 0$; $s_r = \frac{b}{r}\,\frac{1+\Lambda'}{b-a}$	$s_\theta = 0$; $s_r = -\frac{1}{r(1-b)}$
$(m_\theta)_{r=b} = -1 - \Lambda'$; $(s_r)_{r=b} = \frac{\Lambda' b(1-b)+(2b-b^2-a)}{b(b-a)(1-b)}$	
$\dot{w} = \dot{w}_0\,\frac{r-a}{b-a}$	$\dot{w} = \dot{w}_0\,\frac{1-r}{1-b}$

PLATE 34

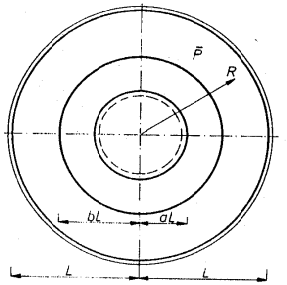

$$\bar{p} = \frac{1}{b}\,\frac{\Lambda'(b-a)(2-b)+(2b-b^2-a)}{(b-a)(1-b)}$$

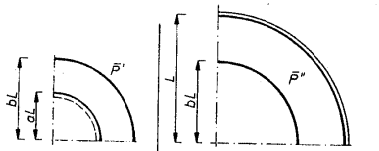

$\bar{p}' = \frac{1}{b}(\Lambda' + \frac{b}{b-a})$	$\bar{p}'' = \frac{1+\Lambda'}{b}(\frac{1}{1-b})$
$m_\theta = -\Lambda'$; $m_r = 1 - \frac{a}{b-a}\,\frac{b-r}{r}$	$m_\theta = 1$; $m_r = -\Lambda' + \frac{(1+\Lambda')b}{1-b}\,\frac{1-r}{r}$
$s_\theta = 0$; $s_r = \frac{1}{r}(\Lambda' + \frac{b}{b-a})$	$s_\theta = 0$; $s_r = -\frac{1+\Lambda'}{r}(\frac{1}{1-b})$
$[m_\theta]_{r=b} = -1 - \Lambda'$; $[s_r]_{r=b} = \frac{\Lambda'(b-a)(2-b)+(2b-b^2-a)}{b(b-a)(1-b)}$	
$\dot{w} = \dot{w}_o\,\frac{r-a}{b-a}$	$\dot{w} = \dot{w}_o\,\frac{1-a}{1-b}$

PLATE 35

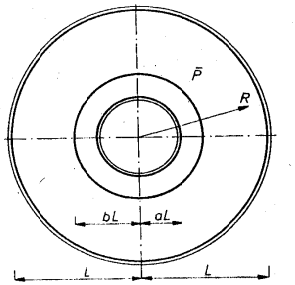

$$\bar{p} = \frac{1+\Lambda'}{b}\,\frac{2b-b^2-a}{(b-a)(1-b)}$$

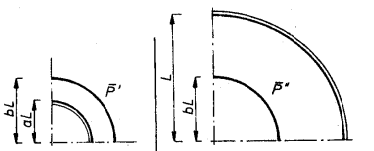

$\bar{p}' = \frac{1+\Lambda'}{b-a}$	$\bar{p}'' = \frac{1+\Lambda'}{b}(\frac{1}{1-b})$
$m_\theta = -\Lambda'$; $m_r = 1 - \frac{a(1+\Lambda')}{(b-a)}\,\frac{b-r}{r}$	$m_\theta = 1$; $m_r = -\Lambda' + \frac{(1+\Lambda')b}{1-b}\,\frac{1-r}{r}$
$s_\theta = 0$; $s_r = \frac{b}{r}\,\frac{1+\Lambda'}{b-a}$	$s_\theta = 0$; $s_r = -\frac{1+\Lambda'}{r}(\frac{1}{1-b})$
$[m_\theta]_{r=b} = -\Lambda' - 1$; $[s_r]_{r=b} = \frac{1+\Lambda'}{b}\,\frac{2b-b^2-a}{(b-a)(1-b)}$	
$\dot{w} = \dot{w}_o\,\frac{r-a}{b-a}$	$\dot{w} = \dot{w}_o\,\frac{1-r}{1-b}$

PLATE 36, [48]

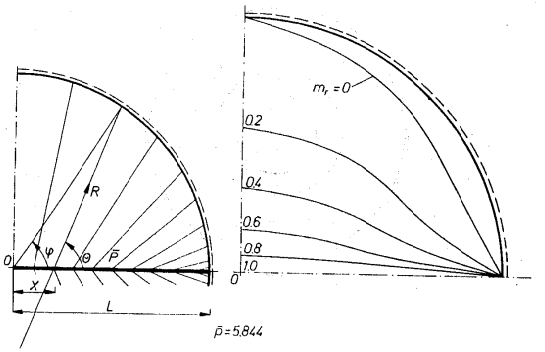

$\bar{p} = 5.844$

numerical solution $\Lambda = 1$

$m_\theta = 1\,;\quad m_r = 1 + A(\Theta) + \frac{B(\Theta)}{r}$											
$s_\theta = 0\,;\quad s_r = \frac{A(\Theta)}{r}$											
$\dot{w}(r)$ - developable surface											
x	0.0	0.1	0.2	0.3	0.4	0.5	0.6	0.7	0.8	0.9	1.0
φ	$\pi/2$	1.281	1.008	0.762	0.552	0.377	0.238	0.133	0.059	0.015	0.000

PLATE 37, [48]

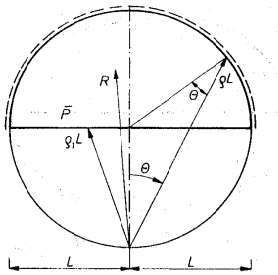

$\bar{p} = 2$

$m_\varphi = 1\,;\quad m_r = -\tan^2\Theta,\quad 0 \leqslant \Theta \leqslant \frac{\pi}{4}$
$s_\theta = 0\,;\quad s_r = \frac{1}{r}\,\frac{1}{\cos^2\Theta}$
$\dot{w} = \frac{\dot{w}_0}{2\cos\Theta - 1}(2\cos\Theta - r)$

PLATE 38

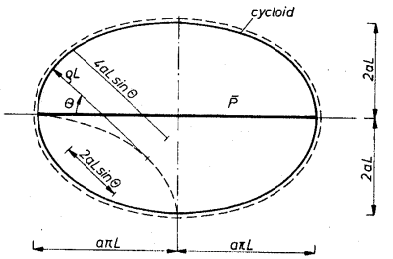

$\bar{p} = 2\pi$

$m_\theta = 1\,;$	$m_r = -1 + \frac{4\sin\theta}{\pi r}$ $\frac{2\sin\theta}{\pi} \leqslant r \leqslant \frac{4\sin\theta}{\pi}$
$s_\theta = 0$	$s_r = -\frac{2}{r}$
$\dot{w} = \frac{\dot{w}_0}{2\sin\theta - 1}\left(2\sin\theta - \frac{\pi}{2} r\right)$	

PLATE 39

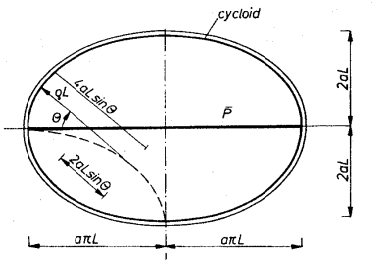

$\bar{p} = 2\pi(1+\Lambda')$

$m_\theta = 1\,;$	$m_r = 1 - 2(1-\Lambda')\left(1 - \frac{2}{r\pi}\sin\theta\right)$ $\frac{2\sin\theta}{\pi} \leqslant r \leqslant \frac{4\sin\theta}{\pi}$
$s_\theta = 0\,;$	$s_r = -\frac{2(1+\Lambda')}{r}$
$\dot{w} = \frac{\dot{w}_0}{2\sin\theta - 1}\left(2\sin\theta - \frac{\pi}{2} r\right)$	

PLATE 40, [48]

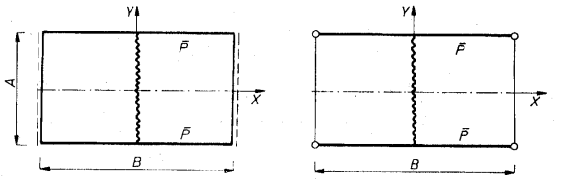

$$\bar{p} = 4\frac{a}{b^2}$$

$$\frac{a}{b} \leq \Lambda \leq 1$$

$m_x = 1 - \frac{4}{b^2}x^2$; $m_y = 0$; $m_{xy} = \frac{4}{b^2}xy$
$s_x = -\frac{4}{b^2}x$; $s_y = \frac{4}{b^2}y$
$\dot{w} = \dot{w}_0 \frac{b-2x}{b}$

PLATE 41

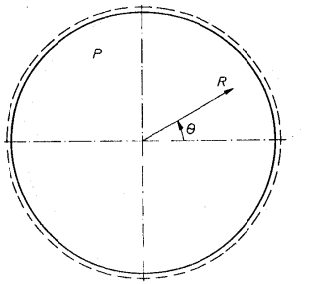

$p = 6$

$m_6 = 1$; $m = 1 - r^2$
$s_\theta = 0$ $s_r = -3r$
$\dot{w} = \dot{w}_0(1-r)$

PLATE 42

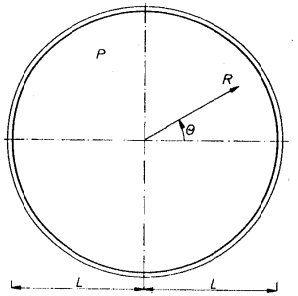

$$p = 6(1 + \Lambda')$$

$m_\theta = 1 \; ; \quad m_r = 1 - (1 + \Lambda')r^2$
$s_\theta = 0 \; ; \quad s_r = -3(1 + \Lambda')r$
$\dot{w} = \dot{w}_0 (1 - r)$

PLATE 43

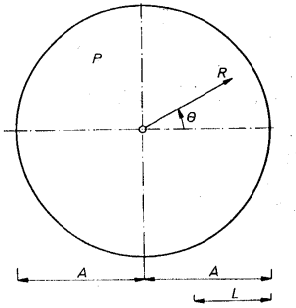

$$p = \frac{3\Lambda'}{a^3}$$

$m_\theta = -\Lambda' \; ; \quad m_r = \frac{1}{2}\Lambda'\left(1 - \frac{r^2}{a^2}\right)$
$s_\vartheta = 0 \; ; \quad s_r = \frac{3}{2}\Lambda'\left(1 - \frac{r^2}{a^2}\right)\frac{1}{r}$
$\dot{w} = \dot{w}_c \frac{r}{a}$

PLATE 44

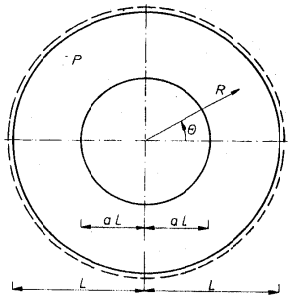

$$p = \frac{6}{(1-a)(2a+1)}$$

$m_\theta = 1\ ;\ m_r = \frac{p}{6}\left((1-r^2)-(1+a)a\frac{1-r}{r}\right)$
$s_\theta = 0\ ;\ s_r = \frac{p}{2}\left(\frac{a^2-r^2}{r}\right)$
$\dot{w} = \frac{\dot{w}_0}{1-a}(1-r)$

PLATE 45

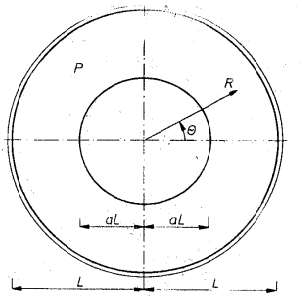

$$p = \frac{6(1+\lambda'-a)}{(1-a)^2(2a+1)}$$

$m_\theta = 1;\ m_r = \frac{\lambda'(a-r)}{r(1-a)} + \frac{p}{6}\left((1-r^2)-(1+a)a\frac{1-r}{r}\right)$
$s_\theta = 0\ ;\ s_r = \frac{p}{2}\left(\frac{a^2-r^2}{r}\right)$
$\dot{w} = \frac{\dot{w}_0}{1-a}(1-r)$

PLATE 46

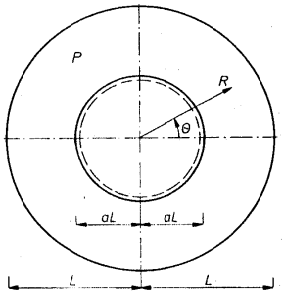

$$p = \frac{6\Lambda'}{(1-a)(2+a)}$$

$m_\theta = -\Lambda'\,;\quad m_r = \frac{p}{6}\left((1-r^2) - \frac{(1+a)a(1-r)}{r}\right)$
$s_\theta = 0\,;\quad s_r = \frac{p}{2}\left(\frac{1-r^2}{r}\right)$
$\dot{w} = \frac{\dot{w}_0}{1-a}(r-a)$

PLATE 47

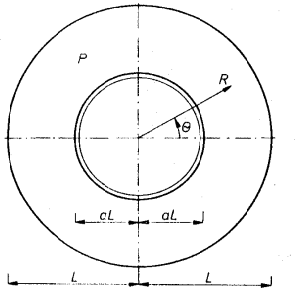

$$p = \frac{6\Lambda'}{(1-a)^2(a+2)}$$

$m_\theta = -\Lambda'\,;\quad m_r = -\frac{\Lambda' a(1-r)}{r(1-a)} + \frac{p}{6}\left((1-r^2) - \frac{(1+a)a(1-r)}{r}\right)$
$s_\theta = 0\,,\quad s_r = \frac{p}{2}\left(\frac{1-r^2}{r}\right)$
$\dot{w} = \frac{\dot{w}_0}{1-a}(r-a)$

PLATE 48, [48]

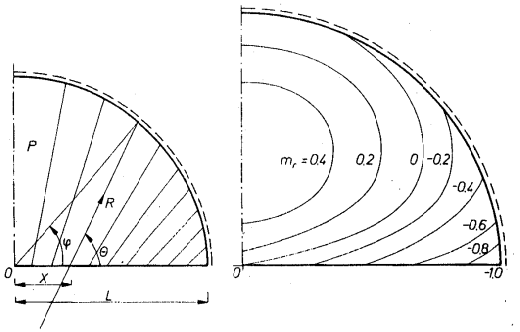

$p = 4.40$

numerical solution $\Lambda' = 1$

$m_\theta = 1$; $m_r = 1 + A(\Theta) + \frac{B(\Theta)}{r} - \frac{pr^2}{6}$											
$s_\theta = 0$ $s_r = \frac{A(\Theta)}{r} - \frac{pr}{2}$											
$\dot{w}(r)$ - developable surface											
x	0.0	0.1	0.2	0.3	0.4	0.5	0.6	0.7	0.8	0.9	1.0
φ	π/2	1.303	1.065	0.864	0.696	0.552	0.425	0.310	0.203	0.100	0.000

PLATE 49, [13]

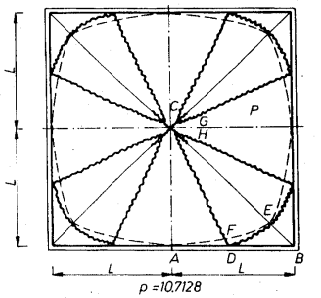

$p = 10.7128$

(numerical solution)
AD/AB = 0.46001
CE/CB = 0.84225
CH/CB = 0.09386
CG/CB = 0.03899

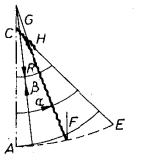

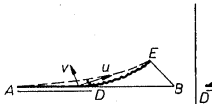

$\Lambda' = 1$

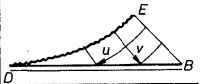

$m_\alpha = 1$, $m_\beta = 1 + A(\alpha) + \frac{B(\alpha)}{r} - \frac{pr^2}{6}$ $m_\beta^{AFE} = -1$	$m_u = 1$; $m_v = -1$	$m_u = 1$; $m_v = -1$
$s_\alpha = 0$; $s_\beta = A(\alpha) - \frac{pr}{2}$	$s_u = \frac{2}{9_v}$; $s_v = -\frac{2}{9_u}$	$s_u = \frac{2}{9_v}$; $s_v = -\frac{2}{9_u}$
$(m_v - m_\beta)_{AFE} = 0$; $[m_n]_{AFE} = [m_{ns}]_{AFE} = [s_n]_{AFE} = 0$		$m_{ns}^{EB} = s_n^{EB} = 0$
$\dot{w}(r)$ developable surface	$\dot{w}(u,v)$ $\dot{w}_u \dot{w}_v < 0$	$\dot{w}(u,v) = 0$

PLATE 50

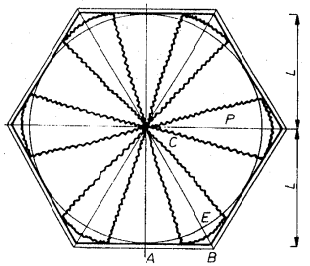

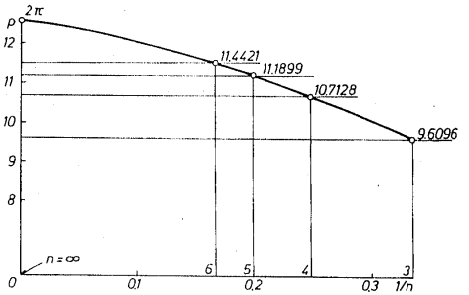

o – numerical results
n – number of polygon sides
moments, shear forces, deflection rates
as for square plate (plate 49)

PLATE 51, [48]

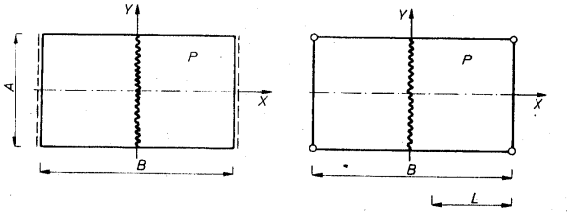

$$p = \frac{q}{D^2}$$

$$\frac{a}{b} \leqslant \Lambda \leqslant 1$$

$m_x = 1 - \frac{4x^2}{b^2}$; $m_y = \frac{a^2}{b^2}(1 - \frac{4y^2}{a^2})$; $m_{xy} = \frac{4}{b^2}xy$
$s_x = -\frac{4x}{b^2}$; $s_y = -\frac{4y}{b^2}$
$\dot{w} = \dot{w}_0 \frac{b-2x}{b}$

PLATE 52

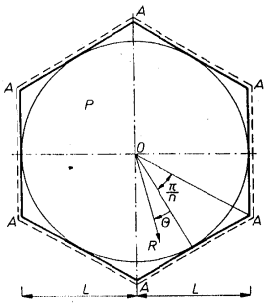

$p = 6 \qquad p_{total} = 6n \tan\frac{\pi}{n}$

n – number of polygon sides $\qquad n \geq \frac{\pi}{\arctan\sqrt{\Lambda}}$

$n = 4$	5	6	7	8	9	10	∞
$p_{total} = 24$	21.80	20.78	20.23	19.88	19.65	19.50	6π
$m_\theta = 1 \qquad m_r = 1 - r^2$							
$s_\theta = 0 \qquad s_r = -3r$							
$(s_r)_{UA} = (m_r)_{OA} = 0$							
$\dot{w} = \dot{w}_0 (1 - r\cos\Theta)$							

PLATE 53

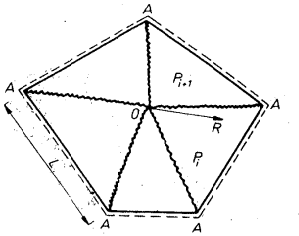

$$p_{total} = 3 \sum (\tan\alpha_i + \tan\gamma_i) s_i^2$$

$$\alpha_i, \gamma_i \leq \arctan\sqrt{\Lambda}$$

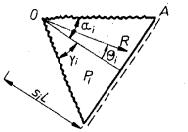

$p_i = \frac{6}{s_i^2} \; ; \quad p_i \neq p_{i+1}$
$m_\theta = 1 \; ; \quad m_r = 1 - \frac{r^2}{s_i^2}$
$s_\theta = 0 \qquad s_r = -\frac{3r}{s_i^2}$
$(m_r)_i = r^2\left(\frac{1}{s_i^2} - \frac{1}{s_{i+1}^2}\right) \; ; \; (s_r)_{OA} = 3r\left(\frac{1}{s_i^2} - \frac{1}{s_{i+1}^2}\right)$
$\dot{w} = \dot{w}_0 \left(1 - \frac{r\cos\Theta_i}{s_i}\right)$

PLATE 54

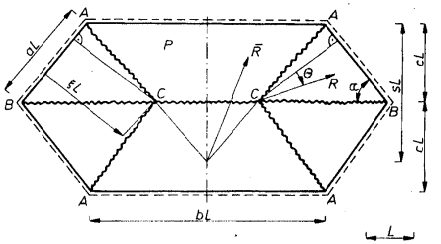

$$p = \frac{6}{(\xi/a)^3}$$

$$\frac{\xi}{a} = -2\frac{a}{b}\sin\alpha + \sqrt{4\left(\frac{a}{b}\right)^2\sin^2\alpha + 3\sin^2\alpha + 2\frac{a}{b}\sin\alpha\,\sin 2\alpha}$$

$$\frac{\pi}{2} - \operatorname{arctan}\sqrt{\Lambda} \leqslant \alpha \leqslant \frac{\pi}{2}$$

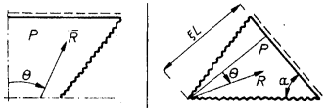

$m_\theta = 1$ $m_r = 1 + \frac{p}{6}\left(3\frac{(s-c)^2}{\cos^2\Theta} - 2\frac{(s-c)^3}{\bar{r}\cos^3\Theta} - \bar{r}^2\right)$	$m_\theta = 1\ ;\quad m_r = 1 - \frac{r^2}{\xi^2}$
$s_\theta = 0\ ;\ s_r = -\frac{p}{2}\left(\bar{r} - \frac{(s-c)^2}{\bar{r}\cos^2\Theta}\right)$	$s_\theta = 0\ ;\quad s_r = -\frac{3r}{\xi^3}$
$[m_r]_{CA} \neq 0\ ;\ [s_r]_{OA} = 0\ ;\ [m_r]_{BCCB} = [s_r]_{BCCB} = 0$	
$\dot{w} = \frac{\dot{w}_0}{c}(s - \bar{r}\cos\Theta)$	$\dot{w} = \dot{w}_0\left(1 - \frac{r\cos\Theta}{\xi}\right)$

$$\sqrt{\Lambda} + \operatorname{cotan}\alpha \geqslant \sin\alpha\ ;\quad \frac{\xi}{a} \geqslant \frac{1}{\operatorname{cotan}\alpha + \sqrt{\Lambda}}$$

PLATE 55, [44]

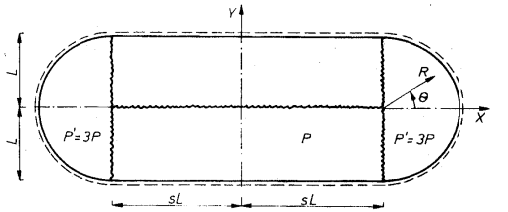

$$p = 2$$

$0 \leqslant s < \infty$

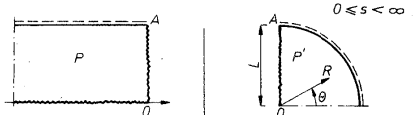

$p = 2$	$p' = 6$
$m_x = 1;\ m_y = 1 - y^2;\ m_{xy} = 0$	$m_\theta = 1\ ;\quad m_r = 1 - r^2$
$s_x = 0\ ;\quad s_y = -2y$	$s_\theta = 0\ ;\quad s_r = -3r$
$[m_r]_{OA} = 0$	$[s_r]_{OA} = \pm r$
$\dot{w} = \dot{w}_0(1-y)\ ;\ -s \leqslant x \leqslant s$	$\dot{w} = \dot{w}_0(1-r)$

PLATE 56

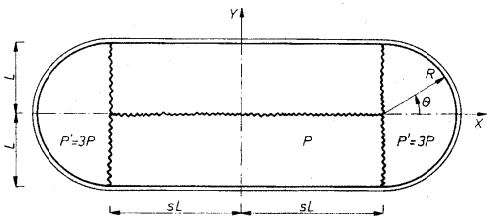

$$p = 2(1+\Lambda')$$

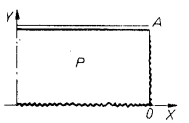

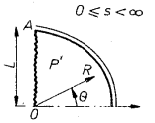

$p = 2(1+\Lambda')$	$p' = 6(1+\Lambda') = 3p$
$m_x = 1;\ m_y = 1-(1+\Lambda')y^2; m_{xy} = 0$	$m_\theta = 1\ ;\ m_r = 1-r^2(1+\Lambda')$
$s_x = 0;\ s_y = -2y(1+\Lambda')$	$s_\theta = 0\ ;\ s_r = -3r(1+\Lambda')$
$[m_r]_{OA} = 0$	$[s_r]_{OA} = \pm r(1+\Lambda')$
$\dot w = \dot w_0(1-y)\ ,\ -s \le x \le s$	$\dot w = \dot w_0(1-r)$

PLATE 57

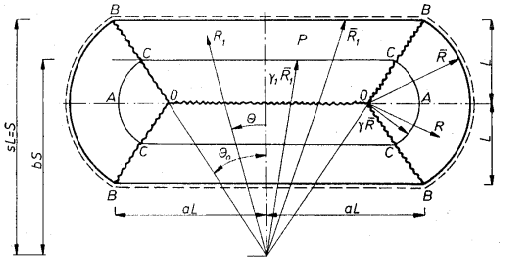

$$p = \frac{6}{s^2(1-b)^2(1+2b)} = \frac{6}{\bar r^2(1-\gamma)^2(1+2\gamma)}$$

$$\gamma \le \frac{2-\Lambda'}{2(1+\Lambda')} \longrightarrow \bar r \le \sqrt{1+\Lambda'}\ ,$$

$$\gamma > \frac{2-\Lambda'}{2(1+\Lambda')} \longrightarrow \bar r < \sqrt{\frac{3}{1+2\gamma}}$$

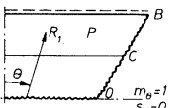

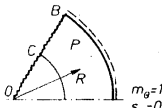

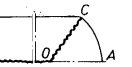

$m_r = 1-\frac{r_1-bs}{s^2(1-b)^2(1+2b)}\left(1+\frac{2bs}{r_1\cos\Theta}\right)$	$m_r = 1-\frac{(r-\gamma\bar r)^2}{\bar r^2(1-\gamma)^2(1+2\gamma)}\left(1+\frac{2\gamma\bar r}{r}\right)$	$m_r = 1;\ m_\theta = 1$
$s_r = -\frac{3}{s^2(1-b)^2(1+2b)}\left(r_1^2-\frac{b^2s^2}{\cos^2\Theta}\right)$	$s_r = -\frac{3(r^2-\gamma^2\bar r^2)}{\bar r^2(1-\gamma)^2(1+2\gamma)}$	$s_r = 0;\ s_\theta = 0$
$[m_r]_{BC} \ne 0\ ;\quad [s_r]_{BC} \ne 0\ ;\quad [m_r]_{CC} = [s_r]_{CC} = 0$		
$\dot w = \dot w_0(s-r_1)\cos\Theta$ $bs/\cos\Theta \le r_1 \le s/\cos\Theta$	$\dot w = \dot w_0\left(1-\frac{r}{\bar r}\right)$	$\dot w = \dot w_0(s-r_1)\cos\Theta$ $(s-1)/\cos\Theta \le r_1 \le bs$

$$\bar r^2 = \frac{3}{1+2\gamma} + \frac{2(1-\gamma)}{(1+2\gamma)^2}\,\frac{1}{a^2}\left(1-\gamma-\sqrt{(1-\gamma)(1-\gamma+2a^2(1+2\gamma)}\right)$$

$$s = \frac{1-\gamma}{1-b}\ ;\quad \frac{a}{s} = \sqrt{\bar r^2-1}\ ;\quad a = \frac{2(1-\gamma)\sqrt{\bar r^2-1}}{3-(1+2\gamma)\bar r^2}$$

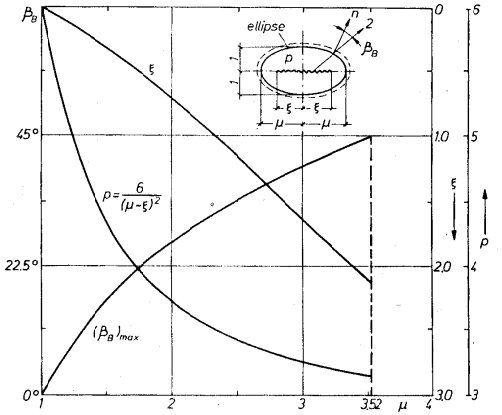

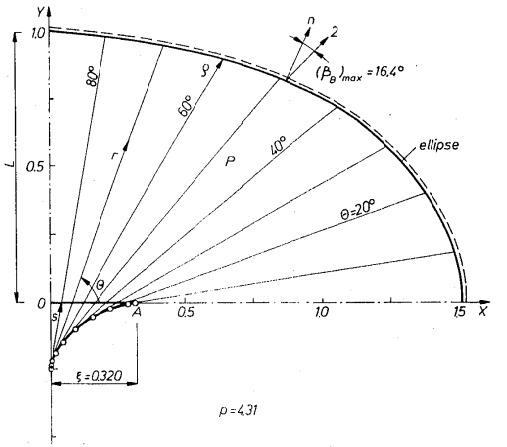

p=4.31

numerical solution $\Lambda'=1$

$m_\theta=1$; $m_r=1-\frac{pr^2}{6}(1-\frac{s}{r})^2(1+\frac{2s}{r})$
$s_\theta=0$, $s_r=\frac{p}{2}(\frac{s^2}{r}-r)$
$\dot{w}=\frac{\dot{w}_0}{\varrho-s}(\varrho-r)$

PLATE 60, [52]

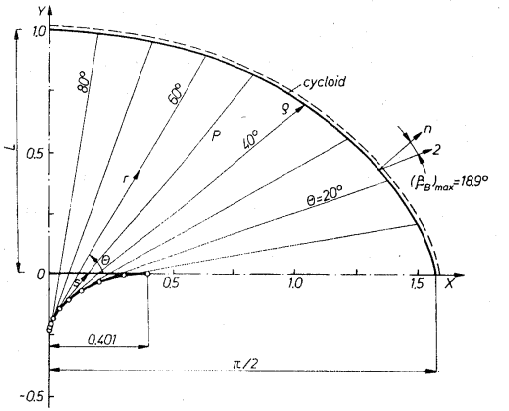

p=4.38

numerical solution $\Lambda'=1$

$m_\theta=1$; $m_r=1-\frac{pr^2}{6}(1-\frac{s}{r})^2(1+\frac{2s}{r})$
$s_\theta=0$; $s_r=\frac{p}{2}(\frac{s^2}{r}-r)$
$\dot{w}=\frac{\dot{w}_0}{\varrho-s}(\varrho-r)$

PLATE 61, [52]

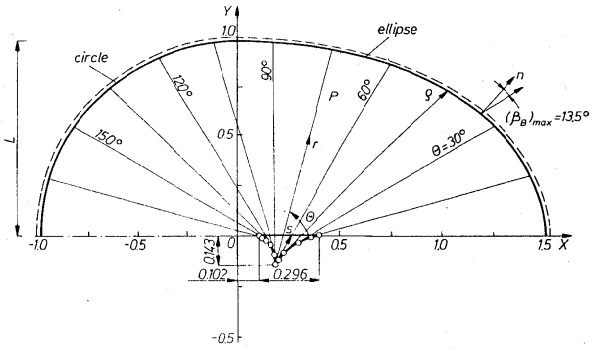

$p = 4.94$

numerical solution $\Lambda'=1$

$m_\theta = 1\ ;\quad m_r = 1 - \frac{pr^2}{6}(1-\frac{s}{r})^2(1+\frac{2s}{r})$
$s_\theta = 0\ ;\quad s_r = \frac{p}{2}(\frac{s^2}{r} - r)$
$\dot{w} = \frac{\dot{w}_0}{\varrho - s}(\varrho - r)$

PLATE 62, [87]

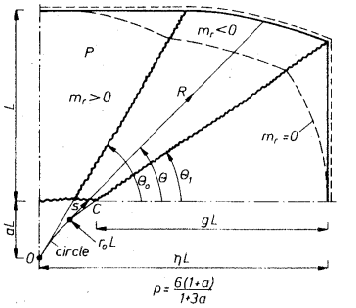

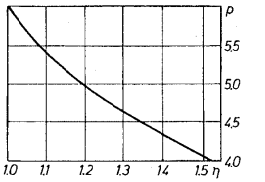

numerical solution $\Lambda'=1$

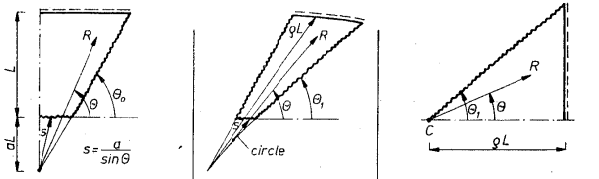

$m_\theta = 1\ ;\quad m_r = 1 - p(\frac{s^2}{2} - \frac{s^3}{3r} + \frac{r^2}{5})$		$m_\theta = 1\ ;\quad m_r = 1 - \frac{pr^2}{6}$
$s_\theta = 0\ ;\quad s_r = p(\frac{s^2}{2r} - \frac{r}{2})$		$s_\theta = 0\ ;\quad s_r = -\frac{pr}{2}$
$\dot{w} = \dot{w}_0(1 + a - r\sin\Theta)$	$\dot{w} = \frac{\dot{w}_0}{\varrho - s}(\varrho - r)$	$\dot{w} = \dot{w}_0(1 - \frac{\cos\Theta}{g}r)$
$g^2 = \frac{1+3a}{1+a}\ ;\quad \Theta_1 = \arccos\frac{a + r_0\cos\Theta_0}{r_0}\ ;$		$r_0 = \frac{c^2 + (\eta - g)^2}{2[(\eta - g)\sin\Theta_0 - a\cos\Theta_0]}$

PLATE 63

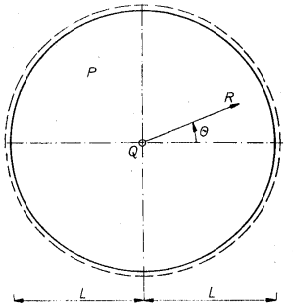

$$p = \frac{6\pi}{3\alpha + \pi}$$

$$q = \alpha p$$

$m_\theta = 1;\quad m_r = 1 - \frac{3\alpha + \pi r^2}{3\alpha + \pi}$
$s_\theta = 0;\quad s_r = -\frac{3(\alpha + \pi r^2)}{(3\alpha + \pi) r}$
$\dot{w} = \dot{w}_0 (1 - r)$

PLATE 64

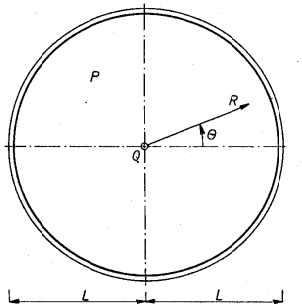

$$p = \frac{6\pi}{3\alpha + \pi} (1 + \Lambda')$$

$$q = \alpha p$$

$m_\theta = 1\ ;\quad m_r = \frac{3\alpha + \pi r^2}{3\alpha + \pi} (1 + \Lambda')$
$s_\theta = 0\ ;\quad s_r = -\frac{3(\alpha + r^2 \pi)}{(3\alpha + \pi) r} (1 + \Lambda')$
$\dot{w} = \dot{w}_0 (1 - r)$

PLATE 65

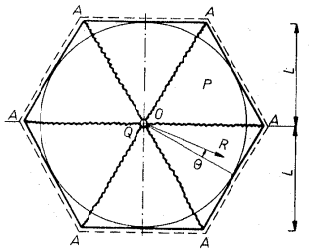

$$p = \frac{6q_o}{q_o + 6\alpha} \qquad q_o = 2n\tan\frac{\pi}{n}$$

$$q = \alpha_i p$$

$$\frac{\pi}{n} \leq \arctan\sqrt{\Lambda}$$

n - number of poligon sides

$m_\theta = 1\ ;\ m_r = (1 - r^2 + \tan^2\theta) - \tan\theta$ $0 \leq \gamma \leq 1 \qquad \gamma = \frac{q_o}{q_o + 6\alpha}$
$s_\theta = 0\ ;\ s_i = \frac{\gamma}{r}(3r^2 - 1 - \tan^2\theta) - \frac{1}{r}(1 + \tan^2\theta)$
$[m_r]_{0A} = [s_r]_{0A} = 0$
$\dot{w} = \dot{w}_0(1 - r\cos\theta)$

PLATE 66

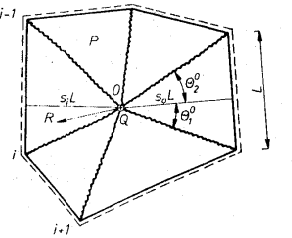

$$p = \beta_o \frac{6}{(\max s_i)^2}\ ; \qquad q = p \sum_{i=0}^{n} \alpha_i$$

$$s_o = \max s_i$$

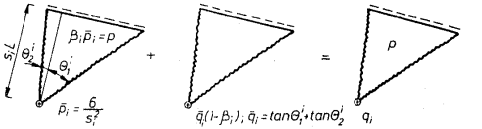

$p = \beta_o \frac{6}{(\max s_i)^2}\ ; \quad q_i = \alpha_i p\ ; \quad i > 0$
$\alpha_i = \psi_i \left(\frac{s_{i-1}^2}{s_i^2} - 1\right) + \frac{\psi_i}{\psi_{i-1}} \frac{s_{i-1}^2}{s_i^2} \alpha_{i-1}\ ; \quad \psi_i = \frac{\bar{q}_i}{\bar{p}_i}\ ; \quad 0 < \alpha_o = \frac{q_o}{p} < \infty$
$m_\theta = 1\ ;\ m_r = \beta_i\left(1 - \frac{r^2}{s_i^2}\right) - (1 - \beta_i)\tan^2\theta^i\ ; \quad \beta_i = \frac{\bar{q}_i}{\bar{p}_i \alpha_i + \bar{q}_i}$ $0 \leq \beta_i \leq 1$
$s_\theta = 0\ ;\ s_r = -3\beta_i \frac{r}{s_i^2} - (1 - \beta_i)\frac{1}{r}(1 + \tan^2\theta^i)$
$[m_r]_{0i} = m_r^{i+1} - m_r^i\ ; \quad [s_r]_{0i} = s_r^{i+1} - s_r^i$
$\dot{w} = \dot{w}_0\left(1 - \frac{r}{s_i}\cos\theta^i\right)\ ; \quad \theta_1^i \leq \theta^i \leq \theta_2^i\ ; \quad \theta_1^i, \theta_2^i \leq \arctan\sqrt{\Lambda}$

PLATE 67, [48]

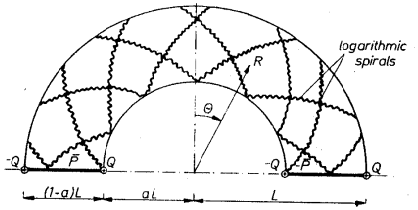

$$q = 2$$
$$\bar{p} = \frac{2}{F}$$

$\Lambda = 1$

$m_\theta = 0\,;\quad m_r = 0\,;\quad m_{r\theta} = 1$
$s_\theta = -\frac{2}{F}\,;\quad s_r = 0$
$\dot{w} = -a^2\Theta$

Literature

[1] Anderheggen, E., Knopfel, H., Finite element limit analysis using linear programming, Int. J. Solids Struct., **8** (1972), 1413 - 1431.

[2] Anderheggen, E., Finite element analysis assuming rigid-ideal plastic material behaviour, Rapport of E.T.H. Zürich, nº 70 (1977), 1 - 17.

[3] Borkowski, A., Jendo, S., Reitman, M., Mathematical Programming, Vol.2 of the series Structural Optimization, ed. by M.A.Save and W.H.Warner, Plenum Press, New York 1989.

[4] Ceradini, G., Gavarini, C., Calcolo a rotura e programmazione lineare continui bi e tridimensionale Nota I Fondamenti scorisi, Giornale del Genio Civile, nº 2 - 3 (1968), 125 - 137; Nota II Applicazioni a piastre e volte di rivoluzione, nº **4** (1968), 163 - 180.

[5] Christiansen, E., Limit analysis in plasticity as a mathematical programming program, Calcolo, **17** (1980), 41 - 65.

[6] Christiansen, E., Limit analysis for plastic plates SIAM J. Math. Anal., **11**, 3 (1980), 514 - 522.

[7] Christiansen, E., Larser, S., Computations in limit analysis for plastic plates, Int. J. Numerical Meth. in Engineering, **19** (1983), 169 - 184.

[8] Cinquini, C., Zanon, P., Limit analysis of circular and annular plates, Ing. Arch. **55**, (1985), 157 - 175.

[9] Collins, J.F., On an analogy between plane strain and plate bending solutions in rigid-perfect plasticity, Int. J. Solid Struct., **7** (1971), 1057 - 1073.

[10] Faccioli, E., Vitiello, E., A finite element, linear programming method for the limit analysis of thin plates, Int. J. Numerical Meth. in Engineering, **5** (1973), 311 - 325.

[11] Eason, G., Velocity fields for circular plates with the Mises yield condition, J. Mech. Phys. Solids, **6** (1958), 231 - 235.

[12] Fox, E.N., Limit analysis for plates: a simply loading problem involving a complex exact solution, Phil. Trans. R. Soc. Lond., A. **272** (1972), 463 - 492.

[13] Fox, E.N., Limit analysis for plates: the exact solution for a clamped square plate of isotropic homogeneous material obeying the square yield criterion and loaded by uniform pressure, Phil. Trans. R. Soc. Lond., A. **277** (1974), 121 - 155.

[14] Guerlement, G., Lamblin, D.O., Analyse limite des plaques circulaires avec la condition de plasticite de von Mises, Bull. Tech. Suisses Romande, **98** (1972), 1 - 8.

[15] Gvozdev, A.A., A Theory of Limit Equilibrium (in Russian), Strojizdat, Moscow 1949.

[16] Haythorthwaite, R.M., Range of yield condition in ideal plasticity, J. Eng. Mech. Div.Proc. ASCE, **87**, EM6 (1961), 117 - 133.

[17] Hill, R., The Mathematical Theory of Plasticity, Clarendon, Oxford 1950.

[18] Hodge, P.G., Jr., Plastic Analysis of Structures, McGraw-Hill, New York 1959.

[19] Hodge, P.G., Jr.,Plastic Analysis of Rotationally Symmetric Plates and Shells, Prentice Hall, Englewood, Cliffs, N.J., 1963.

[20] Hodge, P.G., Jr., Plastic plates theory, Quart. Appl. Math., **22** (1964), 74 - 79.

[21] Hodge, P.G., Jr., Belytschko, T., Numerical methods for the limit analysis of plates, J.Appl.Mech.Transactions ASME, **35** (1968), 797 - 802.

[22] Hodge, P.G., Jr., Belytschko, J., Numerical methods for the limit analysis of plates, Appendix C. Description of computer program, Illinois Institute of Technology, (1968).

[23] Hopkins, H.G., Prager, W., The load carrying capacities of circular plates, J.Mech. Phys. Solids, **2** (1953), 1 - 13 - 13.

[24] Hopkins, H.G., Wang, A., Load carrying capacities for circular plates of perfectly plastic material with arbitrary yield condition, J. Mech. Phys. Solids, **3** (1954), 117 - 129.
[25] Hopkins, H.G., On the plastic theory of plates, Phil. Trans. R. Soc. Lond., A. **241** (1957), 153 - 179.
[26] Hu, L.W., Modified Tresca's yield condition and associated flow rules for anisotropic materials and applications, J. Franklin Institute, **265** (1958), 187 - 204.
[27] Ilyushin, A.A., Plasticity (in Russian), Gostekhizdat, Moscow 1949.
[28] Janas, M., Kinematical compatibility problems in yield line theory, Mag. Concrete Research, **19**, 58 (1967), 33 - 44.
[29] Janas, M., Fondements de la théorie de plasticité et l'analyse limite, Ecole Nationale Supérieure d'Hydraulique et de Mécanique, Université Scientifique Technologique et Médicale, Grenoble 1986.
[30] Johansen, K.W., Brudlinieteorier (in Danish), Gjellerup, Copenhagen 1943; English edition, Yield Line Theory, Cement & Concrete Association, London 1962.
[31] Johnson, W., Upper bounds to the load for the transverse bending of flat rigid- perfectly plastic plates, Int. J. Mech. Sci., **11** (1969), 913 - 938.
[32] Jones, L.L., Wood, R.H., Yield-Line Analysis of Slabs, Chatto and Windus, London 1967.
[33] Kaliszky, S., Limit Analysis of Reinforced Concrete Slabs (in Hungarian), Muszaki Konyvklado, Budapest 1967.
[34] Kaliszky, S., Plasticity, Theory and Engineering Applications, Akadémiai Kiadó, Budapest – Elsevier Science Publ., Amsterdam, The Netherlands 1989.
[35] König, J.A., Rychlewski, J., Limit analysis of circular plates with jump non-homogeneity, Int. J. Solids Struct., **2** (1966), 493 - 513.
[36] König, J.A., Shakedown of Elastic-Plastic Structures, PWN, Warszawa – Elsevier, Amsterdam – Oxford – New York – Tokyo 1987.
[37] Koopman D.C.A., Lance, R.H., On linear programming and plastic limit analysis, J. Mech. Phys. Solids, **13** (1965), 77 - 87.
[38] Kwieciński, M., Collapse Load Design of Slabs-Beam Systems, PWN, Warszawa - Ellis Horwood Ltd, Chichester 1989.
[39] Langendonck, T.V., Teoria Elementar das Charneiras Plasticas, A.B.C.P., Sao Paulo, Brasil, I (1970), II (1975).
[40] Mandel, J., Sur l'unicite du champ des contraintes lors de l'equilibre limite dans un milieu rigide plastique..., C.R. Acad. Sci., Paris, 261 (1965), 35 - 37.
[41] Mansfield, E.H., Studies in collapse analysis of rigid plastic plates with a square diagram, Proc. Roy. Soc., **A241** (1957) 311 - 338.
[42] Markowitz, J., Hu, L.W., Plastic analysis of orhotropic circular plates, J. Eng. Mech. Div., **90**, EM5 (1964), 251 - 292.
[43] Martin, J.B., Plasticity: Fundamentals and General Results, The MIT Press, Massachusetts and London, England 1975.
[44] Massonnet, C.E., Complete solutions describing the limit state of reinforced concrete slabs, Mag. Concrete Research, **19**, 58 (1967), 13 - 32.
[45] Mróz, Z., Sawczuk, A., Load carrying capacities of annular plates (in Russian), Izv. AN USSR, 3 (1960), 72 - 78.
[46] Nguyen Dang Hung, Direct limit analysis via rigid-plastic finit elements, Comp. Meth. Appl. Mech. Engng., **8** (1976), 81 - 116.
[47] Nielsen, M.P., Exact solutions in the plastic plates theory, Bygningstatiske Meddelelser, **34**, 1 (1963), 1 - 28.
[48] Nielsen, M.P., Limit Analysis of Reinforced Concrete Slabs, Acta Polyt. Scand., Ci 26, 1964.
[49] Nielsen, M.P., Limit Analysis and Concrete Plasticity, PrenticeHall, Inc., Englewood Cliffs, New Jersey 1984.
[50] Niepostyn, D., Limit analysis of rectangular plates (in Polish), Arkady, Warszawa 1962.
[51] Niepostyn, D., Limit Analysis of Rotationally Symmetric Plates (in Polish), Arkady, Warszawa 1963.

[52] Ohno, N., Sawczuk, A., A method of limit analysis for plates of arbitrary shape (in Japanese), Trans. JSME, **43** (1977), 2450 - 2458; in English: Journal de Mecanique applique, **3**, 2 (1979), 187 - 203.
[53] Olszak, W., Theory of limit analysis of orthotropic plates (in Polish), Bud. Przem., **2** (1953), 254 - 265.
[54] Olszak, W., Urbanowski, W., The generalised distortion energy in the theory of anisotropic bodies, Bull. Acad. Pol. Sci., Cl.IV, 1957.
[55] Olszak, W., Perzyna P., Sawczuk, A.(editors), Theory of Plasticity (in Polish), PWN Warszawa 1965.
[56] Pell, W.H., Prager, W., Limit design of plates, Proc. 1st US Natl. Congr. Appl. Mech., ASME, New York 1952, 547 - 550.
[57] Prager, W., Discontinuous solutions in the theory of plasticity, Courant Anniv. Vol., Interscience, New York 1948, 289 - 299.
[58] Prager, W., Hodge, P.G. Jr., Theory of Plastic Solids, John Wiley, New York 1951.
[59] Prager, W., Probleme der Plastizitätstheorie, Birkhauser, Basel 1955; English edition: Introduction to Plasticity, Addison-Wesley, Boston 1959.
[60] Ranawera, M.P., Leckie, F.A., Finite element techniques in solid mechanics: Bound methods in limit analysis, University of Southampton, Dept. Civil Engineering, April 1970, 15 - 17.
[61] Rzanitsyn, A., Calculation of Structures with Account for Plastic Properties of Materials (in Russian), Strojizdat, Moskow 1954.
[62] Save, M.A., On yield conditions in generalized stresses, Quart. Appl. Math., **19** (1961), 259 - 267.
[63] Save, M.A., A consistent limit-analysis theory for reinforced concrete slabs, Mag. Concrete Research, **19**, 58 (1967), 3 - 12.
[64] Save M.A., Massonnet, C.E., Plastic Analysis and Design of Plates, Shells and Disks, North-Holland Publ. Comp., Amsterdam 1972.
[65] Save, M.A., Prager, W., Optimality Criteria, Vol.1 of the series Structural Optimization ed. by M.A. Save and W. Prager, Plenum Press, New York 1985.
[66] Sawczuk, A., Sokół-Supel, J., Badin, F., Atlas of Limit Load of Metal Plates and Shells (in print).
[67] Sawczuk, A., Some problems of load carrying capacities of orhotropic and non-homogeneous plates, Arch. Mech. Stos., **8**, 4 (1956), 549 - 553; Actes, IX Congr. Int. Mec. Appl., Vol. 8, Bruxelles 1957, 93 - 102.
[68] Sawczuk, A., Linear theory of anisotropic plasticity and its applications to problems of limit analysis, Arch. Mech. Stos., **11**, 5 (1959), 541 - 557.
[69] Sawczuk, A., Rychlewski, J., On yield surface for plastic shells, Arch. Mech. Stos., **12** (1960), 29 - 53.
[70] Sawczuk, A., On the theory of anisotropic plastic plates and shells, Arch. Mech. Stos., **13**, 3 (1961), 355 - 365.
[71] Sawczuk, A., Janas, M., Zawidzki. J., Problems of limit analysis of plates with mixed boundary conditions (in Polish), Rozpr. Inż., **10** (1962), 245 - 278.
[72] Sawczuk, A., Jaeger, Th., Grenztragfähigkeits-Theorie der Platten, Springer-Verlag, Berlin 1963.
[73] Sawczuk, A., Hodge, P.G., Jr., Limit analysis and yield line theory, J. Appl. Mech., **35** (1968), 357 - 362.
[74] Sawczuk, A., Yield Surfaces, University of Waterloo SM Tech. Note 1, Waterloo 1971.
[75] Sawczuk, A., Janas, M., König, J.A., Plastic Analysis of Structures (in Polish), Ossolineum, Wrocław 1972.
[76] Sawczuk, A., Plastic Plates, CISM Lecture Notes, Udine 1974.
[77] Sawczuk, A., Sokół-Supel, J., Bending of plates with a square yield condition, Bull. Acad. Pol. Sci., **23**, 3 (1975), 141 - 150.
[78] Sawczuk, A., Contribution a l'analyse limite des plaques, Problemes de Rheologie et de Mechanique des Sols, PWN Warszawa 1977, 403 - 417.

[79] Sawczuk, A., Mechanics and Plasticity of Structures, PWN, Warszawa — Ellis Horwood Ltd, Chichester 1989.
[80] Schumann, W., On limit analysis of plates, Quart. Appl. Math., **16** (1958), 61 - 71.
[81] Sobotka, Z., Limit Analysis of Plates (in Polish), Arkady, Warszawa 1975.
[82] Sokół-Supel, J., Plastic plates under concentrated load (in Polish), Rozpr. Inż., **21**, 2 (1973), 311 -345.
[83] Sokół-Supel, J., Discontinuous stress field in plastic plates at collapse under distributed load, Bull. Acad. Pol. Sci., **23**, 4 (1975), 213 - 217.
[84] Sokół-Supel, J., On complete limit analysis solution for point loaded strip, Bull. Acad. Pol. Sci., **23**, 4 (1975), 219 - 223.
[85] Sokół-Supel, J., Grabarski, A, Sawczuk, A., Limit analysis of circular metal plates (in Polish), IPPT Reports 41, 1975.
[86] Sokół-Supel, J., Yield line theory. Tables for uniformly loaded rectangular plates (in Polish), IPPT Reports 19, 1976.
[87] Sokół-Supel, J., Semi-inverse method of obtaining complete solutions in the theory of load carrying capacity of plates (in Polish), Rozpr. Inż., **24**, 4 (1976), 797 - 807.
[88] Sokół-Supel, J., Yield line theory. Collection of solutions for point loaded rectangular plates (in Polish), IPPT Reports 20, 1977.
[89] Sokół-Supel, J., Complete solutions for plastic plates. Collection of solutions (in Polish), IPPT Reports 30, 1978.
[90] Sokół-Supel, J., Numerical method for evaluation of bearing capacity of symmetric circular plates (in Polish), Rozpr. Inż., **26**, 1 (1978), 179 - 191.
[91] Sokół-Supel, J., Sawczuk, A., Complete limit analysis solutions and yield line theory, IABSE Coll. Plasticity in Reinforced Concrete, Copenhagen 1979, Final Report, 137 - 144, Zurich 1979.
[92] Sokół-Supel, A., Sawczuk, A., A systematic study of load carrying capacity of rotationally symmetric plates with Huber-Mises yield condition, Rozpr. Inż., **27**, 2 (1979), 219 - 244.
[93] Wood, R.H., Plastic and Elastic Design of Slabs and Plates, Thames & Hudson, London 1961.
[94] Zawidzki, J., Sawczuk, A., Plastic analysis of fibre-reinforced plates under rotationally symmetric conditions, Int. J. Solids Struct., **3** (1967), 413 - 425.

Subject Index